THESIS / THÈSE

DOCTOR OF SCIENCES

Control theory of area preserving maps - Application to particle accelerator systems

Boreux, Jehan

Award date:
2013

Awarding institution:
University of Namur

[Link to publication](#)

UNIVERSITE DE NAMUR

FACULTE DES SCIENCES
DEPARTEMENT DE MATHEMATIQUE

Control theory of area-preserving maps Application to particle accelerator systems

Thèse présentée par
Jehan Boreux
pour l'obtention du grade
de Docteur en Sciences

Composition du Jury :

Timoteo CARLETTI (Promoteur)
Duccio FANELLI
Anne LEMAITRE
Michel VITTOT
Joseph WINKIN (Président du Jury)

Octobre 2013

Théorie du contrôle des mappings symplectiques
Application aux modèles d'accélérateur de particules
par Jehan Boreux

Résumé : Les accélérateurs de particules sont des outils technologiques permettant d'étudier des échelles *infiniment* petites, e.g. les particules responsables des forces élémentaires, et des échelles *extrêmement* grandes, e.g. l'origine du cosmos. Dans ce travail nous analysons des mappings symplectiques modélisant des accélérateurs circulaires. Parallèlement nous démontrons un théorème *de type contrôle* grâce auquel nous construisons deux nouveaux mappings. Ces systèmes présentent d'excellents comportements dynamiques : une plus grande ouverture dynamique, une réduction du nombre d'orbites chaotiques et un espace des fréquences restreint. Ces résultats ont un fondement analytique et sont validés numériquement par les outils suivants : théorie des formes normales (NF), indicateur de chaos (SALI) et analyse en fréquences d'orbites (FMA). Enfin, une toute nouvelle approche pour contrôler les *systèmes dissipatifs*, proches de systèmes intégrables, est présentée. Les premiers résultats théoriques et numériques afférents sont exposés à l'aide du système de van der Pol.

Control theory of area-preserving maps
Application to particle accelerator systems
by Jehan Boreux

Abstract : Particle accelerators are technological devices which allow studies at both *infinitely* small scale, e.g. particles responsible for elementary forces, and *extremely* large scale, e.g. the origin of cosmos. This work is concerned with area-preserving maps modelling ring accelerators. We prove a theorem on *control* allowing us to build two new maps. These systems exhibit excellent dynamical properties : wider dynamical aperture, reduction of chaos and a reduced frequency space. The results have a strong analitical basis and are validated numerically with the normal form theory (NF), the chaos indicator SALI and the frequency map analysis (FMA). Finally we present a very new direction in the control of dynamical systems : controlling dissipative systems that are perturbations of integrable ones. We give a detailed presentation of the first theoretical and numerical results through the van der Pol model.

He went down south and crossed the border
Left the chaos and disorder
Back there over his shoulder

Jim Morisson, *Celebration of the Lizard*

Remerciements

Un voyage de presque six années se termine et il y a un bon nombre de personnes que je tiens à remercier dans ces quelques lignes pour m'avoir aidé ou tout simplement accompagné lors de la réalisation de cette thèse.

La première personne est évidemment mon promoteur, Timoteo Carletti, sans qui rien de tout cela n'aurait été possible, littéralement. Depuis le début de mon mémoire de fin de Master jusqu'à ces derniers jours de rédaction de thèse, tu t'es montré passionnant et passionné. Ta porte est toujours restée ouverte pour m'expliquer (et me ré-expliquer, itérez !) de nouveaux concepts et ce avec une infinie patience. Tes réponses et conseils judicieux m'ont éclairé et guidé toutes ces années. Même en dehors des "maths", tu t'es montré positif : que ce soit concernant mes petits soucis ou un voyage avec la fucid, je n'ai rencontré que des encouragements. Sincèrement Teo, merci !

Je souhaite remercier Anne Lemaître qui, depuis mes premiers pas en math, s'est toujours montrée à l'écoute et disponible. Au cours des ans, tu m'as apporté énormément, aussi bien scientifiquement qu'humainement. Cette thèse n'existerait pas sans le concours de Michel Vittot. J'ai découvert tes articles qui m'ont orienté vers le contrôle dès mon mémoire pour finalement en faire le sujet de ce manuscrit. Et maintenant on en écrit ensemble, des articles. Merci pour ta passion et ton engouement communicatifs et ce spécialement lorsque tu m'as accueilli à Marseille. Merci aux autres membres du jury, Duccio Fanelli et Joseph Winkin, pour leurs conseils pertinents et leurs remarques constructives ; elles ont permis d'améliorer la qualité et la précision de cet ouvrage.

Merci à tous les membres de ce département bien chaleureux ! En particulier, merci à nos deux secrétaires Pascale et Martine pour leur efficacité et disponibilité constante. Je remercie mes collègues de bureau qui m'ont accompagné au quotidien. Merci Simone pour deux années *à l'italienne* à parler anglais et merci Audrey pour ta convivialité, ton humour et ton écoute de tous les instants durant les quatre années suivantes. Merci aux *vieux* qui ont montré que

Table des matières

Introduction

Context

This thesis has been developed in the field of applied mathematics : starting from a physical problem, hereby the increase of the power of a particle accelerator, we elaborate a theoretical framework where such problem can be tackled and eventually allow us to generalize it to consider new unexpected cases.

Particle accelerators are technological devices which allow studies at both "infinitely small scale", e.g. particles responsible for elementary forces, and "extremely large scale", e.g. the origin of cosmos. In a simplified approach, such devices are composed of basic sequences of elements : focusing and defocusing magnets, accelerating electromagnetic fields and trajectory bending elements as they are used in the case of ring accelerators. The resulting dynamics is nonlinear, and since hadrons lose a negligible part of their energy through synchrotron radiation [Fischer et al., 1995], their motion can be described by a conservative system. This system can thus be modelled by a symplectic map built from the composition of several elementary maps corresponding to each basic element.

One of the main problems found in the dynamics of ring accelerators is to study the stability around the nominal orbit, i.e. the circular orbit passing through the center of the ring. Each component of the ring can be seen as a nonlinear map, that deforms the trajectory far from the reference orbit. Moreover, such maps possess stochastic layers whose effect is the reduction of the stability domain around the nominal circular orbit (the so-called *dynamical aperture* [Giovannozzi et al., 1997]). Such behaviors imply that (chaotic) nearby orbits can drift away after a few ring turns, eventually colliding with the boundaries of the accelerator, and consequently reduce the beam lifetime and the performance of the accelerator.

The first aim of the present work is to provide a reliable improvement of the stability of the beam by increasing the dynamical aperture in a simplified accelerator model, consisting of only one type of element having a sextupole

nonlinearity [Scandale and Turchetti, 1990, Bazzani et al., 1994].

We work in the framework of the *Hamiltonian Control Theory* presented in [Vittot, 2004, Chandre et al., 2005b], where two methods to control symplectic systems have been described, namely using Lie transformations and generating functions. We use the former method, that allows direct determination of the new controlled map; avoiding the possible problems related to coordinate inversion.

The aim of control theory is to improve selected features of a given system, by slightly modifying the Hamiltonian system with the addition of a *small* control term, so that the new system and the original one are conjugated. In other words, they present an equivalent dynamics. This technique is particularly suitable whenever one can directly act on the system and modify it, e.g. in the case of a particle accelerator where the addition of a control term in the Hamiltonian function can be seen as the introduction of a suitable magnet in the accelerator lattice.

In our study, we use the Smaller ALignment Index (SALI) [Skokos, 2001, Bountis and Skokos, 2006] method, which is an efficient indicator for characterizing orbits as chaotic or regular in Hamiltonian flows and symplectic maps.

In parallel we compute the Frequency Map Analysis (FMA) [Laskar, 1990, Laskar, 1999, Nadolski and Laskar, 2003] with which we validate and get complementary information with respect to SALI's results and construct tune footprints of accelerator model including resonances and diffusion indexes.

Then, with the use of the Normal Form (NF) approach [Bazzani et al., 1990, Scandale and Turchetti, 1990] we are able to predict analytically the diffusion directions in the frequency space and provide an analytical support to the FMA results.

Finally, we extend our results to Hamiltonian systems to which a dissipative perturbation is applied. This is a very new direction in which we propose preliminary results.

Structure of the thesis

The thesis is organized as follows. In Chap. 1 we introduce the notations and state important results of Hamiltonian dynamics and area-preserving maps leading to our first result, theorem 1.3.4 : a method to control area-preserving maps. We conclude this chapter by explaining the resulting properties. Examples of others techniques of control are given before the introduction of the Normal Form formalism.

Chap. 2 is dedicated to derive the model of a ring accelerator of particle in the map formalism from the very basic laws of electromagnetism.

In Chap. 3 we give a definition of a *chaotic orbit* and present two numerical

tools to detect such behavior : methods based on deviation vectors and methods based on the analysis of the signals transmitted by the orbit.

We then present our main results in Chap. 4 and Chap. 5. We apply our control method to the previously derived model of accelerator. We analyze the results thanks to the SALI and the FMA. Results are especially convincing ; we observe a significant increase of the dynamical aperture. Finally we reinforce our results by a Normal Form approach on the controlled and un-controlled models allowing us to predict the frequency space shape.

Chap. 6 presents a very new direction in the control of dynamical systems : controlling dissipative systems that are perturbations of integrable ones. We prove a theorem providing a control method for systems expressed by differential operators of order 1 such as vector fields. We expose the first difficulties and solutions through the van der Pol model [van der Pol, 1927].

Contributions

Key results appearing in this document are the subject of different papers : two are already published in peer-reviewed journals, one is in preprint and two are in preparation :

- J. Boreux, T. Carletti, Ch. Skokos and M. Vittot. Hamiltonian control used to improve the beam stability in particle accelerator models. *Communications in Nonlinear Science and Numerical Simulation*, **17** :1725-1738, 2012b.
- J. Boreux, T. Carletti, Ch. Skokos, Y. Papaphilippou and M. Vittot. Efficient control of accelerator maps. *International Journal of Bifurcation and Chaos*, **22**(9) :1250219, 2012a.
- J. Boreux, T. Carletti and Ch. Hubaux. High order explicit symplectic integrators for the Discrete Non Linear Schrödinger equation. *arXiv :1012.3242v1*, 2010.
- J. Boreux, T. Carletti and M. Sansottera. Analysis of the frequency space of controlled particle accelerators maps. In preparation.
- J. Boreux, T. Carletti and M. Vittot. Control of dissipative perturbation of integrable systems - An application to the van der Pol oscillator. In preparation.

In addition, various techniques of control were applied for the first time to simple models (see, for example Sec. 1.3.2). That allows an easier understanding of possibly hard control concepts.

Nonlinear dynamics of area preserving systems : theory and control

Contents

This first chapter is a theoretical one. The aim is to introduce the main notations and the framework, especially the *symplectic maps* and their properties.

We present two main ideas to deal with nonlinear systems or perturbed systems : act by control or by a normal form approach. In this thesis we focus on the first one, by providing proofs and examples both in the continuous and in the discrete time case. We thus shall limit to present the main theoretical features of the second approach ; their significant role will be developed in the application chapter.

In this chapter, we derive our main theoretical result, the *control of area preserving maps*. In order to state this result, we first develop the analogue in Hamiltonian systems thanks to which useful ideas and concepts are introduced.

For the sake of completeness we present other methods of controlling discrete dynamical systems before closing the chapter with the introduction of a powerful tool in nonlinear and perturbations theory.

More precisely, this first chapter is organized in 5 sections. The first section : theory and framework of Hamiltonian dynamics and maps. The following two sections are dedicated to control systems that are continuous in time (Hamiltonian control) or discrete in time (symplectic maps). We then present a short non-exhaustive list in the fourth section of other techniques of control. Finally the Normal Form approach for maps is introduced.

1.1   Theoretical framework

We place ourselves in the framework of Hamiltonian mechanics, where a physical system is described by a set of canonical variablees (see Def. 1.1.2) $\boldsymbol{x} = (\boldsymbol{q}\ \boldsymbol{p})^t$ where $\boldsymbol{q} = (q_1, \ldots, q_n) \in \mathbb{R}^n$ and $\boldsymbol{p} = (p_1, \ldots, p_n) \in \mathbb{R}^n$ are respectively the coordinate and momentum vectors. The system has thus n degrees of freedom.

The dynamics of such system is governed by a scalar function called *the Hamiltonian* $H(\boldsymbol{q}, \boldsymbol{p})$, and the equations of motion read,

$$\begin{cases} \dot{\boldsymbol{q}} = \dfrac{\partial H}{\partial \boldsymbol{p}}, \\[2mm] \dot{\boldsymbol{p}} = -\dfrac{\partial H}{\partial \boldsymbol{q}}. \end{cases} \tag{1.1}$$

The system is thus represented by $2n$ differential equations of order 1.

1.1.1 Poisson brackets

Definition 1.1.1 *If $\boldsymbol{x} = (\boldsymbol{q}\ \boldsymbol{p})^t \in \mathbb{R}^{2n}$, the* Poisson bracket *of two functions f and g is given by*

$$\{f, g\} = \sum_{k=1}^{n} \left(\frac{\partial f}{\partial p_k} \frac{\partial g}{\partial q_k} - \frac{\partial g}{\partial p_k} \frac{\partial f}{\partial q_k} \right). \tag{1.2}$$

Hamilton's equations take the form

$$\dot{q}_k = \{H, q_k\} \qquad \dot{p}_k = \{H, p_k\}, \qquad k = 1, \ldots, n.$$

Let us notice that we do not follow the more common definition which is, for example in [Fasano and Marmi, 2006] :

$$\{f, g\} = \sum_{k=1}^{n} \left(\frac{\partial f}{\partial q_k} \frac{\partial g}{\partial p_k} - \frac{\partial g}{\partial q_k} \frac{\partial f}{\partial p_k} \right).$$

This change is notable but is not of great impact ; the above definitions are equivalent up to a sign change.

Definition 1.1.2 *Canonical variables q_k and p_k are variables in phase space that satisfy*

$$\{q_k, q_l\} = 0 \quad \{p_k, p_l\} = 0 \quad \{p_k, q_l\} = \delta_{kl}.$$

where δ_{kl} is the Kronecker symbol :

$$\delta_{kl} = \left\{ \begin{array}{ll} 1 & if \quad k = l\,, \\ 0 & otherwise. \end{array} \right.$$

1.1.2 Algebra of operators

The framework is the one of Lie structure. For this purpose we consider the vector space $\mathcal{A}$ of C^∞ real functions defined on the phase space. For any $V \in \mathcal{A}$, we define $\{V\}$ as the linear operator acting on $\mathcal{A}$ such that for any $W \in \mathcal{A}$ we have

$$\{V\}W = \{V, W\}$$

where $\{.\,,.\}$ is the Poisson bracket. More formally, if $\mathcal{L}(\mathcal{A})$ is the space of linear operator of $\mathcal{A}$, the map

$$\{\ldots\} : \mathcal{A} \to \mathcal{L}(\mathcal{A}) \quad V \mapsto \{V\}$$

verifies $\forall\, V, W \in \mathcal{A}$

$$\{V\}W = -\{W\}V \tag{1.3}$$

that is to say, the *anti-symmetry* and

$$\{\{V\}W\} = \{V\}\{W\} - \{W\}\{V\} \tag{1.4}$$

the *Jacobi identity*.

The evolution over time of a function $V \in \mathcal{A}$ evaluated on the flow of the Hamiltonian $H \in \mathcal{A}$ is (see Subsec. 1.1.1)

$$\frac{dV}{dt} = \{H\}V, \tag{1.5}$$

whose solution is formally defined by [1]

$$V(t) = e^{t\{H\}}V(0), \tag{1.6}$$

where

$$e^{t\{H\}} = \sum_{k=0}^{\infty} \frac{t^k}{k!} \{H\}^k \in \mathcal{L}(\mathcal{A}). \tag{1.7}$$

Remark 1.1.3 (Convergence) *The series (1.7) is well defined locally : assuming some smoothness in the functions V and H, the ordinary differential equation (1.5) admits a unique solution (see for example [Miller and Michel, 1982]) that is given by this operator $e^{t\{H\}}$.*

Remark 1.1.4 (Composition) *The above notation $\{H\}^k$ refers to the composition of operators with $\{H\}^0$ the identity operator, i.e.*

$$\forall\, H, V \in \mathcal{A} \quad \{H\}^k V = \{H\}^{k-1}(\{H\}V) \quad and \quad \{H\}^0 V = V.$$

It is then obvious that any element $V \in \mathcal{A}$ verifying $\{H\}V = 0$, is a constant of motion under the flow of H

$$\forall\, t \in \mathbb{R} \quad e^{t\{H\}}V = V.$$

The vector space of all this constants of motion is the kernel of the operator $\{H\}$. Let us point out that $Ker\{H\}$ is not trivial (e.g. for any k such that H^k is in $\mathcal{A}$, we have $\{H\}H^k = 0$) and secondly that it is a sub-Lie-algebra of $\mathcal{A}$. Indeed, the composition, in terms of bracket, $\{V\}W$ of two elements $V, W \in Ker\{H\}$ remains in the kernel of $\{H\}$ using (1.4) :

$$\{H\}\{V\}W = \{V\}\{H\}W + \{\{H\}V\}W = 0.$$

Remark 1.1.5 (Vector field) *We consider the action of an operator $\{H\} \in \mathcal{L}(\mathcal{A})$ on a vector field $\mathbf{V} = (V_1, \ldots, V_n)$ (where $\forall i \in \underline{n}\ V_i \subset \mathcal{A}$) componentwise :*

$$\{H\}\mathbf{V} := (\{H\}V_1, \ldots, \{H\}V_n).$$

We can then express the equations of motion of $\boldsymbol{x} \in \mathbb{R}^{2n}$ and their solutions in the compact form

$$\dot{\boldsymbol{x}} = \{H\}\boldsymbol{x} \quad \Rightarrow \quad \boldsymbol{x}(t) = e^{t\{H\}}\boldsymbol{x}(0).$$

---

1. Let us note that Eq. (1.6) holds if H is time-independent ; otherwise, it is always possible to make H autonomous by adding a variable (e.g. the energy) conjugated to time.

1.1.3 Three useful lemmas

The aim of this section is to present and prove three lemmas that will be used later on. Such lemmas can be found in [Bourbaki, 1972] (Chap. 2, §6, nᵒ 4,5) or in [Vittot, 2004].

Lemma 1.1.6

$$\forall V, W \in \mathcal{A} \quad \forall n \in \mathbb{N}_0 \qquad \{\{V\}^n W\} = \sum_{k=0}^{n} \binom{n}{k} \{V\}^{n-k} \{W\} \{-V\}^k \quad (1.8)$$

Proof. By recurrence. The case $n = 1$ is Jacobi (1.4). Let us consider (1.8) true for n and prove it to hold for $n+1$ as well. We develop the left hand side :

$$
\begin{aligned}
\{\{V\}^{n+1} W\} =& \{\{V\}\{V\}^n W\} \\
\overset{1.4}{=}& \{V\}\{\{V\}^n W\} - \{\{V\}^n W\}\{V\} \\
\overset{1.8}{=}& \sum_{k=0}^{n} \binom{n}{k} \{V\}^{n-k+1} \{W\} \{-V\}^k + \sum_{k=0}^{n} \binom{n}{k} \{V\}^{n-k} \{W\} \{-V\}^{k+1} \\
=& \sum_{k=1}^{n} \binom{n}{k} \{V\}^{n+1-k} \{W\} \{-V\}^k + \{V\}^{n+1} \{W\} \\
& + \sum_{k=1}^{n} \binom{n}{k-1} \{V\}^{n+1-k} \{W\} \{-V\}^k + \{W\} \{-V\}^{n+1} \\
=& \sum_{k=1}^{n} \left[\binom{n}{k} + \binom{n}{k-1} \right] \{V\}^{n+1-k} \{W\} \{-V\}^k \\
& + \{V\}^{n+1} \{W\} + \{W\} \{-V\}^{n+1} \\
=& \sum_{k=0}^{n+1} \binom{n+1}{k} \{V\}^{n+1-k} \{W\} \{-V\}^k.
\end{aligned}
$$

$\square$

Lemma 1.1.7

$$\forall V, W \in \mathcal{A} \qquad \{e^{\{V\}} W\} = e^{\{V\}} \{W\} e^{\{-V\}} \qquad (1.9)$$

Proof. We use the previous lemma, sum both side of (1.8) and divide by $k!$ and using the linearity of $\{\ldots\}$, one has

$$
\begin{aligned}
\left\{ \sum_{k \geq 0} \frac{\{V\}^k}{k!} W \right\} &= \sum_{k \geq 0} \frac{1}{k!} \sum_{j=0}^{k} \binom{k}{j} \{V\}^{k-j} \{W\} \{-V\}^j \\
&= \sum_{p,q} \frac{\{V\}^p}{p!} \{W\} \frac{\{V\}^q}{q!} \\
&= \sum_{p} \frac{\{V\}^p}{p!} \{W\} \sum_{q} \frac{\{V\}^q}{q!}.
\end{aligned}
$$

and we conclude using (1.7).

$\square$

Lemma 1.1.8

$$\forall V, W \in \mathcal{A} \qquad \exp(e^{-\{V\}}\{W\}e^{\{V\}}) = e^{-\{V\}}e^{\{W\}}e^{\{V\}} \tag{1.10}$$

Proof. We develop the exponential

$$\exp(e^{-\{V\}}\{W\}e^{\{V\}}) = \sum_{k=0}^{\infty} \frac{1}{k!}(e^{-\{V\}}\{W\}e^{\{V\}})^k$$

and we notice that the general term, once expanded is given by

$$\frac{1}{k!} \overbrace{(e^{-\{V\}}\{W\}\underbrace{e^{\{V\}}}_{=1})(e^{-\{V\}}\{W\}e^{\{V\}})\dots(e^{-\{V\}}\{W\}\underbrace{e^{\{V\}}}_{=1})(e^{-\{V\}}\{W\}e^{\{V\}})}^{k \text{ in total}}$$

so,

$$\exp(e^{-\{V\}}\{W\}e^{\{V\}}) = e^{-\{V\}}\sum_{k=0}^{\infty}\frac{\{W\}^k}{k!}e^{\{V\}}.$$

$\square$

1.1.4   Symplecticity

In the following, the notion of *symplecticity* will be crucial, especially in the applications. Indeed in real systems this often implies energy preservation. Consider the real $2n \times 2n$ matrix

$$\mathcal{J} = \begin{pmatrix} \mathbf{0} & \mathbf{1} \\ -\mathbf{1} & \mathbf{0} \end{pmatrix}, \tag{1.11}$$

with $\mathbf{1}$ and $\mathbf{0}$ respectively the identity and the null matrix, with correct dimensions, e.g. $n \times n$ in (1.11). We notice the following properties of such matrices :

$$\mathcal{J}^{-1} = \mathcal{J}^t = -\mathcal{J} \quad \text{and} \quad \mathcal{J}^2 = -\mathbf{1}.$$

Using the compact notations

$$\boldsymbol{x} = \begin{pmatrix} \boldsymbol{q} \\ \boldsymbol{p} \end{pmatrix} \quad \text{and} \quad \nabla_{\boldsymbol{x}} = \begin{pmatrix} \partial_{\boldsymbol{q}} \\ \partial_{\boldsymbol{p}} \end{pmatrix},$$

we can rewrite Eq. (1.1) as follows

$$\dot{\boldsymbol{x}} = \mathcal{J}\nabla_{\boldsymbol{x}}H(\boldsymbol{x}, t) \tag{1.12}$$

which is nothing but another way to express the operator $\{H\}$ since (see Subsec. 1.1.1) $\dot{\boldsymbol{x}} = \{H\}\boldsymbol{x}$.

Definition 1.1.9 *A real $2n \times 2n$ matrix A is called* symplectic *if*

$$A^t \mathcal{J} A = \mathcal{J},$$

where A^t denotes the transpose matrix of A.

Definition 1.1.10 *A map*

$$T : \mathbb{R}^{2n} \to \mathbb{R}^{2n} \quad \boldsymbol{x} \mapsto T(\boldsymbol{x})$$

is a symplectic map *if its Jacobian matrix is symplectic for all $\boldsymbol{x}$.*

In the following, we shall concentrate on maps of the form

$$T : \mathbb{R}^{2n} \to \mathbb{R}^{2n} \quad \boldsymbol{x} \mapsto T(\boldsymbol{x}) := e^{\{H\}} \boldsymbol{x} \tag{1.13}$$

for some given Hamiltonian function H. We have the following

Lemma 1.1.11 *Maps of the form (1.13) are symplectic maps.*

Proof. We consider the flow of H, denoted by ϕ_t, i.e. for $t \in \mathbb{R}$, we have

$$\phi_t(\boldsymbol{q}(0), \boldsymbol{p}(0)) = (\boldsymbol{q}(t), \boldsymbol{p}(t))$$

where $\boldsymbol{q}(t)$ and $\boldsymbol{p}(t)$ are the solutions of Hamilton's equations with initial conditions $\boldsymbol{q}(0)$ and $\boldsymbol{p}(0)$. Let us also define the Jacobian matrix of the flow at time t by

$$M(\boldsymbol{x}_0, t) = \frac{\partial \phi_t}{\partial \boldsymbol{x}_0}$$

with $\boldsymbol{x}_0 = (\boldsymbol{q}(0) \ \boldsymbol{p}(0))^t$. We have,

$$\begin{aligned}
\frac{\mathrm{d}M}{\mathrm{d}t} &= \frac{\mathrm{d}}{\mathrm{d}t} \frac{\partial \phi_t}{\partial \boldsymbol{x}_0} \\
&= \frac{\partial}{\partial \boldsymbol{x}_0} \frac{\mathrm{d}\phi_t}{\mathrm{d}t} \\
&\overset{1.12}{=} \frac{\partial}{\partial \boldsymbol{x}_0} \mathcal{J} \nabla_{\boldsymbol{x}} H \\
&= \mathcal{J} \frac{\partial \nabla_{\boldsymbol{x}} H}{\partial \boldsymbol{x}} \frac{\partial \boldsymbol{x}}{\partial \boldsymbol{x}_0} \\
&= \mathcal{J} \nabla_{\boldsymbol{x}}^2 H M(\boldsymbol{x}_0, t)
\end{aligned}$$

with $\nabla_{\boldsymbol{x}}^2 H$ the symmetric Hessian matrix of H. We then easily evaluate

$$\begin{aligned}
\frac{\mathrm{d}}{\mathrm{d}t}(M^t \mathcal{J} M) &= \frac{\mathrm{d}M^t}{\mathrm{d}t} \mathcal{J} M + M^t \mathcal{J} \frac{\mathrm{d}M}{\mathrm{d}t} \\
&= M^t (\nabla_{\boldsymbol{x}}^2 H)^t \underbrace{\mathcal{J}^t \mathcal{J}}_{=1} M + M^t \underbrace{\mathcal{J} \mathcal{J}}_{=-1} \nabla_{\boldsymbol{x}}^2 H M \\
&= \boldsymbol{0}.
\end{aligned}$$

In other words, $M^t \mathcal{J} M$ is constant and $M(\boldsymbol{x}_0, 0) = \mathbf{1}$ (at $t = 0$, we stay on $\boldsymbol{x}_0$) implies

$$M(\boldsymbol{x}_0, 0)^t \mathcal{J} M(\boldsymbol{x}_0, 0) = \mathcal{J}.$$

We thus have found the value of the constant : $\mathcal{J}$. $M(\boldsymbol{x}_0, t)$ is a symplectic matrix for all $t \in \mathbb{R}$. In particular, it is true for $t = 1$ and $M(\boldsymbol{x}_0, 1)$ is the Jacobian matrix of the map (1.13).

$\square$

1.1.5   Remarks

We finish this section by giving useful remarks on notations, introducing the $\oplus$ symbol and stating the KAM theorem.

Notations

In this section we denote the next iteration of the map by primed variables :

$$\boldsymbol{x}' = T(\boldsymbol{x}),$$

whereas later, we shall also use the classical n^{th} iterate

$$\boldsymbol{x}(n+1) = T(\boldsymbol{x}(n)),$$

when the number of iterations is important or when which iteration is involved is not clear from the context.

Warped addition

Let us define as in [Chandre et al., 2005b] the warped addition, $\{A\} \oplus \{B\}$, of two operators by

$$e^{\{A\}} e^{\{B\}} := e^{\{A\} \oplus \{B\}}. \tag{1.14}$$

An explicit formula can be obtained using the Baker-Campbell-Hausdorff first in [Dynkin, 1947], later in [Bourbaki, 1972] and more recently in [Casas et al., 2012], where $\{A\} \oplus \{B\}$ is a series whose first terms are

$$\{A\} \oplus \{B\} = \{A\} + \{B\} + \frac{1}{2} (\{A\}\{B\} - \{B\}\{A\}) + \dots, \tag{1.15}$$

hence the warped addition is a deformation of the usual addition between operators.

Big-$\mathcal{O}$ and little-o notations

The big $\mathcal{O}$ notation is used to compare the size of functions around a fixed value.

Definition 1.1.12
$$f(x) \in \mathcal{O}(g(x)) \quad as \quad x \to a$$

$$\Leftrightarrow$$

$$\exists M, \delta \in \mathbb{R}^+ \quad such \ that \quad |f(x)| \leq M|g(x)| \quad for \quad |x - a| < \delta.$$

If $g(x)$ is non-zero for values of x sufficiently close to a, the definition can read

$$f(x) \in \mathcal{O}(g(x)) \quad as \quad x \to a \Leftrightarrow \limsup_{x \to a} \left| \frac{f(x)}{g(x)} \right| < +\infty.$$

This means that around the value a, $f(x)$ is *at most* the same order as $g(x)$.

The little-o notation imposes that the limit equals 0 :

$$f(x) \in o(g(x)) \quad as \quad x \to a \Leftrightarrow \limsup_{x \to a} \left| \frac{f(x)}{g(x)} \right| = 0.$$

This means that around a, $f(x)$ is smaller than $g(x)$.
It comes directly that
$$o(g(x)) \subset \mathcal{O}(g(x)).$$

Everywhere in this document, the value of a is not specified and was set to 0.

KAM theorem

We consider an integrable Hamiltonian system H, i.e. there exists a change of variables such that it depends only on the momentum vector [2] :

$$H(\boldsymbol{q}, \boldsymbol{p}) \equiv H(-, \boldsymbol{p}).$$

Such system has the following solution :

$$\begin{cases} \boldsymbol{q}(t) = \boldsymbol{\omega}(\boldsymbol{p}_0)t + \boldsymbol{q}_0 \\ \boldsymbol{p}(t) = \boldsymbol{p}_0 \end{cases}$$

where $\boldsymbol{q}_0$ and $\boldsymbol{p}_0$ are the initial conditions and $\boldsymbol{\omega} = \frac{\partial H}{\partial \boldsymbol{p}}$. The motion relies on a n dimensional torus with frequency vector $\boldsymbol{\omega}$. The following theorem gives indications on the dynamics when the Hamiltonian system is perturbed.

---

2. We keep the same notations by convenience : H depends only on a new momentum vector $\tilde{\boldsymbol{p}}$ denoted by $\boldsymbol{p}$ directly in the text.

Theorem KAM, developed with the work of Kolmogorov [Kolmogorov, 1954], Moser [Moser, 1962] and Arnold [Arnold, 1963], is fundamental in the study of integrable and quasi-integrable system giving results on their stability (see also [Fasano and Marmi, 2006] for an educational introduction to the subject).

Theorem 1.1.13 *Let us consider a quasi-integrable Hamiltonian system*

$$H(\boldsymbol{p}) + \epsilon V(\boldsymbol{q}, \boldsymbol{p}) \tag{1.16}$$

where $\boldsymbol{q}$ and $\boldsymbol{p}$ are the angle-action vectors : $\boldsymbol{q} \in [0, 2\pi[^n$ and $\boldsymbol{p} \in \mathbb{R}^n$,
If $\boldsymbol{p}_0$ is a point of the action space such that
   – $\boldsymbol{\omega}_0 = \frac{\partial H(\boldsymbol{p}_0)}{\partial \boldsymbol{p}}$ verifies a Diophantine condition [3] ;
   – H is not locally degenerated at $\boldsymbol{p}_0$, i.e.

$$\det \left(\frac{\partial^2 H}{\partial \boldsymbol{p} \partial \boldsymbol{q}} \right) \bigg|_{\boldsymbol{p}=\boldsymbol{p}_0} \neq 0$$

Then, if the perturbation is small enough ($\exists \bar{\epsilon}(\boldsymbol{\omega}_0) > 0$ such that $\epsilon < \bar{\epsilon}(\boldsymbol{\omega}_0)$), the system (1.16) preserves the invariant torus with frequency $\boldsymbol{\omega}_0$ that is a perturbation of the one for H.

In concrete, starting from the Hamiltonian system H, i.e. $\epsilon = 0$, and gradually increasing the perturbation, we observe the deformation and then the destruction of invariant tori (KAM tori).

1.2   Hamiltonian Control

We shall follow the ideas and notations of [Vittot, 2004] where the theory for this control was initially introduced. This theory has been widely applied to several examples from toy models to fusion plasma   [Ciraolo et al., 2004b,   Ciraolo et al., 2004a,   Vittot et al., 2005, Chandre et al., 2005a,   Chandre et al., 2006,   Benzekri et al., 2006, Huang et al., 2006, Macor et al., 2007].

We consider a Hamiltonian system composed of an integrable part H and a (small) perturbation V, namely

$$H + V \, .$$

The goal of this section is to construct a new Hamiltonian system, by slightly perturbing the considered one, so that the new system exhibits better properties such as "more" invariant KAM tori.

A first hypothesis is done in order to build a control term.

---

3. $\boldsymbol{\omega} \in \mathbb{R}^n$ verifies a Diophantine condition if $\exists \gamma > 0$, $\delta > n - 1$ such that $\forall \boldsymbol{k} \in \mathbb{Z}^n \backslash \boldsymbol{0}$, $|\boldsymbol{\omega} \cdot \boldsymbol{k}| \geq \gamma \left(\sum |k_i| \right)^{-\delta}$.

Hypothesis 1.2.1 *We assume the existence of an operator* $\Gamma : \mathcal{A} \to \mathcal{A}$ *that verifies*

$$\{H\}^2\Gamma = \{H\} \tag{1.17}$$

We call this operator *a pseudo-inverse* of $\{H\}$ because the kernel of $\{H\}$ is not reduced to the operator 0.

Having the two operators $\{H\}$ and Γ, we define the *non-resonant* operator $\mathcal{N}$ and the *resonant* operator $\mathcal{R}$ as follow

$$\mathcal{N} = \{H\}\Gamma, \tag{1.18}$$
$$\mathcal{R} = 1 - \mathcal{N}, \tag{1.19}$$

with 1 the identity operator in the algebra $\mathcal{A}$.
Let us notice that the hypothesis 1.2.1 is equivalent to

$$\{H\}\mathcal{R} = 0 \tag{1.20}$$

and thus the range of $\mathcal{R}$ is included in the kernel of $\{H\}$.

Remark 1.2.2 *The operator Γ is not unique : for instance any addition of constant will preserve hypothesis 1.2.1. In fact, any operator of the form*

$$\Gamma' = \Gamma + \mathcal{R}\{B\} \qquad \forall \{B\} \in \mathcal{L}(\mathcal{A})$$

concurs with the hypothesis :

$$\{H\}^2\Gamma' = \{H\}^2\Gamma + \{H\}^2\mathcal{R}\{B\} = \{H\}^2\Gamma = \{H\}$$

because $\{H\}\mathcal{R} = 0$.
This may allow a broader choice of the control according to the problem and the goal to reach.

Remark 1.2.3 *If $\{H\}$ and Γ commute, i.e. $\{H\}\Gamma = \Gamma\{H\}$ (this slightly strengthens hypothesis 1.2.1), then $\mathcal{N}$ and $\mathcal{R}$ are projectors (i.e. $\mathcal{N}^2 = \mathcal{N}$ and $\mathcal{R}^2 = \mathcal{R}$) and $Ker\{H\} = Rg\mathcal{R}$ that is to say, we have a description of the set of constants of the motion. This is the case in the following example.*

The operators in action : a basic example

We shall now give an example on how these operators may act on a simple case. We consider a Hamiltonian system H in action-angle variables $(\boldsymbol{\theta}, \boldsymbol{A}) \in \mathbb{T}^n \times \mathbb{R}^n$ (n being the number of degrees of freedom) :

$$H = \boldsymbol{\omega} \cdot \mathbf{A}$$

with $\boldsymbol{\omega} \in \mathbb{R}^n$ the vector of frequencies

$$\boldsymbol{\omega} = \frac{\partial H}{\partial \mathbf{A}}$$

that we assume to be *non-resonant* and constant.

Definition 1.2.4 *A vector* $\boldsymbol{\omega} \in \mathbb{Z}^n$ *is* resonant *if there exists* $\mathbf{k} \in \mathbb{Z}^n \backslash \{\mathbf{0}\}$ *such that* $\boldsymbol{\omega} \cdot \mathbf{k} = 0$.

Definition 1.2.5 *A vector* $\boldsymbol{\omega} \in \mathbb{Z}^n$ *is* non-resonant *if and only if for* $\mathbf{k} \in \mathbb{Z}^n$ $\quad \boldsymbol{\omega} \cdot \mathbf{k} = 0 \Rightarrow \mathbf{k} = \mathbf{0}$.

We also consider a generic autonomous element V of $\mathcal{A}$ written in its Fourier expansion

$$V = \sum_{\mathbf{k} \in \mathbb{Z}^n} V_{\mathbf{k}} e^{i\,\boldsymbol{\theta} \cdot \mathbf{k}} \tag{1.21}$$

where the elements $V_{\mathbf{k}}$ depend only of the actions : $V_{\mathbf{k}} = V_{\mathbf{k}}(\mathbf{A})$.

The operator $\{H\}$ is nothing but the Poisson brackets :

$$
\begin{aligned}
\{H\}V &= \{H, V\} \\
&= \frac{\partial H}{\partial \boldsymbol{\theta}} \frac{\partial V}{\partial \mathbf{A}} - \frac{\partial V}{\partial \boldsymbol{\theta}} \frac{\partial H}{\partial \mathbf{A}} \\
&= \boldsymbol{\omega} \cdot \frac{\partial V}{\partial \boldsymbol{\theta}} \\
&= \boldsymbol{\omega} \cdot \sum_{\mathbf{k} \in \mathbb{Z}^n} i\,\mathbf{k} V_{\mathbf{k}} e^{i\,\boldsymbol{\theta} \cdot \mathbf{k}}
\end{aligned} \tag{1.22}
$$

The operator $\boldsymbol{\Gamma}$ is not unique [see remark 1.2.2], a possible choice is the following one

$$\Gamma V = \sum_{\substack{\mathbf{k} \in \mathbb{Z}^n \\ \boldsymbol{\omega} \cdot \mathbf{k} \neq 0}} \frac{V_{\mathbf{k}}}{i\,\boldsymbol{\omega} \cdot \mathbf{k}} e^{i\,\boldsymbol{\theta} \cdot \mathbf{k}}$$

and Eq. (1.17) is fulfilled noticing that

$$\{H\}V = \boldsymbol{\omega} \cdot \sum_{\mathbf{k} \in \mathbb{Z}^n} i\,\mathbf{k} V_{\mathbf{k}} e^{i\,\boldsymbol{\theta} \cdot \mathbf{k}} = \boldsymbol{\omega} \cdot \sum_{\substack{\mathbf{k} \in \mathbb{Z}^n \\ \boldsymbol{\omega} \cdot \mathbf{k} \neq 0}} i\,\mathbf{k} V_{\mathbf{k}} e^{i\,\boldsymbol{\theta} \cdot \mathbf{k}}$$

The operator $\mathcal{N}$ is constructed assuming the non-resonant condition (1.2.5) where the condition $\boldsymbol{\omega} \cdot \mathbf{k} \neq \mathbf{0}$ reads then $\mathbf{k} \neq \mathbf{0}$. We have

$$\mathcal{N}V = \sum_{\substack{\mathbf{k} \in \mathbb{Z}^n \\ \mathbf{k} \neq \mathbf{0}}} V_{\mathbf{k}} e^{i\,\boldsymbol{\theta} \cdot \mathbf{k}}$$

or, equivalently

$$\mathcal{N}V = V - V_{\mathbf{0}}.$$

The operator $\mathcal{R}$ is finally

$$\mathcal{R}V = V_{\mathbf{0}}.$$

1.2.1 Control theorem for Hamiltonian systems

We now present the main theorem of this section and its proof following [Vittot, 2004]. We consider a Hamiltonian system composed of an integrable part H and a perturbation V, both element of $\mathcal{A}$. The idea is, if allowed, to add a *control term* such that the flow of the resulting system is in relation with the one of the unperturbed one. More formally, the aim is to design a *conjugation* between the flow of H and the flow of $H + V + f(V)$ where the term $f(V)$ is the control term (we reject the obvious control $f(V) = -V$ by requiring the control to be a perturbation of $H + V$). This is achieved with

Theorem 1.2.6 *Considering the above framework and under hypothesis 1.2.1, we have the following conjugation*

$$\forall t \in \mathbb{R} \qquad e^{t\{H+V+f(V)\}} = e^{-\{\Gamma V\}}e^{t\{H\}}e^{t\{\mathcal{R}V\}}e^{\{\Gamma V\}}$$

with the functions F and $f : \mathcal{A} \to \mathcal{A}$ defined by

$$F(V) :=e^{-\{\Gamma V\}}\mathcal{R}V + \frac{1 - e^{-\{\Gamma V\}}}{\{\Gamma V\}}\mathcal{N}V \qquad (1.23)$$

$$f(V) :=F(V) - V.$$

The second term in (1.23) must be understood as follows :

$$\frac{1 - e^{-\{\Gamma V\}}}{\{\Gamma V\}} = \sum_{k \geq 0}\frac{\{-\Gamma V\}^k}{(k+1)!}.$$

Indeed, using (1.7),

$$\frac{1 - e^{-\{\Gamma V\}}}{\{\Gamma V\}} = \frac{1 - \left(1 + \sum_{k \geq 1}\{-\Gamma V\}^k/k!\right)}{\{\Gamma V\}} = \sum_{k \geq 1}\frac{\{-\Gamma V\}^{k-1}}{k!}.$$

Remark 1.2.7 (One the size of the control) *At first order, using the above development, we have*

$$F(V) = \mathcal{R}V + \mathcal{N}V + \mathcal{O}(V^2) = V + \mathcal{O}(V^2),$$

thus

$$f(V) = V - V + \mathcal{O}(V^2) = \mathcal{O}(V^2).$$

The control is small *in front of the perturbation V (likewise supposed small in front of the integrable part H) which is meaningful with respect to the goals of the control :* slightly *modifying a system, not building a different one. A detailed proof of the smallness of $f(V)$ is given in [Vittot, 2004] p. 6347.*

For practical reasons, we give $f(V)$ in the form of a series :

$$f(V) = \sum_{k \geq 1} \frac{\{-\Gamma V\}^k}{(k+1)!} (k\mathcal{R}V + V). \tag{1.24}$$

Indeed,

$$
\begin{aligned}
f(V) &= F(V) - V \\
&= \sum_{k \geq 0} \frac{\{-\Gamma V\}^k}{k!} \mathcal{R}V + \sum_{k \geq 0} \frac{\{-\Gamma V\}^k}{(k+1)!} \mathcal{N}V - V \\
&= \sum_{k \geq 1} \frac{\{-\Gamma V\}^k}{(k+1)!} (k+1)\mathcal{R}V + \sum_{k \geq 1} \frac{\{-\Gamma V\}^k}{(k+1)!} \mathcal{N}V + \underbrace{\mathcal{R}V + \mathcal{N}V}_{=0} - V \\
&= \sum_{k \geq 1} \frac{\{-\Gamma V\}^k}{(k+1)!} (k\mathcal{R}V + V).
\end{aligned}
$$

It is interesting to raise up that in the case $\mathcal{R}V = 0$, the controlled Hamiltonian system $H + V + f(V)$ is canonically conjugate to H and f takes the form

$$f = \sum_{k=2}^{\infty} f_k, \qquad f_k = -\frac{1}{k}\{\Gamma V\}f_{k-1} \qquad \text{with} \qquad f_1 = V. \tag{1.25}$$

Note that f_k is $\mathcal{O}(V^k)$.

In order to prove the theorem we need to keep in mind lemmas from Subsec. 1.1.3 and the following one.

Lemma 1.2.8

$$\forall V \in \mathcal{A} \qquad H + F(V) = e^{-\{\Gamma V\}}(H + \mathcal{R}V). \tag{1.26}$$

Proof. By the definition (1.18) and the anti-symmetry of the bracket (1.3)

$$
\begin{aligned}
F(V) - e^{-\{\Gamma V\}}\mathcal{R}V &= \frac{1 - e^{-\{\Gamma V\}}}{\{\Gamma V\}}\{H\}\Gamma V \\
&= \frac{1 - e^{-\{\Gamma V\}}}{\{\Gamma V\}}(-\{\Gamma V\}H) \\
&= e^{-\{\Gamma V\}}H - H.
\end{aligned}
$$

$\square$

Proof of Theorem 1.2.6. Both sides of (1.26) are elements of $\mathcal{A}$, we can construct their induced operator and we have

$$
\begin{aligned}
\{H + F(V)\} &= \{e^{-\{\Gamma V\}}(H + \mathcal{R}V)\} \\
&\overset{1.9}{=} e^{-\{\Gamma V\}}\{H + \mathcal{R}V\}e^{\{\Gamma V\}}.
\end{aligned}
$$

The flow of both sides are identical and read $\forall t \in \mathbb{R}$

$$\exp(t\{H + F(V)\}) = \exp(e^{-\{\Gamma V\}}t\{H + \mathcal{R}V\}e^{\{\Gamma V\}})$$
$$\overset{1.10}{=} e^{-\{\Gamma V\}}e^{t\{H+\mathcal{R}V\}}e^{\{\Gamma V\}}$$

Finally, taking into account hypothesis 1.2.1 expressed with the operator $\mathcal{R}$ (1.20) and using Jacobi (1.4), it follows

$$\{H\}\{\mathcal{R}V\} - \{\mathcal{R}V\}\{H\} = \{\{H\}\mathcal{R}V\} = 0.$$

That means that $\{H\}$ and $\{\mathcal{R}V\}$ commute in $\mathcal{L}(\mathcal{A})$ and thus

$$e^{t\{H+\mathcal{R}V\}} = e^{t\{H\}}e^{t\{\mathcal{R}V\}}.$$

This concludes the proof.

$\square$

The flow of the new Hamiltonian system $H + V + f(V)$ is conjugated to the one of $H + \mathcal{R}V$. This ensures that they share the same dynamics. Because a part of the perturbation was removed ($V = \mathcal{R}V + \mathcal{N}V \to \mathcal{R}V$), we expect a new dynamics more regular, less *chaotic*[4]. A complete example is treated in Subsec. 1.2.3.

1.2.2 Higher order control

It is possible to construct higher order term, that is to say, a control whose size is $\mathcal{O}(V^k)$ with $k > 2$. This can be accomplished in different ways (especially considering the non-uniqueness of the operator Γ). We give here an example assuming a non-resonant condition, i.e. $\mathcal{R}V = 0$.

The controlled Hamiltonian system where we emphasize the size of the perturbation and the control by explicitly factorizing V and f with ϵ and ϵ^2 respectively reads

$$H_c = H + \epsilon V + \epsilon^2 f.$$

This Hamiltonian system is integrable. So the initial Hamiltonian system $H + \epsilon V$ can be rewritten as

$$H + \epsilon V + \epsilon^2 f - \epsilon^2 f = \tilde{H} + \tilde{V}$$

with the replacements $\tilde{H} = H_c$, $\tilde{V} = -\epsilon^2 f$. We also consider

$$\tilde{\Gamma} = e^{-\epsilon\{\Gamma V\}}\Gamma e^{\epsilon\{\Gamma V\}}$$

verifying hypothesis 1.2.1 since (1.26) holds. We thus fulfill the conditions to apply theorem 1.2.6 and have the existence of a control term $\epsilon^4 g$ which satisfies

$$H + \epsilon V + \epsilon^4 g = e^{-\epsilon^2\{\tilde{\Gamma}f\}}\left(H_c - \epsilon^2\tilde{\mathcal{R}}f\right).$$

with $\tilde{\mathcal{R}}$ the resonant operator defined as $\tilde{\mathcal{R}} = 1 - \{H_c\}\tilde{\Gamma}$.

We could iterate this procedure to reach other orders.

---

4. More attention to this notion will be given in Chap. 3.

1.2.3   Controlling the forced pendulum model

We consider the following Hamiltonian system [Ciraolo et al., 2004b] with 1.5 degree of freedom

$$H(x, p; t) = \frac{1}{2}p^2 + \epsilon \left(\cos x + \cos(x - t) \right) \tag{1.27}$$

which models a forced pendulum. A plot of the phase space of (1.27) is given in Figure 1.1 for different values of the parameter ϵ. We can see that many KAM tori (see Subsec. 1.1.5) are preserved for small values of ϵ (such as 0.008 or 0.017) while chaotic orbits arise with the increase of the parameter ($\epsilon = 0.034$ or 0.065). In fact, it was shown in [Chandre and Jauslin, 2002] that all KAM tori

FIGURE 1.1: Poincaré sections of the Hamiltonian system (1.27) for $\epsilon = 0.008$, $\epsilon = 0.017$, $\epsilon = 0.034$ and $\epsilon = 0.065$ respectively from up to down and left to right.

vanish when $\epsilon \geq 0.02759$. We now make this Hamiltonian system autonomous

in order to apply the theory previously developed. For this purpose we consider the time t as another angle (let us denote it by τ) whose conjugated action is E. Hamiltonian (1.27) becomes

$$H(x, \tau, p, E) = \frac{1}{2}p^2 + E + \epsilon \left(\cos x + \cos(x - \tau) \right) \tag{1.28}$$

where the angles are $\boldsymbol{\theta} = (x, \tau)$ and the actions are $\boldsymbol{A} = (p, E)$. The integrable part is

$$H(-, -, p, E) = \frac{1}{2}p^2 + E \tag{1.29}$$

whose equations of motion are

$$\begin{cases} \dot{x} = \dfrac{\partial H}{\partial p} = p \\[2mm] \dot{\tau} = \dfrac{\partial H}{\partial E} = 1 \\[2mm] \dot{p} = -\dfrac{\partial H}{\partial x} = 0 \\[2mm] \dot{E} = -\dfrac{\partial H}{\partial \tau} = 0 \end{cases}$$

and the solutions follow straightforwardly

$$\begin{cases} x(t) = x_0 + p_0 t \\ \tau = t \\ p(t) = p_0 \\ E = E_0. \end{cases} \tag{1.30}$$

So for $\epsilon = 0$, we have a complete knowledge of the system and the solutions are tori. The perturbation is (we go back in the t variable, Eq. (1.30) shows this equivalence)

$$V(x, t, p, E) = \epsilon \left(\cos x + \cos(x - t) \right),$$

that we need to express in its Fourier form to apply the operators as in Subsec. 1.2. Using the well-known relation

$$\cos \phi = \frac{e^{i\phi} + e^{-i\phi}}{2}$$

we write

$$V(x, t, p, E) = \frac{\epsilon}{2} \left(e^{ix} + e^{-ix} + e^{i(x-t)} + e^{-i(x-t)} \right)$$

and we have the right form (1.21) with $n = 2$, $\boldsymbol{k} = (k_1, k_2)$ and

$$V_{k_1, k_2} = \begin{cases} \epsilon/2 & \text{if } (k_1, k_2) \in \{(1, 0), (-1, 0), (1, -1), (-1, 1)\} \\ 0 & \text{otherwise} \end{cases}$$

allowing us to calculate the four operators with the perturbation

$$V = \sum_{k_1,k_2 \in \mathbb{Z}} V_{k_1,k_2} e^{i(k_1 x + k_2 t)}.$$

The vector of frequencies is $\boldsymbol{\omega} = (p, 1)$ and then the operators act on any functions $U \in \mathcal{A}$ of the form

$$U(x, t, p, E) = \sum_{k_1,k_2 \in \mathbb{Z}} U_{k_1,k_2}(p, E) e^{i(k_1 x + k_2 t)}$$

as

$$\{H\}U = \sum_{k_1,k_2 \in \mathbb{Z}} i(pk_1 + k_2) U_{k_1,k_2}(p, E) e^{i(k_1 x + k_2 t)} \qquad (1.31)$$

$$\Gamma U = \sum_{\substack{k_1,k_2 \in \mathbb{Z} \\ pk_1 + k_2 \neq 0}} \frac{U_{k_1,k_2}(p, E)}{i(pk_1 + k_2)} e^{i(k_1 x + k_2 t)}$$

$$\mathcal{N}U = \sum_{\substack{k_1,k_2 \in \mathbb{Z} \\ pk_1 + k_2 \neq 0}} U_{k_1,k_2}(p, E) e^{i(k_1 x + k_2 t)}$$

$$\mathcal{R}U = \sum_{\substack{k_1,k_2 \in \mathbb{Z} \\ pk_1 + k_2 = 0}} U_{k_1,k_2}(p, E) e^{i(k_1 x + k_2 t)}. \qquad (1.32)$$

We apply them to the perturbation V and we find

$$\{H\}V = -\epsilon \left(p \sin x + (p - 1) \sin(x - t)\right)$$

$$\Gamma V = \epsilon \left(\frac{1}{p} \sin x + \frac{1}{p - 1} \sin(x - t)\right) \qquad p \neq 0, 1 \qquad (1.33)$$

$$\mathcal{N}V = \epsilon \left(\cos x + \cos(x - t)\right) = V$$

$$\mathcal{R}V = 0.$$

Since $\mathcal{R}V = 0$, we can use the simplifications and notations of (1.25) and compute the series of f by recursion. The first term is

$$f_2 = -\frac{1}{2} \{\Gamma V\} V = \frac{1}{2} \frac{\partial(\Gamma V)}{\partial p} \frac{\partial V}{\partial x},$$

since V does not depend of p. We can calculate it explicitly :

$$f_2 = -\frac{\epsilon^2}{2} \left(\sin x + \sin(x - t)\right) \left(\frac{\sin x}{p^2} + \frac{\sin(x - t)}{(p - 1)^2}\right) \quad p \neq 0, 1.$$

The other terms of the series can be found in the same way. But because there is an infinite number of them we cannot compute f exactly.
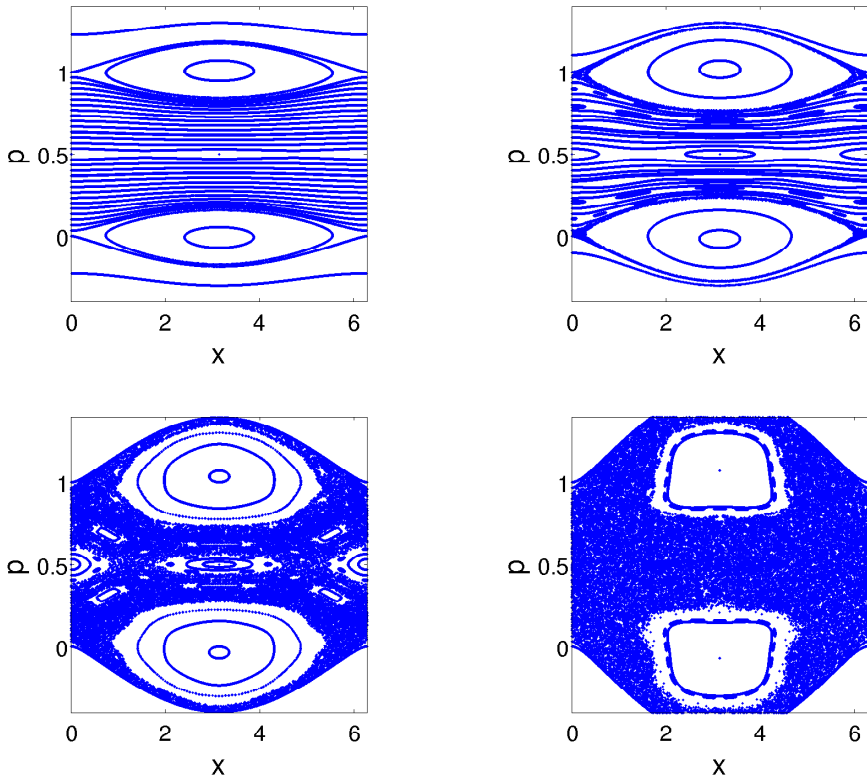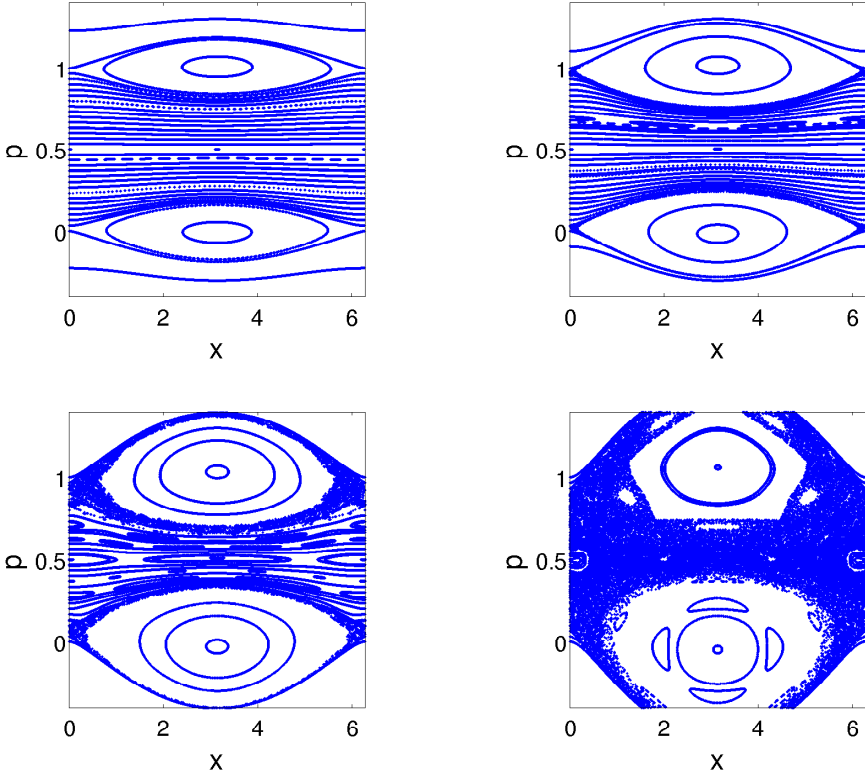
FIGURE 1.2: Poincaré sections of the controlled Hamiltonian system (1.35) for $\epsilon = 0.008$, $\epsilon = 0.017$, $\epsilon = 0.034$ and $\epsilon = 0.065$ respectively from up to down and left to right.

We now present two ways to pull through of this issue.

A possible simplification is to restrict the sum at its first term previously calculated : f_2. Roughly speaking this term is bigger in front of the other because $f_k = \mathcal{O}(V^k)$ and approximating the size of V by ϵ small, $|\epsilon| << 1$, it comes that f_2 is the leading term (see Chap. 4, Sec. 4.1 for a more detailed discussion of that kind of truncation of the control).

In order to present numerical results, it is convenient to use adapted integrators, symplectic ones.

Remark 1.2.9 (Symplectic integrator) *As seen before the formal solution*

of Hamilton equations is

$$\boldsymbol{x}(t) = e^{t\{H\}}\boldsymbol{x}(0).$$

where $\boldsymbol{x} = (\mathbf{q}, \mathbf{p})$.

The goal of a symplectic scheme is to preserve some properties of the Hamiltonian systems such as the conservation of H and the symplecticity of the flow (see Sec. 1.1.4) that most of the generic numerical methods fail to do.

In [Hairer et al., 2006] various methods are exposed. In the following, we limited ourselves to present the scheme based on the Campbell-Baker-Hausdorff (CBH) theorem (see [Nadolski and Laskar, 2002] for example) : if H can be decomposed as

$$H = A + \epsilon B \tag{1.34}$$

then, its solution is (see the warped addition, Eq. (1.15))

$$e^{t\{H\}} = e^{t\{A\}}e^{t\{\epsilon B\}} + \mathcal{O}(t\epsilon).$$

This formula is especially convenient when the flows of A and B, that are $e^{t\{A\}}$ and $e^{t\{B\}}$ respectively are known. Then the integrator with time step τ reads

$$\boldsymbol{x}_{k+1} = e^{\tau\{A\}}e^{\tau\{\epsilon B\}}\boldsymbol{x}_k.$$

The algorithm is : knowing $\boldsymbol{x}_k$, compute

$$\tilde{\boldsymbol{x}}_k = e^{\tau\{\epsilon B\}}\boldsymbol{x}_k$$

$$\boldsymbol{x}_{k+1} = e^{\tau\{A\}}\tilde{\boldsymbol{x}}_k$$

The obvious cases where we have the knowledge of the solution of a Hamiltonian system is when it only depends on the momentum vector or only on the coordinate vector.

Using the (CBH) and more generally the development of Eq. (1.15), efficient integrators of higher order have been derived, for example, the very spread [Yoshida, 1990] and [Laskar and Robutel, 2001].

For that purpose, we shall fix the value of p in the control f_2 at p^*. The Hamiltonian system $V + f_2$ is now independent of the actions, we can compute explicitly $e^{t\{V+f_2\}}$ and use symplectic schemes to integrate the controlled Hamiltonian

$$H + V + f_2|_{p=p^*}. \tag{1.35}$$

The first resonances lie around $p = 0$ and $p = 1$ as it is visible with the operator ΓV, Eq.(1.36), or in the control term. For that reason, we choose $p^* = 1/2$ between the two resonances.

We present in Figure 1.2 the equivalent plots of Figure 1.1 but with the addition of the control $f_2|_{p=p^*}$.

The Poincaré sections exhibit much more regularity and we can observe the reconstruction of KAM tori in the $\epsilon = 0.034$ case while none remains in the non-controlled Hamiltonian system for the same value of ϵ. A zoom around
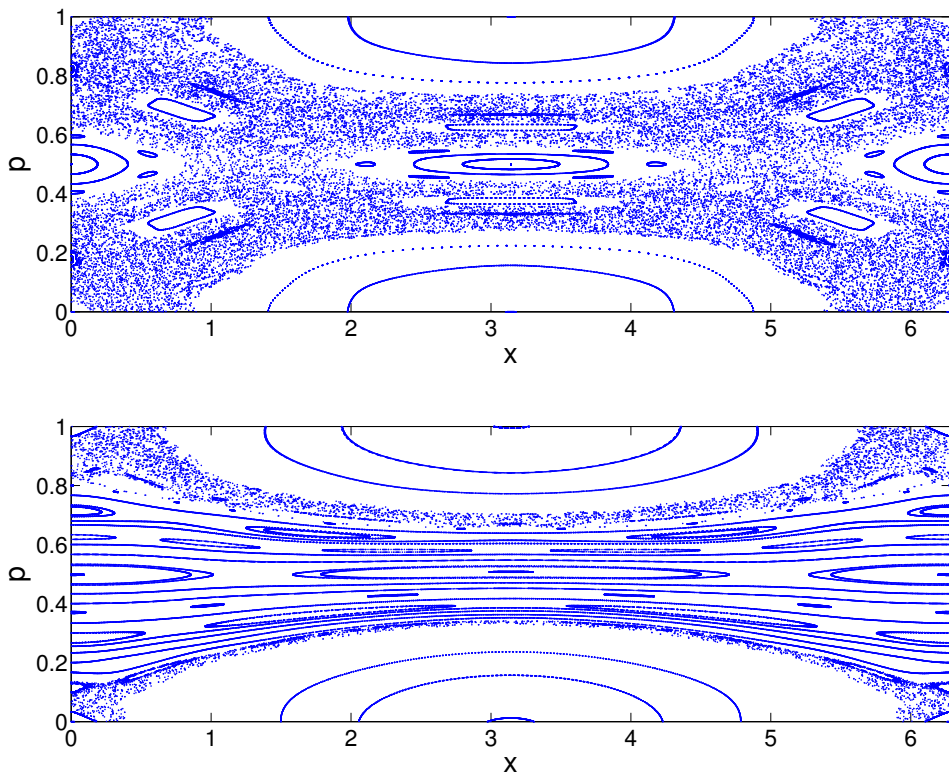
FIGURE 1.3: Comparison of Poincaré sections of the perturbed Hamiltonian system (1.27) and the controlled one (1.35) for $\epsilon = 0.034$ and $p^* = 1/2$.

$p = 1/2$ is given Figure 1.3 for $\epsilon = 0.034$ in the uncontrolled case (above) and in the controlled one (down). We clearly see the improvement and the re-apparition of tori.

Another way to struggle the issues inherent in computing a series is to make a shift of ω in the variable p such that the considered integrable part is linear in the action :

$$H = E + \omega p$$

and the perturbation becomes

$$V = \epsilon \left(\cos x + \cos(x - t) \right) + \frac{p^2}{2}.$$

Operators defined by Equations (1.31)-(1.32) are still valid and we find

$$\{H\}V = -\epsilon\left(\omega\sin x + (\omega-1)\sin(x-t)\right)$$

$$\Gamma V = \epsilon\left(\frac{1}{\omega}\sin x + \frac{1}{\omega-1}\sin(x-t)\right) \qquad (1.36)$$

$$\mathcal{N}V = \epsilon\left(\cos x + \cos(x-t)\right)$$

$$\mathcal{R}V = \frac{p^2}{2}.$$

with $\omega \neq 0, 1$ (chosen irrational) and after some calculations

$$f = \epsilon p\left(\frac{\cos x}{\omega} + \frac{\cos(x-t)}{\omega-1}\right) + \epsilon^2\left(\frac{\cos x}{\omega} + \frac{\cos(x-t)}{\omega-1}\right)^2.$$
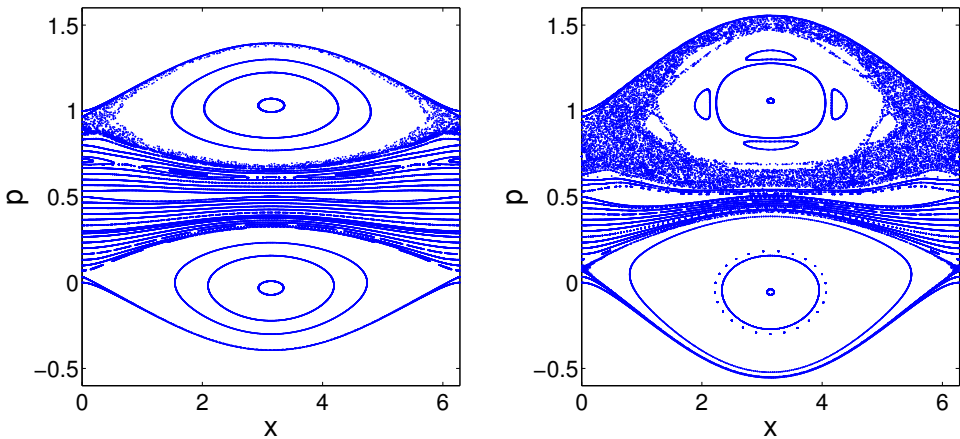
FIGURE 1.4: Poincaré sections of the controlled Hamiltonian system (1.37) for $\epsilon = 0.034$ (left) and $\epsilon = 0.065$ (right) and $\omega = (3 + \sqrt{5})/2$.

We immediately see the advantage of this method : we have been able to compute exactly the control term [5]. On the other hand, this control is of order ϵ, the same as the perturbation. We use the same "trick" as we did before to have a Hamiltonian system that is computable by symplectic integrators : we put $p = 0$ in the control term. Doing this manipulation, the control is of order ϵ^2 and the full Hamiltonian system, back in the original momenta, reads

$$\frac{1}{2}p^2 + \epsilon\left(\cos x + \cos(x-t)\right) + \epsilon^2\left(\frac{\cos x}{\omega} + \frac{\cos(x-t)}{\omega-1}\right)^2. \qquad (1.37)$$

---

5. The terms of the series (1.24) vanish for $k \geq 3$: V and $\mathcal{R}V$ are quadratic in p while ΓV does not depend on p such that after two iterations $\{\Gamma V\}(k\mathcal{R}V + V) = 0$.

The value of ω is chosen irrational to avoid resonance problems. In the example, it is fixed to $\frac{3+\sqrt{5}}{2}$.

The Poincaré sections of this Hamiltonian system are presented Figure 1.4. The chaos has considerably been reduced and a significant number of KAM tori were reconstructed.

Even if phase spaces presented in Figure 1.4 present a more regular shape by comparison with those of Figure 1.2, it does not mean that the last method we used is the best one : we did several approximations and truncations so that the control is not the one planned by the theorem. The control term should be chosen according to the studied problem and the inherent constraints.

We can summarize this section by concluding that we have built different robust [6] control terms responding to several criteria and showing very good properties.

1.3   Control theory : discrete time

In the following we shall be interested in controlling a quasi-integrable symplectic map in such a way that it will allow us to obtain a new, *controlled*, map "closer" to the integrable part of the original map. The controlled map is expected to have a smaller number of escaping orbits and a larger region occupied by invariant curves in a neighborhood of the origin. For this purpose, we apply the method presented in [Chandre et al., 2005b], with the modification that in the present case the integrable part is not expressed in action-angle variables.

The developments to come are similar to those of the previous section in the philosophy being our goal the construction of a conjugation between the controlled map and a suitable part of the original map. As we shall present it, the difference states in the meaning of "*addition* of a control term". In the continuous time, we added a term to the initial Hamiltonian system ("classical "addition of C^∞ functions), while in control of maps, we shall consider a warped addition $\oplus$ (see remark 1.1.5).

1.3.1   Controlling maps : a theorem

We now state which maps we shall be interested in : *integrable* maps and their *perturbation*. Then we propose the construction of *controlled* maps.

---

6. We shall come back to robustness when we analyze the discrete in time controls, next section.

Let us consider an integrable symplectic map defined through its generator H

$$\mathbf{x}' = e^{\{H\}}\mathbf{x}\,, \tag{1.38}$$

and consider the quasi-integrable perturbation of the former

$$\mathbf{x}' = T(\mathbf{x}) = e^{\{H\}}e^{\{V\}}\mathbf{x}\,, \tag{1.39}$$

where $\mathbf{x} \in \mathbb{R}^{2n}$ and V is a perturbation, namely $V = o(H)$.

Remark 1.3.1 *The term* quasi-integrable *is taken from Hamiltonian systems. In fact, most of the time, we shall know the time-1 flow of V, namely $e^{\{V\}}$ because the model we are interested in can be decomposed in basic maps. But we shall (unlikely) rarely know the generator M such that $e^{\{M\}} = e^{\{H\}}e^{\{V\}}$ as it is explained remark 1.1.5.*

Remark 1.3.2 *It is obvious that the composition of two symplectic maps remains symplectic and thus the map T, defined in (1.39), is symplectic.*

The aim is to construct a third map, the *control map*, whose generator F is small in front of the initial system (e.g. it satisfies $F = o(V)$). We desire the *controlled map*

$$T_{\text{ctrl}} = e^{\{H\}}e^{\{V\}}e^{\{F\}}\,, \tag{1.40}$$

to be conjugated to a map T_*, closer to $e^{\{H\}}$ than T (see (1.44) below).

Let us now focus on the following unperturbed map

$$1 - e^{-\{H\}}\,, \tag{1.41}$$

and observe that $1-e^{-\{H\}}$ is not invertible, e.g. its kernel contains any smooth function of H. Indeed, consider any $f \in C^\infty(\mathbb{R})$ and notice that $\{H\}f(H) = 0$:

$$\{H\}f(H) = \frac{\partial H}{\partial p}\frac{\partial f(H)}{\partial q} - \frac{\partial H}{\partial q}\frac{\partial f(H)}{\partial p} = \frac{\partial H}{\partial p}\frac{\partial H}{\partial q}f'(H) - \frac{\partial H}{\partial q}\frac{\partial H}{\partial p}f'(H) = 0$$

then $\left(1 - e^{-\{H\}}\right)f(H) = 0$ using the definition of $e^{-\{H\}}$.

To outmatch this difficulty we make the assumption of the existence of a "pseudo-inverse" of this operator.

Hypothesis 1.3.3 *We assume the existence of an operator $\mathcal{G} : \mathcal{A} \to \mathcal{A}$ that satisfies*

$$\mathcal{G}\left(1 - e^{-\{H\}}\right)\mathcal{G} = \mathcal{G}\,. \tag{1.42}$$

Given this operator, we define the *non-resonant* and the *resonant* operators by

$$\mathcal{N} := \left(1 - e^{-\{H\}}\right)\mathcal{G} \quad \text{and} \quad \mathcal{R} := 1 - \mathcal{N}\,, \tag{1.43}$$

which are projectors, i.e. $\mathcal{N}^2 = \mathcal{N}$ and $\mathcal{R}^2 = \mathcal{R}$.

The main theoretical result of this section is then stated in the following

Theorem 1.3.4 *Under the above hypotheses we have*

$$e^{\{\mathcal{G}V\}}T_{ctrl}e^{-\{\mathcal{G}V\}} = e^{\{H\}}e^{\{\mathcal{R}V\}} := T_*\,, \tag{1.44}$$

where

$$T_{ctrl} = e^{\{H\}}e^{\{V\}}e^{\{F\}}\,,$$

with a control term given by

$$e^{\{F\}} = e^{-\{V\}}e^{\{(\mathcal{N}-\mathcal{G})V\}}e^{\{\mathcal{R}V\}}e^{\{\mathcal{G}V\}}\,. \tag{1.45}$$

Proof. Using the warped addition, we can rewrite the controlled map into the form

$$T_{ctrl} = e^{\{H\}\oplus\{V\}\oplus\{F\}}\,, \tag{1.46}$$

where the control term (1.45) becomes

$$\{F\} = -\{V\} \oplus \{(\mathcal{N} - \mathcal{G})\,V\} \oplus \{\mathcal{R}V\} \oplus \{\mathcal{G}V\}\,. \tag{1.47}$$

From (1.43) we have :

$$\mathcal{N} - \mathcal{G} = -e^{-\{H\}}\mathcal{G}\,. \tag{1.48}$$

Using lemmas 1.9 and 1.10, we also have the relation

$$(-\{H\}) \oplus (-\{\mathcal{G}V\}) \oplus \{H\} = -\{e^{-\{H\}}\mathcal{G}V\}\,, \tag{1.49}$$

hence, combining (1.48) and (1.49), we can rewrite (1.47) as

$$\{F\} = -\{V\} \oplus (-\{H\}) \oplus (-\{\mathcal{G}V\}) \oplus \{H\} \oplus \{\mathcal{R}V\} \oplus \{\mathcal{G}V\}\,. \tag{1.50}$$

By rearranging the terms we can get

$$\{\mathcal{G}V\} \oplus \{H\} \oplus \{V\} \oplus \{F\} \oplus (-\{\mathcal{G}V\}) = \{H\} \oplus \{\mathcal{R}V\}\,,$$

which is nothing but (1.44) rewritten using the warped addition.

$\square$

Remark 1.3.5 *Let us observe that the control term is, as required, small compared to* V*. In fact from* (1.47) *and by using the approximated formula for the warped addition* (1.15)*, we obtain*

$$\begin{aligned}
\{F\} &= -\{V\} \oplus \{(\mathcal{N} - \mathcal{G})\,V\} \oplus \{\mathcal{R}V\} \oplus \{\mathcal{G}V\} \\
&= -\{V\} + \{\mathcal{N}V\} - \{\mathcal{G}V\} + \{\mathcal{R}V\} + \{\mathcal{G}V\} + o(V) \\
&= o(V)\,,
\end{aligned}$$

where we use the relation $\mathcal{N} + \mathcal{R} = 1$*.*

We now give a convenient way to calculate the first order of F (i.e. of order V^2) that we denote by F_2. We place ourselves in the particular non-resonant case : we assume $\mathcal{R}V = 0$.
Using the warped addition with equation (1.45) of Theorem 1.3.4, we obtain

$$e^{\{F\}} = e^{-\{V\}}e^{\{(\mathcal{N}-\mathcal{G})V\}}e^{\{\mathcal{R}V\}}e^{\{\mathcal{G}V\}} = e^{-\{V\}\oplus\{(\mathcal{N}-\mathcal{G})V\}\oplus\{\mathcal{R}V\}\oplus\{\mathcal{G}V\}},$$

and thus

$$\begin{aligned}
\{F\} &= -\{V\} \oplus \{(\mathcal{N} - \mathcal{G})V\} \oplus \{\mathcal{R}V\} \oplus \{\mathcal{G}V\} \\
&= -\{V\} \oplus \{(1 - \mathcal{G})V\} \oplus \{\mathcal{G}V\} \\
&= \left[\frac{1}{2}\underbrace{(\{V\}\{\mathcal{G}V\} - \{\mathcal{G}V\}\{V\})}_{\overset{(1.4)}{=}\{\{V\}\mathcal{G}V\}} - \{\mathcal{G}V\} \right] \oplus \{\mathcal{G}V\} + o(\{V\}^2) \\
&= \frac{1}{2}\{\{V\}\mathcal{G}V\} + \frac{1}{4}\underbrace{\{\{\{V\}\mathcal{G}V\}\mathcal{G}V\}}_{=o(V^2)} + o(V^2) \\
&= \frac{1}{2}\{\{V\}\mathcal{G}V\} + o(\{V\}^2)\,,
\end{aligned} \tag{1.51}$$

where we explicitly used the assumption $\mathcal{R}V = 0$ to remove the third term on the right hand side on the first equation and hence we wrote $\mathcal{N}V = V$. We are thus able to define the non-resonant control term, up to order V^2, to be

$$F_2 = \frac{1}{2}\{V\}\mathcal{G}V = \frac{1}{2}\{V, \mathcal{G}V\}\,, \tag{1.52}$$

and so

$$F = F_2 + o(V^2)\,. \tag{1.53}$$

Remark 1.3.6 (Robustness) *In the following, we shall show that choosing F_2 instead of F leads to good results. This means that the control is* robust *: the initial system $H \oplus V$ can be modified by terms of order $o(V^2)$ without damaging the quality of the controlled system.*

1.3.2   Controlling the Hénon map

We now aim to give a full example of the previously detailed scheme of control. We choose the well known Hénon map whose dynamics was studied for example in [Hénon, 1969]. We come back to this map in Chap. 2, where we explain the motivation of such map and in Chap. 4 and 5, where we exhibit more advanced numerical results. For now, we concentrate on some particular properties of the map and the construction of a control term.

The Hénon map

The map is of the form

$$\begin{pmatrix} x' \\ p' \end{pmatrix} = R(\omega) \begin{pmatrix} x \\ p + x^2 \end{pmatrix} \quad ; \quad R(\omega) = \begin{pmatrix} \cos\omega & \sin\omega \\ -\sin\omega & \cos\omega \end{pmatrix}, \tag{1.54}$$

i.e. it is the composition of a rotation of angle ω with the operation which adds the quantity x^2 to p leaving the coordinate x unchanged. We show in Fig. 1.5 initial conditions leading to non-escaping orbits after 10^4 iterations.
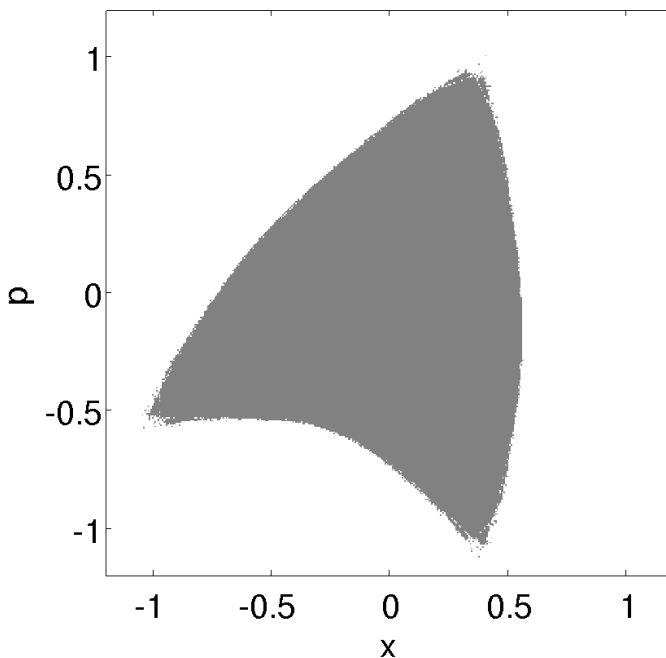
FIGURE 1.5: Initial conditions leading to non-escaping orbits of the Hénon map (1.54) after 10^4 iterations. We take 400 by 400 initial conditions in the square $[-1.2, 1.2]^2$ with $\omega = 2\pi q_x$ and $q_x = 0.61803$.

Performing the change of variables

$$z = x - ip, \quad \bar{z} = x + ip, \quad z \in \mathbb{C} \tag{1.55}$$

we can rewrite (1.54) simply as

$$z' = e^{i\omega} \left(z - \frac{i}{4}(z + \bar{z})^2 \right) \qquad z \in \mathbb{C}, \tag{1.56}$$

where $\bar{z}$ denotes the complex conjugate of z. Being the initial map a real one we can therefore omit the equation in the latter variable,

$$\bar{z}' = e^{-i\omega} \left(\bar{z} + \frac{i}{4}(z + \bar{z})^2 \right) \qquad z \in \mathbb{C} \, ;$$

all the information is contained in (1.56).

The *a priori* unusual choice $z = x - ip$ is made in order to have $e^{i\omega}$ as factor. The more classical definition $z = x + ip$ implies a factor $e^{-i\omega}$. As it will be shown below, both choices are equivalent but in this case, we won't have to carry the minus sign.

Remark 1.3.7 *Every quadratic area-preserving map can be written in the form of (1.56). We can check it easily. Let us consider a generic quadratic map :*

$$u' = e^{i\omega} \left(u + \frac{a}{2}u^2 + bu\bar{u} + \frac{c}{2}\bar{u}^2 \right) ,$$

and impose the preservation of the area (the determinant of its Jacobian matrix equals 1) :

$$\left| \frac{\partial(u', \bar{u}')}{\partial(u, \bar{u})} \right| = 1 + (a + \bar{b})u + (\bar{a} + b)\bar{u} + (a\bar{b} - b\bar{c})u^2 + (a\bar{a} - c\bar{c})u\bar{u} + (\bar{a}b - \bar{b}c)\bar{u}^2 = 1,$$

that is to say, parameters a, b and c satisfy

$$a = -\bar{b} \qquad c = \frac{\bar{a}^2}{a}.$$

The map reads then

$$u' = e^{i\omega} \left(u + \frac{1}{2a}(au - \bar{a}\bar{u})^2 \right) ,$$

which is nothing but (1.56) after the change of variable $u = z/2ia$.

It is also interesting to notice that the inverse of such a quadratic map remains a quadratic map. Indeed, we easily obtain

$$z = e^{-i\omega}z' + \frac{i}{4} \left(e^{-i\omega}z' + e^{i\omega}\bar{z}' \right).$$

In the literature, one can find different definitions of the Hénon map. For the sake of completeness, we present four other definitions and the way to obtain them from the initial Hénon map :

1. reflection with respect to the x axis : $z \to \bar{z}$

$$z' = e^{-i\omega} \left(z + \frac{i}{4}(z + \bar{z})^2 \right) \qquad \begin{pmatrix} x' \\ p' \end{pmatrix} = R(-\omega) \begin{pmatrix} x \\ p - x^2 \end{pmatrix} ;$$

2. reflection with respect to the p axis : $z \to -\bar{z}$

$$z' = e^{-i\omega}\left(z - \frac{i}{4}(z + \bar{z})^2\right) \qquad \begin{pmatrix} x' \\ p' \end{pmatrix} = R(-\omega)\begin{pmatrix} x \\ p + x^2 \end{pmatrix};$$

3. reflection with respect to the origin : $z \to -z$

$$z' = e^{i\omega}\left(z + \frac{i}{4}(z + \bar{z})^2\right) \qquad \begin{pmatrix} x' \\ p' \end{pmatrix} = R(\omega)\begin{pmatrix} x \\ p - x^2 \end{pmatrix}; \qquad (1.57)$$

4. rotation of $\pi/2$: $z \to -iz$

$$z' = e^{i\omega}\left(z - \frac{1}{4}(z - \bar{z})^2\right) \qquad \begin{pmatrix} x' \\ p' \end{pmatrix} = R(\omega)\begin{pmatrix} x + p^2 \\ p \end{pmatrix}.$$

The map as time-1 flow

The control is designed through composition of maps of the form (1.13). We thus need to express the map of Hénon in such a form. We propose the following integrable Hamiltonian system

$$H(p_H, x_H) = \omega\frac{x_H^2 + p_H^2}{2}$$

whose equations of motion have the following solutions

$$\begin{aligned} x_H(t) &= x_{H0}\cos(\omega t) + p_{H0}\sin(\omega t) \\ p_H(t) &= -x_{H0}\sin(\omega t) + p_{H0}\cos(\omega t) \end{aligned}$$

where $\mathbf{x}_{H0} \equiv (x_{H0}\ p_{H0})^t$ are the initial conditions. It follows that

$$\mathbf{x}_H(t) = e^{t\{H\}}\mathbf{x}_{H0} = R(\omega t)\mathbf{x}_{H0}.$$

Pursuing the same scheme with the perturbation

$$V(p_V, x_V) = -\frac{x_V^3}{3}$$

we find

$$\mathbf{x}_V(t) = e^{t\{V\}}\mathbf{x}_{V0} = \begin{pmatrix} x_{V0} \\ p_{V0} + x_{V0}^2 t \end{pmatrix}.$$

Finally, using these two Hamiltonian systems at time $t = 1$, we can rewrite the Hénon map (1.54) as

$$\begin{pmatrix} x' \\ p' \end{pmatrix} = e^{\{H\}}e^{\{V\}}\begin{pmatrix} x \\ p \end{pmatrix}.$$

We now fulfill the framework of theorem 1.3.4 with $\mathbf{x} = (x\ p)^t$.

Controlled Hénon map

We here expose the main steps leading to a computable control. Those steps are fully detailed in the more general 4-dimensional case studied in Sec. 4.1 Chap. 4.

We choose the complex variables define in (1.55). In these variables, the generators of the map are

$$H(z, \bar{z}) = \omega \frac{z\bar{z}}{2}$$

and

$$V(z, \bar{z}) = \frac{-1}{24} (z + \bar{z})^3 \ .$$

The linear operator $\{H\}$ acting on any complex monomial $z^n \bar{z}^m$ $(n, m \in \mathbb{N})$ reads then

$$\{H\} z^n \bar{z}^m = i\omega(n - m) z^n \bar{z}^m$$

from which the relations follow

$$\{H\}^k z^n \bar{z}^m = [i\omega(n - m)]^k z^n \bar{z}^m \qquad \text{and} \qquad e^{\{H\}} z^n \bar{z}^m = e^{i\omega(n-m)} z^n \bar{z}^m.$$

We also need to find one operator $\mathcal{G}$ satisfying hypothesis 1.42. We can easily check that

$$\mathcal{G} z^n \bar{z}^m = \frac{1}{1 - e^{-i\omega(n-m)}} \mathcal{N} z^n \bar{z}^m$$

with

$$\mathcal{N} z^n \bar{z}^m = \begin{cases} 0 & \text{if } \omega(n - m) = 2k\pi \text{ for some } k \in \mathbb{Z} \\ z^n \bar{z}^m & \text{otherwise} \end{cases}$$

fits the requirements assuming a non-resonant condition for ω. Because $\mathcal{G}$ is linear and V is a sum of monomials, we can evaluate $\mathcal{G}V$ in complex variables.

Back in the original variables, we find

$$\mathcal{G}V(p, x) = \frac{1}{6 \sin(\omega)(1 + 2\cos(\omega))} \left(p^3 (\cos(\omega) + 1)^2 \right.$$
$$\left. + 3px^2 \cos(\omega)(\cos(\omega) + 1) + x^3 \sin(\omega)(2\cos(\omega) + 1) \right)$$

and

$$F_2(p, x) = \frac{x^2}{12 \sin(\omega)(1 + 2\cos(\omega))} \left(3p^2 (\cos(\omega) + 1)^2 + 3x^2 \cos(\omega)(\cos(\omega) + 1) \right)$$

We obtained F_2 exactly, but we need $e^{\{F_2\}}$ that cannot be explicitly found because we are not able to compute the infinite series. As in the continuous case, we consider different possibilities in order to compute it : truncation or

fixing some variables to constant quantities.

In this example, we first choose to truncate the series. For this purpose, we introduce the quantity

$$C_k(F_2) = \sum_{l=0}^{k} \frac{\{F_2\}^l}{l!}$$

that we call *truncated control map of order k*. It is just an approximation of the predicted exact control map since $C_\infty(F_2) = e^{\{F_2\}}$, or

$$\lim_{k \to +\infty} C_k(F_2) = e^{\{F_2\}}.$$

Of course maps of that form may not (and usually will not) be symplectic. This is discussed later, Chap. 4 Sec. 4.1.

We show in Fig. 1.6 non-escaping orbits after 10^4 iterations for the initial map (1.54) (plot (a)) and the *truncated controlled map of order k* :

$$e^{\{H\}}e^{\{V\}}C_k(F_2) \tag{1.58}$$

with $k = 4$ (plot (b)). We clearly see a decrease of the amount of initial condi-
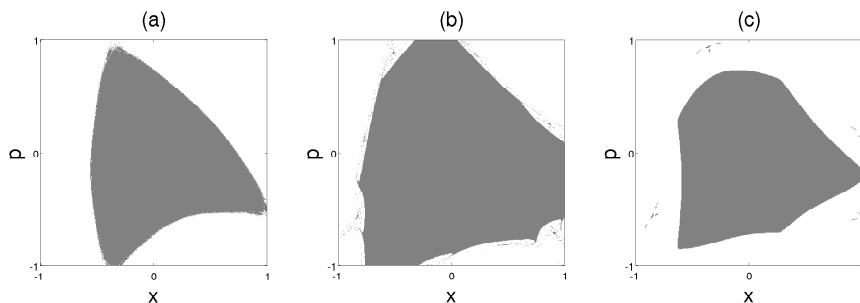
FIGURE 1.6: Non-escaping orbits of the Hénon map after 10^4 iterations : panel (a) without control, panel (b) with control $C_4(F_2)$ and panel (c) with control $e^{\{F_{2c}\}}$. Grey dots for remaining initial conditions, white for escaping initial conditions.

tions that escaped. To reinforce this statement we calculate the percentage of non escaping orbits at a distance r from the origin. This is reported on Fig. 1.7. For the uncontrolled map, 100% of the orbits remain up to a radius $r = 0.55$ while this radius is increased to $r = 0.72$ for the controlled map (1.58).
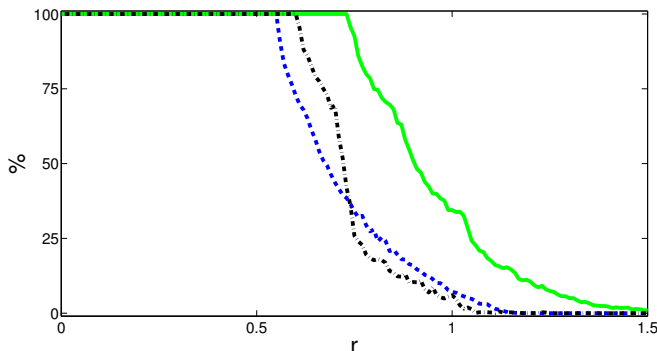
FIGURE 1.7: Percentage of non-escaping orbit versus the distance to the origin. The blue line corresponds to the non controlled map, the green line to the controlled map with the add $C_4(F_2)$ and the black one to the control whose generator is F_{2c}.

In Chap. 3 we shall present tools that will allow us to show that those remaining orbits have good dynamical properties.

Instead of a truncation of the series, another method to compute the map generated by F is to decrease the number of variables by fixing the momentum p to a constant p_c and thus make F independent of the momenta : $F_{2c}(x) \equiv F_2(p_c, x)$. We are then able to express $e^{\{F_{2c}\}}$:

$$e^{\{F_{2c}\}} \left(\begin{array}{c} x \\ p \end{array} \right) = \left(\begin{array}{c} e^{\{F_{2c}\}} x \\ e^{\{F_{2c}\}} p \end{array} \right) = \left(\begin{array}{c} x \\ p - 2\alpha p_c^2 x - 4\beta x^3 \end{array} \right)$$

where

$$\alpha = \frac{(\cos(\omega) + 1)^2}{4 \sin(\omega)(1 + 2\cos(\omega))} \quad \text{and} \quad \beta = \frac{\cos(\omega)(\cos(\omega) + 1)}{4 \sin(\omega)(1 + 2\cos(\omega))}.$$

We show in Fig. 1.6 (plot (c)), the non-escaping orbits after 10^4 iterations for the map

$$e^{\{H\}} e^{\{V\}} e^{\{F_{2c}\}}.$$

We also reported on Fig. 1.7 the percentage of non-escaping orbit at distance r from the origin. This percentage is of 100% up to a radius 0.6. The improvement is smaller than the one of the truncated control but the map is symplectic. Other criteria can be taken into account to compare the controlled maps and quantify their *goodness*. They will be developed in Chap. 3, Chap. 4 and Chap. 5.

1.4 On other control methods

In this section, we briefly present and analyze two other *philosophies* used to control dynamical systems : automatic control and control by tuning parameters.

1.4.1 Automatic control

Roughly speaking, we consider a dynamical system dependent of an *input* usually denoted by u that can be modified through time. The system reads

$$\dot{\boldsymbol{x}} = f(\boldsymbol{x}(t), \boldsymbol{u}(t), t) \quad \text{or} \quad \boldsymbol{x}_{n+1} = f(\boldsymbol{x}_n, \boldsymbol{u}_n, n)$$

if the system is continuous in time or discrete in time respectively. The main idea is to modify $\boldsymbol{u}$ along the orbit such that the system (or more specifically the state) satisfies or reaches specific properties such as (un-)stability, or behavior of certain quantities.

This represents a whole field in applied mathematics and in engineering with sub-fields such as control and systems [Hinrichsen and Pritchard, 2005], linear systems [Callier and Desoer, 1991] or optimal control [Locatelli, 2001]. This is a pretty new field in mathematics that gained attention in the 20th century with the advancement of technology : nowadays it is applied almost everywhere in our daily routine, from the design of the water tank of the ordinary flush toilet to the design of a lateral and longitudinal control of a Boeing (and thus the autopilot) or in the satellite's attitude control [Franklin et al., 2010].

We would like to stress out that this set of theories has an **a priori** radically different approach than those of the previous sections even if they are close in the goals : to change, adapt the system to reach, keep certain behaviors. Here, these changes are made *during* the evolution of the system while in Secs. 1.2 and 1.3 it is carried out *before*, in the design of the system.

In fact such approach may be linked to the one presented Sec. 1.2 as it is explained and the end of the following example.

As example, we present the Ott-Grebogi-Yorke control method applied to the Hénon map. We follow the original paper [Ott et al., 1990] and the scheme detailed in [Flake, 1998].

We consider a 2D chaotic non-linear map [7] depending on one system parameter u. This parameter is assumed available for external adjustment. With respect to the discretization of time, the parameter reads u_n and the system

$$\boldsymbol{x}_{n+1} = f(\boldsymbol{x}_n, u_n) \tag{1.59}$$

---

7. The generalization to higher dimension is exposed in [Ott et al., 1990] but in the present section, we restrain ourselves to controlling chaos in lower dimensional dynamical systems.

where $\boldsymbol{x}_n \in \mathbb{R}^2$, $u_n \in \mathbb{R}$ and $n \in \mathbb{N}$. We also assume that the map has a saddle [8] fixed point that we denote by $\boldsymbol{x}_F$ (the fixed point is independent of $u_n \ \forall n$).

We linearize the map around $\boldsymbol{x}_F$ and $u \sim 0$. To that end, we shall require that u_n is of order $||\boldsymbol{x} - \boldsymbol{x}_F||$. This means that the control will be effective locally and, there, small. We obtain

$$\boldsymbol{x}_{n+1} \approx f(\boldsymbol{x}_F, 0) + M(\boldsymbol{x}_n - \boldsymbol{x}_F) + \boldsymbol{b}\, u_n$$

where M is the Jacobian matrix of the map and $\boldsymbol{b}$ is the derivative of the map with respect to the control, both evaluated at the fixed point without control ($u = 0$). Finally, to simplify further calculation, we impose a linear control :

$$u_n = \boldsymbol{k} \cdot (\boldsymbol{x}_n - \boldsymbol{x}_F)$$

where $\boldsymbol{k}$ is a vector of $\mathbb{R}^2$. With the following notations

$$\boldsymbol{d}_n = \boldsymbol{x}_n - \boldsymbol{x}_F \quad \text{and} \quad C = M + \boldsymbol{b}\,\boldsymbol{k}^t$$

we write down a new, linear, map [9]

$$\boldsymbol{d}_{n+1} = C\,\boldsymbol{d}_n. \tag{1.60}$$

The fixed point $\boldsymbol{x}_F$ will be stable if the difference $\boldsymbol{x}_n - \boldsymbol{x}_F$ tends to $\boldsymbol{0}$, i.e. if the moduli of the eigenvalues of C are smaller than 1. So we are looking for $\boldsymbol{k}$ achieving this condition.

We know that one of the eigenvalues, λ_u, of M has a modulus greater than 1 in the unstable direction $\boldsymbol{e}_u$. In the same way, we denote by λ_s and $\boldsymbol{e}_s$ the stable eigenvalue and its corresponding eigenvector. Let us write $\boldsymbol{d}_n$ in the eigenbasis $(\boldsymbol{e}_s, \boldsymbol{e}_u)$:

$$\boldsymbol{d}_n = a_s \boldsymbol{e}_s + a_u \boldsymbol{e}_u.$$

We thus have, without considering the control,

$$\begin{aligned} \boldsymbol{d}_{n+1} &= M\boldsymbol{d}_n \\ &= M(a_s \boldsymbol{e}_s + a_u \boldsymbol{e}_u) \\ &= \lambda_s a_s \boldsymbol{e}_s + \lambda_u a_u \boldsymbol{e}_u. \end{aligned}$$

Now, we can state the required value for $\boldsymbol{k}$: we want to fix it in such a way that the dynamics on the escaping direction $\lambda_u a_u \boldsymbol{e}_u$ vanishes.
We introduce an orthonormal basis : a couple of vectors $(\boldsymbol{g}_s, \boldsymbol{g}_u)$ satisfying

$$\boldsymbol{g}_s \cdot \boldsymbol{e}_u = \boldsymbol{g}_u \cdot \boldsymbol{e}_s = 0 \quad \text{and} \quad \boldsymbol{g}_s \cdot \boldsymbol{e}_s = \boldsymbol{g}_u \cdot \boldsymbol{e}_u = 1 \tag{1.61}$$

---

8. This is an hypothesis often assumed in the control strategy.
9. We used $f(\boldsymbol{x}_F, 0) = \boldsymbol{x}_F$ because $\boldsymbol{x}_F$ is a fixed point.

that allows us to write the matrix M in the following form

$$M = \lambda_s \boldsymbol{e}_s \boldsymbol{g}_s^t + \lambda_u \boldsymbol{e}_u \boldsymbol{g}_u^t.$$

Then we left multiply (1.60) by $\boldsymbol{g}_u$ and impose that $\boldsymbol{g}_u \cdot \boldsymbol{d}_{n+1} = 0$, that is to say that $\boldsymbol{d}_{n+1}$ has no component in the $\boldsymbol{e}_u$ direction. Let us develop the left hand side of the condition :

$$\begin{aligned} \boldsymbol{g}_u \cdot \boldsymbol{d}_{n+1} &= \boldsymbol{g}_u \cdot (M + \boldsymbol{b}\boldsymbol{k}^t)\boldsymbol{d}_n \\ &= \boldsymbol{g}_u \cdot (\lambda_s \boldsymbol{e}_s \boldsymbol{g}_s^t + \lambda_u \boldsymbol{e}_u \boldsymbol{g}_u^t + \boldsymbol{b}\boldsymbol{k}^t)\boldsymbol{d}_n \\ &= (\lambda_u \boldsymbol{g}_u^t + \boldsymbol{g}_u \cdot \boldsymbol{b}\boldsymbol{k}^t)\boldsymbol{d}_n. \end{aligned}$$

to have $\boldsymbol{g}_u \cdot \boldsymbol{d}_{n+1} = 0$. The solution is

$$\boldsymbol{k} = -\frac{\lambda_u}{\boldsymbol{g}_u \cdot \boldsymbol{b}}\boldsymbol{g}_u.$$

We now apply this scheme to the Hénon map [10] [Hénon, 1976]

$$f(x, y) = \begin{pmatrix} a_v - x^2 + by \\ x \end{pmatrix}. \tag{1.62}$$

We assume that we can make a_v vary by a small quantity around a that has been initially fixed. Consequently, we write a_v as $a_v = a + u$, where u is the control parameter. The map (1.62) reads

$$f(x, y) = \begin{pmatrix} a - x^2 + by \\ x \end{pmatrix} + \begin{pmatrix} u \\ 0 \end{pmatrix}.$$

The unstable fixed point for the uncontrolled map is located at (x_F, y_F) where

$$x_F = y_F = \frac{b - 1 + \sqrt{(b - 1)^2 + 4a}}{2}.$$

We easily find the Jacobian matrix M and the vector $\boldsymbol{b}$ evaluated on this point :

$$M = \begin{pmatrix} -2x_F & b \\ 1 & 0 \end{pmatrix} \quad \text{and} \quad \boldsymbol{b} = \begin{pmatrix} 1 \\ 0 \end{pmatrix},$$

the corresponding eigenvalues,

$$\lambda_u = -x_F - \sqrt{x_F^2 + b} \quad \text{and} \quad \lambda_s = -x_F + \sqrt{x_F^2 + b}$$

---

10. Let us point out that this is not the same kind of map as those analyzed in Sec. 1.3 even if they have the same name. In fact, for particular values of the parameter a_v and b there exists a change of variable such that the maps are equivalent, see [Polymilis et al., 1997] for details.

and the eigenvectors

$$\boldsymbol{e}_u = \frac{1}{\sqrt{\lambda_u^2 + 1}} \left(\begin{array}{c} \lambda_u \\ 1 \end{array} \right) \quad \text{and} \quad \boldsymbol{e}_s = \frac{1}{\sqrt{\lambda_s^2 + 1}} \left(\begin{array}{c} \lambda_s \\ 1 \end{array} \right).$$

In order to compute the control term u, we need the vector $\boldsymbol{g}_u$ of the orthonormal basis. Let us denote e_{ui} the ith component of $\boldsymbol{e}_u$ and similarly for $\boldsymbol{e}_s$. The vector

$$\boldsymbol{g}_u = \frac{1}{e_{u1}e_{s2} - e_{u2}e_{s1}} \left(\begin{array}{c} e_{s2} \\ -e_{s1} \end{array} \right)$$

verifies conditions of Eqs. (1.61). With this last vector we can compute $\boldsymbol{k}$ and thus u_n at each time step. We also want to include a constraint on the size of the control, that is to say u_n shouldn't exceed a determined quantity u^*. We include this rule in the definition of u_n :

$$u_n = \begin{cases} 0 & \text{if } |\boldsymbol{k} \cdot (\boldsymbol{x}_n - \boldsymbol{x}_F)| \geq u^* \\ \boldsymbol{k} \cdot (\boldsymbol{x}_n - \boldsymbol{x}_F) & \text{otherwise.} \end{cases}$$

Of course other smoother transitions are possible.

The following computations where performed with $a = 1.29$ and $b = 0.3$. With these values, the unstable fixed point is located at $x_F \approx 0.838486$. In Figs. 1.8, we first show the behavior of the system when the control is not applied. The orbit follows a chaotic attractor and has an unpredictable behavior as one can see on the right panel of Fig. 1.8.
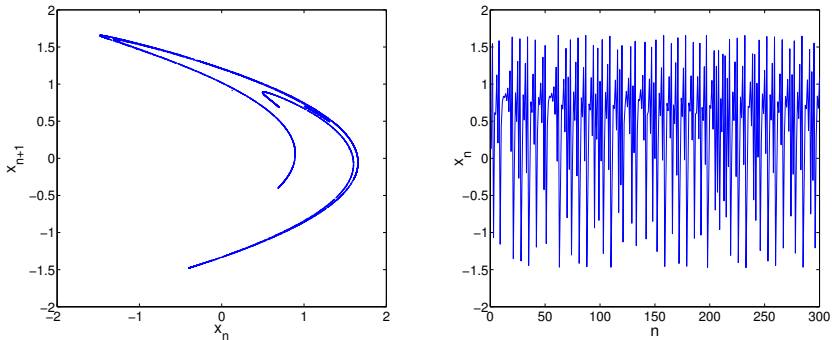
FIGURE 1.8: The Hénon map without control. On the left side, the chaotic attractor ($n = 1000$ iterations). On the right side, the chaotic behavior of the variable x (and thus also y) as a function of the time for the first 300 iterations.

We now show in Fig. 1.9, the evolution of x_n with control. We observe small variations around the fixed point already after 4 iterations : we have $\max_{n \geq 4} |x_n - x_F| = 0.0284$. The control is thus working and moreover it is

quick to reach its goal even for a distant initial condition ($x_0 = 0.5$). We used the value $u^* = 0.01$, that is to say, we controlled the system with a "force" less than half a percent (considering the amplitude of Figs. 1.8).
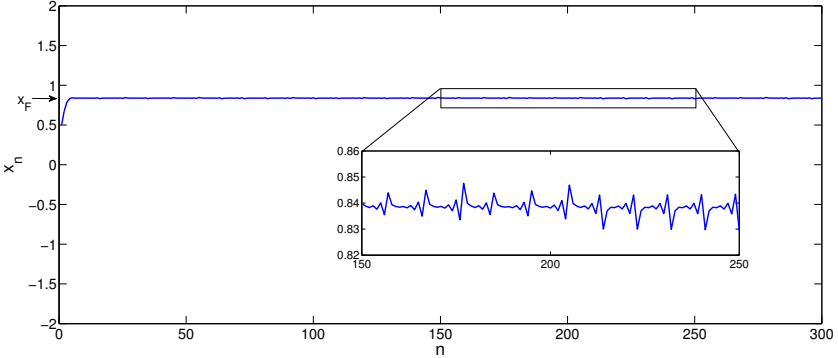
FIGURE 1.9: The controlled Hénon map with $u^* = 0.01$ for first 300 iterations. After 5 iterations, the rest remains close (< 0.03) to the objective value x_F.

The control should be independent of the initial condition. In order to convince ourselves, we switch it on and off, i.e. it is present or absent, along the integration. We observe that when it is off, the orbit follows the chaotic attractor while when it is on, the system tends rapidly to the fixed point and then oscillates (lightly) around it. This is presented by Fig. 1.10 : we switched the control on after 50 iterations, removed it after 150 to finally put it back at 200 iterations. We remark a delay in the occurrence of the chaotic behavior after $n = 150$. Those iterations are probably already in the stable direction of the saddle node and thus the absence of the control is not yet visible.

Finally, we test the robustness of the control by introducing some noise. We consider the system

$$f(x, y) = \begin{pmatrix} a - x^2 + by \\ x \end{pmatrix} + \begin{pmatrix} u \\ 0 \end{pmatrix} + \epsilon \begin{pmatrix} \delta_1 \\ \delta_2 \end{pmatrix}.$$

where $\boldsymbol{\delta} = (\delta_1\, \delta_2)^t$ has its values drawn from a standard uniform distribution on the open interval $(-0.5, 0.5)$ and ϵ is a new parameter giving the size of the external noise. We see in Fig. 1.11 (where we also switched-on and off the control for windows identical to Fig. 1.10) that even with a noise up to 2 times greater than the size of the control ($\epsilon = 0.05$ and $u^* = 0.01$), the method remains efficient. The behavior is the same, only the size of the oscillations around x_F increased to 0.0303 (without noise it was 0.0284).

Remark 1.4.1 (Link with Sec. 1.2) *A branch of the* automatic control *is concerned by the so-called* port controlled Hamiltonian systems with dissipa-
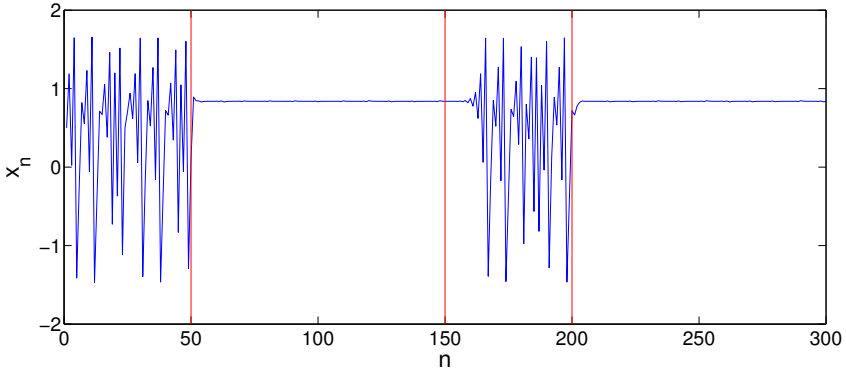
FIGURE 1.10: The controlled Hénon map with $u^* = 0.01$ with control switched-on and off. Control off from $n = 0$ to $n = 50$ and from $n = 150$ to $n = 200$.

tion. For example, in [Maschke et al., 2000], they consider the system

$$\begin{cases} \dot{\boldsymbol{x}} = [\mathcal{J}(\boldsymbol{x}) - R(\boldsymbol{x})]\nabla_{\boldsymbol{x}} H(\boldsymbol{x}) + g(\boldsymbol{x})\boldsymbol{u} \\ \boldsymbol{y} = g(\boldsymbol{x})^t \nabla_{\boldsymbol{x}} H(\boldsymbol{x}) \end{cases} \tag{1.63}$$

which state-dynamics, when considered lossless, reads

$$\dot{\boldsymbol{x}} = \mathcal{J}(\boldsymbol{x})\nabla_{\boldsymbol{x}} H(\boldsymbol{x}) + g(\boldsymbol{x})\boldsymbol{u}.$$

That later equation describes a dynamics analogue to the one of the controlled Hamiltonian (see theorem 1.2.6) $\tilde{H} + f$ (with $\tilde{H} = H + V$) :

$$\dot{\boldsymbol{x}} = \mathcal{J}\nabla_{\boldsymbol{x}}\tilde{H}(\boldsymbol{x}) + \mathcal{J}\nabla_{\boldsymbol{x}} f(\boldsymbol{x}).$$

The comparison is not pushed any further in the present work but would be interesting : first in order to compare the methods and the results but mainly to propose new directions by merging concepts and techniques of both control strategies.
Let us finally point out that the comparison can also be considered with the technique exposed in the last chapter where dissipation is allowed, that is, in Eq. (1.63), when $R \neq 0$.

1.4.2   Control by tuning parameters

Dynamical systems can depend on parameters alterable during the experience (e.g. see previous Subsec. 1.4.1) or to be set before running it. In the following, we consider that hypothesis ; parameters should be fixed and thus well chosen before to start the experiment. Of course this choice can radically change the results.
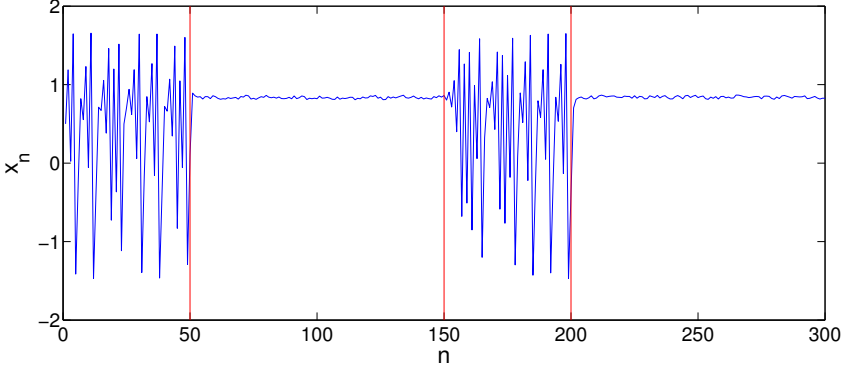
FIGURE 1.11: The controlled Hénon map with $u^* = 0.01$ with control switched-on and off and noise ($\epsilon = 0.05$). The controlled system is robust exhibiting a similar behavior as the one without noise.

A naive approach would be to test all the range of admissible parameters in order to find the right ones. Even if it is possible in some cases, most of the time this solution is not applicable : for example there could be an infinity of possibilities (imagine a continuous parameter $p \in [0, 1]$) or running the experiment could cost a lot or take too much time.

For these reasons, it is often needed to find a correct value for the parameters *a priori*. In this paragraph, we present an example of control using a parameter. We follow the ideas of [Hanson and Cary, 1984] applied to the standard map [Chirikov, 1979]. Let us notice that the essence of this method was applied to control Hamiltonian systems like (1.27) in [Bachelard et al., 2006].

We consider a two dimensional symplectic map depending on different parameters $p_1, p_2, \ldots, p_l$ regrouped under the vectorial notation $\boldsymbol{p}$ (to be fixed at the beginning) :

$$\boldsymbol{x}_{n+1} = T(\boldsymbol{x}_n, \boldsymbol{p}) \tag{1.64}$$

together with a periodic point $\boldsymbol{x}^*$ of order q (independent of $\boldsymbol{p}$), i.e.

$$T^q(\boldsymbol{x}^*, \boldsymbol{p}) = \boldsymbol{x}^*$$

where

$$T^q(\boldsymbol{x}^*, \boldsymbol{p}) = T(T^{q-1}(\boldsymbol{x}^*, \boldsymbol{p}), \boldsymbol{p}) \quad \text{with} \quad T^1 \equiv T \,.$$

We also consider the Jacobian matrix of the map denoted by $M(\boldsymbol{x}^*, \boldsymbol{p})$ that gives us, at first order, the evolution of the distance between the fixed point $\boldsymbol{x}^*$ and a point $\boldsymbol{x}^* + \boldsymbol{\delta x}^*$ in its vicinity. With $\boldsymbol{\delta} \equiv T^q(\boldsymbol{x}^* + \boldsymbol{\delta x}^*, \boldsymbol{p}) - T^q(\boldsymbol{x}^*, \boldsymbol{p})$, this distance, one has

$$\boldsymbol{\delta} = M^q \boldsymbol{\delta x}^* \tag{1.65}$$

where
$$M^q = M(T^{q-1}(\boldsymbol{x}^*, \boldsymbol{p})) \cdots M(T(\boldsymbol{x}^*, \boldsymbol{p})) M(\boldsymbol{x}^*, \boldsymbol{p})$$

is called the monodromy matrix. The relation (1.65) can be characterized by the eigenvalues of M^q. Also, being T symplectic, the determinant of M is the unity and so is the one of M^q. Therefore, the eigenvalues of M^q only depend on its trace :
$$\lambda_{1,2} = \frac{\mathrm{tr} M^q \pm \sqrt{(\mathrm{tr} M^q)^2 - 4}}{2}.$$

In [Greene, 1968, Greene, 1979], Greene studied the persistence and destruction of rotational invariant tori with sequences of periodic orbits. He characterized these orbits by the so called

Greene's residue
Considering previous notations, the Greene's residue is
$$r = \frac{1}{2} - \frac{\mathrm{tr} M^q}{4}$$

Using it, he also proposed a heuristic criterion ensuring the existence of an invariant torus with irrational frequency ω :

Greene's criterion
Considering periodic orbits of rational frequencies $\omega_n = p_n/q_n$, an invariant torus with frequency
$$\omega = \lim_{n \to \infty} \omega_n,$$
exists if
$$\lim_{n \to \infty} r_n = 0,$$
where r_n is the residue of the periodic orbit with frequency ω_n. On the contrary, if an invariant torus does not exist, the residues diverge to infinity.

If the eigenvalues are equal to 1, the residue vanishes. Based on these tools, [Hanson and Cary, 1984] wrote :

> "In particular, for an integrable system without island structure the fixed points on a rational surface have zero residue. This leads us to an empirical rule : to make a system more integrable, one should minimize the residues of the fixed points."

We can thus propose an ideal scheme to reduce chaos in a system : starting with a map like (1.64), one should find periodic orbits (of possibly long period) and use the set of parameters in order to make their Greene's residues as small as possible (ideally zero). Of course this is not always possible : for example the number of parameters p_i can be much smaller than the number of fixed points.

We apply this procedure (following [Chandre, 2006]) to the standard map [Chirikov, 1979]

$$T \left(\begin{array}{c} A_n \\ \phi_n \end{array} \right) = \left(\begin{array}{c} A_{n+1} \\ \phi_{n+1} \end{array} \right) = \left(\begin{array}{c} A_n + \epsilon \sin \phi_n \\ \phi_n + A_{n+1} \mod 2\pi \end{array} \right) . \tag{1.66}$$

We present in Fig. 1.12, the Poincaré section of the map with $\epsilon = 1.5$. Chaos is nearly everywhere : there remains no KAM tori for that value of ϵ (and higher). We add a control depending on a parameter p (the form, $\sin 2\phi_n$, is taken from
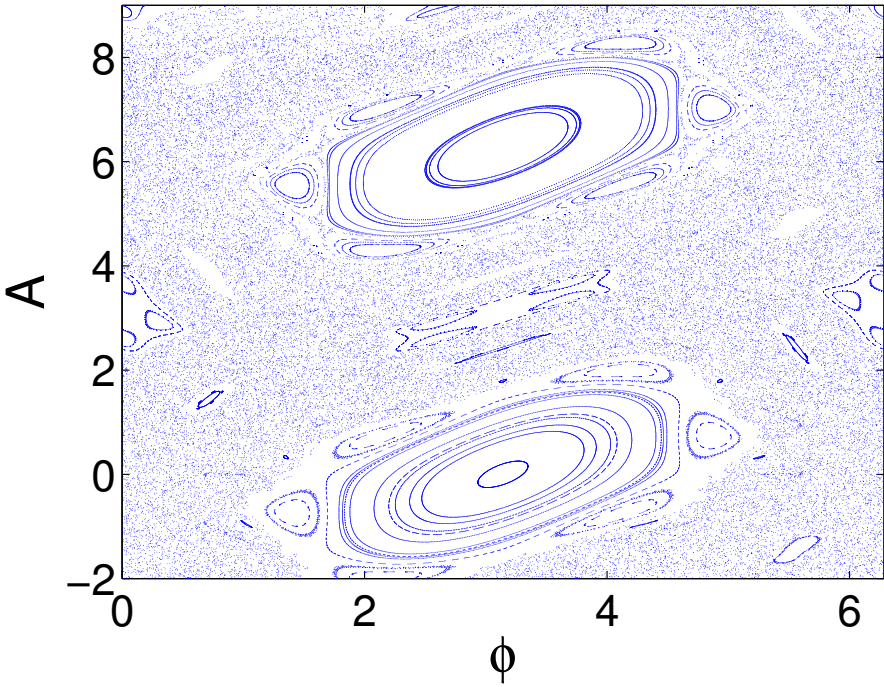
FIGURE 1.12: Poincaré section of the standard map (1.66) with $\epsilon = 1.5$. Every KAM tori have disappeared under the perturbation.

another control strategy exposed before [Chandre et al., 2005b]) to the map to obtain :

$$\left(\begin{array}{c} A_{n+1} \\ \phi_{n+1} \end{array} \right) = \left(\begin{array}{c} A_n + \epsilon \sin \phi_n + p \sin 2\phi_n \\ \phi_n + A_{n+1} \mod 2\pi \end{array} \right) \tag{1.67}$$

and we are looking for a good value of p reducing chaos and luckily re-establishing KAM tori.

We find that $\boldsymbol{x}^* = (\pi\,\pi)^t$ is a fixed point of (1.67) of period 2 :

$$T\left(\begin{array}{c} \pi \\ \pi \end{array}\right) = \left(\begin{array}{c} \pi \\ 0 \end{array}\right) \quad \text{and} \quad T^2\left(\begin{array}{c} \pi \\ \pi \end{array}\right) = T\left(\begin{array}{c} \pi \\ 0 \end{array}\right) = \left(\begin{array}{c} \pi \\ \pi \end{array}\right).$$

We also compute the Jacobian matrix

$$M(A,\phi) = \left(\begin{array}{cc} 1 & \epsilon\cos\phi + 2p\cos 2\phi \\ 1 & 1 + \epsilon\cos\phi + 2p\cos 2\phi \end{array}\right)$$

and the monodromy matrix of $(\pi\,\pi)^t$ reads

$$M(\pi,0)M(\pi,\pi) = \left(\begin{array}{cc} 1 + \epsilon + 2p & 4p^2 + 4p - \epsilon^2 \\ 2 + \epsilon + 2p & 4p^2 + 6p + 1 - \epsilon - \epsilon^2 \end{array}\right)$$

The trace of the later matrix is $4p^2 + 8p + 2 - \epsilon^2$ that we want equal to 2 in order to set to zero the residue of $\boldsymbol{x}^*$. It gives two solutions $p_\pm$:

$$p_\pm = -1 \pm \sqrt{1 + \frac{\epsilon^2}{4}}$$

or, at first approximation

$$p_+ \approx \frac{\epsilon^2}{8} \quad \text{and} \quad p_- \approx -2 - \frac{\epsilon^2}{8}.$$

The first, p_+ is of order ϵ^2, that is small in front of the initial system while p_- is of order 1. Following previous considerations (e.g. remark 1.2.7) on what a *good* size for a control should be, we compute the controlled standard map with p_+. Results are exposed Fig. 1.13 where KAM tori were reconstructed for values of A around π.

So it worked well in this case. But we would like to warn about that method : it is empirical ! In the above developed example, we zeroed *only one* fixed point residue while, ideally, every fixed points residue should be zeroed. Also the choice of the control is very important : here we have chosen a control $p\sin 2\phi_n$ calculated with a strong background of theory.

In order to illustrate that the method is empirical, we choose a slightly different basis for the control, $\sin 4\phi_n$, and apply the same procedure. The points $(\pi\,\pi)^t$ remains a fixed point of period 2 and we find two values zeroing the residue :

$$p_\pm = -\frac{1}{2} \pm \sqrt{\frac{1}{4} + \frac{\epsilon^2}{16}}.$$

The same arguments apply : we choose p_+ being $\mathcal{O}(\epsilon^2)$ and find the Poincaré section presented Fig. 1.14 where we cannot see any improvement from Fig. 1.12.

In conclusion, even if it *can* work sometimes, and thus it is worth considering it according to the problem, we cannot (always) link the linear stability of a fixed point to the stability in its vicinity in the nonlinear system.
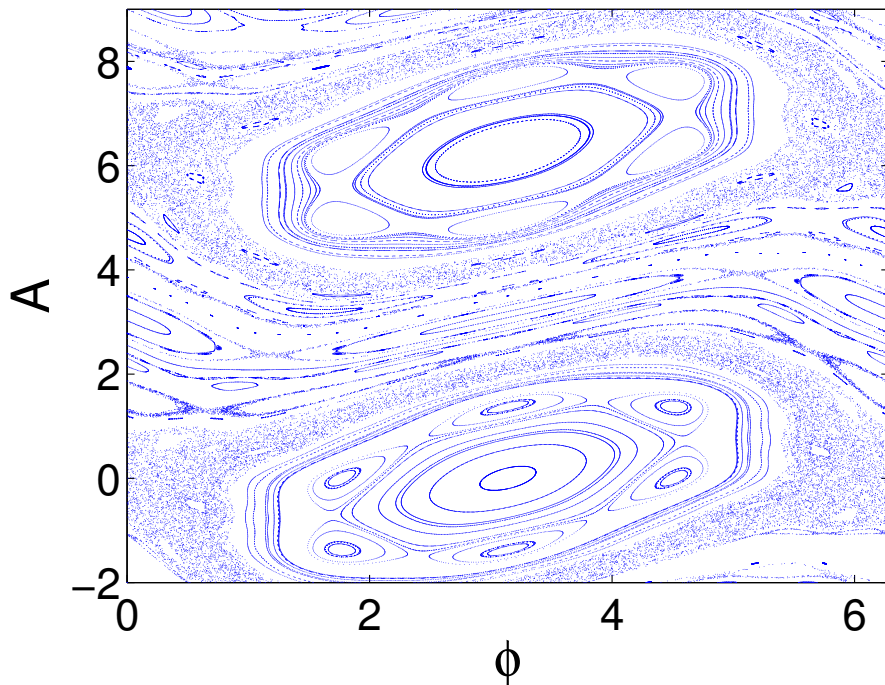
FIGURE 1.13: Poincaré section of the controlled standard map (1.67) with $\epsilon = 1.5$ and $p_+ = -1 + \sqrt{1 + \epsilon^2/4}$. There remain KAM tori despite the perturbation.

1.5   Normal Forms

In this section we introduce the normal form approach for symplectic maps. While in the previous sections, we dealt with nonlinearities by controlling the system, the goal of the normal form approach is to find a different representation of the system in order to describe it more precisely, more completely.

We present the main ideas and results of [Bazzani et al., 1990] where authors develop the normal form for non-resonant symplectic maps of $\mathbb{R}^{2n}$ in the neighborhood of an elliptic fixed point [11].

Previous works on such construction were done for Hamiltonian systems such [Birkhoff, 1927, Gustavson, 1966, Meyer, 1974] but do not give an easy generalization to symplectic maps in more than two dimensions. Dedication to this particular work can be found in [Servizi and Turchetti, 1986]

---

11. The Jacobian matrix evaluated on an elliptic fixed point has purely imaginary eigenvalues. The dynamics around such a point is circular motion in first approximation.
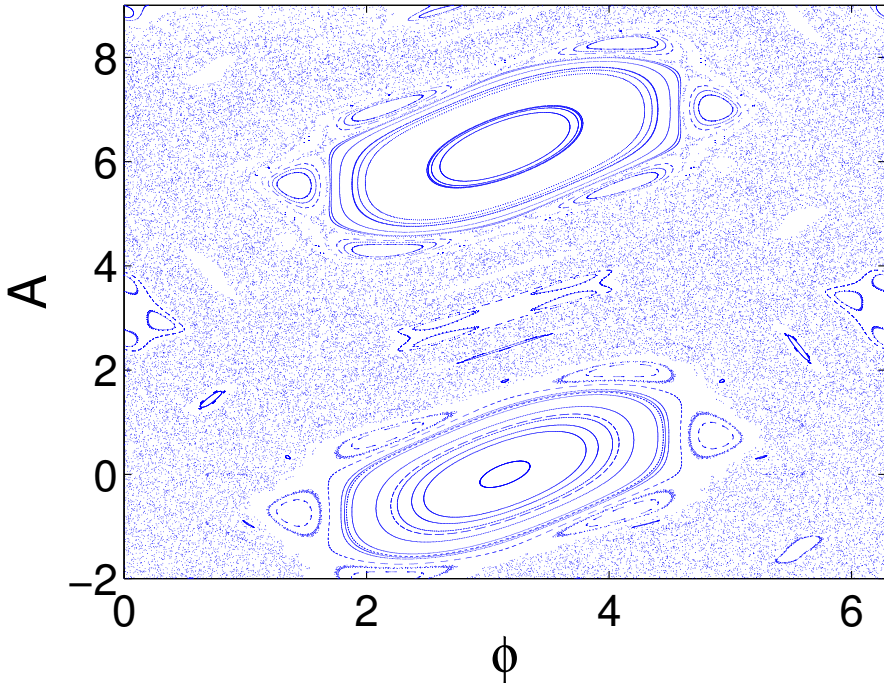
FIGURE 1.14: Poincaré section of the controlled standard map (1.67) with $\epsilon = 1.5$, $p \sin 4\phi_n$ instead of $p \sin 2\phi_n$ and $p = -1 + \sqrt{1 + \epsilon^2/4}$. The control does not improve the stability around $(\pi \, \pi)^t$.

or [Bazzani, 1988] before [Bazzani et al., 1990]. More recently a new algorithm dedicated to compute a normal form for maps was presented in [Giorgilli, 2013].

We are looking for the construction of a change of variables such that in the new variables, the system (a map or a Hamiltonian system) takes a simpler form, i.e. exhibits more invariants, explicit (interpolating [12]) flows or symmetries than the original system. The new system is said to be in *normal form*.

First we state the notations, the desired normal form and the linked results. Secondly we apply it to the Hénon map.

---

12. In the case of maps.

1.5.1 Notations and results

We consider a $2n$, $n \geq 1$, dimensional area preserving map (see Def. 1.1.10) defined by

$$\begin{cases} \boldsymbol{q}' = f(\boldsymbol{q}, \boldsymbol{p}) \\ \boldsymbol{p}' = g(\boldsymbol{q}, \boldsymbol{p}) \end{cases} \tag{1.68}$$

with $(\boldsymbol{q}, \boldsymbol{p}) \in \mathbb{R}^n \times \mathbb{R}^n$ and $\boldsymbol{f}$, $\boldsymbol{g}$ are real analytic functions for which the origin is an elliptic fixed point :

Definition 1.5.1 *A point* $(\boldsymbol{q}^*, \boldsymbol{p}^*)$ *is* elliptic *if the Jacobian matrix of the map (1.68) at this point admits only pure imaginary eigenvalues.*

We directly switch to complex variable as we did in Eq. (1.55) but keeping the $+$ sign :

$$\boldsymbol{z} = \boldsymbol{q} + i\boldsymbol{p} \qquad \text{and} \qquad \bar{\boldsymbol{z}} = \boldsymbol{q} - i\boldsymbol{p}$$

with i such that $i^2 = -1$ and the bar-symbol, $\bar{}$, denoting the complex conjugate (applying to every components z_k, $k = 1 \ldots n$). We also define

$$F = f + ig \,.$$

The initial map in real variables (1.68) reads now in complex variables

$$\boldsymbol{z}' = F(\boldsymbol{z}, \bar{\boldsymbol{z}}) \,. \tag{1.69}$$

We choose a norm on $\mathbb{C}^n$:

$$||\boldsymbol{z}|| := \max_{1 \leq i \leq n} |z_i| \qquad \boldsymbol{z} \in \mathbb{C}^n$$

and consider a holomorphic function $G : \mathbb{C}^{2n} \to \mathbb{C}^d$ on a polydisk

$$D_r := \{(\boldsymbol{z}, \boldsymbol{w}) \in \mathbb{C}^{2n} \ : \ ||\boldsymbol{z}|| \leq r, ||\boldsymbol{w}|| \leq r\}$$

with the jth component of G denoted by G^j and $G(\boldsymbol{0}) = \boldsymbol{0}$. The Taylor series of G is then

$$G(\boldsymbol{z}, \boldsymbol{w}) = \sum_{\boldsymbol{k} \in \mathbb{N}^{2n}, \ |\boldsymbol{k}| \geq 1} \boldsymbol{G_k} z_1^{k_1} w_1^{k_2} \ldots z_n^{k_{2n-1}} w_n^{k_{2n}} \tag{1.70}$$

where $|\boldsymbol{k}| = \sum_{i=1}^n |k_i|$ and $\boldsymbol{G_k} \in \mathbb{C}^n$. We also define its projection on the subspace of polynomials of order d with

$$[G]_d(\boldsymbol{z}, \boldsymbol{w}) := \sum_{k_1 + \cdots + k_{2n} = d} \boldsymbol{G_k} z_1^{k_1} w_1^{k_2} \ldots z_n^{k_{2n-1}} w_n^{k_{2n}} \,.$$

We thus have that

$$G(\boldsymbol{z}, \boldsymbol{w}) = \sum_{d \geq 1} [G]_d(\boldsymbol{z}, \boldsymbol{w}).$$

In the following we assume a Diophantine condition :

Definition 1.5.2 *The frequencies* $\boldsymbol{\omega}$ *satisfy a* Diophantine condition *if for some constants* $\gamma > 0$ *and* $\eta \geq n$ *one has*

$$|e^{i\boldsymbol{k}\cdot\boldsymbol{\omega}} - 1| \geq \gamma^{-1}|\boldsymbol{k}|^{-\eta} \text{ for all } \quad \boldsymbol{k} \in \mathbb{Z}^n\backslash\{\boldsymbol{0}\}$$

This condition is *stronger* than a non-resonant condition by requiring the term $|e^{i\boldsymbol{k}\cdot\boldsymbol{\omega}} - 1|$ not to be *too* small.

Remark 1.5.3 (A result from Normal Form theory) *With the above notations and considerations it was proven by [Bazzani et al., 1990] the exponentially long stability for a given set of initial conditions close to the origin. Unfortunately, the region described in this theorem is very small (a circle of radius* $10^{-2}, 10^{-3}$ *according to the examples) by comparison with what we shall obtain and thus not suitable for practical applications : see the application Chap. 5.*

We now introduce more formally the normal form.

Considering the vector $\boldsymbol{\omega} = (\omega_1 \ldots \omega_n)^t$ we introduce the notation

$$e^{i\boldsymbol{\omega}} = \text{diag}(e^{i\omega_1} \ldots e^{i\omega_n})$$

and then

$$e^{i\boldsymbol{\omega}}\boldsymbol{z} = (e^{i\omega_1} z_1 \ldots e^{i\omega_n} z_n)$$

We are looking for the following kind of map :

Definition 1.5.4 *A map* G *is a* normal form *if*

$$G(e^{i\boldsymbol{\omega}}\boldsymbol{z}, e^{-i\boldsymbol{\omega}}\bar{\boldsymbol{z}}) = e^{i\boldsymbol{\omega}}G(\boldsymbol{z}, \bar{\boldsymbol{z}})$$

So we are looking for a change of variables :

$$\boldsymbol{z} = \Phi(\boldsymbol{\zeta}, \bar{\boldsymbol{\zeta}}) \tag{1.71}$$

close to the identity such that the map in these variables :

$$\boldsymbol{\zeta}' = U(\boldsymbol{\zeta}, \bar{\boldsymbol{\zeta}})$$

is a normal form.

Φ *close to the identity* means that it will take the following form :

$$\Phi(\boldsymbol{\zeta}, \bar{\boldsymbol{\zeta}}) = \boldsymbol{\zeta} + \sum_{d\geq 2}[\Phi]_d(\boldsymbol{\zeta}, \bar{\boldsymbol{\zeta}}).$$

We have the following diagram representing the considered map and the conjugation equation with its normal form :

$$
\begin{array}{ccc}
\boldsymbol{z} & \overset{F}{\longrightarrow} & \boldsymbol{z}' \\
\Phi \uparrow & & \uparrow \Phi \\
\boldsymbol{\zeta} & \underset{U}{\longrightarrow} & \boldsymbol{\zeta}'
\end{array}
$$

Theorem 1.5.5 *A symplectic map G in normal form with $\boldsymbol{\omega}$ non-resonant takes the form*

$$
G(\boldsymbol{z}, \bar{\boldsymbol{z}}) = e^{i\Omega(\boldsymbol{z}, \bar{\boldsymbol{z}})} \boldsymbol{z} \tag{1.72}
$$

where

$$
\Omega(\boldsymbol{z}, \bar{\boldsymbol{z}}) = \Omega(|z_1|^2, \ldots, |z_n|^2)
$$

is real valued function.

The result shows that, in the new variables, the map is simply a rotation with a non-constant angle.

Proof. Let us consider only the jth component of G, namely G^j, that reads, expanded in integer series

$$
G^j(\boldsymbol{z}, \bar{\boldsymbol{z}}) = \sum_{|\boldsymbol{k}| \geq 1} G^j_{\boldsymbol{k}} z_1^{k_1} \bar{z}_1^{k_2} \ldots z_n^{k_{2n-1}} \bar{z}_n^{k_{2n}}. \tag{1.73}
$$

Considering $\boldsymbol{G}$ to be in normal form, we have

$$
\begin{aligned}
G^j(e^{i\boldsymbol{\omega}} \boldsymbol{z}, e^{-i\boldsymbol{\omega}} \bar{\boldsymbol{z}}) &= e^{i\omega_j} G^j(\boldsymbol{z}, \bar{\boldsymbol{z}}) \\
&= \sum_{|\boldsymbol{k}| \geq 1} G^j_{\boldsymbol{k}} z_1^{k_1} \bar{z}_1^{k_2} \ldots z_n^{k_{2n-1}} \bar{z}_n^{k_{2n}} e^{i\omega_j}
\end{aligned} \tag{1.74}
$$

and, using Eq. (1.73) :

$$
G^j(e^{i\boldsymbol{\omega}} \boldsymbol{z}, e^{-i\boldsymbol{\omega}} \bar{\boldsymbol{z}}) = \sum_{|\boldsymbol{k}| \geq 1} G^j_{\boldsymbol{k}} z_1^{k_1} \bar{z}_1^{k_2} \ldots z_n^{k_{2n-1}} \bar{z}_n^{k_{2n}} e^{i\omega_1(k_1-k_2)} \ldots e^{i\omega_n(k_{2n-1}-k_{2n})}.
$$

$$\tag{1.75}$$

We want Eqs. (1.74) and (1.75) to be equal. We obtain it if (considering the general case where $G^j_{\boldsymbol{k}} \neq 0$) :

$$
\begin{cases}
k_{2m-1} = k_{2m} & \text{for} \quad m = 1 \ldots n\,, m \neq j \\
k_{2j-1} = k_{2j} + 1
\end{cases} \tag{1.76}
$$

With this condition, Eq. (1.73) reads

$$G^j(\boldsymbol{z}, \bar{\boldsymbol{z}}) = z_j \sum_{|\boldsymbol{k}| \geq 1} G^j_{\boldsymbol{k}} |z_1|^2 \cdots |z_n|^2$$

$$=: z_j \phi_j(|z_1|^2, \ldots, |z_n|^2)$$

$$=: z_j e^{\Psi_j(|z_1|^2, \ldots, |z_n|^2)}$$

and we can write, including all components

$$G(\boldsymbol{z}, \bar{\boldsymbol{z}}) = e^{\Psi(|z_1|^2, \ldots, |z_n|^2)} \boldsymbol{z}.$$

Now we consider the symplectic condition in the complex variables $(\boldsymbol{z}, \bar{\boldsymbol{z}})$:

$$\{G^j, \bar{G}^k\} = \delta_{jk}. \tag{1.77}$$

We also use the notation $\rho_l = z_l \bar{z}_l$ and remark that

$$\frac{\partial \Psi_j}{\partial z_l} = \sum_m \frac{\partial \Psi_j}{\partial \rho_m} \frac{\partial \rho_m}{\partial z_l} = \frac{\partial \Psi_j}{\partial \rho_l} \bar{z}_l.$$

Now, we develop the left hand side of Eq. (1.77) :

$$\{G^j, \bar{G}^k\} = \{z_j e^{\Psi_j}, \bar{z}_k e^{\bar{\Psi}_k}\}$$

$$= \sum_{l=1}^n \frac{\partial}{\partial z_l}\left(z_j e^{\Psi_j}\right) \frac{\partial}{\partial \bar{z}_l}\left(\bar{z}_k e^{\bar{\Psi}_k}\right) - \frac{\partial}{\partial \bar{z}_l}\left(z_j e^{\Psi_j}\right) \frac{\partial}{\partial z_l}\left(\bar{z}_k e^{\bar{\Psi}_k}\right)$$

$$= \sum_{l=1}^n \left[\left(\delta_{jl} e^{\Psi_j} + z_j e^{\Psi_j} \frac{\partial \Psi_j}{\partial \rho_l} \bar{z}_l\right)\left(\delta_{kl} e^{\bar{\Psi}_k} + \bar{z}_k e^{\bar{\Psi}_k} \frac{\partial \bar{\Psi}_k}{\partial \rho_l} z_l\right)\right.$$

$$\left. - \left(z_j e^{\Psi_j} \frac{\partial \Psi_j}{\partial \rho_l} z_l\right)\left(\bar{z}_k e^{\bar{\Psi}_k} \frac{\partial \bar{\Psi}_k}{\partial \rho_l} \bar{z}_l\right)\right]$$

$$= \delta_{kj} e^{\Psi_j + \bar{\Psi}_k} + e^{\Psi_j + \bar{\Psi}_k} \bar{z}_k \frac{\partial \bar{\Psi}_k}{\partial \rho_j} z_j + e^{\Psi_j + \bar{\Psi}_k} \bar{z}_k \frac{\partial \bar{\Psi}_j}{\partial \rho_k} z_j.$$

Condition (1.77) becomes

$$\delta_{jk} = e^{\Psi_k + \bar{\Psi}_k}\left[\delta_{jk} + \rho_k\left(\frac{\partial \bar{\Psi}_k}{\partial \rho_k} + \frac{\partial \Psi_k}{\partial \rho_k}\right)\right]$$

This is solved if

$$\bar{\Psi}_k + \Psi_k = 0$$

whose solution is

$$\Psi_k = i\Omega_k$$

with Ω real. This concludes the proof.

$\square$

Using the desired normal form (1.72) and the change of variables (1.71), we want to find the change of variables Φ and the rotation vector Ω such that the following functional equation

$$F(\Phi(\boldsymbol{\zeta},\bar{\boldsymbol{\zeta}}),\bar{\Phi}(\boldsymbol{\zeta},\bar{\boldsymbol{\zeta}})) = \Phi(e^{i\Omega}\boldsymbol{\zeta}, e^{-i\Omega}\bar{\boldsymbol{\zeta}}) \qquad (1.78)$$

is solved. Since no analytical solutions are known to exist in a neighborhood of the origin, we solve Eq. (1.78) order by order considering Φ and Ω polynomial functions of type (1.70). The solution (Φ, U) is not unique : if it satisfies (1.78) then the couple (Φ^*, U) where

$$\Phi^* := e^{i\Xi}\Phi \qquad (1.79)$$

with $\Xi = \Xi(|\zeta_1|^2, \ldots, |\zeta_n|^2)$ real, is also a solution. In [Bazzani et al., 1994] it is explicitly stated :

Theorem 1.5.6 *Let us consider the functional equation (1.78) where the normal form is done with respect to the group generated by the linear part $e^{i\boldsymbol{\omega}}$. Then it is possible to compute the normal form solution, i.e. the Taylor expansion at all orders of Φ and U ; this solution is unique up to a gauge group (see Eq. 1.79).*

Invariant. It is interesting to show that there exists an invariant, the so-called *interpolating* Hamiltonian system, H such that

$$\boldsymbol{\zeta}' = e^{\{H\}}\boldsymbol{\zeta}.$$

Indeed, a direct computation of the time-one flow of H gives

$$e^{\{H\}}\zeta_d := \sum_{l\geq 0}\frac{\{H\}^l}{l!}\zeta_d = \sum_{l\geq 0}\frac{1}{l!}\left(\frac{\partial H}{\partial\rho_d}\right)^l\zeta_d = e^{\frac{\partial H}{\partial\rho_d}}\zeta_d \qquad d = 1\ldots n$$

where $\rho_d = \zeta_d\bar{\zeta}_d$. And thus we have the following relation

$$i\Omega_d = \frac{\partial H}{\partial\rho_d} \qquad d = 1\ldots n$$

This Hamiltonian system is thus purely complex and depends only on the modulus of each component of $\boldsymbol{\zeta}$: $H(\boldsymbol{\zeta},\bar{\boldsymbol{\zeta}}) \equiv H(|\zeta_1|^2, \ldots, |\zeta_n|^2)$.

Different algorithms exist in order to solve Eq. (1.78) up to a certain order giving the change of coordinates and its inverse, the interpolating Hamiltonian system and other informations, see [Bazzani et al., 1995, Todesco et al., 1997] [13] or, more recently [Giorgilli, 2013].

In the following we calculate the first orders for a specific map with $n = 1$ so that we can understand the first steps of the iterative process.

---

13. The described programs are for the case $n = 2$.

1.5.2   Application to the Hénon map

We consider the Hénon map (1.57) :

$$z' = e^{i\omega}\left(z + \frac{i}{4}(z + \bar{z})^2\right) \tag{1.80}$$

with $z \in \mathbb{C}$. We are thus in the case $n = 1$ of the previous paragraph, i.e. a $2D$ map in real variables. We consider a non-resonant condition on ω and because we are interested in rotation, we write that condition as follows

$$\frac{\omega}{2\pi} \in \mathbb{R}/\mathbb{Q}.$$

We conjugate (1.80) to a normal form

$$\zeta' = U(\zeta, \bar{\zeta}) = e^{i\Omega(\zeta\bar{\zeta})}\zeta$$

via the close to identity conjugation

$$z = \Phi(\zeta, \bar{\zeta}) = \zeta + \sum_{d \geq 2}[\Phi]_d(\zeta, \bar{\zeta})$$

The unknown functions U and Φ are determined with the functional Eq. (1.78), in compact form :

$$F \circ \Phi = \Phi \circ U \tag{1.81}$$

where $\circ$ denotes the composition : for instance $F \circ \Phi = F(\Phi, \bar{\Phi})$.

We shall now explicitly compute the first orders of the normal form and the conjugation. For that reason, we express F, U and Φ emphasizing the coefficients with the following developments

$$z' = F(z, \bar{z}) = \sum_{d \geq 1}[F]_d(z, \bar{z}) = e^{i\omega}z + \sum_{d \geq 2}\sum_{k=0}^{d}f_{k,d-k}z^k\bar{z}^{n-k},$$

$$\zeta' = U(\zeta, \bar{\zeta}) = \sum_{d \geq 1}[U]_d(\zeta, \bar{\zeta}) = e^{i\Omega_0}\zeta + \sum_{d \geq 2}\sum_{k=0}^{d}u_{k,d-k}\zeta^k\bar{\zeta}^{n-k},$$

and

$$z = \Phi(\zeta, \bar{\zeta}) = \sum_{d \geq 1}[\Phi]_d(\zeta, \bar{\zeta}) = \zeta + \sum_{d \geq 2}\sum_{k=0}^{d}\phi_{k,d-k}\zeta^k\bar{\zeta}^{n-k}.$$

We proceed a bit differently for the normal form because of its special form, i.e. it has no contribution of even order :

$$[U]_{2k}(\zeta, \bar{\zeta}) = 0 \quad \forall k \in \mathbb{N},$$

and the odd contribution will always be of type $\zeta^k \bar{\zeta}^{k-1}$ with $k \geq 1$. Indeed, Ω depends only on $\zeta\bar{\zeta}$ and thus :

$$\Omega(\zeta\bar{\zeta}) = \Omega_0 + \Omega_2 \zeta\bar{\zeta} + \mathcal{O}(|\zeta|^4).$$

so that

$$U(\zeta, \bar{\zeta}) = \exp(i\Omega(\zeta\bar{\zeta}))\zeta = e^{i\Omega_0}\zeta + ie^{i\Omega_0}\Omega_2\zeta^2\bar{\zeta} + \mathcal{O}(|\zeta|^5).$$

Before going on let us give the coefficient of the initial map F :

$$f_{02} = f_{20} = \frac{i}{4}e^{i\omega} \qquad f_{11} = 2f_{20} \qquad f_{k,d-k} = 0 \quad d \geq 3, \ 0 \leq k \leq d.$$

First order.

The projection of Eq. (1.81) on the subspace of polynomials of order 1 gives :

$$[F \circ \Phi]_1(\zeta, \bar{\zeta}) = e^{i\omega}\zeta$$

and

$$[\Phi \circ U]_1(\zeta, \bar{\zeta}) = e^{i\Omega_0}\zeta.$$

It comes that

$$\Omega_0 = \omega.$$

Second order.

We proceed similarly on the subspace of polynomials of order 2 for the functional equation :

$$
\begin{aligned}
[F \circ \Phi]_2(\zeta, \bar{\zeta}) &= [e^{i\omega}\Phi(\zeta, \bar{\zeta}) + [F]_2(\Phi, \bar{\Phi})]_2 \\
&= e^{i\omega}[\Phi]_2(\zeta, \bar{\zeta}) + [F]_2(\zeta, \bar{\zeta}) \\
&= e^{i\omega}(\phi_{20}\zeta^2 + \phi_{02}\bar{\zeta}^2 + \phi_{11}\zeta\bar{\zeta}) + f_{20}\zeta^2 + f_{02}\bar{\zeta}^2 + f_{11}\zeta\bar{\zeta}
\end{aligned}
\tag{1.82}
$$

and

$$
\begin{aligned}
[\Phi \circ U]_2(\zeta, \bar{\zeta}) &= [U(\zeta, \bar{\zeta}) + [\Phi]_2(U, \bar{U})]_2 \\
&= e^{2i\omega}\phi_{20}\zeta^2 + e^{-2i\omega}\phi_{02}\bar{\zeta}^2 + \phi_{11}\zeta\bar{\zeta}.
\end{aligned}
\tag{1.83}
$$

By equating both sides of the functional equation at order 2, that is Eqs (1.82) and (1.83), we get the system

$$
\begin{cases}
e^{i\omega}\phi_{20} + f_{20} = e^{2i\omega}\phi_{20} \\
e^{i\omega}\phi_{02} + f_{02} = e^{-2i\omega}\phi_{02} \\
e^{i\omega}\phi_{11} + f_{11} = \phi_{11}
\end{cases}
$$

which is solved by

$$
\begin{cases}
\phi_{20} = \dfrac{i}{4(e^{i\omega} - 1)} \\[3mm]
\phi_{02} = \dfrac{ie^{3i\omega}}{4(1 - e^{3i\omega})} \\[3mm]
\phi_{11} = \dfrac{ie^{i\omega}}{2(1 - e^{i\omega})}
\end{cases}
$$

because of the non-resonance condition such solution is well defined.

Third order.

We proceed similarly. The left hand side of order 3 of the functional equation is

$$[F \circ \Phi]_3(\zeta, \bar{\zeta}) = e^{i\omega}[\Phi]_3(\zeta, \bar{\zeta}) + [[F]_2(\Phi, \bar{\Phi})]_3$$

whose parts are

$$e^{i\omega}[\Phi]_3(\zeta, \bar{\zeta}) = e^{i\omega} \left(\phi_{30}\zeta^3 + \phi_{03}\bar{\zeta}^3 + \phi_{21}\zeta^2\bar{\zeta} + \phi_{12}\zeta\bar{\zeta}^2 \right)$$

and

$$[[F]_2(\Phi, \bar{\Phi})]_3 = \frac{i}{4} \left[\left(\zeta + [\Phi]_2(\zeta, \bar{\zeta}) + \bar{\zeta} + \overline{[\Phi]_2(\zeta, \bar{\zeta})} \right)^2 \right]_3$$

$$= \frac{i}{2} e^{i\omega} \left(\zeta^3(\phi_{20} + \bar{\phi}_{02}) + \zeta^2\bar{\zeta}(\phi_{20} + \bar{\phi}_{02} + \phi_{11} + \bar{\phi}_{11}) \right.$$

$$\left. + \bar{\zeta}^3(\phi_{02} + \bar{\phi}_{20}) + \zeta\bar{\zeta}^2(\phi_{02} + \bar{\phi}_{20} + \phi_{11} + \bar{\phi}_{11}) \right) .$$

Now, the right hand side of order 3 is

$$[\Phi \circ U]_3 = [\Phi]_3(e^{i\omega}\zeta, e^{-i\omega}\bar{\zeta}) + [[\Phi]_2(U, \bar{U})]_3 + [U]_3(\zeta, \bar{\zeta})$$

with

$$[\Phi]_3(e^{i\omega}\zeta, e^{-i\omega}\bar{\zeta}) = e^{3i\omega}\phi_{30}\zeta^3 + e^{-3i\omega}\phi_{03}\bar{\zeta}^3 + e^{i\omega}\phi_{21}\zeta^2\bar{\zeta} + e^{-i\omega}\phi_{12}\zeta\bar{\zeta}^2 ,$$

$$[[\Phi]_2(U, \bar{U})]_3 = 0$$

and

$$[U]_3(\zeta, \bar{\zeta}) = ie^{i\omega}\Omega_2\zeta^2\bar{\zeta}.$$

Therefore one has

$$\begin{cases} (e^{3i\omega} - e^{i\omega})\phi_{30} = \dfrac{i}{2}e^{i\omega}(\phi_{20} + \bar{\phi}_{02}) \\[2mm] (e^{-3i\omega} - e^{i\omega})\phi_{03} = \dfrac{i}{2}e^{i\omega}(\phi_{02} + \bar{\phi}_{20}) \\[2mm] ie^{i\omega}\Omega_2 = \dfrac{i}{2}e^{i\omega}(\phi_{20} + \bar{\phi}_{02} + \phi_{11} + \bar{\phi}_{11}) \\[2mm] (e^{-i\omega} - e^{i\omega})\phi_{12} = \dfrac{i}{2}e^{i\omega}(\phi_{02} + \bar{\phi}_{20} + \phi_{11} + \bar{\phi}_{11}) \end{cases}$$

which is solved by

$$\begin{cases} \phi_{30} = \dfrac{i(\phi_{20} + \bar{\phi}_{02})}{2(e^{2i\omega} - 1)} \\[3mm] \phi_{03} = \dfrac{i(\phi_{02} + \bar{\phi}_{20})e^{4i\omega}}{2(1 - e^{i\omega})} \\[3mm] \Omega_2 = \dfrac{1}{2}(\phi_{20} + \bar{\phi}_{02} + \phi_{11} + \bar{\phi}_{11}) \\[3mm] \phi_{12} = \dfrac{i(\phi_{02} + \bar{\phi}_{20} + \phi_{11} + \bar{\phi}_{11})e^{2i\omega}}{2(1 - e^{2i\omega})} \end{cases}$$

We notice that we do not have conditions on ϕ_{21}. As we already pointed out there is no unique solution for the NF. This value can be fixed in order to make Φ symplectic for example.

The procedure we followed for the first 3 orders can be generalized, see for example the program ARES [Bazzani et al., 1995] or follow [Giorgilli, 2013]. We used the later to plot in Fig. 1.15, the normal form of the Hénon map in the z and ζ planes. We used 10^3 iterations and the coefficients of the normal form were taken up to order 6.
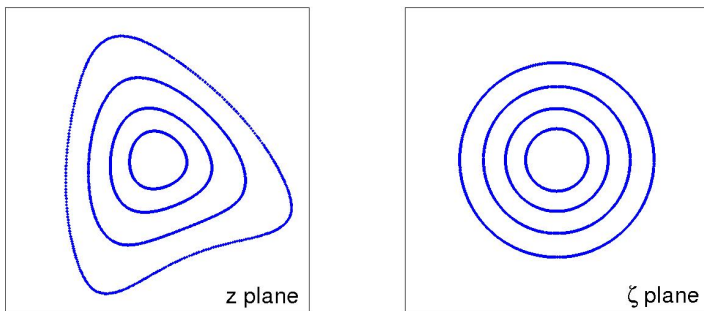

FIGURE 1.15: Map (1.80) in the z plane (left) and in the normal form ζ plane (right).

Chapitre 2

The model

Contents

   The goal of this chapter is to derive a 4 dimensional map mo-
delling the dynamics of a circular particle accelerator. We sketch
the main steps and approximations in order to pass from Lorentz
equation to the map.
Two sections compose the chapter. In the first one we make some
assumptions and approximations, we present a development of the
magnetic field and obtain a set of 2 ordinary differential equations
of order 2 representing the dynamics under study. In the second
part we first consider the linear terms of these equations and intro-
duce the ingredients of maps. Finally we consider one way, the *thin
lens approximation*, to include nonlinearities in the maps.

   These two sections are the result of various readings, often pre-
senting same concepts with different scale of details or interpreta-
tion. We mainly focused on
   – [Scandale and Turchetti, 1990], proceedings treating nonlinear
     problems in particle accelerator where we especially consulted
     the contributions of Turchetti, Bountis, Giorgilli and Forest ;
   – [Turner, 1994] focusing on the work of Rossbach and Schmüser
     in parallel with [Steffen, 1985] and [Lee, 2012] for the first
     section ;
   – [Bazzani et al., 1994, Scandale and Turchetti, 1990] for the se-
     cond section.
We found details and useful complementary information in the follo-
wing references [Servizi and Turchetti, 1986], [Bazzani et al., 1988],
[Henke et al., 1992], [Forest, 1998], [Wilson, 2001], [Close, 2004],
[Chao and Chou, 2008] and [MacKay and Conte, 2012].

2.1   Equations of motion

2.1.1   In a fixed coordinate system

In accelerator physics, there is one curve, *the design orbit*, that all particles
should follow (see Fig. 2.1). This is the ideal case : in reality many particles
will deviate from that orbit. In order to make these deviations small, focusing
forces are required. In this chapter we consider curved orbits for which bending
forces are also needed. We thus need both bending and focusing forces. This
is effectively obtained with electromagnetic fields which exert on the particles
the Lorentz force

$$\boldsymbol{F} = e(\boldsymbol{E} + \boldsymbol{v} \times \boldsymbol{B}) \tag{2.1}$$

where e is the electron charge and $\boldsymbol{E}$ and $\boldsymbol{B}$ respectively the electric and ma-
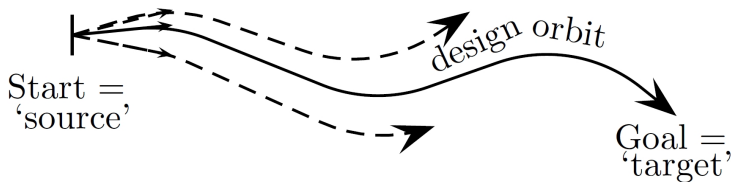gnetic fields.

FIGURE 2.1: A curved design orbit where bending elements are required (magnets).

Standard values for high velocities $v \approx c$ and moderate [1] magnetic field of 1 Tesla give

$$Bv \approx 3 \cdot 10^8 \frac{m}{s} \frac{Vs}{m^2} = 3 \cdot 10^8 \frac{V}{m}.$$

Thus a magnetic field of one Tesla gives the same bending force as an electric field of 300 million Volts per meter for relativistic particles. Because of this large scale separation, we therefore only consider transverse magnetic fields. Eq. 2.1 thus becomes

$$\boldsymbol{F} = e(\boldsymbol{v} \times \boldsymbol{B}) \tag{2.2}$$

where we consider relativistic particles.

Also, we consider the total energy of the particle

$$E = \frac{m_0 c^2}{\sqrt{1 - \frac{v^2}{c^2}}}$$

and we recall [Benson, 1999] that its variation with time in the presence of an external force is

$$\dot{E} = \boldsymbol{v} \cdot \boldsymbol{F}$$

where we use the *dot* notation $(\dot{\ }) = \frac{d}{dt}(\ )$. Since $\boldsymbol{v}$ is perpendicular (Eq. (2.2)) to $\boldsymbol{v} \times \boldsymbol{B}$ which is proportional to $\boldsymbol{F}$, we have that $\boldsymbol{v} \cdot \boldsymbol{F} = 0$ and thus the energy and the relativistic mass are constant in static magnetic fields. Finally the equation of motion reads

$$\dot{\boldsymbol{v}} = \frac{e}{m}(\boldsymbol{v} \times \boldsymbol{B}) \tag{2.3}$$

where we use the relation $\boldsymbol{F} = m\dot{\boldsymbol{v}}$.

---

1. Neodymium magnets, available in classical stores, and used, for example, in hard disk drive, produce a magnetic field of the order of 1 Tesla [Thiry, 2002].

We now fix a Cartesian coordinate system $\{y, x, s\}$ [2] and rewrite the position vector $\boldsymbol{r}$ in such coordinates :

$$\boldsymbol{r} = y\boldsymbol{y}_0 + x\boldsymbol{x}_0 + s\boldsymbol{s}_0$$
$$\boldsymbol{v} = \dot{\boldsymbol{r}} = \dot{y}\boldsymbol{y}_0 + \dot{x}\boldsymbol{x}_0 + \dot{s}\boldsymbol{s}_0$$
$$\dot{\boldsymbol{v}} = \ddot{\boldsymbol{r}} = \ddot{y}\boldsymbol{y}_0 + \ddot{x}\boldsymbol{x}_0 + \ddot{s}\boldsymbol{s}_0$$

that we can insert in Eq. 2.3. The result is

$$\ddot{y} = \frac{e}{m}(\dot{x}B_s - \dot{s}B_x)$$
$$\ddot{x} = \frac{e}{m}(\dot{s}B_y - \dot{y}B_s)$$
$$\ddot{s} = \frac{e}{m}(\dot{y}B_x - \dot{x}B_y)$$

where the components of the magnetic field in this coordinate system were used : $\boldsymbol{B} = (B_y \; B_x \; B_s)^t$.

As we shall see in the following, it is convenient to follow the evolution of a particle along the s axis instead of the classical time t. For that purpose, we insert primed variables instead of dotted ones :

$$y' = \frac{dy}{ds} \quad \text{and} \quad x' = \frac{dx}{ds}.$$

We find [3]

$$\dot{y} = y'\dot{s} \qquad\qquad\qquad \dot{x} = x'\dot{s} \qquad\qquad (2.4)$$
$$\ddot{y} = y''\dot{s}^2 + y'\ddot{s} \qquad\qquad \ddot{x} = x''\dot{s}^2 + x'\ddot{s} \qquad\qquad (2.5)$$

and thus

$$\ddot{s} = \frac{e}{m}\dot{s}(y'B_x - x'B_y)v^2 = \dot{s}^2 + \dot{y}^2 + \dot{x}^2 = \dot{s}^2(1 + y'^2 + x'^2). \qquad (2.6)$$

We thereby obtain the trajectory equations in the fixed coordinate system along the s variable

$$\boxed{\begin{aligned} y'' &= \tfrac{v}{\dot{s}}\tfrac{e}{p}\left(x'B_s - (1 + y'^2)B_x + x'y'B_y\right) \\ x'' &= -\tfrac{v}{\dot{s}}\tfrac{e}{p}\left(y'B_s - (1 + x'^2)B_y + x'y'B_x\right) \end{aligned}}$$

with

$$\frac{v}{\dot{s}} = \sqrt{1 + y'^2 + x'^2} \quad \text{and} \quad p = mv$$

---

2. The choice of the letters and the order y, x and s is classical in particle accelerator physics literature.

3. $\ddot{y} = \frac{d}{dt}(\dot{y}) = \frac{d}{dt}(y'\dot{s}) = \frac{ds}{dt}\frac{d}{ds}(y'\dot{s}) = \dot{s}\left(\frac{d}{ds}(y')\dot{s} + \frac{d}{ds}(\dot{s})y'\right) = y''\dot{s}^2 + y'\underbrace{\frac{ds}{dt}\frac{d}{ds}\frac{ds}{dt}}_{=\ddot{s}}$

2.1.2 In a curved coordinate system

Homogeneous field, radius and curvature

From now on we consider the design orbit to be a circle and study a simplified case where there is only a vertical constant magnetic field :

$$B_x \equiv B_s \equiv 0 \qquad \text{and} \qquad B_y \equiv B = \text{const.}$$

Then, comparing the pseudo centrifugal force and the Lorentz force it comes

$$evB_y = -\frac{mv^2}{\rho} \Rightarrow \frac{e}{p}B_y = -\frac{1}{\rho}$$

that quantifies the magnetic field B_y at first order and conversely for ρ. To convince ourselves, we can obtain the same result evaluating the curvature [4] :

$$\kappa := \frac{x''}{(1 + x'^2)^{3/2}} = \frac{e}{p}B_y = \text{const.} =: -\frac{1}{\rho}.$$

Curved coordinate system

We choose the reference trajectory, the center of the beam, in the plane $y \equiv 0$ and we want to describe particle trajectories nearby that reference trajectory. We introduce a right handed rectangular system of coordinate $\{y, x, s\}$ that follows this trajectory, see Fig. 2.2.
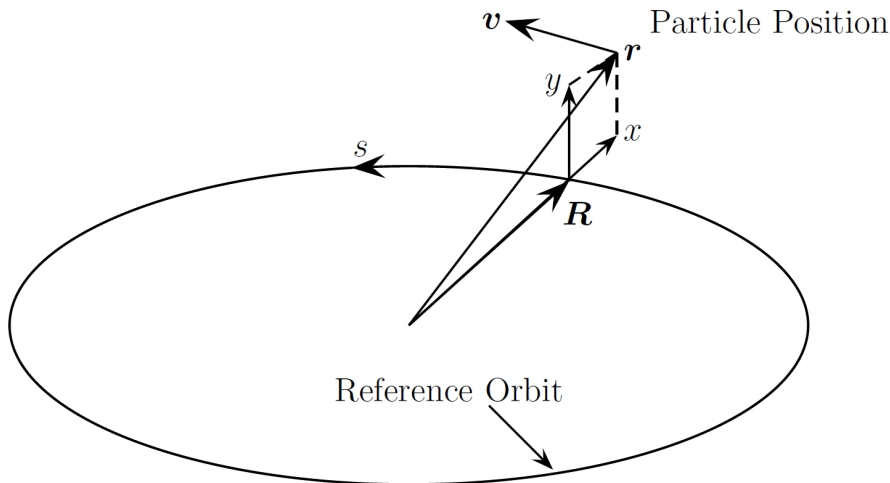

FIGURE 2.2: Curved system coordinates

It is also often (e.g. [Turner, 1994]) described thanks to a cylindrical coordinate system $\{y, r, \phi\}$: put $r = \rho + x$ and for s small, $\phi = s/\rho$.

---

4. We set $y'_0 = 0$ as initial condition to simplify the calculations.

Equations of motion

We now write down the trajectory equations in the curved coordinate system. First, we recall the derivatives with respect to time of the moving axis :

$$\begin{cases} \dot{\boldsymbol{y}}_0 = \boldsymbol{0} \\[2mm] \dot{\boldsymbol{x}}_0 = \dfrac{\dot{s}}{\rho}\boldsymbol{s}_0 \\[2mm] \dot{\boldsymbol{s}}_0 = -\dfrac{\dot{s}}{\rho}\boldsymbol{x}_0 \end{cases}$$

With the vector $\boldsymbol{R}$ joining the fixed frame to the moving one, i.e. $\boldsymbol{R} = \rho\boldsymbol{x}_0$, we find the following equations for the position, the speed and the acceleration :

$$\boldsymbol{r} = \boldsymbol{R} + y\boldsymbol{y}_0 + x\boldsymbol{x}_0 \tag{2.7}$$

$$\dot{\boldsymbol{r}} = \dot{y}\boldsymbol{y}_0 + \dot{x}\boldsymbol{x}_0 + \dot{s}(1 + \frac{x}{\rho})\boldsymbol{s}_0 \tag{2.8}$$

$$\ddot{\boldsymbol{r}} = \ddot{y}\boldsymbol{y}_0 + \left(\ddot{x} - \frac{\dot{s}^2}{\rho}(1 + \frac{x}{\rho}) \right)\boldsymbol{x}_0 + \left(2\dot{x}\frac{\dot{s}}{\rho} + \ddot{s}(1 + \frac{x}{\rho}) \right)\boldsymbol{s}_0 \tag{2.9}$$

where we use $\dot{\boldsymbol{R}} = \dot{s}\boldsymbol{s}_0$.

We set again

$$y' = \frac{dy}{ds} \quad \text{and} \quad x' = \frac{dx}{ds}.$$

Thus we find that

$$\frac{v}{\dot{s}} = \sqrt{\left(1 + \frac{x}{\rho} \right)^2 + y'^2 + x'^2}$$

and, by differentiation,

$$\frac{\ddot{s}}{\dot{s}^2} = -\frac{1}{2}\frac{(v^2/\dot{s}^2)'}{v^2/\dot{s}^2}$$

We can now write the equation of motion using the Lorentz equation (2.3) :

$$\boxed{\begin{aligned} y'' + \frac{\ddot{s}}{\dot{s}^2}y' &= \frac{v}{\dot{s}}\frac{e}{p}\left(x'B_s - (1 + \frac{x}{\rho})B_x \right) \\ x'' + \frac{\ddot{s}}{\dot{s}^2}x' - \frac{1}{\rho}(1 + \frac{x}{\rho}) &= -\frac{v}{\dot{s}}\frac{e}{p}\left(y'B_s - (1 + \frac{x}{\rho})B_y \right) \end{aligned}} \tag{2.10}$$

2.1.3   Magnetic field expansion

In this paragraph we derive an expansion of the magnetic field $\boldsymbol{B}$. There exist different (and various) ways to proceed : expansion of the magnetic field $\boldsymbol{B}$, expansion of the vector potential $\boldsymbol{A}$, expansion of the scalar potential V or other combinations in different choices of coordinates. These choices are related to the specificity of the considered problem [Wilson, 2001]. Following [Turner, 1994],

we present an expansion both in $\boldsymbol{A}$ and V.

We shall use complex variables and for that reason we use the conventional coordinates notation $z = x + iy$ where y is the vertical coordinate and x the horizontal one.

Also we consider the magnets to be long in front of their section radius : in this way the effect of the field at the termination of the magnet will be rather small. We thus do not consider these edge effects. Let us remark that this assumption is dedicated to this specific problem and that in many other cases these side contributions should be (and are) taken into account.

We consider a two dimensional field that verifies the second of the Maxwell's equations :

$$\nabla \cdot \boldsymbol{B} = 0 \,.$$

It comes that there exists a vector potential $\boldsymbol{A}$ such that

$$\boldsymbol{B} = \nabla \times \boldsymbol{A} \,.$$

The vector potential $\boldsymbol{A}$ has only a component in the s direction because of the transversality of the magnetic field :

$$\boldsymbol{A} = \left(\begin{array}{c} 0 \\ 0 \\ A_s \end{array} \right)$$

and we can write $\boldsymbol{B}$ in this component

$$\boldsymbol{B} = \left(\begin{array}{c} B_y \\ B_x \\ B_s \end{array} \right) = \nabla \times \boldsymbol{A} = \left(\begin{array}{c} \partial A_s / \partial y \\ -\partial A_s / \partial x \\ 0 \end{array} \right) \,.$$

This implies that $\boldsymbol{B}$ derives from a scalar potential V :

$$\boldsymbol{B} = -\nabla V$$

and we find the relations

$$B_x = -\frac{\partial V}{\partial x} = \frac{\partial A_s}{\partial y} \qquad \text{and} \qquad B_y = -\frac{\partial V}{\partial y} = -\frac{\partial A_s}{\partial x} \,. \qquad (2.11)$$

We now define a complex potential function of $z = x + iy$ by

$$\varphi(z) = A_s(x,y) + iV(x,y)$$

with Eqs. (2.11) being the Cauchy-Riemann conditions for the real and imaginary part of an analytic function. Indeed, we have that

$$\frac{\partial \varphi}{\partial x} + i \frac{\partial \varphi}{\partial y} = 0.$$

The complex function $\varphi(z)$ is thus analytic and therefore can be expanded in a power series :

$$\varphi(z) = \sum_{n=0}^{\infty} \varphi_n z^n \qquad \text{with} \qquad \varphi_n = \lambda_n + i\mu_n . \tag{2.12}$$

This series is convergent within a radius r_c.

It is also convenient to introduce the largest conceivable deviation of beam particles from the reference orbit. We denote [5] this quantity by r_0. For example, $r_0 = 1$cm for the LHC [Lee, 2012]. We shall also call B_{main} the magnitude of the main field component. Those two quantities allow us to rescale the coefficients λ_n and μ_n to obtain the *normal* multipole coefficients b_n and the *skew* multipole coefficients a_n :

$$b_n = -\frac{n\lambda_n}{B_{main}}r_0^{n-1} \qquad \text{and} \qquad a_n = \frac{n\mu_n}{B_{main}}r_0^{n-1} \tag{2.13}$$

with $b_0 = a_0 = 0$ since they will not contribute to the magnetic field.

Now, using Eqs. (2.12) and (2.13), we find

$$
\begin{aligned}
A_s(x,y) =& \Re \sum_{n=0}^{\infty} \varphi_n z^n \\
=& -B_{main}\left(b_1 x + a_1 y + \frac{b_2}{2r_0}(x^2 - y^2) + \frac{a_2}{r_0}xy + \frac{b_3}{3r_0^2}(x^3 - 3xy^2) + \right. \\
& \left. \frac{a_3}{3r_0^2}(3x^2 y - y^3) + \frac{b_4}{4r_0^3}(x^4 - 6x^2 y^2 + y^4) + \frac{a_4}{r_0^3}(x^3 y - xy^3) \pm \dots \right) \\
V(x,y) =& \Im \sum_{n=0}^{\infty} \varphi_n z^n \\
=& B_{main}\left(a_1 x - b_1 y + \frac{a_2}{2r_0}(x^2 - y^2) - \frac{b_2}{r_0}xy + \frac{a_3}{3r_0^2}(x^3 - 3xy^2) - \right. \\
& \left. \frac{b_3}{3r_0^2}(3x^2 y - y^3) + \frac{a_4}{4r_0^3}(x^4 - 6x^2 y^2 + y^4) - \frac{b_4}{r_0^3}(x^3 y - xy^3) \pm \dots \right)
\end{aligned}
$$

---

5. We distinguished r_0 and r_c because r_c depends on the series expansion while r_0 is chosen as parameter according to the accelerator. In this case $r_0 \approx r_c$.

We can now express the magnetic field, using for example the gradient of V :

$$
\begin{aligned}
B_x(x,y) = B_{main} & \left(-a_1 + \frac{b_2}{r_0}y - \frac{a_2}{r_0}x - \frac{a_3}{r_0^2}(x^2 - y^2) + \right. \\
& \left. \frac{b_3}{r_0^2}2xy - \frac{a_4}{r_0^3}(x^3 - 3xy^2) + \frac{b_4}{r_0^3}(3x^2y - y^3) \pm \dots \right) \\
B_y(x,y) = B_{main} & \left(b_1 + \frac{a_2}{r_0}y + \frac{b_2}{r_0}x + \frac{a_3}{r_0^2}2xy + \right. \\
& \left. \frac{b_3}{r_0^2}(x^2 - y^2) + \frac{a_4}{r_0^3}(3x^2y - y^3) + \frac{b_4}{r_0^3}(x^3 - 3xy^2) \pm \dots \right)
\end{aligned}
$$

or, in a more compact form,

$$
B_y + iB_x = B_{main} \sum_{n=1}^{\infty} (b_n + ia_n) \left(\frac{x}{r_0} + i\frac{y}{r_0} \right)^{n-1} \tag{2.14}
$$

Similarly, we can use polar coordinates (r, ϕ) :

$$
x = r\cos\phi \quad y = r\sin\phi \quad z^n = r^n(\cos n\phi + i\sin n\phi)
$$

to get

$$
B_\phi(r,\phi) = B_{main} \sum_{n=1}^{\infty} (b_n \cos n\phi + a_n \sin n\phi) \left(\frac{r}{r_0} \right)^{n-1}
$$

$$
B_r(r,\phi) = B_{main} \sum_{n=1}^{\infty} (-a_n \cos n\phi + b_n \sin n\phi) \left(\frac{r}{r_0} \right)^{n-1}
$$

From the last set of equations, it comes that

$$
|(\boldsymbol{B})_n| = \sqrt{(B_r)_n^2 + (B_\phi)_n^2} = B_{main} \left(\frac{r}{r_0} \right)^{n-1} \sqrt{a_n^2 + b_n^2}
$$

i.e. the magnitude of the $2n$-pole field component is independent of the direction, and it gives a reason to the normalization (2.13) : a_n and b_n express the field contribution of the nth multipole to the main field.

We have shown in the very first simple case (see § 2.1.2) that $B_y = -\frac{1}{\rho}\frac{p}{e}$, i.e. a dipole acting vertically. This corresponds to $B_{main} = p/e$ and $b_1 = -1/\rho$. Similarly, we can increase the order to find (see details in [Turner, 1994]) the values of table 2.1 where g is the gradient of the magnetic field.

Remark 2.1.1 (Scaling the magnetic field) *In order to introduce the map formalism, we shall need a scaled[6] version [Lee, 2012, Floyd et al., 1942] of the magnetic field (2.14) :*

---

6. $\frac{k_n}{(n-1)!} \leftarrow \frac{b_n}{r_0^{n-1}}$, $\frac{j_n}{(n-1)!} \leftarrow \frac{a_n}{r_0^{n-1}}$, $B_{main} \leftarrow B_0\rho$ and $B_0\kappa \leftarrow -B_{main}(b_1 + ia_1)$

Normal dipole ($n = 1$)	
$B_x(x, y) = 0$	$B_y(x, y) = B_{vert}$
Skew dipole ($n = 1$)	
$B_x(x, y) = -B_{hor}$	$B_y(x, y) = 0$
Normal quadripole ($n = 2$)	
$B_x(x, y) = -gy$	$B_y(x, y) = -gx$
Skew quadripole ($n = 2$)	
$B_x(x, y) = gx$	$B_y(x, y) = -gy$
Normal sextupole ($n = 3$)	
$B_x(x, y) = g'xy$	$B_y(x, y) = \frac{1}{2}g'(x^2 - y^2)$
Skew sextupole ($n = 3$)	
$B_x(x, y) = \frac{1}{2}g'(x^2 - y^2)$	$B_y(x, y) = -g'xy$

TABLE 2.1: Values of magnetic field for normal and skew dipoles, quadripoles and sextupoles.

$$B_y(x, y; s) + iB_x(x, y; s) = B_0 \left(\rho \sum_{n=1}^{\infty} [k_n(s) + ij_n(s)] \frac{(x + iy)^n}{n!} - \kappa(s) \right).$$

The multipolar coefficients k_n and j_n are respectively the normal and skew gradients :

$$k_n(s) \equiv \frac{1}{B_0\rho} \left. \frac{\partial^n B_y}{\partial x^n} \right|_{(0,0;s)} \qquad j_n(s) \equiv \frac{1}{B_0\rho} \left. \frac{\partial^n B_x}{\partial y^n} \right|_{(0,0;s)}$$

2.1.4   Equations of motion for a single particle

Performing the following approximations

$$\frac{v}{\dot{s}} \approx 1 + \frac{x}{\rho} \tag{2.15}$$

$$\ddot{s} \approx 0 \tag{2.16}$$

$$\frac{1}{p} \approx \frac{1}{p_0}(1 - \frac{\Delta p}{p_0}) \tag{2.17}$$

Eqs. (2.10) become with the notations of remark 2.1.1 :

$$\frac{d^2x}{ds^2} + \left(\frac{1}{\rho(s)^2} - k_1(s) \right) x = \Re \left[\sum_{n=2}^{\infty} \frac{k_n(s) + ij_n(s)}{n!}(x + iy)^n \right] \tag{2.18a}$$

$$\frac{d^2y}{ds^2} + k_1(s)y = -\Im \left[\sum_{n=2}^{\infty} \frac{k_n(s) + ij_n(s)}{n!}(x + iy)^n \right] \tag{2.18b}$$

In this form such equations cannot be solved exactly. That is why we introduce a discrete time version : the maps that allow us to tackle the problem.

2.2 Maps

In this section we derive the equation of motion of a one-turn map of a linear lattice with a single normal sextupole.

We introduce the transfer map and concentrate on the linear motion solving Hill's equations (see Eqs. (2.21)). We can therefore introduce the Courant-Snyder coordinates. Finally, non-linearities are taken into account.

2.2.1 The one turn map

Considering a circular accelerator composed of L magnetic elements $\mathcal{M}^{(m)}$ ($m = 1 \ldots L$), sketched in Fig. 2.3, we introduce the *transfer map* $M^{(m)}$.
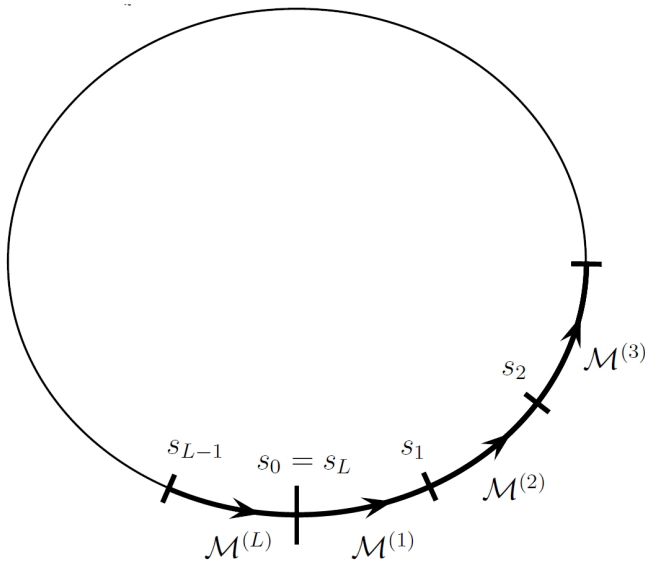

FIGURE 2.3: Sketch of a circular accelerator composed of L magnetic elements $\mathcal{M}^{(m)}$.

$M^{(m)}$ denotes the function that transforms the phase space coordinates at the beginning of the element magnet $\mathcal{M}^{(m)}$ to the coordinates at the end of the element. Explicitly,

$$M^{(m)} : \mathbb{R}^4 \to \mathbb{R}^4 \qquad \boldsymbol{x}(s_m) = M^{(m)}(\boldsymbol{x}(s_{m-1})).$$

We put $s_0 = 0$ and the total length of the accelerator will then be s_L.

Remark 2.2.1 ($M^{(m)}$ is symplectic) *Equations of motion (2.18) can be derived from the time dependent (here s whose evolution is considered linear)*

Hamiltonian function

$$H(x, p_x, y, p_y; s) = \frac{p_x^2 + p_y^2}{2} + \left(\frac{1}{\rho(s)^2} - k_1(s) \right) \frac{x^2}{2} + k_1(s) \frac{y^2}{2}$$
$$- \Re \left[\sum_{n=2}^{\infty} \frac{k_n(s) + ij_n(s)}{(n+1)!} (x + iy)^{n+1} \right] .$$

Therefore $M^{(m)}$ is the Hamiltonian flow that propagates the initial condition $\boldsymbol{x}(s_{m-1})$ to $\boldsymbol{x}(s_m)$. It was shown in Chap. 1 Sec. 1.1 that such a map is symplectic.

We now consider a full turn : we want to propagate $\boldsymbol{x}(s_0)$ to $\boldsymbol{x}(s_L)$. This is accomplished with the *one-turn map* M which is the composition of L transfer maps of single element :

$$M = M^{(L)} \circ M^{(L-1)} \circ \cdots \circ M^{(2)} \circ M^{(1)},$$

and thus, it follows that $\boldsymbol{x}(s_L) = M(\boldsymbol{x}(s_0))$. Except when it is explicitly stated, we shall focus mainly on such full turn. For this reason, we adopt the following notations

$$\boldsymbol{x} \equiv \boldsymbol{x}(s_0) \quad \text{and} \quad \boldsymbol{x}' \equiv \boldsymbol{x}(s_L) \tag{2.19}$$

that are more compact. We thus denotes one iteration of M by (see also Fig. 2.4)

$$\boldsymbol{x}' = M(\boldsymbol{x}).$$

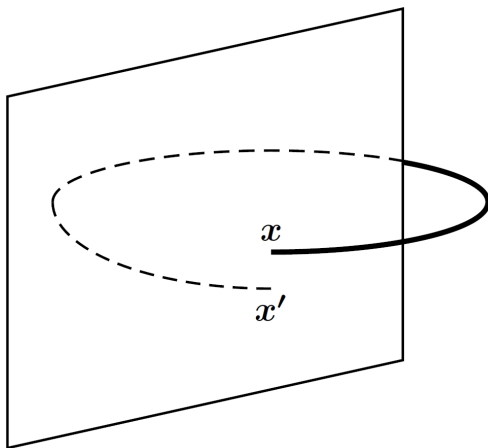In the following, we pay attention to the linearization of the Eqs. (2.18).

FIGURE 2.4: The effect of the one-turn map M in a circular accelerator.

Because we choose the reference orbit passing through the origin, we have that $M(\mathbf{0}) = \mathbf{0}$ and thus M has no constant term and we write the decomposition

$$M(\mathbf{x}) = L(\mathbf{x}) + \text{ higher order terms.}$$

where L is the linear part, $L(\mathbf{x}) \equiv L\mathbf{x}$. For example, the linear map representing a drift in the positions of length l is (see Fig. 2.5)

$$L_{\text{drift}} = \begin{pmatrix} 1 & l & 0 & 0 \\ 0 & 1 & 0 & 0 \\ 0 & 0 & 1 & l \\ 0 & 0 & 0 & 1 \end{pmatrix}. \tag{2.20}$$
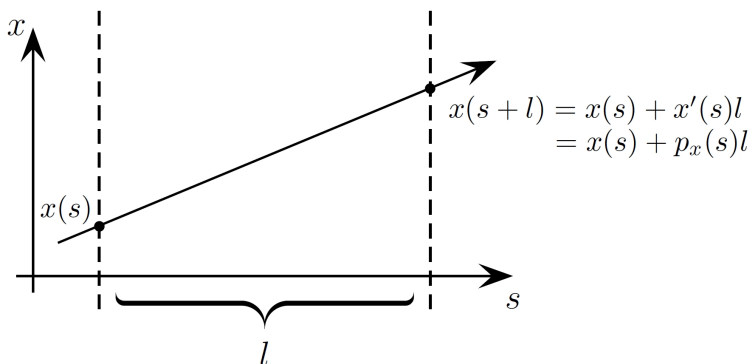

FIGURE 2.5: Representation of a drift of length l with initial momenta p_x.

2.2.2   Hill's equations

We consider the linearized version of Eqs (2.18) :

$$\frac{d^2 x}{ds^2} + \left(\frac{1}{\rho(s)^2} - k_1(s) \right) x = 0 \,, \tag{2.21a}$$

$$\frac{d^2 y}{ds^2} + k_1(s)y = 0 \,. \tag{2.21b}$$

They both have the same structure and they are called in the literature *Hill's equations* [Lee, 2012].

Because they have the structure of a linear oscillator with varying frequency we propose the solutions of the form

$$x(s) = \sqrt{\epsilon_x \beta_x(s)} \sin(\psi_x(s) + \delta_x) \tag{2.22a}$$

$$y(s) = \sqrt{\epsilon_y \beta_y(s)} \sin(\psi_y(s) + \delta_y). \tag{2.22b}$$

The amplitudes are $\beta_x(s)$ and $\beta_y(s)$, the phase advances are $\psi_x(s)$ and $\psi_y(s)$. The 4 constants ϵ_x, ϵ_y, δ_x and δ_y are determined by the initial conditions. Let us stress out that these 4 quantities are thus constants of motion.

Substituting Eqs. (2.22) in Eqs. (2.21), we obtain the following conditions

$$
\begin{cases}
\psi_x' \beta_x' + \psi_x'' \beta_x = 0 \\
\psi_y' \beta_y' + \psi_y'' \beta_y = 0 \\
\beta_x' \dfrac{1}{2} - \beta_x'^2 \dfrac{1}{4\beta_x} - \beta_x \psi_x'^2 + \beta_x \left(\dfrac{1}{\rho^2} - k_1(s) \right) = 0 \\
\beta_y' \dfrac{1}{2} - \beta_y'^2 \dfrac{1}{4\beta_y} - \beta_y \psi_y'^2 + \beta_y k_1(s) = 0
\end{cases}
$$

The first two equations give the relation between amplitude and phase advance :

$$
\psi_x(s) = c_x \int_0^s \frac{d\sigma}{\beta_x(\sigma)} \qquad \psi_y(s) = c_y \int_0^s \frac{d\sigma}{\beta_x(\sigma)}
$$

The constants c_x and c_y can be chosen to fix $\psi_x(0)$ and $\psi_y(0)$. The functions β_x and β_y, dependent on the magnetic field, can be chosen to be periodic (see [Lee, 2012]). In accelerator physics, those quantities have specific names
  – β_x and β_y are the *beta functions*;
  – the constants ϵ_x and ϵ_y are the *emittances*;
  – q_x and q_y are the *linear tunes* of the machine where

$$
q_x = \frac{\psi_x(s_L)}{2\pi} \qquad \text{and} \qquad q_y = \frac{\psi_y(s_L)}{2\pi} .
$$

With this formalism in place, we can write Eqs. (2.22) as

$$
\boldsymbol{x}(s) = T(s)R(s)\boldsymbol{w}
$$

if we define

$$
\boldsymbol{w} =
\begin{pmatrix}
\sqrt{\epsilon_x} \sin \delta_x \\
\sqrt{\epsilon_x} \sin \delta_x \\
\sqrt{\epsilon_y} \sin \delta_y \\
\sqrt{\epsilon_y} \sin \delta_y
\end{pmatrix}
\qquad \text{and} \qquad
T(s) =
\begin{pmatrix}
\sqrt{\beta_x(s)} & 0 & 0 & 0 \\
\dfrac{-\alpha_x(s)}{\sqrt{\beta_x(s)}} & \dfrac{1}{\sqrt{\beta_x(s)}} & 0 & 0 \\
0 & 0 & \sqrt{\beta_y(s)} & 0 \\
0 & 0 & \dfrac{-\alpha_y(s)}{\sqrt{\beta_y(s)}} & \dfrac{1}{\sqrt{\beta_y(s)}}
\end{pmatrix}
$$

where

$$
\alpha_x(s) = -\frac{\beta_x'}{2} \qquad \alpha_y(s) = -\frac{\beta_y'}{2}
$$

and R is a the direct sum of two rotation matrices :

$$
R(\psi_x(s), \psi_y(s)) =
\begin{pmatrix}
\cos \psi_x(s) & \sin \psi_x(s) & 0 & 0 \\
-\sin \psi_x(s) & \cos \psi_x(s) & 0 & 0 \\
0 & 0 & \cos \psi_y(s) & \sin \psi_y(s) \\
0 & 0 & -\sin \psi_y(s) & \cos \psi_y(s)
\end{pmatrix} .
$$

T is invertible and thus $\boldsymbol{w} = T(0)^{-1}\boldsymbol{x}(0)$ since $\boldsymbol{x}(0) = T(0)\boldsymbol{w}$ where we recall that we have chosen $s_0 = 0$. T is also periodic and it comes that $T(s_L) = T(0)$. Using the notations (2.19) and putting $T \equiv T(0)$, we write down the one-turn linear map :

$$\boldsymbol{x}' = L\boldsymbol{x}\,, \qquad L = TRT^{-1}$$

The matrix L is called the *Twiss matrix* and its explicit form is

$$L = \begin{pmatrix} L_x & 0 \\ 0 & L_y \end{pmatrix}$$

where

$$L_x = \begin{pmatrix} \cos(2\pi q_x) + \alpha_x \sin(2\pi q_x) & \beta_x \cos(2\pi q_x) \\ -\frac{1+\alpha_x^2}{\beta_x}\sin(2\pi q_x) & \cos(2\pi q_x) - \alpha_x \sin(2\pi q_x) \end{pmatrix}$$

and

$$L_y = \begin{pmatrix} \cos(2\pi q_y) + \alpha_y \sin(2\pi q_y) & \beta_y \cos(2\pi q_y) \\ -\frac{1+\alpha_y^2}{\beta_y}\sin(2\pi q_y) & \cos(2\pi q_y) - \alpha_y \sin(2\pi q_y) \end{pmatrix}$$

with β_x, β_y, α_x and α_y evaluated at $s = 0$.

2.2.3   Courant-Snyder coordinates

The *Courant-Snyder coordinates* [Courant and Snyder, 1958] are obtained by left multiplying the one-turn map $\boldsymbol{x}' = L\boldsymbol{x}$ by T^{-1}. The motion becomes the direct sum of two rotations :

$$\hat{\boldsymbol{x}}' = R\hat{\boldsymbol{x}}$$

where the change of coordinates is

$$\hat{\boldsymbol{x}} = T^{-1}\boldsymbol{x}.$$

We have the commuting diagram, representing such transformation :

$$
\begin{array}{ccc}
\boldsymbol{x} & \xrightarrow{\ L\ } & \boldsymbol{x}' \\[4pt]
T\uparrow & & \uparrow T \\[4pt]
\hat{\boldsymbol{x}} & \xrightarrow[\ R\ ]{} & \hat{\boldsymbol{x}}'
\end{array}
$$

The previous invariants ϵ_x and ϵ_y become

$$\epsilon_x = \hat{x}^2 + \hat{p}_x^2 \quad \text{and} \quad \epsilon_y = \hat{y}^2 + \hat{p}_y^2\,.$$

In the old coordinates, we have a symplectic linear map that preserves the areas in the planes (x, p_x) and (y, p_y). The orbits, in these planes are ellipses, in the new coordinates, they become circles with the same areas. This effect is sketched in Fig. 2.6.
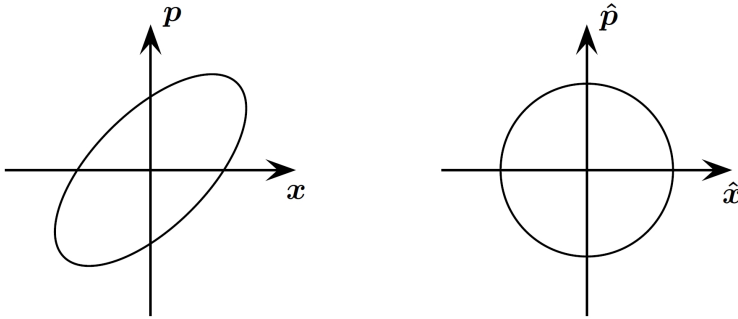

FIGURE 2.6: Effect on the Courant-Snyder change of coordinates on the phase space.

We summarize the notations in the linear motion :

1. Initial coordinates :

$$\boldsymbol{x}' = L\boldsymbol{x}\,, \qquad \boldsymbol{x} = (x, p_x, y, p_y)$$

2. Courant-Snyder coordinates :

$$\hat{\boldsymbol{x}}' = R(\boldsymbol{\omega})\hat{\boldsymbol{x}}\,, \quad \hat{\boldsymbol{x}} = (\hat{x}, \hat{p}_x, \hat{y}, \hat{p}_y)\,, \quad \begin{cases} \hat{x} = \beta_x^{-1/2} x \\ \hat{p}_x = \beta_x^{-1/2}(\alpha_x x + \beta_x p_x) \\ \hat{y} = \beta_y^{-1/2} y \\ \hat{p}_y = \beta_y^{-1/2}(\alpha_y y + \beta_y p_y) \end{cases}$$

where $\boldsymbol{\omega} = (\psi_x, \psi_y) = (2\pi q_x, 2\pi q_y)$

3. The emittances in both coordinates

$$\epsilon_x = \frac{1}{\beta_x}\left(x^2 + (\alpha_x x + \beta_x p_x)^2\right) = \hat{x}^2 + \hat{p}_x^2$$

$$\epsilon_y = \frac{1}{\beta_y}\left(y^2 + (\alpha_y y + \beta_y p_y)^2\right) = \hat{y}^2 + \hat{p}_y^2.$$

2.2.4   Non-Linearities

In this subsection, we use the thin lens approximation [7] in order to derive a map representing the motion of Eqs. (2.18) including the non-linearities.

---

7. Because the non-linearities act on a single, *thin*, physical place. In opposition to the *thick* approximation considering the full length l of the magnet element.

We first transform the 2 second order ordinary differential Eqs (2.18) into a system of 4 ordinary differential equations of first order :

$$\frac{d\boldsymbol{x}}{ds} = A(s)\boldsymbol{x} + f(x, y; s), \tag{2.23}$$

where

$$A(s) = \begin{pmatrix} 0 & 1 & 0 & 0 \\ k_1(s) - \frac{1}{\rho^2(s)} & 0 & 0 & 0 \\ 0 & 0 & 0 & 1 \\ 0 & 0 & -k_1(s) & 0 \end{pmatrix},$$

and

$$f(x, y; s) = \begin{pmatrix} 0 \\ f_x(x, y; s) \\ 0 \\ f_y(x, y; s) \end{pmatrix} \tag{2.24}$$

with

$$f_x(x, y; s) = \Re \left[\sum_{n=2}^{\infty} \frac{k_n(s) + ij_n(s)}{n!} (x + iy)^n \right]$$

$$f_y(x, y; s) = -\Im \left[\sum_{n=2}^{\infty} \frac{k_n(s) + ij_n(s)}{n!} (x + iy)^n \right].$$

Eq. (2.23) can be formally solved with the following integral form

$$\boldsymbol{x}(s) = L(s, s_{m-1})\boldsymbol{x}(s_{m-1}) + \int_{s_{m-1}}^{s} L(s, t) f(x, y; t) dt$$

$$= L(s, s_{m-1}) \left(\boldsymbol{x}(s_{m-1}) + \int_{s_{m-1}}^{s} L(s_{m-1}, t) f(x, y; t) dt \right) \tag{2.25}$$

where $\boldsymbol{x}(s_{m-1})$ is the initial condition and $L(s, s_{m-1})$ is the linear transfer map satisfying the conditions

$$\frac{dL(s, s_{m-1})}{ds} = A(s)L(s, s_{m-1})$$

$$L(s_{m-1}, s_{m-1}) = I$$

$$L(s_{m-2}, s_{m-1})L(s_{m-1}, s) = L(s_{m-2}, s)$$

2.2.5 Thin lens approximation

A solution of Eq. (2.25) can be obtained by the *thin lens approximation*. We consider that the non-linearity is concentrated in a finite number of places of $[s_{m-1}, s_m]$.
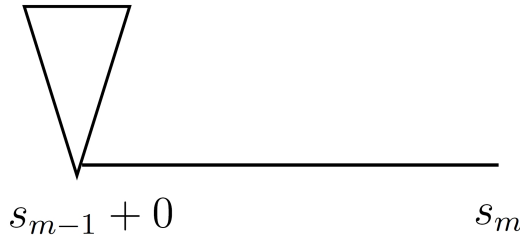
$$s_{m-1} + 0 \qquad\qquad\qquad\qquad s_m$$

FIGURE 2.7: Location of the action of the nonlinearities in the one-kick approximation for one magnet : all the nonlinearities act in a single spot at the very beginning of the element.

The next developments assume the latter fact to hold at only one place : at the beginning of the element, just after s_{m-1}, see Fig. 2.7.

We denote that location by $s_{m-1} + 0$. This method is called *the one-kick approximation* : the non-linear content acts only on $s_{m-1}+0$ by the replacement

$$f(x, y; s) \rightarrow f(x, y; s) l\delta(s - (s_{m-1} + 0)) \tag{2.26}$$

where the δ-function has the following properties :

$$\int_{0-\epsilon}^{0+\epsilon} \delta(s)ds = 1$$

$$\int_{0-\epsilon}^{0+\epsilon} \delta(s)f(x, y; s)ds = f(x, y; 0)$$

for any positive ϵ.

In the substitution (2.26), the addition of l should be understood as a weight function such that the initial size of the non-linearity is conserved.

The transfer map for the rest of the element is straightforward : from $s_{m-1}+\epsilon$ to s_m, non-linearities are not considered and we thus have

$$\boldsymbol{x}(s_m) = L(s_m, s_{m-1} + \epsilon)\boldsymbol{x}(s_{m-1} + \epsilon).$$

Now, we consider what effect has the non linearity from s_{m-1} to $s_{m-1} + \epsilon$. We execute the computation for x and p_x. Results are similar in the y and p_y variables. Considering the solution on integral form Eq. (2.25) and the value of f given Eq. (2.24) with its substitution, one calculates

$$\int_{s_{m-1}}^{s_{m-1}+\epsilon} \frac{dx}{ds}ds = x(s_{m-1} + \epsilon) - x(s_{m-1}) = \mathcal{O}(\epsilon),$$

and

$$\int_{s_{m-1}}^{s_{m-1}+\epsilon} \frac{dp_x}{ds}ds = p_x(s_{m-1} + \epsilon) - p_x(s_{m-1}) = lf_x(x, y; s_{m-1}) + \mathcal{O}(\epsilon).$$

In the limit $\epsilon \to 0$, one obtains the *kick map* :

$$
\begin{pmatrix} x \\ p_x \\ y \\ p_y \end{pmatrix}_{s=s_{m-1}+0}
=
\begin{pmatrix} x \\ p_x + l f_x(x,y;s) \\ y \\ p_y + l f_y(x,y;s) \end{pmatrix}_{s=s_{m-1}}
$$

and the one kick approximation is then

$$
\boldsymbol{x}_{\text{one-kick}}(s_m) = L(s_m, s_{m-1})(\boldsymbol{x}(s_{m-1}) + l f(x,y;s_{m-1})).
$$

For instance, the one-kick map of a drift (see Eq. (2.20)) with non-linearities is

$$
\begin{pmatrix} x \\ p_x \\ y \\ p_y \end{pmatrix}_{s_m}
=
\begin{pmatrix} 1 & l & 0 & 0 \\ 0 & 1 & 0 & 0 \\ 0 & 0 & 1 & l \\ 0 & 0 & 0 & 1 \end{pmatrix}
\begin{pmatrix} x \\ p_x + \Re \sum_{n=2}^{\infty} \frac{K_n(s) + i J_n(s)}{n!}(x+iy)^n \\ y \\ p_y - \Im \sum_{n=2}^{\infty} \frac{K_n(s) + i J_n(s)}{n!}(x+iy)^n \end{pmatrix}_{s_{m-1}}
\tag{2.27}
$$

where

$$
K_n = l k_n \qquad \text{and} \qquad J_n = l j_n.
$$

Finally, we give the map we shall deal with in the following chapters. It is the map (2.27) of a linear lattice with a single normal sextupole ($n = 2$) in the one kick approximation :

$$
\begin{pmatrix} x' \\ p'_x \\ y' \\ p'_y \end{pmatrix}
= L
\begin{pmatrix} x \\ p_x + \frac{K_2}{2}(x^2 - y^2) \\ y \\ p_y - K_2 xy \end{pmatrix}
\tag{2.28}
$$

or, in the Courant-Snyder coordinates (see Subsec. 2.2.3),

$$
\begin{pmatrix} \hat{x}' \\ \hat{p}'_x \\ \hat{y}' \\ \hat{p}'_y \end{pmatrix}
= R(\boldsymbol{\omega})
\begin{pmatrix} \hat{x} \\ \hat{p}_x + \frac{K_2}{2} \beta_x^{\frac{3}{2}}\left(\hat{x}^2 - \frac{\beta_y}{\beta_x}\hat{y}^2\right) \\ \hat{y} \\ \hat{p}_y - K_2 \beta_x^{\frac{3}{2}} \frac{\beta_y}{\beta_x} \hat{x}\hat{y} \end{pmatrix}.
\tag{2.29}
$$

This map was extensively study, for example in [Scandale and Turchetti, 1990, Bountis and Kollmann, 1994, Vrahatis et al., 1996, Bountis and Skokos, 2006, Vrahatis et al., 1997, Boreux et al., 2012b, Boreux et al., 2012a].

Chapitre 3

Chaos : indicators

Contents

The aim of this chapter is to introduce in details the numerical *tools* used to analyze and describe dynamical systems and specifically those we shall use in the application chapter.

In the first section, we take the time to present a definition of a *chaotic orbit*. Being such definition a not trivial one, we introduce other ingredients than the most spread one : sensitive dependence on initial conditions.

In Sec. 3.2, we present *Chaos Indicators* based on deviation vectors : the Maximum Lyapunov Exponent [Benettin et al., 1980], the Smaller ALignement Index [Skokos, 2001] and the Mean Exponential Growth of Nearby Orbits [Cincotta and Simó, 2000].

Sec. 3.3 is dedicated to the study of spectral methods [Guzzo and Benettin, 2001, Laskar, 1999]. We treat the Frequency Map Analysis of Laskar based on the analysis of a time series constructed by the coordinates of the orbit under study. For such an orbit, we recover the first frequencies and their corresponding amplitude that we can use in order to characterize its chaoticity.

A last section is dedicated to give an example on which the indicators are used and briefly compare them. We then conclude that all *tools*, that is to say chaos indicators based on deviation vectors and based on signal analysis, perform a good analysis. While the first class is only dedicated to detect chaos, the second one can provide other information on an orbit (in particular its main frequencies). If both available, both should be used, if only to check each other results.

3.1   Chaos

As we introduced the dynamical systems in Chap. 1, they essentially come in two classes :

1. *Continuous time dynamical systems* : expressed by differential equations, for example
$$\dot{\boldsymbol{x}} = f(\boldsymbol{x}, t) \, ;$$

2. *Discrete time dynamical systems* : expressed by "difference" equations, for example
$$\boldsymbol{x}(n+1) = f(\boldsymbol{x}, n).$$

Considering such systems, we previously already have given some ingredients of *chaos* : destruction/absence of regular behavior, close initial conditions lea-

ding to strongly different orbits. We now give it a precise definition following [Banks et al., 2003]

Definition 3.1.1 *Let V be a set. We say that a map $f : V \to V$, is* chaotic *on V if :*

1. *f has* sensitive dependence on initial conditions*;*

2. *f is* transitive*;*

3. *periodic points are dense in V.*

In this definition we use the concept of sensitive dependence on initial conditions :

Definition 3.1.2 *f has* sensitive dependence on initial conditions *at $\boldsymbol{x}$ if there exists $\delta > 0$ such that, for any neighborhood I of $\boldsymbol{x}$, there exists $\boldsymbol{y} \in I$ and $n \geq 0$, such that $||f^n(\boldsymbol{x}) - f^n(\boldsymbol{y})|| > \delta$.*

This definition means that there exist points arbitrarily close to $\boldsymbol{x}$ that will eventually be δ-distant from each other after n iterations. So sensitivity refers to the behaviors of two orbits which diverge (see remark 3.1.4 on the rate of the divergence) away from each other as iterations proceed.

Let us also remark that, behind the mathematical concepts, it also means that in a system sensitive to initial conditions, a very small error on the knowledge or measure of an initial condition can be rapidly amplified.

This concept is maybe the most spread one in the idea of chaos. For instance, the *butterfly effect* (or the *domino effect* : chain of event leading to large-scale alterations), inspired by the article of Lorenz [Lorenz, 1963] and its strange attractor, see Fig. 3.1.
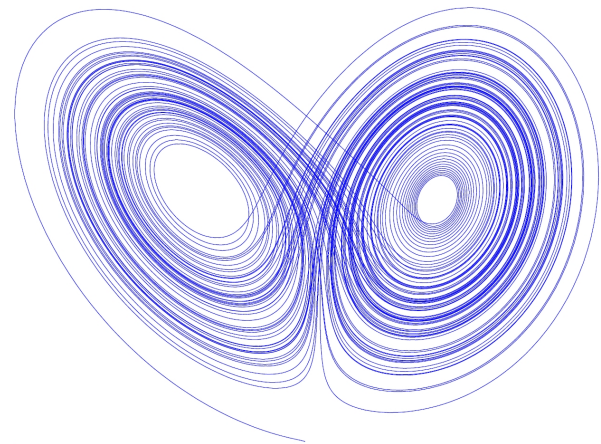

FIGURE 3.1: The strange attractor of Lorenz.

While the first condition compares at least *two* orbits, the idea of chaos can also be seen from *one* orbit exhibiting an *irregular* behavior, see for example Fig. 3.2 that shows the first iterations of a particular initial condition. This orbit wanders all over the domain (in this case $[0,1]$). This is linked (considering
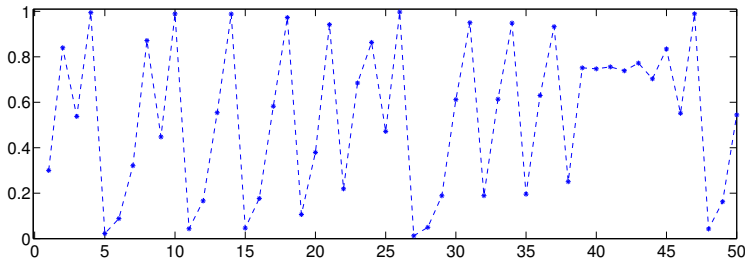

FIGURE 3.2: The first 50 iterations of the logistic map $Q_4(x) = 4x(1-x)$ with initial condition $x_0 = 0.3$.

intervals instead of points) to the concept of transitivity :

Definition 3.1.3 *A map $f : V \to V$ is* transitive *if for every pair of not empty disjoint subsets I and J of V there is an n such that $f^n(I) \cap J \neq \emptyset$.*

This definition imposes the existence of points that move from any arbitrarily small subsets to any other arbitrarily small subsets ; roughly speaking there are points going everywhere.
Let us remark that this property does not always imply chaos. For example, the map

$$x \mapsto x + \sqrt{2} \mod 1$$

fills all its domain, $[0,1]$, but is not chaotic.

Finally the last condition seems quite opposite to the previous ones since one might think of periodic orbit as ingredient of regularity and predictability. In fact these periodic orbits can be unstable and thus when another point approaches a periodic one it is pushed away. This is the contribution to chaos.

This *full* definition of chaos is hard to check for a particular orbit. In fact, in practice, mainly the condition on the sensitivity on initial conditions will be tested to characterize an orbit as chaotic or regular. We present such techniques in the rest of the chapter.

Remark 3.1.4 (Exponential divergence) *When motion exhibits a sensitive dependence on initial conditions, we expect that two trajectories starting very close together will* rapidly *diverge from each other. In many examples, this speed of divergence is* exponential, *that is to say, if the initial distance between*

two initial conditions is δ_0, then after a time t, it will be

$$\delta(t) \sim \delta_0 e^{\lambda t} \tag{3.1}$$

where λ is called the Liapunov exponent. *For example, in the case of the Lorenz attractor (see Fig. 3.1), $\lambda \sim 0.9$. The link (3.1) has sense only for a finite time span (in order to keep the orbits in the considered domain). Many references, such as [Strogatz, 1994] or [Hilborn, 1994] include this criteria to the definition of chaos.*

3.2   Deviation vectors

3.2.1   Tangent map

In order to introduce chaos indicators, we first need to define deviation vectors. Deviation vectors are meant to represent a second orbit, close to the considered one, see Fig. 3.3.
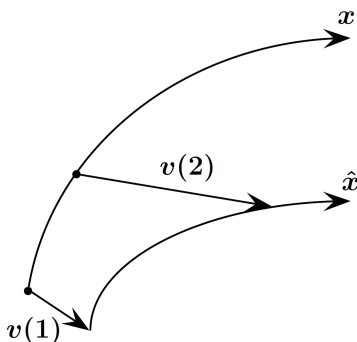

FIGURE 3.3: Evolution of a deviation vector $\boldsymbol{v}$ along the orbit of $\boldsymbol{x}$.

Considering thus $\hat{\boldsymbol{x}} = \boldsymbol{x} + \boldsymbol{v}$, where $\boldsymbol{v}$ is the so-called *deviation vector*, we have

$$\hat{\boldsymbol{x}}' = f(\hat{\boldsymbol{x}}) = f(\boldsymbol{x} + \boldsymbol{v}) = f(\boldsymbol{x}) + M(\boldsymbol{x})\boldsymbol{v} + \mathcal{O}(\boldsymbol{v})^2 \,,$$

where M is the Jacobian matrix of the map f. Since, $\hat{\boldsymbol{x}}' = \boldsymbol{x}' + \boldsymbol{v}'$ and $\boldsymbol{x}' = f(\boldsymbol{x})$, we find the *tangent map*; the evolution of $\boldsymbol{v}$ at first order :

$$\boldsymbol{v}' = M(\boldsymbol{x})\,\boldsymbol{v}$$

or, when the iterate is explicit :

$$\boldsymbol{v}(n+1) = M(\boldsymbol{x}(n))\,\boldsymbol{v}(n)\,. \tag{3.2}$$

Initial conditions, $\boldsymbol{v}(0)$, are chosen according to the indicator, often randomly.

Various recent references (see for example [Darriba et al., 2012, Maffione et al., 2011, Skokos, 2010] and references therein) treat the way of computing such indicators. This is not the direct concern of this section : we restrain the discussion in defining 3 of these indicators and then give a few directions to compare them.

3.2.2   The Maximum Lyapunov Exponent

Following [Benettin et al., 1980], we define the *maximal Lyapunov exponent*, or *largest Lyapunov characteristic number* (LCN) λ_1 of an orbit $(\boldsymbol{x}(n))_{n\geq 0}$ as the limit for $n \to \infty$ of the quantity

$$L_1(n) = \frac{1}{n} \ln \frac{||\boldsymbol{v}(n)||}{||\boldsymbol{v}(0)||}, \quad \text{i.e.} \quad \lambda_1 = \lim_{n\to\infty} L_1(n) \tag{3.3}$$

where $\boldsymbol{v}(0)$, $\boldsymbol{v}(n)$ are deviation vectors from the orbit at $n = 0$ and $n > 0$ iterations, respectively, whose equations of motion are given in Eq. (3.2).

The LCN measures the rate of exponential divergence of initially nearby orbits in the phase space of the dynamical system as time goes to infinity.

Based (only) on the first criterion of chaos (see Def. 3.1.2), we have the following rule

---

For a given orbit $(\boldsymbol{x}(n))_{n\geq 0}$ and its associated largest Lyapunov characteristic number λ_1

$$\lambda_1 > 0 \quad \Rightarrow \quad (\boldsymbol{x}(n))_{n\geq 0} \quad \text{CHAOTIC}$$

For $\lambda_1 = 0$, both scenarii could have occurred : for example the deviation vector has a polynomial divergence and the orbit is chaotic, or the deviation vector remains constant and the orbit is regular.

Numerically speaking, the main problem of this indicator is the need for computing very large time scales in order to qualify λ_1 to be zero or not. Moreover, as it is point out in [Bountis and Skokos, 2012]

> "Their values vary significantly in time and may only be used in the long time limit when the exponents have converged with satisfactory accuracy."

This drawback was overcome with different new indicators. We present two of them : the SALI and the MEGNO.

3.2.3   The Smaller ALignement Index

The Smaller ALignement Index (SALI) was introduced in [Skokos, 2001] and was applied in various works such [Bountis and Skokos, 2006,

Petalas et al., 2008, Boreux et al., 2012b, Boreux et al., 2012a].

In order to compute the SALI we need to follow the time evolution of 2 deviation vectors. Also, only their direction will be important, we thus consider them normalized from step to step :

$$\hat{\boldsymbol{v}}_i(n) = \frac{\boldsymbol{v}_i(n)}{||\boldsymbol{v}_i(n)||}, \quad i = 1, 2\,.$$

The SALI is defined as

$$SALI(n) = \min\{||\hat{\boldsymbol{v}}_1(n) + \hat{\boldsymbol{v}}_2(n)||, ||\hat{\boldsymbol{v}}_1(n) - \hat{\boldsymbol{v}}_2(n)||\}$$

whence it is obvious that $SALI(n) \in [0, \sqrt{2}]$, see Fig. 3.4.
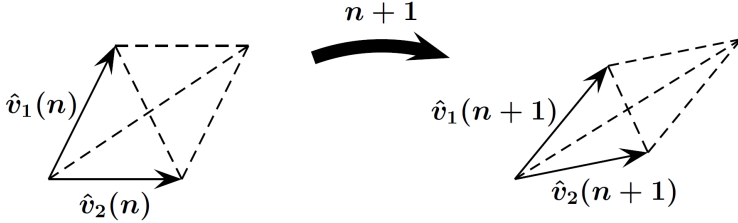

FIGURE 3.4: Evolution of the construction of the SALI by following the respective position of two deviation vectors along the iterates.

In the case of an ordered orbit, the two vectors evolve tangentially to the torus that supports the orbit. They keep different directions : they do not align and thus the SALI remains constant.
On the contrary, in the case of a chaotic orbit, the deviation vectors eventually go in the unstable direction and SALI *falls exponentially* to zero [Skokos et al., 2007].

The rule is thus (apart from the case of remark 3.2.1)

For a given orbit $(\boldsymbol{x}(n))_{n \geq 0}$ and its associated $(SALI(n))_{n \geq 0}$

$$SALI(n) > 0 \quad \forall n \in \mathbb{N} \quad \Rightarrow \quad (\boldsymbol{x}(n))_{n \geq 0} \quad \text{REGULAR}$$
$$SALI(n) \to 0 \ (\text{exponentially}) \quad \Rightarrow \quad (\boldsymbol{x}(n))_{n \geq 0} \quad \text{CHAOTIC}$$

Remark 3.2.1 (2D maps) *In the case of an ordered orbit for a 2D map, the torus on which the orbit is confined is unidimensional and thus the deviation vectors eventually align and SALI goes to zero. Hopefully SALI tends to*

zero, both for ordered and chaotic cases, but following completely different time rates [Skokos, 2001] : the rule becomes

---

For a given $2D$ orbit $(\boldsymbol{x}(n))_{n \geq 0}$ and its associated $(SALI(n))_{n \geq 0}$

$$SALI(n) \to 0 \text{ as } n^{-2} \quad \Rightarrow \quad (\boldsymbol{x}(n))_{n \geq 0} \quad REGULAR$$
$$SALI(n) \to 0 \text{ as } e^{-n} \quad \Rightarrow \quad (\boldsymbol{x}(n))_{n \geq 0} \quad CHAOTIC$$

Remark 3.2.2 (Initial conditions) *Generally speaking, the initial conditions for the deviation vectors can be chosen randomly. However, in practice, in order to avoid a random choice of initial vectors (nearly) aligned, they can be chosen orthogonal to each other.*

Let us remark that a generalization for higher dimensional system of this method exists : the Generalized ALignement Index (GALI) based on k deviation vectors, introduced in [Skokos et al., 2007].

3.2.4   The Mean Exponential Growth of Nearby Orbits

The Mean Exponential Growth factor of Nearby Orbits (MEGNO) and the mean-MEGNO were introduced in [Cincotta and Simó, 2000] for continuous systems and later in [Cincotta et al., 2003] where the MEGNO and the mean-MEGNO are generalized and defined for maps. This pair of indicators has been a success especially in astronomy and astrodynamics [Goździewski et al., 2001, Breiter et al., 2005, Valk et al., 2009, Hinse et al., 2010, Mestre et al., 2011, Compère et al., 2012, Hubaux et al., 2013].

The MEGNO is defined for maps after n iterations by

$$Y(n) = \frac{2}{n} \sum_{k=1}^{n} k \ln \left(\frac{||\boldsymbol{v}(k)||}{||\boldsymbol{v}(k-1)||} \right)$$

where $\boldsymbol{v}$ is a deviation vector. If the orbit is chaotic, $Y(n)$ oscillates around the asymptote $\lambda_1 \frac{n}{2}$. If the orbit is confined on an invariant torus, it oscillates around the fixed value 2 (see [Cincotta et al., 2003]).

In order to eliminate the oscillations, let us also consider the mean-MEGNO

$$\overline{Y}(n) = \frac{1}{n} \sum_{k=1}^{n} Y(k) \, .$$

While $Y(n)$ may not converge nor admit a limit for $n \to \infty$, it was proven [Cincotta and Simó, 2000] that the asymptotic value of $\overline{Y}$ yields to a clear characterization of the regular or chaotic nature of orbits.

We summarize its behavior by the following :

For a given orbit $(\boldsymbol{x}(n))_{n \geq 0}$ and its associated mean-MEGNO

$$\overline{Y}(n) \to 0 \quad \Rightarrow \quad (\boldsymbol{x}(n))_{n \geq 0} \quad \text{REGULAR PERIODIC}$$
$$\overline{Y}(n) \to 2 \quad \Rightarrow \quad (\boldsymbol{x}(n))_{n \geq 0} \quad \text{REGULAR QUASI-PERIODIC}$$
$$\overline{Y}(n) \sim \frac{\lambda_1 n}{2} \quad \Rightarrow \quad (\boldsymbol{x}(n))_{n \geq 0} \quad \text{CHAOTIC}$$

3.3 Frequency Map Analysis

In this section we introduce another method, the *Frequency Map Analysis* (FMA), of characterizing an orbit as chaotic or regular. FMA is based on the analysis of a time series that allows to recover the main frequencies (and their corresponding amplitude) of a signal. Thanks to its precision it has been used with success in several studies. For example let us mention applications to the Solar System [Laskar, 1990] and Extra Solar Systems [Gayon et al., 2008], to Particle Accelerators [Nadolski and Laskar, 2003] or in Space Geodesy [Delsate et al., 2010].

We present here the sketch of the method following [Laskar, 1993b, Laskar, 1999].

3.3.1 The Method

We consider a function $f(t)$ with values in the complex domain :

$$f(t) = \sum_{k=1}^{\infty} a_k e^{i\nu_k t}, \tag{3.4}$$

whose we suppose a numeric knowledge on a finite time span $[-T, T]$. The frequency analysis algorithm dwells in searching a quasi-periodic approximation of the initial function such that it is a finite number of elementary trigonometric monomials, e.g.

$$\tilde{f}(t) = \sum_{k=1}^{N} \tilde{a}_k e^{i\tilde{\nu}_k t}.$$

The frequencies $\tilde{\nu}_k$ and their corresponding amplitudes $\tilde{a}_k$ are determined following an iterative process.
The first frequency $\tilde{\nu}_1$ is found maximizing the function

$$\phi(\nu) = \langle f(t), e^{i\nu t} \rangle$$

where the scalar product $\langle f(t), g(t) \rangle$ is defined by

$$\langle f(t), g(t) \rangle = \frac{1}{2T} \int_{-T}^{T} f(t) \overline{g}(t) \chi(t) dt$$

and where $\chi(t)$ is a weight function, positive, even and such that

$$\frac{1}{2T} \int_{-T}^{T} \chi(t)dt = 1.$$

Even if many candidates fulfill the conditions to be the weight function, the Hanning window filter, $\chi_1(t)$ is often chosen :

$$\chi_1(t) = 1 + \cos(\pi t/T) \,,$$

whose generalization is

$$\chi_p(t) = \frac{2^p(p!)^2}{(2p)!} (1 + \cos(\pi t/T))^p \,. \tag{3.5}$$

As a result, the first periodic term $e^{i\tilde{\nu}_1 t}$ is found. Its complex amplitude is obtained by orthogonal projection of $f(t)$ on $e^{i\tilde{\nu}_1 t}$. The remaining frequencies $\tilde{\nu}_2, \ldots, \tilde{\nu}_N$ and their complex amplitudes $\tilde{a}_2, \ldots, \tilde{a}_N$ are found similarly considering the initial function lightened of the already found parts $\tilde{a}_k e^{i\tilde{\nu}_k t}$. For example, in order to find $\tilde{\nu}_2$ we consider (instead of the initial function $f(t)$) the function

$$f(t) - \tilde{a}_1 e^{i\tilde{\nu}_1 t} \,.$$

Let us finally point out that generally the functions $e^{i\tilde{\nu}_k t}$ are not orthogonal, it is thus necessary to orthogonalize the set of functions $(e^{i\tilde{\nu}_k t})_k$, when projecting f iteratively.

This procedure leads to the following result :

Theorem 3.3.1 (Proposition 1 of [Laskar, 1999]) *For a KAM solution $f(t)$ of the form (3.4) and using the weight function (3.5), the application of the frequency analysis algorithm over the time span $[-T, T]$, as described above, provides a determination $\tilde{\nu}_1$ of the frequency ν_1 with a precision $\nu_1 - \tilde{\nu}_1$ having the asymptotic expression for $T \to \infty$*

$$\nu_1 - \tilde{\nu}_1 = \frac{(-1)^{p+1}\pi^{2p}(p!)^2}{A_p T^{2p+2}} \sum_{\boldsymbol{k} \in \mathbb{Z}^n} \frac{\Re(a_{\boldsymbol{k}})}{\Omega_{\boldsymbol{k}}^{2p+1}} \cos(\Omega_{\boldsymbol{k}} T) + o\left(\frac{1}{T^{2p+2}}\right),$$

with

$$\Omega_{\boldsymbol{k}} = \langle \boldsymbol{k}, \boldsymbol{\nu} \rangle - \nu_1 \,; \quad A_p = -\frac{2}{\pi^2}\left(\frac{\pi^2}{6} - \sum_{j=1}^{p} \frac{1}{j^2}\right).$$

In particular, the use of a Hanning window ($p = 1$) ensures that for a KAM solution, the accuracy of determining the main frequencies will be proportional to $1/T^4$ which will usually be several orders of magnitude better than a classic Fast Fourier Transform method, where the precision is only proportional to $1/T$.

3.3.2 Chaotic orbits

Second derivative

Let F be the frequency map that associates a frequency to a signal on a time span $[0, T]$. This map should be regular for action corresponding to regular motion, in fact the map should be C^∞ [Laskar, 1993a]. On the contrary, for chaotic motion (corresponding to jumps in the frequencies), the map is no longer a diffeomorphism.

An estimate of the first derivative of F can be computed using

$$\delta F(y) = F(y) - F(y - h) = hF'(\zeta) \quad \zeta \in [y - h, y];$$

and for the estimate of the second derivative, we have

$$\delta\delta F(y) = F(y) - 2F(y - h) + F(y - 2h) = h^2 F''(\zeta) \quad \zeta \in [y - 2h, y].$$

Let us set the error when computing F to ϵ. Then the error committed computing δF is 2ϵ and the one computing $\delta\delta F$ is 4ϵ. Considering that the first and second derivatives are of the order of the unity in regular motion, we need $2\epsilon < h$ for the computation of the first derivative and $4\epsilon < h^2$ for the computation of the second derivative in order to have a relevant result.

This is the reason why the estimate of the second derivative $\delta\delta F$ can be used as a chaos indicator. It is a more useful tool than the estimate of the derivative δF; if we want an accuracy of 10^{-8}, we need a step size of 10^{-4} while we should use the same order with the estimate of the first derivative.

Regrettably this indicator is not usable in the future studied cases : in order to be precise, the step size h should be small while in map theory it is fixed to $h = 1$. We therefore do not insist on this indicator.

Diffusion index

In the case of regular motion, orbits lay on a torus with fixed frequencies. The analysis of the diffusion of the frequency with respect to time can thus give an estimate of the chaoticity of a considered orbit [Laskar, 1993a].

For that purpose, we decompose the time span $[-T, T]$ into two time spans, for example $[-T, 0]$ and $[0, T]$, on which we evaluate the main frequency. We obtain $\nu_1^{(1)}$ and $\nu_1^{(2)}$. Then the diffusion index D is

$$D = \left| \frac{\nu_1^{(2)} - \nu_1^{(2)}}{\nu_1^{(2)}} \right| \tag{3.6}$$

The smaller D is, the lesser is the frequency diffusion and the orbit is regular. On the contrary, if the diffusion is important the orbit is considered chaotic because it is not characterized by a unique frequency.

Def. (3.6) of D can be largely modified. We can take more than 2 sub-intervals, for example if we consider n sub-interval $T_k \subset [-T, T]$ $(k = 1 \dots n)$

and the corresponding frequencies $\nu_1^{(k)}$ $(k = 1 \ldots n)$ then D takes the form

$$D = \max_{i,j} \left| \nu_1^{(i)} - \nu_1^{(j)} \right| . \tag{3.7}$$

We can also consider only adjacent intervals : we choose Def. (3.7) with $j \leftarrow i + 1$.

Sometimes, it is interesting to consider *more than one* signal associated to *one* initial condition (see [Nadolski and Laskar, 2003] and Chap. 5), for example considering two signals, we find two main frequencies, for instance ν_x and ν_y, and the diffusion index is

$$D = \sqrt{\left(\nu_x^{(1)} - \nu_x^{(2)} \right)^2 + \left(\nu_y^{(1)} - \nu_y^{(2)} \right)^2} \tag{3.8}$$

Finally, we present a combination of the two last possibilities in the case of two signals :

$$D = \sqrt{\left(\max_{i,j} \left| \nu_x^{(i)} - \nu_x^{(j)} \right| \right)^2 + \left(\max_{i,j} \left| \nu_y^{(i)} - \nu_y^{(j)} \right| \right)^2} . \tag{3.9}$$

Similarly to the previous section, we summarize when we consider an orbit as chaotic or not according to the value of D.

For a given orbit $(\boldsymbol{x}(n))_{n \geq 0}$ and its associated diffusion index D,

$$D \sim 0 \quad \Rightarrow \quad (\boldsymbol{x}(n))_{n \geq 0} \quad \text{REGULAR}$$
$$D > 0 \quad \Rightarrow \quad (\boldsymbol{x}(n))_{n \geq 0} \quad \text{CHAOTIC}$$

Remark 3.3.2 (The signal) *The signal presented in the beginning by $f(t)$ can usually be chosen freely. For example if $\boldsymbol{x} \in \mathbb{R}^2$, we can choose $f(t) = x_1 \pm i x_2$ or $f(t) = x_2 \pm i x_1$ or other combinations (see Chap. 5 for an application in $\mathbb{R}^4$).*

3.4   Application and comparison

In this section, we analyze the Hénon map (see Sec. 1.3.2 and remark that it corresponds to a flat beam of the Eq. (2.29) that we shall investigate in Chap. 4, Sec. 4.2) :

$$\begin{pmatrix} x' \\ p' \end{pmatrix} = R(\omega) \begin{pmatrix} x \\ p + x^2 \end{pmatrix} \quad ; \quad R(\omega) = \begin{pmatrix} \cos \omega & \sin \omega \\ -\sin \omega & \cos \omega \end{pmatrix},$$

with the different indicators presented before. We set $\omega = 2\pi q_x$ with $q_x = 0.61803$ and the number of iterations to 10^4. We consider initial conditions in the square $(x, p) \in [-1.2, 1.2]^2$ with a discretization mesh
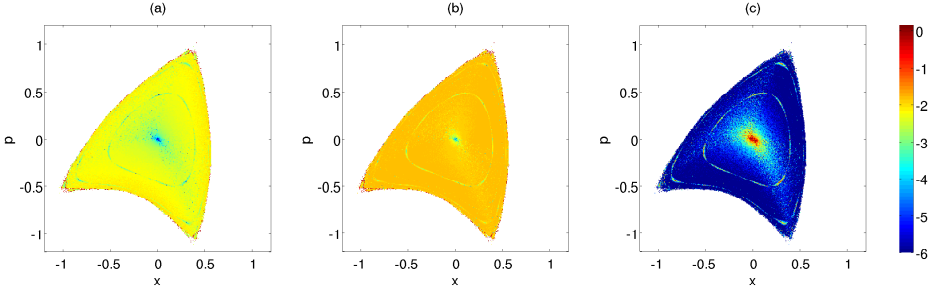
FIGURE 3.5: From left to right : the $\log_{10}$ of λ_1, $\overline{Y}$ and $SALI$ for different initial conditions. The three indicators exhibit the same structure.

of $6 \cdot 10^{-3}$. We showed only initial conditions leading to non-escaping or-bits. We first plot the results of indicators based on deviation vectors in Fig. 3.5.

The indicators give us the same information : very stable orbits near the origin and on two groups of islands. This stable zone at the origin may seem bigger with the SALI indicator. We used a logarithmic scale in order to make distinction between dots.
Also, the SALI panel is composed with many values close to 0. We have to keep in mind that it tends to zero both for regular and chaotic orbits of $2D$ maps, but with different time rates.

We then produced comparable plots using the frequency map analysis. It is reported in Fig. 3.6. In this case, we considered only one signal : $z = x + ip$.
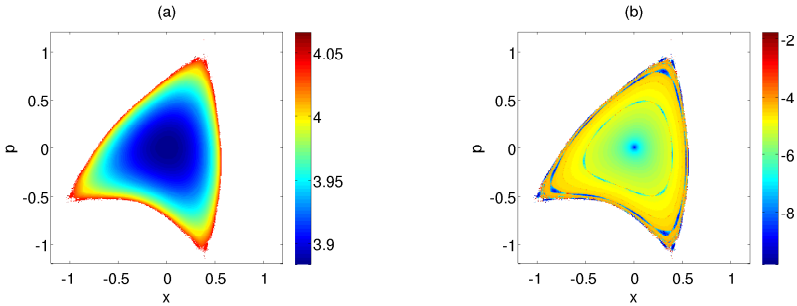

FIGURE 3.6: Panel (a) : Frequency of the all signal. Panel (b) : $\log_{10}$ of the diffusion index.

We first show the main frequency obtained on the full signal. We observe a variation of that frequency according to the distance to the origin. Then we plot $\log_{10} D$ where we choose the diffusion index of Eq. (3.7). Structures arise : even for initial conditions "far " from the origin, we observe zones where the frequency remains constant along the signal.

Let us finally insist that these structures are identical to those obtained with deviation vectors. Frequency map analysis is thus also a good chaos indicator.

Our goal was to present the indicators and not to compare them. Such comparison was recently presented [1] first for maps in [Maffione et al., 2011] and extended to general continuous time systems in [Darriba et al., 2012]. They conclude indicating which indicator or which combination of indicators should be used according to the goal pursued.

---

1. They treat only deviation vectors based methods : they do not incorporate the FMA.
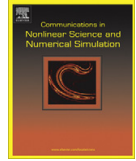
Control of a particle accelerator model

Contents

This chapter merges different parts previously developed. The scheme is logical : we apply the control theorem 1.3.4 to the model of particle accelerator, Eq. (2.29), derived in Chap. 2. In order to convince ourselves of the effectiveness of the new map, we use the SALI to highlight the results. They are promising.

These results have already been published in peer-reviewed journals. We include the two articles, namely [Boreux et al., 2012b] and [Boreux et al., 2012a], once we have given a brief presentation.

4.1 Hamiltonian control used to improve the beam stability in particle accelerator models

In the following article, the $4D$ model of Eq. (2.29) of a ring particle accelerator is first expressed as composition of maps expressed as *time-one flow* of a Hamiltonian function (see Eq. (1.13), p. 11). Then the control theorem 1.3.4 can be applied. The resulting new, controlled, map is expressed as a series. In order to implement it, we perform a truncation and discuss its validity because of the loss of symplecticity. Then we present the gains such as the increase of the dynamical aperture or the decrease of the number of chaotic orbits. We have chosen the chaos indicator SALI to complete this task.

Hamiltonian control used to improve the beam stability in particle accelerator models

J. Boreux [a,*], T. Carletti [a], Ch. Skokos [b], M. Vittot [c]

[a] Namur Center for Complex Systems, naXys, University of Namur, Rempart de la Vierge 8, Namur 5000, Belgium
[b] Max Planck Institute for the Physics of Complex Systems, Nöthnitzer Str. 38, D-01187 Dresden, Germany
[c] Centre de Physique Théorique CNRS, Luminy Case 907, 13288 Marseille Cedex 9, France

ABSTRACT

We derive a Hamiltonian control theory which can be applied to a 4D symplectic map that models a ring particle accelerator composed of elements with sextupole nonlinearity. The controlled system is designed to exhibit a more regular orbital behavior than the uncontrolled one. Using the Smaller Alignment Index (SALI) chaos indicator, we are able to show that the controlled system has a dynamical aperture up to 1.7 times larger than the original model.

© 2011 Elsevier B.V. All rights reserved.

1. Introduction

Particle accelerators are technological devices which allow studies at both "infinitely small scale", e.g. particles responsible for elementary forces, and "extremely large scale", e.g. the origin of cosmos. In a simplified approach, such devices are composed of basic elements sequence: focusing and defocusing magnets, accelerating electromagnetic fields and trajectory bending elements as they are used in the case of ring accelerators. The resulting dynamics is nonlinear, and can be described, in the absence of strong damping, by a conservative system. This system can be modeled by a symplectic map built from the composition of several elementary maps corresponding to each basic magnetic element.

One of the main problems found in the dynamics of ring accelerators is to study the stability around the nominal orbit, i.e. the circular orbit passing through the centre of the ring. Each component of the ring can be seen as a nonlinear map, that deforms the trajectory at large amplitude. Moreover, such maps possess stochastic layers whose effect is the reduction of the stability domains around the nominal circular orbit (the so-called *dynamical aperture* – DA) [1]. Such behaviors imply that (chaotic) nearby orbits can drift away after a few ring turns, eventually colliding with accelerator's boundaries, and consequently reduce the beam lifetime and the performance of the accelerator.

The aim of the present paper is to derive a reliable improvement of the stability of the beam by increasing the DA in a simplified accelerator model, consisting of only one type of element having a sextupole nonlinearity [2–5].

We work in the framework of the *Hamiltonian control theory* presented in [7,8], where two methods to control symplectic maps have been described, namely using Lie transformations and generating functions. In the present paper we use the

---

* Corresponding author.
  E-mail addresses: jehan.boreux@fundp.ac.be (J. Boreux), timoteo.carletti@fundp.ac.be (T. Carletti), hskokos@pks.mpg.de (Ch. Skokos), vittot@cpt.univ-mrs.fr (M. Vittot).

former method, that allows direct determination of the new controlled map; avoiding the possible problems related to coordinate inversion.

The aim of control theory is to improve selected features of a given system, by slightly modifying its Hamiltonian with the addition of a *small* control term, so that the new system and the unperturbed one are conjugated namely, they have the same dynamics. This technique is particularly suitable whenever one can directly act on the system and modify it, e.g. in the case of a particle accelerator where the addition of a control term in the Hamiltonian function can be seen as the introduction of a suitable magnet in the accelerator lattice.

In our study, we use the Smaller Alignment Index (SALI) [6,10–12] method, which is an efficient indicator for characterising orbits as chaotic or regular in Hamiltonian flows and symplectic maps. The SALI is computed using the time evolution of two deviation vectors along the studied orbit.

The paper is organized as follows: we introduce the model in Section 2 and present a general result for the control of symplectic maps in Section 3. We apply the theory to the symplectic map model of a standard ring accelerator in Section 4. We briefly recall the SALI chaos indicator in Section 5, while Section 6 presents our numerical results on the behavior of the constructed model. Finally, in Section 7 we summarize our conclusions. Further technical details can be found in Appendix A.

2. The model

Let us consider a system consisting of a charged particle and a simplified accelerator ring with linear frequencies (tunes) q_x, q_y, with a localized thin sextupole magnet (for more details the interested reader is referred to [2]). The magnetic field of this element modifies the orbit once the particle passes through it. The basic model is:

$$
\begin{pmatrix} x_1' \\ x_2' \\ x_3' \\ x_4' \end{pmatrix} = \begin{pmatrix} \cos \omega_1 & -\sin \omega_1 & 0 & 0 \\ \sin \omega_1 & \cos \omega_1 & 0 & 0 \\ 0 & 0 & \cos \omega_2 & -\sin \omega_2 \\ 0 & 0 & \sin \omega_2 & \cos \omega_2 \end{pmatrix} \begin{pmatrix} x_1 \\ x_2 + x_1^2 - x_3^2 \\ x_3 \\ x_4 - 2x_1 x_3 \end{pmatrix} = T \begin{pmatrix} x_1 \\ x_2 \\ x_3 \\ x_4 \end{pmatrix},
\tag{1}
$$

where $x_1(x_3)$ denote the deflection from the ideal circular orbit in the horizontal (vertical) direction before the particle enters the element and $x_2(x_4)$ are the associated momentum. Primed variables denote positions and momenta after the particle left the element. The parameters ω_1 and ω_2 are related to the accelerator's tunes[1] q_x and q_y by the relations $\omega_1 = 2\pi q_x$ and $\omega_2 = 2\pi q_y$. The first matrix in (1) describes the linear motion of a particle, which corresponds to a simple rotation in the phase space. The nonlinearity induced by the thin sextupole magnet is modeled by the 2nd order polynomial expression in (1). The particle dynamics at the nth turn, can be described by the sequence $\left(x_1^{(n)}, x_2^{(n)}, x_3^{(n)}, x_4^{(n)} \right)_{n \geqslant 0}$, where the $(n+1)$th positions and momenta are defined as a function of the nth ones by (1).

The map (1) decomposes in an integrable part and a quadratic perturbation, respectively the system is associated to the following Hamiltonian (see Appendix A)

$$
H(x_1, x_2, x_3, x_4) = -\omega_1 \frac{x_1^2 + x_2^2}{2} - \omega_2 \frac{x_3^2 + x_4^2}{2} \quad \text{and} \quad V(x_1, x_2, x_3, x_4) = -\frac{x_1^3}{3} + x_1 x_3^2,
\tag{2}
$$

more precisely (1) can be written in terms of Poisson brackets[2] as

$$
\vec{x}' = T(\vec{x}) = e^{\{H\}} e^{\{V\}} \vec{x}.
\tag{3}
$$

Here $\vec{x} = (x_1, x_2, x_3, x_4)^{\mathrm{T}}$, with $^{\mathrm{T}}$ denoting the transpose of a matrix, and by definition, for any function f defined in the phase space, $\{H\}f = \{H, f\} = (\nabla H)^{\mathrm{T}} J \nabla f$, with $J = \begin{pmatrix} \mathbf{0} & \mathbf{1} \\ -\mathbf{1} & \mathbf{0} \end{pmatrix}$, being the symplectic constant matrix,

$$
e^{\{H\}} f = \sum_{n \geqslant 0} \frac{\{H\}^n}{n!} f \quad \text{and} \quad \{H\}^n f = \{H\}^{n-1}(\{H\}f).
\tag{4}
$$

Maps of the form (1) have already been studied in [6] where it has been shown that chaotic orbits reduce the DA to a hypersphere of radius ~ 0.39 in the 4-dimensional phase space (see Figs. 5 and 6 of [6]). The goal of the present paper is to show that the stability region of the nominal circular orbit can be increased once the map (1) is controlled by an appropriately designed map.

3. Control theory for symplectic maps

The aim of Hamiltonian theory is to provide mathematic tools to be able to modify the dynamics of a symplectic system. With this, it is possible to manipulate intrinsic features, e.g. to reduce the chaotic regions in phase space or to build invariant tori.

---

[1] Such parameters have been fixed throughout this work to the values $q_x = 0.61803$ and $q_y = 0.4152$, corresponding to a non-resonant condition (see [5]).

[2] In the literature one can sometimes find the alternative equivalent notation $\{H\} = L_H$.

In the following we will be interested in controlling a quasi-integrable symplectic map in such a way that it will allow us to obtain a new, *controlled* map "closer" to the integrable part of the original map, and thus increase the stability region around the nominal circular orbit. This is of great importance since chaos diffusion channels in phase space with unpredictable consequences in configuration space. The controlled map is expected to have a smaller number of escaping orbits and a larger region occupied by invariant curves in a neighbourhood of the origin. For this purpose, we apply the method presented in [8], with the modification that in the present case the integrable part is not expressed in action-angle variables. In particular, the integrable part is a rotation, so the present theory applies to perturbations of rotations, instead of maps close to identity.

Let us consider an integrable symplectic map defined through its infinitesimal generator[3] H

$$\vec{x}' = e^{\{H\}}\vec{x} \tag{5}$$

and consider the quasi-integrable map perturbation of the former

$$\vec{x}' = T(\vec{x}) = e^{\{H\}}e^{\{V\}}\vec{x}, \tag{6}$$

where $\vec{x} \in \mathbb{R}^{2N}$ and V is a perturbation, namely $V = o(H)$. The aim of Hamiltonian control theory, is to construct a third map, the *control map*, whose generator F is small (it satisfies $F = o(V)$). The *controlled map*

$$T_{ctrl} = e^{\{H\}}e^{\{V\}}e^{\{F\}}, \tag{7}$$

will be conjugated to a map T_*, closer to $e^{\{H\}}$ than T (see (11) below). We note that the use of the exponential of a Poisson bracket, ensures that such maps are symplectic by construction.

To be more precise, let us define the unperturbed map

$$\mathcal{A}^{-1} = e^{-\{H\}} \tag{8}$$

and observe that $(1 - \mathcal{A}^{-1})$ is not invertible, since its kernel contains any smooth function of H. Thus we assume the existence of a "pseudo-inverse" operator, $\mathcal{G}$, that should satisfy (see [8] for details)

$$\mathcal{G}(1 - \mathcal{A}^{-1})\mathcal{G} = \mathcal{G}. \tag{9}$$

At this point we can define the *non-resonant* and the *resonant* operators

$$\mathcal{N} := (1 - \mathcal{A}^{-1})\mathcal{G} \quad \text{and} \quad \mathcal{R} := 1 - \mathcal{N}, \tag{10}$$

which are projectors, i.e. $\mathcal{N}^2 = \mathcal{N}$ and $\mathcal{R}^2 = \mathcal{R}$.

Our main theoretical result can be stated in the following theorem:

Theorem 3.1. *Under the above hypotheses and defining* $S = \mathcal{G}V$ *we have*

$$e^{\{S\}}T_{ctrl}e^{-\{S\}} = e^{\{H\}}e^{\{\mathcal{R}V\}} := T_*, \tag{11}$$

where

$$T_{ctrl} = e^{\{H\}}e^{\{V\}}e^{\{F\}} \tag{12}$$

with a control term given by

$$e^{\{F\}} = e^{-\{V\}}e^{\{(\mathcal{N}-\mathcal{G})V\}}e^{\{\mathcal{R}V\}}e^{\{\mathcal{G}V\}}. \tag{13}$$

Remark 3.2 (*Warped addition*). Let us define as in [8] the warped addition, $\{A\} \oplus \{B\}$, of two operators by

$$e^{\{A\}}e^{\{B\}} := e^{\{A\}\oplus\{B\}}. \tag{14}$$

An explicit formula can be obtained using the Baker-Campbell-Hausdorff formula [9], where $\{A\} \oplus \{B\}$ is a series whose first terms are

$$\{A\} \oplus \{B\} = \{A\} + \{B\} + \frac{1}{2}(\{A\}\{B\} - \{B\}\{A\}) + \cdots, \tag{15}$$

hence the warped addition is a deformation of the usual addition between operators.

Proof. Using this warped addition, we can rewrite the controlled map into the form

$$T_{ctrl} = e^{\{H\}\oplus\{V\}\oplus\{F\}}, \tag{16}$$

---

[3] In [8] a similar theory has been developed for a general symplectic map devoid of an infinitesimal generator.

where the control term (13) becomes

$$\{F\} = -\{V\} \oplus \{(\mathcal{N} - \mathcal{G})V\} \oplus \{\mathcal{R}V\} \oplus \{\mathcal{G}V\}. \tag{17}$$

From (10) we have:

$$\mathcal{N} - \mathcal{G} = -\mathcal{A}^{-1}\mathcal{G}. \tag{18}$$

One can easily prove (see Appendix A of [8]) that

$$(-\{H\}) \oplus (-\{S\}) \oplus \{H\} = -\{\mathcal{A}^{-1}S\}, \tag{19}$$

hence, recalling the definition of S and (18), we can rewrite (17) as

$$\{F\} = -\{V\} \oplus (-\{H\}) \oplus (-\{S\}) \oplus \{H\} \oplus \{\mathcal{R}V\} \oplus \{S\}. \tag{20}$$

By rearranging the terms we can easily get

$$\{S\} \oplus \{H\} \oplus \{V\} \oplus \{F\} \oplus (-\{S\}) = \{H\} \oplus \{\mathcal{R}V\}, \tag{21}$$

which is nothing but (11) rewritten using the warped addition. □

Remark 3.3. Let us observe that the control term is, as required, small compared to V. In fact from (17) and by using the approximated formula for the warped addition (15), we obtain

$$\{F\} = -\{V\} \oplus \{(\mathcal{N} - \mathcal{G})V\} \oplus \{\mathcal{R}V\} \oplus \{\mathcal{G}V\} \tag{22}$$

$$= -\{V\} + \{\mathcal{N}V\} - \{\mathcal{G}V\} + \{\mathcal{R}V\} + \{\mathcal{G}V\} + o(V) = o(V), \tag{23}$$

where we use the relation $\mathcal{N} + \mathcal{R} = 1$.

Under the assumption of absence of resonances, i.e. $\mathcal{R}V = 0$, the $o(V)$ term in the control map can be explicitly computed to give (see Appendix A)

$$F = \frac{1}{2}\{V\}\mathcal{G}V + o(V^2). \tag{24}$$

4. The control term for the non-resonant map

In this section we derive the controlled map presented in Section 3 in case of maps of the form (1). To implement the theory we need to diagonalize the operator $\{H\}$. For this reason we introduce complex variables

$$\zeta_1 = x_2 + ix_1 \quad \text{and} \quad \zeta_2 = x_4 + ix_3 \tag{25}$$

and rewrite H as

$$H(\zeta_1, \zeta_2) = -\frac{\omega_1}{2}|\zeta_1|^2 - \frac{\omega_2}{2}|\zeta_2|^2. \tag{26}$$

The Poisson bracket with H now takes the form

$$\{H\} = i\omega_1(\bar{\zeta}_1\partial_{\bar{\zeta}_1} - \zeta_1\partial_{\zeta_1}) + i\omega_2(\bar{\zeta}_2\partial_{\bar{\zeta}_2} - \zeta_2\partial_{\zeta_2}). \tag{27}$$

Hence, for any $\vec{n} = (n_1, n_2) \in \mathbb{N}^2$ and $\vec{m} = (m_1, m_2) \in \mathbb{N}^2$ we obtain

$$\{H\}\zeta^{\vec{n}}\bar{\zeta}^{\vec{m}} = i(\omega_1 m_1 - \omega_1 n_1 + \omega_2 m_2 - \omega_2 n_2)\zeta^{\vec{n}}\bar{\zeta}^{\vec{m}} = i\vec{\omega} \cdot (\vec{m} - \vec{n})\zeta^{\vec{n}}\bar{\zeta}^{\vec{m}}. \tag{28}$$

Here we introduced the vector $\vec{\omega} = (\omega_1, \omega_2)$ and use the compact notation $\zeta^{\vec{n}} = \zeta_1^{n_1}\zeta_2^{n_2}$ for the complex vector $\zeta = (\zeta_1, \zeta_2)$. The operator $\{H\}$ is diagonal in these variables and thus map (8) is straightforwardly obtained as

$$\mathcal{A}^{-1}\zeta^{\vec{n}}\bar{\zeta}^{\vec{m}} = e^{-\{H\}}\zeta^{\vec{n}}\bar{\zeta}^{\vec{m}} = e^{-i\vec{\omega}\cdot(\vec{m}-\vec{n})}\zeta^{\vec{n}}\bar{\zeta}^{\vec{m}}. \tag{29}$$

Once we have this map, we can compute the operators $\mathcal{G}$, $\mathcal{N}$ and $\mathcal{R}$. For all $\vec{n}$ and $\vec{m} \in \mathbb{N}^2 \setminus \{0\}$, such that $\vec{n} \neq \vec{m}$ and

$$\vec{\omega} \cdot (\vec{m} - \vec{n}) \neq 2k\pi \quad \forall k \in \mathbb{Z} \tag{30}$$

(which defines the *non-resonance condition*), we get

$$\mathcal{G}\zeta^{\vec{n}}\bar{\zeta}^{\vec{m}} = \frac{1}{1 - e^{-i\vec{\omega}\cdot(\vec{m}-\vec{n})}}\mathcal{N}\zeta^{\vec{n}}\bar{\zeta}^{\vec{m}}, \tag{31}$$

with

$$\mathcal{N}\zeta^{\vec{n}}\bar{\zeta}^{\vec{m}} = \begin{cases} \zeta^{\vec{n}}\bar{\zeta}^{\vec{m}} & \text{if } \vec{\omega} \cdot (\vec{m} - \vec{n}) \neq 2k\pi \quad \forall k \in \mathbb{Z}, \\ 0 & \text{otherwise}. \end{cases} \tag{32}$$

In the rest of the paper, we will assume the above non-resonant condition (30) to hold for the considered values of q_x and q_y. Let us remark that this is not a limitation of the actual theory, but just a working assumption. We could equivalently have chosen to work in the resonant regime, using a different control term suitable for resonant dynamics.

The explicit computations are as follows: first we need to express V in terms of complex variables; next we compute $S = \mathcal{G}V$, and transform back to the original variables. Finally we compute the exponential $e^{\{\mathcal{G}V\}}$. Actually, even if $\mathcal{G}V$ is a polynomial of degree three in the variables x_1, x_2, x_3, x_4 the map $e^{\{\mathcal{G}V\}}$ is given by an infinite series. The terms of this series can be sequentially computed, but the degree of complexity (i.e. the number of involved terms) increase very fast. To simplify the computations we decided to use the *approximated* generator of the control map (24) already truncated at order 2

$$F_2 = \frac{1}{2}\{V\}\mathcal{G}V. \tag{33}$$

We note that F_2 is composed by about 20 terms. A detailed discussion of the whole procedure needed to obtain F_2, as well as its explicit formula, are presented in Appendix A.

We now face another difficulty, namely the computation of the control map from the generator F_2. This is equivalent to perform the sum

$$e^{\{F_2\}} = 1 + \{F_2\} + \frac{1}{2}\{F_2\}^2 + \cdots, \tag{34}$$

whose complexity once again grows very fast. We thus introduce a second approximation to our construction, by computing only a finite number of terms in the above sum. So, we define a *truncated control map of order k*

$$C_k(F_2) = \sum_{l=0}^{k} \frac{\{F_2\}^l}{l!} \tag{35}$$

and a *truncated controlled map of order k*

$$T_k(F_2) = e^{\{H\}}e^{\{V\}}C_k(F_2) = TC_k(F_2). \tag{36}$$

Since the exact control map $e^{\{F_2\}}$ given by (34) is symplectic, the controlled map (7) will also be symplectic. On the other hand, we cannot expect the kth order control map $C_k(F_2)$ to be symplectic. We know that a map is symplectic if its Jacobian matrix A verifies (in its definition domain) the equality

$$A^{\mathrm{T}}JA - J = 0, \tag{37}$$

Thus, in order to check the *symplecticity defect* of $T_k(F_2)$ we compute the norm D_k of matrix $A_k^{\mathrm{T}}JA_k - J$, where A_k is the Jacobian of $T_k(F_2)$ given by (36). The results are presented in Fig. 1 for orders $k = 1$ up to $k = 5$, in the region $(x_1, x_3) \in [-1, 1] \times [-1, 1]$, $x_2 = x_4 = 0$. The results indicate that $T_k(F_2)$ is a good approximation of a symplectic map for $k \geqslant 4$, because we get $D_k \lesssim 10^{-4}$ for a large portion ($\gtrsim 53\%$) of variables values. We note that in the central region of the truncated controlled map, where the actual physical process of beam's evolution occurs, the symplectic character of the map is established even better since there $D_k \lesssim 10^{-8}$. As expected, the larger the order k, the closer to symplecticity the approximation is.

The main objective of the addition of a control term is to increase the size of the stability region around the central periodic orbit. This increase leads to decrease the number of escaping orbits,[4] as we can see from the results presented in Fig. 2, where we plot in black the initial conditions on the square $(x_1, x_3) \in [-1, 1] \times [-1, 1]$, $x_2 = x_4 = 0$, giving rise to orbits that do not escape up to 10^5 iterations of the map. In particular, we consider in Fig. 2(a) the original uncontrolled map (1), and in Figs. 2(b)–(d), the k order controlled map $T_k(F_2)$ for $k = 1$ to $k = 5$, respectively. One can easily see that the region of non-escaping orbits for the original map is smaller than the one of the controlled maps. This observation can be quantified by considering initial conditions inside a circle centered at the origin of each panel of Fig. 2 (which represent the actual physical plane since the initial momenta are $x_2^{(0)} = x_4^{(0)} = 0$) with radius $r^2 = x_1^{(0)^2} + x_3^{(0)^2}$, and evaluate the number of escaping and non-escaping orbits as a function of the circle radius for $T_k(F_2)$ with $k = 1$ up to $k = 5$. Results reported in Fig. 3 support the previous claim, by clearly showing that controlled maps of orders 3, 4 and 5 behave very similarly and lead to an increase of the non-escaping region. Let us note that the behavior of the controlled maps of orders $k = 1$ (Fig. 2(b)) and $k = 2$ (Fig. 2(c)) is somewhat misleading if it is not analyzed together with the information from the symplecticity defect (see Fig. 1(a) and (b), respectively). In fact, these maps are strongly dissipative and produce a strong shift of orbits towards the origin, preventing them from escaping. This dissipation effect is not physical, as it is not observed in real accelerators, and therefore we do not discuss further the $k = 1$ and $k = 2$ controlled maps.

---

[4] An orbit $\left(x_1^{(k)}, x_2^{(k)}, x_3^{(k)}, x_4^{(k)}\right)_{0 \leqslant k \leqslant N}$ is defined as non-escaping if for all $k \leqslant N x_1^{(k)^2} + x_2^{(k)^2} + x_3^{(k)^2} + x_4^{(k)^2} \leqslant R^2$ for a certain R (in the simulations we used $R^2 = 10$ and $N = 10^4, 10^5$) and escaping otherwise.
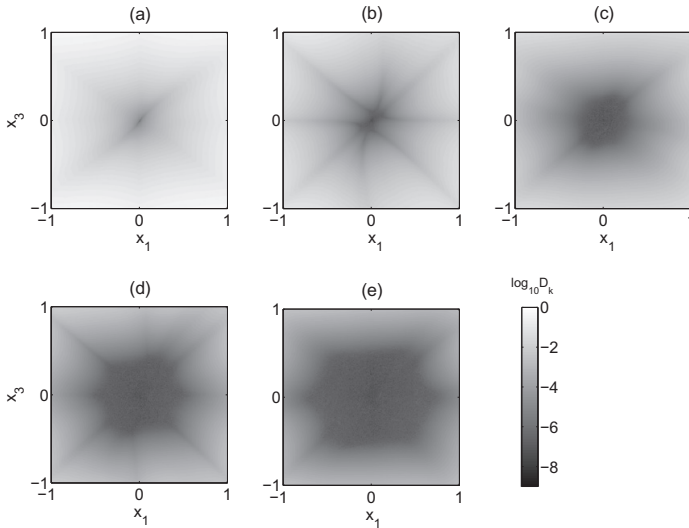
Fig. 1. The simplicity defect of the controlled map $T_k(F_2)$ (36). Plot of $\log_{10}D_k$, where $D_k = \left\| A_k^T J A_k - J \right\|$ and A_k is the Jacobian of the k-order controlled map $T_k(F_2)$ given by (36), for 16000 uniformly distributed values in the square $(x_1, x_3) \in [-1, 1] \times [-1, 1]$, $x_2 = x_4 = 0$, for (a) $k = 1$, (b) $k = 2$, (c) $k = 3$, (d) $k = 4$ and (e) $k = 5$. The percentage of orbits with $\log_{10}D_k < -4$ is 0.5%, 11%, 28%, 53% and 73% for $k = 1, 2, 3, 4$ and 5 respectively. The gray scale corresponds to the value of $\log_{10}D_k$: the darker the color, the smaller the value of $\log_{10}D_k$ is, and hence the closer the map is to a symplectic one.
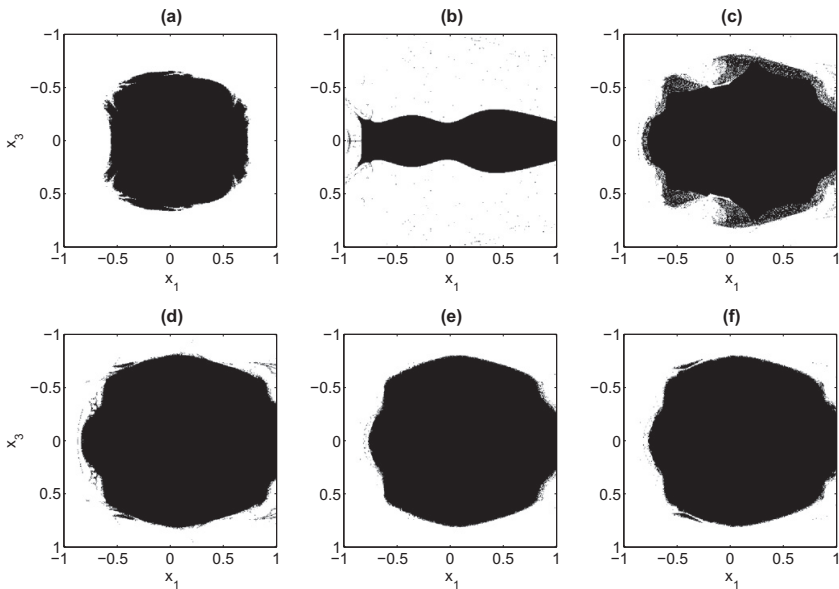
Fig. 2. Non-escaping regions of controlled map $T_k(F_2)$ as a function of the truncation order k. 16000 uniformly distributed initial conditions in the square $(x_1, x_3) \in [-1, 1] \times [-1, 1]$, $x_2^{(0)} = x_4^{(0)} = 0$ are iterated up to $n = 10^5$ using (a) the uncontrolled map (1) and (b)–(f) the $k = 1$ to $k = 5$ order controlled map $T_k(F_2)$ (36), respectively. Initial conditions corresponding to non-escaping orbits up to $n = 10^5$ are coloured in black, while escaping orbits are colored in white.
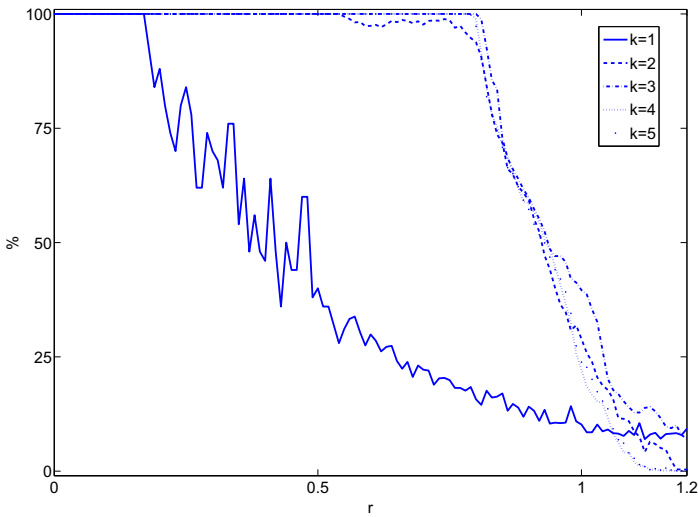
Fig. 3. Percentages of non-escaping orbits for the controlled map $T_k(F_2)$ (36) as a function of the distance from the origin in the physical space (x_1, x_3). We iterate initial conditions in a circle of radius r centred at the origin of plane (x_1, x_3), with $x_2^{(0)} = x_4^{(0)} = 0$, and compute the percentages of non-escaping orbits during $n = 10^5$ iterations, for the controlled map $T_k(F_2)$ with $k = 1, 2, 3, 4, 5$, as a function of r.

From the results of Figs. 2 and 3 we see that the addition of even the lower order ($k = 3$) control term, having an acceptable symplecticity defect, increases drastically the size of the region of non-escaping orbits around the central periodic orbit. A further increase of the order of the control term results to less significant increment of this region, while the computational effort for constructing the controlled map increases considerably. In fact, $T_1(F_2)$ contains around 100 elementary terms, i.e. monomials in $x_1 \ldots x_4$, while this number is almost doubled for each order, so that $T_5(F_2)$ contains around 2000 terms. Also the CPU time needed to evolve the orbits increases with the order. For example, while the integration of one orbit using $T_1(F_2)$ takes about 1.4 times the CPU time needed to integrate the original map (1), the use of $T_5(F_2)$ needs almost 21.5 times more.

Thus we conclude that the $T_4(F_2)$ controlled map, which can be considered quite accurately to be symplectic, is sufficient to get significant increment of the percentage of non-escaping orbits, without paying an extreme computational cost.

5. The SALI method

The Smaller Alignment Index (SALI) [10] has been proved to be an efficiently simple method to determine the regular or chaotic nature of orbits in conservative dynamical systems. Thanks to its properties, it has already been successfully distinguished between regular and chaotic motion both, in symplectic maps and Hamiltonian flows [11–15].

For the sake of completeness, let us briefly recall the definition of the SALI and its behavior for regular and chaotic orbits, restricting our attention to $2N$-dimensional symplectic maps. The interested reader can consult [10] for a more detailed description. To compute the SALI of a given orbit of such maps, one has to follow the time evolution of the orbit itself and also of two linearly independent unitary deviation vectors $\hat{v}_1^{(0)}$, $\hat{v}_2^{(0)}$. The evolution of an orbit of a map T is described by the discrete-time equations of the map

$$\vec{x}^{(n+1)} = T(\vec{x}^{(n)}), \tag{38}$$

where $\vec{x}^{(n)} = \left(x_1^{(n)}, x_2^{(n)}, \ldots, x_{2N}^{(n)} \right)^{\mathrm{T}}$, represents the orbit's coordinates at the nth iteration. The deviation vectors $\vec{v}_1^{(n)}$, $\vec{v}_2^{(n)}$ at time n are given by the tangent map

$$\vec{v}_i^{(n+1)} = A(\vec{x}^{(n)}) \cdot \vec{v}_i^{(n)}, \quad i = 1, 2, \tag{39}$$

where A denotes the Jacobian matrix of map (38), evaluated at the points of the orbit under study. Then, according to [10] the SALI for the given orbit is defined as

$$\mathrm{SALI}(n) = min\left\{ \left\| \hat{v}_1^{(n)} + \hat{v}_2^{(n)} \right\|, \left\| \hat{v}_1^{(n)} - \hat{v}_2^{(n)} \right\| \right\}, \tag{40}$$

where $\|\cdot\|$ denotes the usual Euclidean norm and $\hat{v}_i = \frac{\vec{v}_i}{\|\vec{v}_i\|}$, $i = 1, 2$ are unitary normalised vectors.

In the case of chaotic orbits, the deviation vectors $\hat{v}_1$, $\hat{v}_2$ eventually become aligned in the direction defined by the maximal Lyapunov characteristic exponent (LCE), and SALI (n) falls exponentially to zero. An analytical study of SALI's behavior for chaotic orbits was carried out in [12] where it was shown that

$$\text{SALI}(n) \propto e^{-(\sigma_1 - \sigma_2)n} \tag{41}$$

with σ_1, σ_2 being the two largest LCEs.

On the other hand, in the case of regular motion the orbit lies on a torus and the vectors $\hat{v}_1$, $\hat{v}_2$ eventually fall on its tangent space, following a n^{-1} time evolution, having in general different directions. This behavior is due to the fact that for regular orbits, the norm of a deviation vector increases linearly in time. Thus, the normalization procedure brings about a decrease of the magnitude of the coordinates perpendicular to the torus, at a rate proportional to n^{-1}, and so $\hat{v}_1$, $\hat{v}_2$ eventually fall on the tangent space of the torus. In this case, the SALI oscillates about non-zero values (for more details see [11]).

The simplicity of SALI's definition, its completely different behavior for regular and chaotic orbits and its rapid convergence to zero in the case of chaotic motion are the main advantages that make SALI an ideal chaos detection tool. Recently a generalization of the SALI, the so-called Generalized Alignment Index (GALI) has been introduced [16,17], which uses information of more than two deviation vectors from the reference orbit. Since the advantages of GALI over SALI become relevant in the case of multi-dimensional systems, in the present paper we apply the SALI method for the dynamical study of the 4D map (1).

6. Dynamics of the controlled map

As already mentioned, the goal of constructing the controlled map $T_{ctrl} = Te^{\{F\}}$ is to increase the percentage of regular orbits up to a given (large) number of iterations, or equivalently increase the size of the stability region around the nominal circular trajectory (i.e. the DA). Because the presence of chaotic regions can induce a large drift in the phase space, that eventually could lead to the escape of orbits, the achievement of a larger DA can be qualitatively inspected by checking via the SALI method the regular or chaotic nature of orbits in a neighborhood of the origin (see Fig. 4). We note that we define an orbit to be chaotic whenever SALI $(t) < 10^{-8}$, and regular for the contrary.
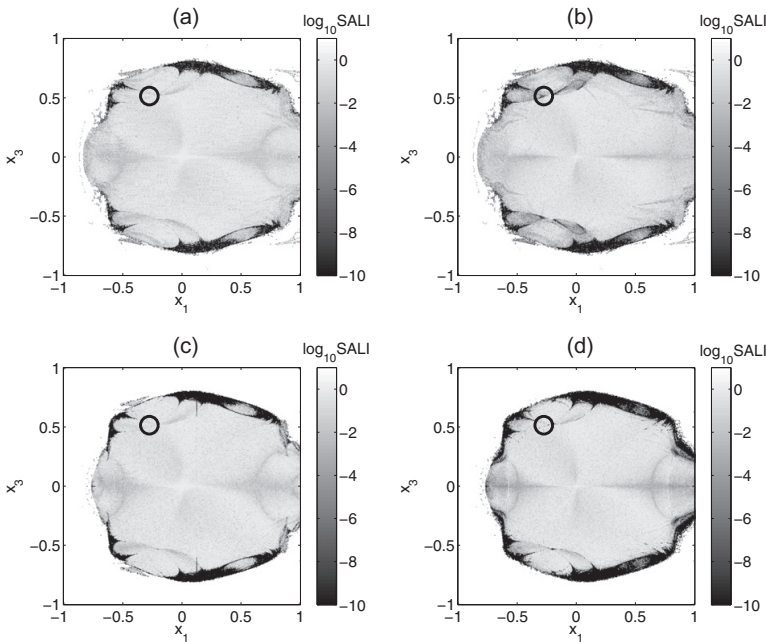

Fig. 4. Stability analysis in the (x_1, x_3) plane. 16000 uniformly distributed initial conditions in the square $(x_1, x_3) \in [-1, 1] \times [-1, 1]$, $x_2^{(0)} = x_4^{(0)} = 0$ are integrated using the $T_3(F_2)$ ((a) and (b)), and the $T_4(F_2)$ controlled map ((c) and (d)), up to $n = 10^4$ ((a) and (c)) and $n = 10^5$ iterations ((b) and (d)). The gray scale represents the value of $\log_{10}$SALI for each orbit at the end of the integration time. The lighter the color the more stable is the orbit, while white color denotes that an orbit escaped before the total number of iterations was reached. The black circle indicate the initial condition of the orbit studied in Fig. 5.
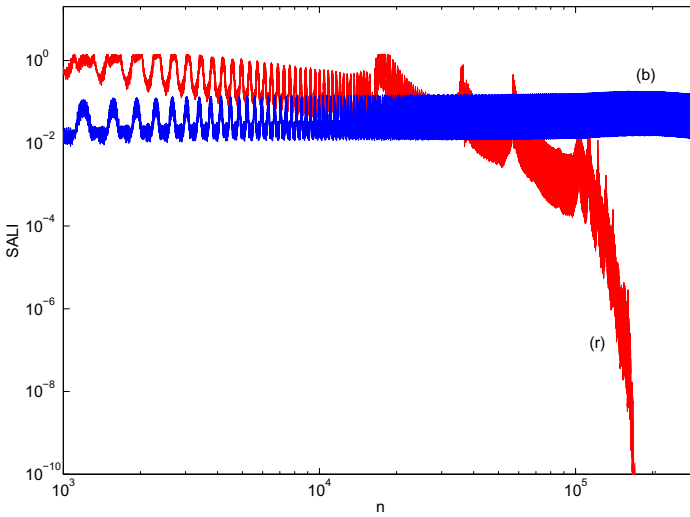
Fig. 5. Dynamics of two orbits with the same initial conditions for the 3rd and 4th order controlled maps. Time evolution of the SALI for the orbit with initial conditions $\vec{x}^{(0)} = (-0.50, 0, -0.65, 0)^{\mathsf{T}}$ (see Fig. 4), using the $T_3(F_2)$ [(r) red curve] and the $T_4(F_2)$ controlled map [(b) blue curve]. (For interpretation of the references to colour in this figure legend, the reader is referred to the web version of this article.)

In Fig. 4 (which should be compared with Fig. 5 of [6]) we observe a strong enlargement of the region of regular orbits. This region is characterized by large SALI values. In particular, for 10^4 iterations of the $T_4(F_2)$ map, 54% of the considered orbits are regular, while for the uncontrolled map this percentage reduces to 33%. This improvement can be also confirmed by visual inspection of Fig. 2, where the regions of non-escaping orbits are shown for different orders of the controlled map (36).

In Fig. 4(a) and (b) we see that there exist orbits of the $T_3(F_2)$ map, which are characterized as regular up to $n = 10^4$ iterations, while they show their chaotic character once they are iterated up to $n = 10^5$. Such orbits correspond to the dark regions marked by a black circle in Fig. 4(b) (for comparison this circle is also plotted in all panels of Fig. 4). This discrepancy is absent for the $T_4(F_2)$ map, which shows almost the same geometrical shape for the non-escaping region when we pass from 10^4 to 10^5 iterations. In order to better understand this behavior we followed the evolution of a single orbit with initial condition $\vec{x}^{(0)} = (-0.50, 0, -0.65, 0)^{\mathsf{T}}$ –inside the black circle in Fig. 4 – for both the $T_3(F_2)$ and the $T_4(F_2)$ controlled maps, computing the corresponding SALI values up to 2×10^5 iterations. The results are reported in Fig. 5 and clearly show that the orbit behaves regularly up to $n \approx 10^5$ iterations of the $T_3(F_2)$ map, since its SALI values are different from zero, but later on a sudden decrease of SALI to zero denotes the chaotic character of the orbit. This behavior clearly implies this is a slightly chaotic, sticky orbit, which remains close to a torus for long time intervals ($n \approx 10^5$), while later on it enters a chaotic region of the phase space. It is interesting to note that iterating the same initial condition by the $T_4(F_2)$ map we get a regular behavior at least up to $n = 2 \times 10^5$.
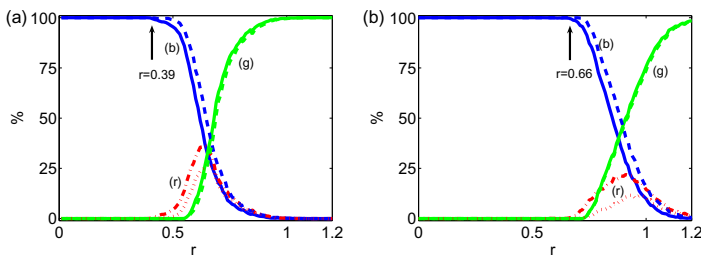

Fig. 6. Dynamical aperture of the (a) original map (1) and (b) the $T_4(F_2)$ controlled map (36). The percentages of regular [(b) blue curves], escaping [(g) green curves] and chaotic [(r) red curves] orbits after $n = 10^4$ (dashed curves) and $n = 10^5$ iterations (solid curves) for initial conditions in a 4D sphere centred at the origin $x_1 = x_2 = x_3 = x_4 = 0$, as a function of the sphere radius r. Each point corresponds the average value over 5000 initial conditions. The largest radius at which the percentage of regular orbits is still 100%, is marked by an arrow in each panel. (For interpretation of the references to colour in this figure legend, the reader is referred to the web version of this article.)

In order to provide additional numerical evidence of the effectiveness of the controlled map (36) in increasing the DA, we consider initial conditions inside a 4D sphere centered at the origin $x_1 = x_2 = x_3 = x_4 = 0$ of the map, with radius, $r^2 = x_1^{(0)^2} + x_2^{(0)^2} + x_3^{(0)^2} + x_4^{(0)^2}$. We compute the number of regular, escaping and chaotic orbits as a function of the sphere radius. The corresponding results are reported in Fig. 6(b), while in Fig. 6(a) we reproduce Fig. 6 of [6] for comparison. From this figure we observe a strong increase of the DA, since the largest sphere containing 100% regular orbits has a radius $r \approx 0.66$, while this radius was $r \approx 0.39$ for the original uncontrolled map. We also observe that increasing the total number of iterations from 10^4 to 10^5 (dashed and solid lines in Fig. 6 respectively) increases the percentage of chaotic orbits, but the radius of the 4D sphere containing only regular orbits does not change significantly.

7. Conclusions

In this paper we considered a simple model of a ring particle accelerator with sextupole nonlinearity that can be described by a symplectic map. In the framework of Hamiltonian control theory, we were able to control the dynamics of the original system, by providing a suitable control map, resulting in a small "perturbation" of the initial map. This control map has been constructed with the aim of DA enlargement of the particle accelerator, and thus improving the beam's lifetime and the accelerator's performance.

In particular, the theoretical framework we developed allows a 1-parameter family of approximated controlled maps. We performed several numerical simulations in order to choose "the best" approximated controlled map $T_k(F_2)$ (36), taking into account the complexity of the map, i.e. the number of terms by which it is composed, the CPU time needed to perform the numerical iteration of orbits, and the accuracy of the results in terms of the symplectic character of the map. We find that the 4th order controlled map $T_4(F_2)$ is an optimal choice for the controlled system.

Using this controlled map we succeeded in achieving our initially set goal, since the $T_4(F_2)$ map exhibits a DA with a radius more than 1.7 times larger than the one for the original map (see Fig. 6).

Acknowledgement

Appendix A. Computation of the control term

The aim of this section is to introduce further details for the construction of the control term and of the controlled map, and to provide explicit formulas for the interested reader.

A.1. Notations

Let us first introduce some notations and recall some useful relations.

- **Lie brackets and operators.** Let $\mathcal{X}$ be the vector space of C^∞ real or complex functions of $2N$ variables (p, q). For any $F, G \in \mathcal{X}$, the Lie bracket is given by

$$\{F, G\} := \sum_{i=1}^{N} [\partial_{p_i} F \partial_{q_i} G - \partial_{q_i} F \partial_{p_i} G], \tag{A.1}$$

where $\partial_x f \equiv \frac{\partial f}{\partial x_i}$ denotes the partial derivative with respect to the variable x_i.

Using the above definition, we can define a linear operator, induced by an element F of $\mathcal{X}$, acting on $\mathcal{X}$

$$\begin{aligned} \{F\} : \mathcal{X} &\to \mathcal{X}, \\ G &\mapsto \{F\}G := \{F, G\}. \end{aligned} \tag{A.2}$$

This operator is *linear*, *antisymmetric* and verifies the *Jacobi identity*

$$\forall F, G \in \mathcal{X} \quad \{\{F\}G\} = \{F\}\{G\} - \{G\}\{F\}. \tag{A.3}$$

- **Exponential.** We define the exponential of such an operator $\{F\}$, by

$$e^{\{F\}} := \sum_{k=0}^{\infty} \frac{\{F\}^k}{k!}, \tag{A.4}$$

which is also an operator acting on $\mathcal{X}$. The power of an operator is the composition: $\{F\}^k G = \{F\}^{k-1}(\{F\}G)$.

We observe that in the case of the Hamiltonian function H, the exponential provides the flow, namely $e^{\{H\}}x_0 = x(t)$, of the Hamilton equations

$$\begin{cases} \dot{p} & = -\partial_q H, \\ \dot{q} & = \partial_p H. \end{cases} \tag{A.5}$$

- **Vector field.** The action of the above defined operators, can be extended to vector fields "component by component"

$$\forall F, G, H \in \mathcal{X}, \quad \{F\} \begin{pmatrix} G \\ H \end{pmatrix} := \begin{pmatrix} \{F\}G \\ \{F\}H \end{pmatrix}. \tag{A.6}$$

A.2. Mappings as time-1 flows

We show now that map (1) can be seen as the time-1 flow of a given Hamiltonian system. More precisely we show that

$$T \begin{pmatrix} x_1 \\ x_2 \\ x_3 \\ x_4 \end{pmatrix} = \begin{pmatrix} \cos(\omega_1) & -\sin(\omega_1) & 0 & 0 \\ \sin(\omega_1) & \cos(\omega_1) & 0 & 0 \\ 0 & 0 & \cos(\omega_2) & -\sin(\omega_2) \\ 0 & 0 & \sin(\omega_2) & \cos(\omega_2) \end{pmatrix} \begin{pmatrix} x_1 \\ x_2 + x_1^2 - x_3^2 \\ x_3 \\ x_4 - 2x_1x_3 \end{pmatrix} = e^{\{H\}}e^{\{V\}} \begin{pmatrix} x_1 \\ x_2 \\ x_3 \\ x_4 \end{pmatrix}, \tag{A.7}$$

where

$$H(x_1, x_2, x_3, x_4) = -\omega_1 \frac{x_1^2 + x_2^2}{2} - \omega_2 \frac{x_3^2 + x_4^2}{2} \tag{A.8}$$

and

$$V(x_1, x_2, x_3, x_4) = -\frac{x_1^3}{3} + x_1 x_3^2. \tag{A.9}$$

Let us observe that H is the sum of two non-interacting harmonic oscillators with frequencies ω_1 and ω_2, hence its dynamics is explicitly given by

$$\begin{cases} x_1(t) & = A\cos(\omega_1 t) - B\sin(\omega_1 t), \\ x_2(t) & = B\cos(\omega_1 t) + A\sin(\omega_1 t), \\ x_3(t) & = C\cos(\omega_2 t) - D\sin(\omega_2 t), \\ x_4(t) & = D\cos(\omega_2 t) + C\sin(\omega_2 t). \end{cases} \tag{A.10}$$

By definition $\vec{y} = e^{\{H\}}\vec{x}$ is the solution at time 1 with initial condition $\vec{x} = (x_1, x_2, x_3, x_4)^{\mathsf{T}}$, hence we obtain

$$\begin{cases} y_1 & = \cos(\omega_1)x_1 - \sin(\omega_1)x_2, \\ y_2 & = \sin(\omega_1)x_1 + \cos(\omega_1)x_2, \\ y_3 & = \cos(\omega_2)x_3 - \sin(\omega_2)x_4, \\ y_4 & = \sin(\omega_2)x_3 + \cos(\omega_2)x_4, \end{cases} \tag{A.11}$$

that is

$$e^{\{H\}} \begin{pmatrix} x_1 \\ x_2 \\ x_3 \\ x_4 \end{pmatrix} = \begin{pmatrix} \cos(\omega_1) & -\sin(\omega_1) & 0 & 0 \\ \sin(\omega_1) & \cos(\omega_1) & 0 & 0 \\ 0 & 0 & \cos(\omega_2) & -\sin(\omega_2) \\ 0 & 0 & \sin(\omega_2) & \cos(\omega_2) \end{pmatrix} \begin{pmatrix} x_1 \\ x_2 \\ x_3 \\ x_4 \end{pmatrix}. \tag{A.12}$$

From (A.9) and the definition (A.2) we easily get

$$\begin{aligned} \{V\} &:= \partial_{x_2}V\partial_{x_1} - \partial_{x_1}V\partial_{x_2} + \partial_{x_4}V\partial_{x_3} - \partial_{x_3}V\partial_{x_4}, \\ &= (x_1^2 - x_3^2)\partial_{x_2} - 2x_1x_3\partial_{x_4}. \end{aligned} \tag{A.13}$$

This means that once applied to a vector $\vec{x}$ only the second and fourth components of $\{V\}\vec{x}$ will be non-zero and moreover they only depend on the first and third components of $\vec{x}$, hence $\{V\}^2\vec{x} = \vec{0}$. We can thus conclude that $\forall k \geqslant 2$ and $\forall \vec{x} \in \mathbb{R}^4$, we get $\{V\}^k\vec{x} = \vec{0}$. Finally using the definition (A.4) we obtain

$$e^{\{V\}}\vec{x} = \sum_{k=0}^{\infty} \frac{\{V\}^k}{k!}\vec{x} = I\vec{x} + \{V\}\vec{x} = \begin{pmatrix} x_1 \\ x_2 + x_1^2 - x_3^2 \\ x_3 \\ x_4 - 2x_1x_3 \end{pmatrix}. \tag{A.14}$$

A.3. Computation of the generator F under the assumption $\mathcal{R}V \equiv 0$

Let us recall that the composition of maps expressed by exponential defines the warped addition

$$e^{\{A\}}e^{\{B\}} := e^{\{A\}\oplus\{B\}}, \tag{A.15}$$

whose first terms are

$$\{A\} \oplus \{B\} = \{A\} + \{B\} + \frac{1}{2}(\{A\}\{B\} - \{B\}\{A\}) + \cdots. \tag{A.16}$$

Using the warped addition with Eq. (13) of Theorem 3.1, we obtain

$$e^{\{F\}} = e^{-\{V\}}e^{\{(\mathcal{N}-\mathcal{G})V\}}e^{\{\mathcal{R}V\}}e^{\{\mathcal{G}\mathcal{V}\}} = e^{-\{V\}\oplus\{(\mathcal{N}-\mathcal{G})V\}\oplus\{\mathcal{R}V\}\oplus\{\mathcal{G}\mathcal{V}\}} \tag{A.17}$$

and thus

$$\{F\} = -\{V\} \oplus \{(\mathcal{N}-\mathcal{G})V\} \oplus \{\mathcal{R}V\} \oplus \{\mathcal{G}\mathcal{V}\} = -\{V\} \oplus \{(1-\mathcal{G})V\} \oplus \{\mathcal{G}\mathcal{V}\} + o(V^2)$$

$$= \left[\frac{1}{2}\underbrace{(\{V\}\{\mathcal{G}\mathcal{V}\} - \{\mathcal{G}\mathcal{V}\}\{V\})}_{=(A.3)\ V\}\mathcal{G}\mathcal{V}\}} -\{\mathcal{G}\mathcal{V}\} \right] \oplus \{\mathcal{G}\mathcal{V}\} + o(V^2) = \frac{1}{2}\{\{V\}\mathcal{G}\mathcal{V}\} + \frac{1}{4}\underbrace{\{\{\{V\}\mathcal{G}\mathcal{V}\}\mathcal{G}\mathcal{V}\}}_{=o(V^2)} + o(V^2)$$

$$= \frac{1}{2}\{\{V\}\mathcal{G}\mathcal{V}\} + o(V^2), \tag{A.18}$$

where we explicitly used the assumption $\mathcal{R}V = 0$ to remove the third term on the right hand side on the first equation and hence to write $\mathcal{N}V = V$. We are thus able to define the non-resonant control term, up to order V^2, to be

$$F_2 = \frac{1}{2}\{V\}\mathcal{G}V = \frac{1}{2}\{V, \mathcal{G}V\}. \tag{A.19}$$

A.4. The operator $\mathcal{G}$

To get the explicit formula for F_2 we need to compute the expression of $\mathcal{G}$. From definition (9) the operator $\mathcal{G}$ should satisfy

$$\mathcal{G}(1 - e^{-\{H\}})\mathcal{G} = \mathcal{G}. \tag{A.20}$$

To construct it, it will be more convenient to use complex variables

$$\zeta_1 = x_2 + ix_1 \quad \text{and} \quad \zeta_2 = x_4 + ix_3. \tag{A.21}$$

Then the function H becomes

$$H(\zeta_1, \zeta_2) = -\frac{\omega_1}{2}\zeta_1\bar{\zeta}_1 - \frac{\omega_2}{2}\zeta_2\bar{\zeta}_2 \tag{A.22}$$

and using

$$\frac{\partial}{\partial x_1} = \frac{\partial\zeta_1}{\partial x_1}\frac{\partial}{\partial\zeta_1} + \frac{\partial\bar{\zeta}_1}{\partial x_1}\frac{\partial}{\partial\bar{\zeta}_1} = i\frac{\partial}{\partial\zeta_1} - i\frac{\partial}{\partial\bar{\zeta}_1}, \tag{A.23}$$

$$\frac{\partial}{\partial x_2} = \frac{\partial\zeta_1}{\partial x_2}\frac{\partial}{\partial\zeta_1} + \frac{\partial\bar{\zeta}_1}{\partial x_2}\frac{\partial}{\partial\bar{\zeta}_1} = \frac{\partial}{\partial\zeta_1} + \frac{\partial}{\partial\bar{\zeta}_1} \tag{A.24}$$

for (x_1, x_2), the operator $\{H\}$ becomes

$$\partial_{x_2}H\partial_{x_1} - \partial_{x_1}H\partial_{x_2} = 2i(\partial_{\zeta_1}H\partial_{\bar{\zeta}_1} - \partial_{\bar{\zeta}_1}H\partial_{\zeta_1}) = i\omega_1(\bar{\zeta}_1\partial_{\bar{\zeta}_1} - \zeta_1\partial_{\zeta_1}) \tag{A.25}$$

with a similar expression holding for (x_3, x_4). Hence for any $\vec{n} = (n_1, n_2) \in \mathbb{N}^2$ and $\vec{m} = (m_1, m_2) \in \mathbb{N}^2$ we obtain

$$\{H\}\zeta^{\vec{n}}\bar{\zeta}^{\vec{m}} = i(\omega_1 m_1 - \omega_1 n_1 + \omega_2 m_2 - \omega_2 n_2)\zeta^{\vec{n}}\bar{\zeta}^{\vec{m}} = i\vec{\omega}\cdot(\vec{m}-\vec{n})\zeta^{\vec{n}}\bar{\zeta}^{\vec{m}}, \tag{A.26}$$

where we introduced the vector $\vec{\omega} = (\omega_1, \omega_2)$ and we used the compact notation $\zeta^{\vec{n}} = \zeta_1^{n_1}\zeta_2^{n_2}$, for the complex vector $\zeta = (\zeta_1, \zeta_2)$.

We note that from the knowledge of the operators' action on such monomials $\zeta^{\vec{n}}\bar{\zeta}^{\vec{m}}$, we can reconstruct the operator action on any regular function. The operators are linear and they will be applied on polynomials in the $\vec{x}$ variable, which are nothing more than polynomials in the complex variables.

Let us now compute the time-1 flow of $\{H\}$ by using complex variables. Starting from (A.26) and then proceeding by induction, we can easily prove that for all $k \in \mathbb{N}$

$$\{H\}^k \zeta^{\vec{n}} \bar{\zeta}^{\vec{m}} = (i\vec{\omega} \cdot (\vec{m} - \vec{n}))^k \zeta^{\vec{n}} \bar{\zeta}^{\vec{m}} \tag{A.27}$$

and finally

$$e^{\{H\}} \zeta^{\vec{n}} \bar{\zeta}^{\vec{m}} = \sum_{k=0}^{\infty} \frac{(i\vec{\omega} \cdot (\vec{m} - \vec{n}))^k}{k!} \zeta^{\vec{n}} \bar{\zeta}^{\vec{m}} = e^{i\vec{\omega} \cdot (\vec{m} - \vec{n})} \zeta^{\vec{n}} \bar{\zeta}^{\vec{m}}. \tag{A.28}$$

Similarly $e^{-\{H\}} \zeta^{\vec{n}} \bar{\zeta}^{\vec{m}} = e^{-i\vec{\omega} \cdot (\vec{m} - \vec{n})} \zeta^{\vec{n}} \bar{\zeta}^{\vec{m}}$.

Assuming a non-resonance condition

$$\vec{\omega} \cdot (\vec{m} - \vec{n}) \neq 2k\pi \quad \forall \vec{n} \neq \vec{m} \in \mathbb{N}^2 \setminus \{0\} \quad \text{and} \quad \forall k \in \mathbb{Z}, \tag{A.29}$$

a possible choice for the operator $\mathcal{G}$ is the following

$$\mathcal{G} \zeta^{\vec{n}} \bar{\zeta}^{\vec{m}} := \frac{1}{1 - e^{-i\vec{\omega} \cdot (\vec{m} - \vec{n})}} \mathcal{N} \zeta^{\vec{n}} \bar{\zeta}^{\vec{m}} \tag{A.30}$$

with

$$\mathcal{N} \zeta^{\vec{n}} \bar{\zeta}^{\vec{m}} = \begin{cases} \zeta^{\vec{n}} \bar{\zeta}^{\vec{m}} & \text{if } \vec{\omega} \cdot (\vec{m} - \vec{n}) \neq 2\pi k, \\ 0 & \text{otherwise.} \end{cases} \tag{A.31}$$

It is easy to check that the operator $\mathcal{G}$ defined by (A.30) verifies (A.20). In order to do so we introduce the compact notation

$$Z_{n,m} := \zeta^{\vec{n}} \bar{\zeta}^{\vec{m}} \quad \text{and} \quad \Box_{n,m} := e^{-i\vec{\omega} \cdot (\vec{m} - \vec{n})}. \tag{A.32}$$

Developing the left hand side of (A.20) and using the linearity of all operators, we get

$$\mathcal{G}\left(1 - e^{-\{H\}}\right) \mathcal{G} Z_{n,m} = (\mathcal{G} - \mathcal{G} e^{-\{H\}}) \frac{1}{1 - \Box_{n,m}} Z_{n,m}, \tag{A.33}$$

$$= \frac{1}{1 - \Box_{n,m}} \mathcal{G} Z_{n,m} - \frac{1}{1 - \Box_{n,m}} \mathcal{G} e^{-\{H\}} Z_{n,m}, \tag{A.34}$$

$$= \frac{1}{(1 - \Box_{n,m})^2} Z_{n,m} - \frac{1}{1 - \Box_{n,m}} \mathcal{G}(\Box_{n,m} Z_{n,m}), \tag{A.35}$$

$$= \frac{1}{(1 - \Box_{n,m})^2} Z_{n,m} - \frac{\Box_{n,m}}{(1 - \Box_{n,m})^2} Z_{n,m}, \tag{A.36}$$

$$= \frac{1}{1 - \Box_{n,m}} Z_{n,m} = \mathcal{G} Z_{n,m}. \tag{A.37}$$

A.5. Expression of the control term F_2

The function F_2 is defined by (A.19), where V is a known function. The term $\mathcal{G}V$ will be computed starting from the previously obtained expression of $\mathcal{G}$. To construct F_2 we first have to express V in the complex variables (A.21):

$$V(\zeta_1, \zeta_2) = -\frac{1}{24} i\zeta_1^3 + \frac{1}{8} i\bar{\zeta}_1 \zeta_1^2 - \frac{1}{8} i\bar{\zeta}_1^2 \zeta_1 + \frac{1}{24} i\bar{\zeta}_1^3 + \frac{1}{8} i\zeta_1 \zeta_2^2 - \frac{1}{4} i\zeta_1 \zeta_2 \bar{\zeta}_2 + \frac{1}{8} i\zeta_1 \bar{\zeta}_2^2 - \frac{1}{8} i\bar{\zeta}_1 \zeta_2^2 + \frac{1}{4} i\bar{\zeta}_1 \zeta_2 \bar{\zeta}_2 - \frac{1}{8} i\bar{\zeta}_1 \bar{\zeta}_2^2. \tag{A.38}$$

By the linearity of the operator, and by using (A.30), we easily compute $\mathcal{G}V$. In particular we apply $\mathcal{G}$ to each term of (A.38). Then using the inverse change of coordinates

$$x_1 = \frac{1}{2} i(\bar{\zeta}_1 - \zeta_1) \quad \text{and} \quad x_2 = \frac{1}{2}(\zeta_1 + \bar{\zeta}_1) \tag{A.39}$$

(similar expressions hold for (x_3, x_4) and $(\zeta_2, \bar{\zeta}_2)$), we can go back to the original variables $\vec{x}$. The obtained expression after some algebraic simplifications is

$$\mathcal{G}V = -1/6 \csc(3/2\omega_1)[x_2 \cos(1/2\omega_1) + x_1 \sin(1/2\omega_1)][x_1^2 - 3x_3^2 + x_2^2 + (2x_1^2 - 6x_3^2 + x_2^2)\cos(\omega_1) - x_1 x_2 \sin(\omega_1)]$$

$$+ 1/4 \frac{\sin(\omega_2)}{\cos(\omega_1 - \omega_2) - \cos(\omega_2)} - 1/4 \frac{(-x_2 x_4^2 + x_2 x_3^2 + 2x_1 x_4 x_3)\sin(\omega_2)}{\cos(\omega_2) - \cos(\omega_1 + \omega_2)}. \tag{A.40}$$

Then the explicit expression of the control term F_2 is

$$F_2 = 1/2(x_1^2 - x_3^2)\Big(-1/6 \csc(3/2\omega_1)\cos(1/2\omega_1)(x_1^2 - 3x_3^2 + x_2^2 + (2x_1^2 - 6x_3^2 + x_2^2)\cos(\omega_1) - x_1 x_2 \sin(\omega_1))$$

$$- 1/6 \csc(3/2\omega_1)(x_2 \cos(1/2\omega_1) + x_1 \sin(1/2\omega_1))(2x_2 + 2x_2 \cos(\omega_1) - x_1 \sin(\omega_1))$$

$$- 1/4 \frac{(x_3^2 - x_4^2)\sin(\omega_2)}{\cos(\omega_2) - \cos(\omega_1 + \omega_2)}\Big) + 1/4 \frac{x_1 x_3 (2x_1 x_3 - 2x_2 x_4)\sin(\omega_2)}{\cos(\omega_2) - \cos(\omega_1 + \omega_2)}. \tag{A.41}$$

References

[1] Giovanozzi M, Scandale W, Todesco E. Part Accel 1997;56:195.
[2] Bountis T, Tompaidis S, Turchetti G, Scandale W, editors, Singapore: World Scientific; 1991. p. 112.
[3] Bountis T, Kollmann M. Physica D 1994;71:122.
[4] Vrahatis MN, Bountis T, Kollmann M. Int J Bifurcat Chaos 1996;6(8):1425.
[5] Vrahatis MN, Isliker H, Bountis T. Int J Bifurcat Chaos 1997;7(12):2707.
[6] Bountis T, Skokos Ch. Nucl Instrum Methods Phys Res Sect A 2006;561:173.
[7] Vittot M. J Phys A Math Gen 2004;37:6337.
[8] Chandre C, Vittot M, Elskens Y, Ciraolo G, Pettini M. Physica D 2005;208:131.
[9] Bourbaki N. Eléments de Mathématiques: groupes et Algèbres de Lie (Hermann Ed. Paris); 1972.
[10] Skokos Ch. J Phys A 2001;34:10029.
[11] Skokos Ch, Antonopoulos Ch, Bountis T, Vrahatis MN. Prog Theor Phys Suppl 2003;150:439.
[12] Skokos Ch, Antonopoulos Ch, Bountis TC, Vrahatis MN. J Phys A 2004;37:6269.
[13] Széll A, Érdi B, Sándor ZS, Steves B. MNRAS 2004;347:380.
[14] Panagopoulos P, Bountis TC, Skokos Ch. J Vib Acoust 2004;126:520.
[15] Manos T, Athanassoula E. In: Proceedings of Semaine de l' Astrophysique Française Journées de la SF2A, Caloli F, Contini T, Hameury, JM, Pagani, L, editors (EDP-Science Conference Series); 2005. p. 631.
[16] Skokos Ch, Bountis T, Antonopoulos Ch. J Phys D 2007;231:30.
[17] Skokos Ch, Bountis T, Antonopoulos Ch. Eur Phys J Sp T 2008;165:5.

4.2 Efficient control of accelerator maps

In the following article, we consider results obtained in the previous section and derived two new maps.

First we look for a symplectic version of the 4 dimensional version of the controlled map. We achieve this goal by setting the momenta constant in the generator of the control F. Thus the series $e^{\{F\}}$ becomes a sum and the map is symplectic. Moreover it exhibits an excellent behavior : a dynamical aperture of radius 0.79 (it was 0.39 for the initial map and 0.66 for the truncation version of the controlled map) and a strong decrease of the chaotic zones.
Finally, and maybe more importantly, its independence of the momenta gives it a realistic physical meaning.

Secondly, we present similar results for the $2D$ Hénon map (see Subsec. 1.3.2). There is an interest [Raubenheimer, 1993] in such $2D$ systems meaning that the beam is very flat and can be considered uni-dimensional. Of course lowering the number of degrees of freedom in the model makes it easier to implement, simulate and finally interpret.
We applied the control method. Similarly to the full $4D$ model, we needed to operate a truncation. We showed that after a certain order the gain is close to 0. Results are good : increase of the dynamical aperture with a decrease of the number of chaotic orbits.

EFFICIENT CONTROL OF ACCELERATOR MAPS

JEHAN BOREUX* and TIMOTEO CARLETTI†
Namur Center for Complex Systems, naXys,
University of Namur, Rempart de la Vierge 8,
Namur 5000, Belgium
*jehan.boreux@fundp.ac.be
†timoteo.carletti@fundp.ac.be

CHARALAMPOS SKOKOS
Max Planck Institute for the Physics of Complex Systems,
Nöthnitzer Str. 38, D-01187 Dresden, Germany

Center for Research and Applications of Nonlinear Systems,
University of Patras, GR-26500 Patras, Greece
hskokos@pks.mpg.de

YANNIS PAPAPHILIPPOU
CERN, CH-1211 Geneva 23, Switzerland
yannis@cern.ch

MICHEL VITTOT
Centre de Physique Théorique,
Aix-Marseille Universite, CNRS-UMR 7332, USTV,
FRUMAM F-13288 Marseille, cedex 9, France
vittot@cpt.univ-mrs.fr

Recently, the Hamiltonian Control Theory was used in [Boreux *et al.*, 2012] to increase the dynamic aperture of a ring particle accelerator having a localized thin sextupole magnet. In this paper, these results are extended by proving that a simplified version of the obtained general control term leads to significant improvements of the dynamic aperture of the uncontrolled model. In addition, the dynamics of flat beams based on the same accelerator model can be significantly improved by a reduced controlled term applied in only one degree of freedom.

Keywords: Hamiltonian control; particle accelerators; dynamical aperture; symplectic maps; SALI method.

1. Introduction

Hamiltonian Control Theory has been developed in [Vittot, 2004; Chandre *et al.*, 2005] aiming to improve some selected features of a given Hamiltonian system (like to reduce its chaotic behavior), by adding a "small control term" which slightly alters the Hamiltonian of the system.

This technique was adapted in [Boreux *et al.*, 2012] to the case of symplectic maps. In particular,

it was applied to a four-dimensional (4D) map which models a simplified accelerator ring with sextupole nonlinearity, succeeding to increase the stability domain around the nominal circular orbit (the so-called dynamic aperture — DA). This procedure allowed the construction of a sequence of control terms of increasing complexity, that successively improve the dynamics of the original map. Actually, the larger the DA became, the functional

complexity of the control term increased, and the required CPU time for the evolution of orbits grew. Real accelerators are composed of such simplified maps (see for example [Forest, 1998]). Thus, we believe that the study of these maps can guide the research for increasing the DA of more complicated models.

The aim of the present paper is to show that simplified versions of the general control term can also lead to a significant increase of the DA. For accelerators, the addition of a control term can be interpreted as the addition of an extra magnet. Since magnetic fields depend only on spatial variables we investigate the efficiency of a modified control term obtained by neglecting the dependence on the momenta of the general control term constructed in [Boreux *et al.*, 2012].

In many real accelerators, the vertical extent of the beam is much smaller than its horizontal size. Such cases can be approximated by considering ideal, flat beams of zero height, whose dynamics is described by a restriction of the general 4D accelerator model to a two-dimensional subspace. We also apply our control theory to a 2D map model of this type, improving the stability of the flat beam.

2. The Model of a Simplified Accelerator Ring

As in [Bountis & Tompaidis, 1991; Bountis & Skokos, 2006a; Boreux *et al.*, 2012] we consider a simplified accelerator ring with linear frequencies (tunes) q_x, q_y, having a localized thin sextupole magnet. The evolution of a charged particle is modeled by the 4D symplectic map

$$\begin{pmatrix} x'_1 \\ x'_2 \\ x'_3 \\ x'_4 \end{pmatrix} = \begin{pmatrix} \cos\omega_1 & -\sin\omega_1 & 0 & 0 \\ \sin\omega_1 & \cos\omega_1 & 0 & 0 \\ 0 & 0 & \cos\omega_2 & -\sin\omega_2 \\ 0 & 0 & \sin\omega_2 & \cos\omega_2 \end{pmatrix} \begin{pmatrix} x_1 \\ x_2 + x_1^2 - x_3^2 \\ x_3 \\ x_4 - 2x_1x_3 \end{pmatrix} = T_S \begin{pmatrix} x_1 \\ x_2 \\ x_3 \\ x_4 \end{pmatrix}. \tag{1}$$

where x_1 (x_3) denotes the initial deflection from the ideal circular orbit in the horizontal (vertical) direction before the particle enters the element, and x_2 (x_4) is the associated momentum. Primes denote positions and momenta after one turn in the ring. The parameters ω_1 and ω_2 are related to the accelerator's tunes q_x and q_y by $\omega_1 = 2\pi q_x$ and $\omega_2 = 2\pi q_y$. In our study, we set $q_x = 0.61803$ and $q_y = 0.4152$ corresponding to a regular orbit as shown in [Vrahatis *et al.*, 1997].[1] The particle dynamics at the nth turn, can be described by the sequence $(x_1(n), x_2(n), x_3(n), x_4(n))_{n\geq 0}$, where the $(n+1)$th positions and momenta are defined as a function of the nth ones by (1).

3. Theoretical Considerations and Numerical Techniques

For sake of completeness, let us briefly recall the theoretical framework developed in [Boreux *et al.*, 2012]. Map (1) naturally decomposes in a integrable part, the rotation by angles ω_1, ω_2 in the planes x_1, x_2 and x_3, x_4 respectively, and a quadratic

"perturbation", and can be obtained as the time-1 flow of the following Hamiltonian systems

$$H(x_1, x_2, x_3, x_4) = -\omega_1 \frac{x_1^2 + x_2^2}{2}$$
$$- \omega_2 \frac{x_3^2 + x_4^2}{2} \quad \text{and} \tag{2}$$

$$V(x_1, x_2, x_3, x_4) = -\frac{x_1^3}{3} + x_1 x_3^2.$$

Using the notation of the Poisson bracket — which is defined by $\{H\}f := \{H, f\} = \sum_j \frac{\partial H}{\partial p_j}\frac{\partial f}{\partial q_j} - \frac{\partial H}{\partial q_j}\frac{\partial f}{\partial p_j}$ for any function $f(p, q)$ — map (1) can be written as

$$\mathbf{x}' = T_S(\mathbf{x}) = e^{\{H\}}e^{\{V\}}\mathbf{x}, \tag{3}$$

where $\mathbf{x} = (x_1, x_2, x_3, x_4)^{\mathrm{T}} \in \mathbb{R}^4$, ($^{\mathrm{T}}$) denotes the transpose of a matrix, and the exponential map is defined as $e^{\{H\}}f = \sum_{n\geq 0} \frac{\{H\}^n}{n!}f$, with $\{H\}^n f = \{H\}^{n-1}(\{H\}f)$.

---

[1]We remark that in the theory we developed q_x and q_y have been considered as parameters. So, our results can be straightforwardly applied to other cases, remaining valid for tunes satisfying a nonresonant condition (see Sec. 3). We also note that our method can be easily adapted to the resonant case, but the construction of a new control term is required.

Assuming that the perturbation V is small close to the origin, so that $V = o(H)$, we can construct a *control map* whose generator F is small with respect to V (i.e. it satisfies $F = o(V)$). Moreover, the *controlled map*

$$T_{\text{ctrl}} = e^{\{H\}} e^{\{V\}} e^{\{F\}}, \qquad (4)$$

is symplectic and conjugated to a map T_*, closer to $e^{\{H\}}$ than T_S (for more details the reader is referred to [Boreux *et al.*, 2012]). Assuming furthermore, that a nonresonant condition is satisfied for the particular choice of the q_x and q_y values of map (1), the generator F of the control map $e^{\{F\}}$ is

$$F = \frac{1}{2}\{V\}\mathcal{G}V + o(V^2), \qquad (5)$$

where $\mathcal{G}$ is a "pseudo-inverse" operator, which satisfies $\mathcal{G}(1 - e^{-\mathcal{H}})\mathcal{G} = \mathcal{G}$ (see [Chandre *et al.*, 2005] for more details).

Even truncating the generator F at order two and using

$$F_2 = \frac{1}{2}\{V\}\mathcal{G}V, \qquad (6)$$

as an *approximate generator*, the control map $e^{\{F_2\}}$ cannot, in general, be written in a closed analytic form. So, we define a *truncated control map of order k*

$$C_k(F_2) = \sum_{l=0}^{k} \frac{\{F_2\}^l}{l!}, \qquad (7)$$

and a *truncated controlled map of order k*:

$$T_k(F_2) = e^{\{H\}} e^{\{V\}} C_k(F_2) = T_S C_k(F_2). \qquad (8)$$

Following [Boreux *et al.*, 2012], the Smaller Alignment Index (SALI) method of chaos detection is used to determine the regular or chaotic nature of orbits of map (1) and its controlled version (4). We note that an orbit is considered to escape and collide with the accelerator's vacuum chamber if at some time $n \sum_{i=1}^{4} x_i^2(n) > 10$. For the evaluation of SALI, the tangent of the studied map is computed and employed for following the evolution of two initially linearly independent unit deviation vectors $\hat{v}_1(0)$ and $\hat{v}_2(0)$, defining the index as

$$\text{SALI}(n) = \min\{\|\hat{v}_1(n) + \hat{v}_2(n)\|,$$
$$\|\hat{v}_1(n) - \hat{v}_2(n)\|\}, \qquad (9)$$

where $\|\cdot\|$ denotes the usual Euclidean norm and $\hat{v}_i(n) = \frac{\mathbf{v}_i(n)}{\|\mathbf{v}_i(n)\|}$, $i = 1, 2$ are vectors of unit norm.

The behavior of SALI, and its generalization, the so-called Generalized Alignment Index (GALI), has been studied in detail in [Skokos, 2001; Skokos *et al.*, 2003, 2004, 2007]. According to these studies, in 4D maps the SALI of chaotic orbits tends exponentially to zero as $\text{SALI}(n) \propto e^{-(\sigma_1 - \sigma_2)n}$ (with σ_1, σ_2 being the two largest Lyapunov characteristic exponents of the orbit), while it fluctuates around positive values, i.e. $\text{SALI}(n) \propto \text{const}$, for regular orbits. In the case of 2D maps, the SALI tends to zero both for regular and chaotic orbits, as $\text{SALI}(n) \propto 1/n^2$ and $\text{SALI}(n) \propto e^{-\sigma_1 n}$, respectively. Thus, the completely different behaviors of SALI for regular and chaotic orbits allow us to clearly distinguish between the two cases both for 4D and 2D maps.

In the following, we consider an orbit to be chaotic if $\text{SALI}(n) \leq 10^{-8}$ after n iterations. We note that in our studies we typically have $\text{SALI}(n) \gtrsim 10^{-2}$ for regular orbits. Consequently the chosen threshold value ($\text{SALI}(n) \leq 10^{-8}$) safely guarantees the chaotic nature of orbits.

4. The Controlled 4D Map

In [Boreux *et al.*, 2012] it was shown that the fourth order controlled map $T_4(F_2)$, is a very good choice for the controlled system, since it succeeded to considerably increase the DA of the accelerator, keeping also the required CPU time for the evolution of large sets of initial conditions, at acceptable levels.

The computed generator F_2 is a complicated function of both the positions x_1, x_3 and the momenta x_2, x_4 of map (1), and its specific expression is given in the Appendix of [Boreux *et al.*, 2012].

A simple approach for investigating the global dynamics of 4D accelerator maps, used in [Bountis & Skokos, 2006a; Boreux *et al.*, 2012], was the computation of the maximal radius of a four-dimensional hypersphere centered at $(x_1, x_2, x_3, x_4) = (0, 0, 0, 0)$, containing only regular orbits up to a finite but large number of iterations. This approach provides a reliable indication of the size of the DA. Application of this methodology in [Boreux *et al.*, 2012] showed that the controlled map $T_4(F_2)$ has better stability properties than the uncontrolled map (1). Nevertheless, one should keep in mind that the center of these hyperspheres does not bear any

particular physical meaning, as it does not correspond to an experimentally realizable beam configuration.

From a physical point of view, it is more meaningful to study the dynamics of the nominal orbit having $x_1(0) = x_3(0) = 0$ for different momenta x_2, x_4. For this purpose, we consider four-dimensional hyperspheres, centered at $(0, x_2, 0, x_4)$ and compute for different values of x_2, x_4, the radius R of the largest hypersphere which contains only regular orbits.

The outcome of this investigation is presented in Fig. 1, where the x_2, x_4 coordinates of the centers of the considered hyperspheres are colored according to the value of radius R for the uncontrolled map (1) [Fig. 1(a)], and the $T_4(F_2)$ map [Fig. 1(b)]. For both maps, the largest value of R is obtained for $x_2 = x_4 = 0$ (i.e. the value obtained in [Boreux *et al.*, 2012]), while R decreases as the hypershere's center is moved away from $x_2 = x_4 = 0$. This implies that large values of the momenta introduce instabilities and chaotic behavior, which reduce the size of the stability domain.

Nevertheless, the controlled map $T_4(F_2)$ succeeded to increase the stability region, since $R > 0$ for larger values of x_2 and x_4, with respect to the original map. In addition, R attains larger values in the central region of the (x_2, x_4) plane for the controlled map $T_4(F_2)$, being $R \approx 0.6$, which suggests a significant increase of the stability domain around the nominal orbit of the accelerator.

As it has already been mentioned, the controlled map $T_4(F_2)$ has a complicated functional form, depending both on spatial variables x_1, x_3

and on the conjugate momenta x_2, x_4. From a practical point of view, the addition of a control map (7) can be thought as the addition of an appropriate magnetic element in the ring. On the other hand, the vector potential of a Maxwellian magnetic field which is transverse to the particle motion (i.e. without any longitudinal dependence) is a function of these transverse positions and not momenta. It is legitimate then to investigate the efficiency of a modified control term, obtained by neglecting the dependence of F_2 on momenta. In practice, this means that we set $x_2 = x_4 = 0$ in the expression of F_2 obtained in [Boreux *et al.*, 2012], getting

$$
F_2^{(0)}(x_1, x_3) := F_2(x_1, 0, x_3, 0)
$$

$$
= \frac{1}{2}(x_1^2 - x_3^2)\left\{ -\frac{1}{6}\csc\left(\frac{3\omega_1}{2}\right)\cos\left(\frac{\omega_1}{2}\right) \right.
$$

$$
\times [x_1^2 - 3x_3^2 + (2x_1^2 - 6x_3^2)\cos(\omega_1)]
$$

$$
+ \frac{1}{6}\csc\left(\frac{3\omega_1}{2}\right)x_1^2\sin\left(\frac{\omega_1}{2}\right)\sin(\omega_1)
$$

$$
\left. - \frac{1}{4}\frac{x_3^2\sin(\omega_2)}{\cos(\omega_2) - \cos(\omega_1 + \omega_2)} \right\}
$$

$$
+ \frac{1}{2}\frac{x_1^2 x_3^2 \sin(\omega_2)}{\cos(\omega_2) - \cos(\omega_1 + \omega_2)}. \qquad (10)
$$

This is a fourth order polynomial in the positions which may be transformed with some variable rescaling to the vector potential of an octupole magnet with normal symmetry [Wiedemann, 2007]

$$
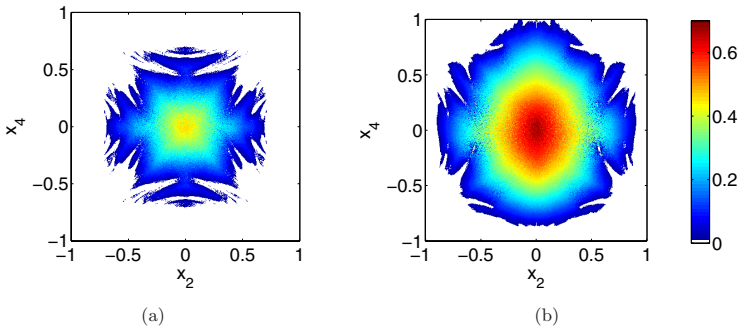V_{\text{oct}} = b_4 \text{Re}[(x_1 + ix_3)^4], \qquad (11)
$$

Fig. 1. The x_2, x_4 coordinates of the centers $(0, x_2, 0, x_4)$ of the four-dimensional hyperspheres containing only regular orbits for (a) the uncontrolled map (1), and (b) the $T_4(F_2)$ map. Each point is colored according to the value of the hypersphere of radius R (with white color corresponding to $R = 0$), and all orbits are evolved up to 10^4 iterations.

where b_4 denotes the multipole coefficient related to the magnet field strength. Since $F_2^{(0)}$ does not depend on the momenta, the control map $e^{\{F_2^{(0)}\}}$, can be explicitly computed. The action of this map on x_2 is given by

$$e^{\{F_2^{(0)}\}}x_2 = x_2 + \{F_2^{(0)}\}x_2 + \frac{\{F_2^{(0)}\}^2}{2!}x_2 + \cdots$$

$$= x_2 - \frac{\partial F_2^{(0)}}{\partial x_1}, \qquad (12)$$

because $\{F_2^{(0)}\}x_2$ does not depend on the momenta and consequently $\{F_2^{(0)}\}^m x_2 = 0$ for all integers $m \geq 2$. Similar relations hold also for the other variables, i.e. $\{F_2^{(0)}\}^m x_4 = 0$ for all integers $m \geq 2$ and $\{F_2^{(0)}\}x_1 = \{F_2^{(0)}\}x_3 = 0$. Thus, no truncation of the form (7) is needed, and consequently the simplified controlled map

$$T_C^{(0)} = e^{\{H\}}e^{\{V\}}e^{\{F_2^{(0)}\}}, \qquad (13)$$

is symplectic by construction, as a composition of three explicitly known symplectic maps.

Since map $T_C^{(0)}$ is not explicitly constructed by the Hamiltonian Control Theory, it is interesting to check its performance in controlling map (1) and increasing its DA. Following [Bountis & Skokos, 2006a; Boreux *et al.*, 2012], the SALI method is used to determine the regular or chaotic nature of orbits of map $T_C^{(0)}$. In order to directly compare these results with the ones obtained in previous studies, the values of $\log_{10}$ SALI after 10^5 iterations are plotted in Fig. 2, to describe the dynamics in the two-dimensional subspace $x_2(0) = x_4(0) = 0$,

for the uncontrolled map (1) [Fig. 2(a)], the $T_4(F_2)$ controlled map (8) [Fig. 2(b)], and the simplified map $T_C^{(0)}$ (13) [Fig. 2(c)]. Chaotic orbits are characterized by small SALI values and are located in the blue colored domains, regular orbits are colored red, while white regions correspond to orbits that escape in less than 10^5 iterations. Figure 2 shows that both controlled maps, $T_4(F_2)$ and $T_C^{(0)}$, increase the DA of the accelerator. It is remarkable that the simplified controlled map $T_C^{(0)}$ not only increases the region of nonescaping orbits, with respect to the original system, but also decreases drastically the number of chaotic orbits.

In order to perform a more global investigation of the dynamics of these maps we consider, as was done in [Bountis & Skokos, 2006a; Boreux *et al.*, 2012], initial conditions inside a four-dimensional hypersphere centered at $x_1 = x_2 = x_3 = x_4 = 0$, and compute the percentages of regular and chaotic orbits as a function of the hypersphere radius r (Fig. 3). From the red curves in Fig. 3, it is observed that the $T_C^{(0)}$ map significantly increases the domain of regular motion, not only with respect to the original map (black curves in Fig. 3), but also with respect to the controlled map $T_4(F_2)$ (blue curves in Fig. 3). In addition, map $T_C^{(0)}$ has the smallest percentage of chaotic orbits among the studied models, which means that orbits of this map either escape or they are regular.

Thus, map $T_C^{(0)}$ (13) controls the original system (1) more efficiently than map $T_4(F_2)$ (8). Additional advantages of this map is its simplicity, since it depends only on the spatial variables, and the fact that it is symplectic by construction. Another
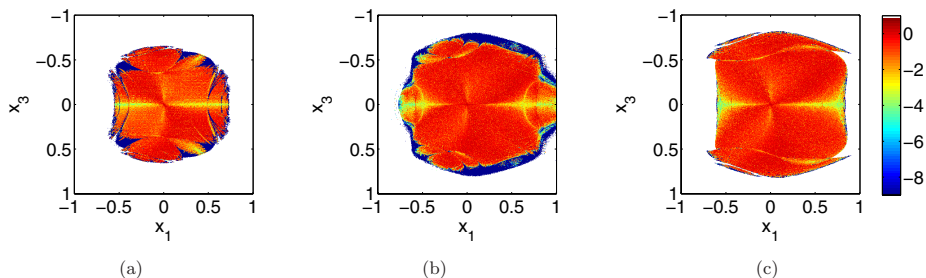

Fig. 2.   Regions of different SALI values on the (x_1, x_3) plane of (a) the uncontrolled map (1), (b) the $T_4(F_2)$ controlled map (8), and (c) the $T_C^{(0)}$ simplified controlled map (13). 16 000 uniformly distributed initial conditions in the square $(x_1, x_3) \in [-1, 1] \times [-1, 1]$, $x_2(0) = x_4(0) = 0$ are followed for 10^5 iterations, and they are colored according to their final $\log_{10}$ SALI value. The white colored regions correspond to orbits that escape in less than 10^5 iterations.
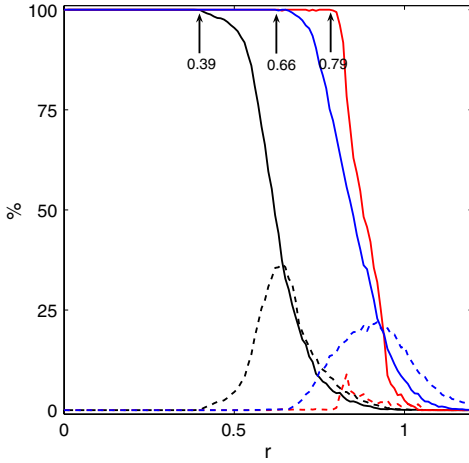
Fig. 3. The percentages of regular (solid curves) and chaotic (dashed curves) orbits after $n = 10^5$ iterations of the original map (1) (black curves), the $T_4(F_2)$ controlled map (8) (blue curves), and the $T_C^{(0)}$ simplified controlled map (13) (red curves), in a four-dimensional hypersphere centered at $x_1 = x_2 = x_3 = x_4 = 0$, as a function of the hypersphere radius r. The largest radii at which the percentage of regular orbits is 100%, are also marked.

feature, which could be of major practical importance, is that the generator $F_2^{(0)}$ (10) of the simplified control map $T_C^{(0)}$ can be considered as the potential induced by a magnetic element, since it depends only on spatial variables.

These results show that the simplified controlled map $T_C^{(0)}$ works better than the controlled map $T_4(F_2)$ which is also able to enlarge the DA with respect to T_S. Then, a natural task would be to compare $T_C^{(0)}$ with T_{ctrl} or with $T_\infty(F_2)$. We note that we were not able to find a closed analytic form for the latter maps due to the cumbersome involved summations. Thus, these comparisons remain open problems which we plan to address in the future. However, we remark that the finite number of terms involved in $T_4(F_2)$ possibly allows the attribution of a real magnetic element to this map, while probably this will not be feasible for maps T_{ctrl} and $T_\infty(F_2)$.

5. Flat Beams: The Controlled 2D Map

In many particle accelerators the beam is very flat, i.e. its vertical extent is much smaller than the

horizontal one. A simple, first, approach in investigating the dynamics of a flat beam of the 4D map (1) is to neglect the vertical coordinate x_3 and its corresponding momentum x_4, and pass from the initial 4D map to the 2D map

$$\begin{pmatrix} x_1' \\ x_2' \end{pmatrix} = \begin{pmatrix} \cos\omega_1 & -\sin\omega_1 \\ \sin\omega_1 & \cos\omega_1 \end{pmatrix} \begin{pmatrix} x_1 \\ x_2 + x_1^2 \end{pmatrix}$$

$$=: T^{2D} \begin{pmatrix} x_1 \\ x_2 \end{pmatrix}, \tag{14}$$

whose dynamics was studied for example in [Bountis & Skokos, 2006b].

Following for this map, the procedure described in Sec. 3, truncated control $C_k^{2D}(F_2^{2D})$ and controlled $T_k^{2D}(F_2^{2D})$ maps of order k are constructed, in analogy to Eqs. (7) and (8), respectively. As before, the controlled map is not necessarily symplectic. Since a map is symplectic if its Jacobian matrix $\mathbf{A}$ satisfies (in its definition domain) the equality $\mathbf{A}^T \mathbf{J} \mathbf{A} - \mathbf{J} = \mathbf{0}$ (with $\mathbf{J} = \begin{pmatrix} \mathbf{0} & \mathbf{1} \\ -\mathbf{1} & \mathbf{0} \end{pmatrix}$ being the standard symplectic constant matrix), the symplectic nature of $T_k^{2D}(F_2^{2D})$ can be checked by computing the norm D_k of $\mathbf{A}_k^T \mathbf{J} \mathbf{A}_k - \mathbf{J}$, for the Jacobian matrix $\mathbf{A}_k$ of the map. The results of this computation are presented in Fig. 4, for orders $k = 4$, $k = 6$, and $k = 8$, in the region $(x_1, x_2) \in [-1, 1] \times [-1, 1]$, and show that $T_k^{2D}(F_2^{2D})$ is a good approximation of a symplectic map for $k \geq 6$, since $D_k \lesssim 10^{-6}$ for a large portion ($\gtrsim 77$ %) of variable values. As expected, the larger the order k, the closer the map $T_k^{2D}(F_2^{2D})$ numerically approaches the symplectic condition.

In order to check whether the controlled map $T_k^{2D}(F_2^{2D})$ with $k \geq 4$ increases the DA of the flat beam, we use again the SALI to determine the nature of orbits in the (x_1, x_2) plane, keeping in mind that SALI tends to zero both for regular and chaotic orbits of 2D maps, but with time rates which allow the clear distinction between the two cases. In particular, many initial conditions are tracked for 10^4 iterations in the (x_1, x_2) plane, and colored according to their final $\log_{10}$ SALI value, for the T^{2D} [Fig. 5(a)], the $T_6^{2D}(F_2^{2D})$ [Fig. 5(b)], and the $T_8^{2D}(F_2^{2D})$ map. Orbits with SALI $\leq 10^{-10}$ are characterized as chaotic and are colored in blue, while the remaining ones are regular. Similarly to Fig. 2 white regions correspond to escaping orbits. This distinction is based on the theoretical prediction that for regular orbits SALI $\propto 1/n^2 = 10^{-8}$ at

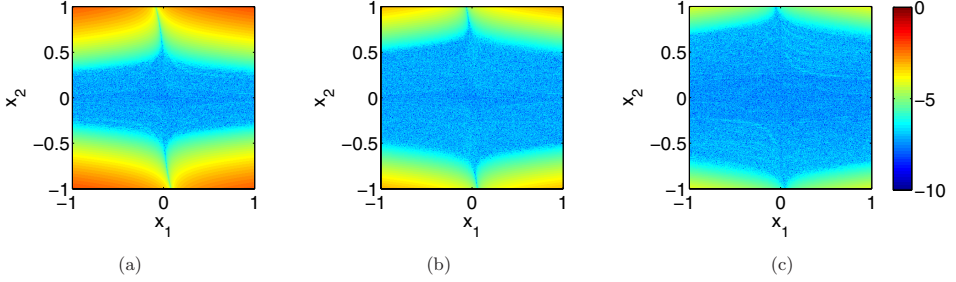(a)   (b)   (c)

Fig. 4. Plot of $\log_{10} D_k$, where D_k is the norm of matrix $A_k^T J A_k - J$, and A_k is the Jacobian of the controlled map $T_k^{2D}(F_2^{2D})$, for 16 000 uniformly distributed values in the square $(x_1, x_2) \in [-1, 1] \times [-1, 1]$, for (a) $k = 4$, (b) $k = 6$, and (c) $k = 8$. The percentages of orbits with $\log_{10} D_k < -6$ are 53%, 77%, and 94% respectively for $k = 2$, 4, and 6. The color scale corresponds to the value of $\log_{10} D_k$; the smaller the value of $\log_{10} D_k$ is (blue region), the closer the map is to a symplectic one.

(a)   (b)   (c)

(d)   (e)   (f)
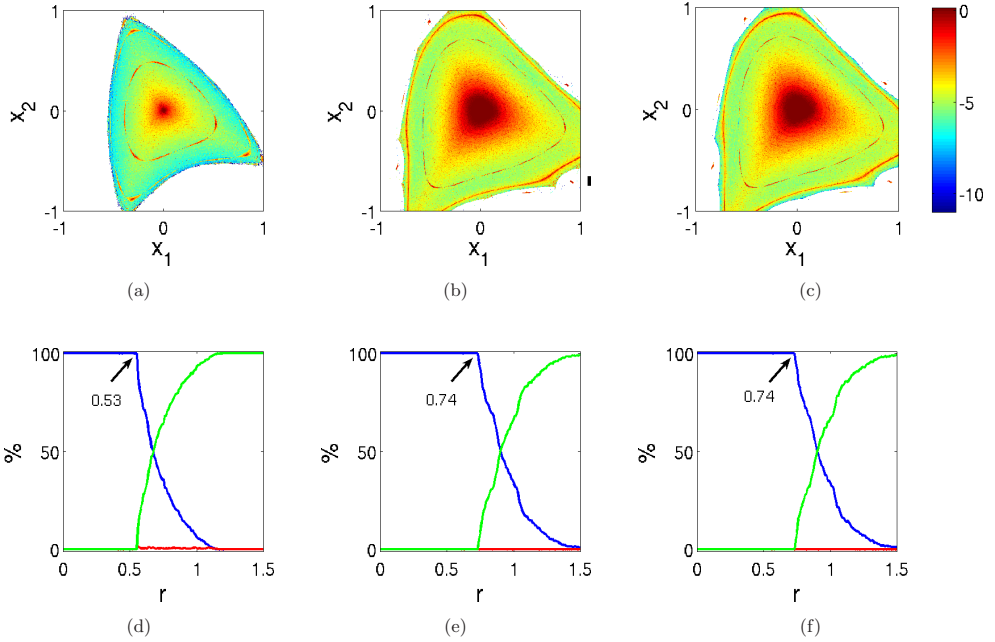
Fig. 5. (Upper row) Regions of different SALI values on the (x_1, x_2) plane of (a) the uncontrolled 2D map (14), (b) the $T_6^{2D}(F_2^{2D})$ controlled map, and (c) the $T_8^{2D}(F_2^{2D})$ controlled map. 16 000 uniformly distributed initial conditions in the square $(x_1, x_2) \in [-1, 1] \times [-1, 1]$ are followed for 10^4 iterations, and they are colored according to their final $\log_{10}$ SALI value. The white colored regions correspond to orbits that escape in less than 10^4 iterations. (Lower row) The percentages of regular (blue curves), chaotic (red curves), and escaping (green curves) orbits after $n = 10^4$ iterations of the maps of the upper row, in a circle centered at $x_1 = x_2 = 0$, as a function of its radius r. The largest radii at which the percentage of regular orbits is 100%, are marked in panels (d)–(f). Panels in the same columns correspond to the same map.

$n = 10^4$. In Figs. 5(d)–5(f) the percentages of regular (blue curves), chaotic (red curves), and escaping (green curves) orbits of these three maps are plotted as a function of the radius r of a circle centered at the origin $x_1 = x_2 = 0$.

In all models the number of chaotic orbits is practically negligible, which means that orbits are either regular or escaping. The two controlled maps succeed to increase the DA of the beam, because the domain of nonescaping orbits increases [Figs. 5(a)–5(c)]. Although this domain does not have a cyclical shape, the radius of the largest cycle containing only regular orbits increases from $r \approx 0.53$ for the uncontrolled map T^{2D} (14), to $r \approx 0.74$ for both controlled maps $T_6^{2D}(F_2^{2D})$ and $T_8^{2D}(F_2^{2D})$. Since both controlled maps give essentially the same results, we conclude that the sixth order truncation of the controlled map is sufficient for controlling the flat beam.

6. Summary and Discussion

In this paper, the results of the application of control theory to a simple 4D accelerator map [Boreux *et al.*, 2012], are being extended by using simplified versions of the control maps. In the first case, the momentum dependence of the control term is artificially removed, so as the control map is a function of the spatial coordinates and thus resembles the magnetic vector potential of a multipole magnet. In addition, this control map is symplectic by construction in contrast to the original one, thus avoiding the associated problems of having to choose an appropriate order of truncation in the Lie representation, for which the map satisfies numerically the symplectic condition. The efficiency of the simplified control map is remarkable, not only achieving the increase of the DA, but also shows a better performance as compared to the complete control map. The remaining important issue regarding the possibility to approximate in practice this magnetic field by a multipole magnet is still open, and will be addressed in a future study. In this respect, and based on the knowledge that control theory can be efficiently used to increase the DA of a toy model, the studies can be extended by investigating the possibility of imposing a control map with the functional form similar to Eq. (11), and compute the associated multipole coefficients which achieve the best increase in the DA.

In the second case, the same theory is applied to a 2D version of the map, modeling flat beams, as it is the case in electron and positron low emittance rings (i.e. with small beam sizes), where the vertical beam size is several orders of magnitude smaller than the horizontal one and thus the dynamic studies can be restricted to that plane. This 2D control map presents the same characteristics as the original map, i.e. increase of the DA, for a truncation order equal to six.

In all our studies, the SALI indicator was mainly used for showing the improvement of control in the DA. In future work, we plan to apply the frequency map analysis method (e.g. see [Laskar, 1999] and references therein) in this map in order to understand the dynamical details of this improvement with respect to resonance excitation and diffusion.

Acknowledgments

References

Boreux, J., Carletti, T., Skokos, Ch. & Vittot, M. [2012] "Hamiltonian control used to improve the beam stability in particle accelerator models," *Commun. Nonlin. Sci. Numer. Simulat.* **17**, 1725–1738.

Bourbaki, N. [1972] *Eléments de Mathématiques: Groupes et Algèbres de Lie* (Hermann Ed. Paris).

Bountis, T. & Tompaidis, S. [1991] *Future Problems in Nonlinear Particle Accelerators*, eds. Turchetti, G. & Scandale, W. (World Scientific, Singapore), p. 112.

Bountis, T. & Skokos, Ch. [2006a] "Application of the SALI chaos detection method to accelerator mappings," *Nucl. Instr. Meth. Phys. Res. — Sect. A* **561**, 173–179.

Bountis, T. & Skokos, Ch. [2006b] "Space charges can significantly affect the dynamics of accelerator maps," *Phys. Lett. A* **358**, 126–133.

Chandre, C., Vittot, M., Elskens, Y., Ciraolo, G. & Pettini, M. [2005] "Controlling chaos in area-preserving maps," *Physica D* **208**, 131–146.

Forest, E. [1998] *Beam Dynamics, A New Attitude and Framework* (Harwood Academic, Chur, Switzerland).

Laskar, J. [1999] "Introduction to frequency map analysis," *Proc. 3DHAM95 NATO Advanced Institute*, ed. Simoó, C. (SAgaro, June 1995).

Skokos, Ch. [2001] "Alignment indices: A new, simple method for determining the ordered or chaotic nature of orbits," *J. Phys. A* **34**, 10029–10043.

Skokos, Ch., Antonopoulos, C., Bountis, T. & Vrahatis, M. N. [2003] "How does the Smaller Alignment Index (SALI) distinguish order from chaos?" *Prog. Theor. Phys. Supp.* **150**, 439–443.

Skokos, Ch., Antonopoulos, Ch., Bountis, T. & Vrahatis, M. N. [2004] "Detecting order and chaos in Hamiltonian systems by the SALI method," *J. Phys. A* **37**, 6269–6284.

Skokos, Ch., Bountis, T. & Antonopoulos, Ch. [2007] "Geometrical properties of local dynamics in Hamiltonian systems: The Generalized Alignment Index (GALI) method," *Physica D* **231**, 30–54.

Vittot, M. [2004] "Perturbation theory and control in classical or quantum mechanics by an inversion formula," *J. Phys. A* **37**, 6337.

Vrahatis, M. N., Isliker, H. & Bountis, T. C. [1997] "Structure and breakdown of invariant tori in a 4-D mapping model of accelerator dynamics," *Int. J. Bifurcation and Chaos* **7**, 2707.

Widemann, H. [2007] *Particle Accelerator Physics* (Springer Verlag Ed., NY).

Chapitre 5

Analysis of the frequency space

Contents

We begin this chapter by taking stock of the results obtained in Chap. 4. We keep track of three maps : the initial one, the controlled one with truncation and the one with momenta fixed in the control part.
We then shift to the frequency space, cherished in the particle accelerators world. We use the numerical frequency map analysis and the analytical normal form approach to analyze the maps in this space. We finally obtain new results on dissipation directions and the shape of the frequency space.

5.1   Interlude

We here summarize what maps we shall consider and their parameters for the rest of the chapter. The attention on escaping time and inherent problems is discussed. Finally we introduce the remaining two sections of the chapter.

From now on and till the end of this chapter, we shall focus exclusively on 3 models. We follow the results of Secs. 4.1 and 4.2 where we have concluded that with $N = 10^4$ iterations, we have a satisfactory level of precision in order to describe the dynamics of the maps. This number of iterations is especially sufficient for the following reasons : in the normal form approach, results are analytical ones and no iterations are needed, in the frequency map analysis, Theorem 3.3.1 of Chap. 3 insures accuracy as $1/N^4$. The considered maps are the 3 following ones :

1. **The initial model (IM)**

$$\boldsymbol{x}' = e^{\{H\}}e^{\{V\}}\boldsymbol{x}$$

   that is symplectic and nonlinear (with nonlinear terms up to order 2)

2. **The controlled model of order 4 (CMo4)**

$$\boldsymbol{x}' = e^{\{H\}}e^{\{V\}} \sum_{k=0}^{4} \frac{\{F\}^k}{k!}\boldsymbol{x}$$

   that is *close* to symplecticity, nonlinear (with nonlinear terms up to order 18) and not *too* heavy from a computational point of view

3. **The controlled model with null momenta (CMp0)**

$$\boldsymbol{x}' = e^{\{H\}}e^{\{V\}}e^{\{F(x_1,0,x_3,0)\}}\boldsymbol{x}$$

   that is symplectic and nonlinear (with nonlinear terms up to order 3)

We recall that the Hamiltonian systems H, V and F are

$$H(x_1, x_2, x_3, x_4) = -\omega_1 \frac{x_1^2 + x_2^2}{2} - \omega_2 \frac{x_3^2 + x_4^2}{2},$$

$$V(x_1, x_2, x_3, x_4) = -\frac{x_1^3}{3} + x_1 x_3^2,$$

and [1]

$$
\begin{aligned}
F = {}& 1/2(x_1^2 - x_3^2)\Bigg(-1/6 \csc(3/2\omega_1) \cos(1/2\omega_1)(x_1^2 - 3x_3^2 + x_2^2 \\
& + (2x_1^2 - 6x_3^2 + x_2^2)\cos(\omega_1) - x_1 x_2 \sin(\omega_1)) \\
& - 1/6 \csc(3/2\omega_1)\Big(x_2 \cos(1/2\omega_1) + x_1 \sin(1/2\omega_1) \Big)(2x_2 + 2x_2 \cos(\omega_1) \\
& - x_1 \sin(\omega_1)) - 1/4 \frac{(x_3^2 - x_4^2)\sin(\omega_2)}{\cos(\omega_2) - \cos(\omega_1 + \omega_2)} \Bigg) \\
& + 1/4 \frac{x_1 x_3 (2x_1 x_3 - 2x_2 x_4)\sin(\omega_2)}{\cos(\omega_2) - \cos(\omega_1 + \omega_2)} \\
& + 1/8 \frac{\left(5\, x_1{}^2 x_3{}^2 - x_1{}^2 x_4{}^2 + x_3{}^2 x_4{}^2 + 4\, x_1\, x_3\, x_2\, x_4 - x_3{}^4 \right)\sin(\omega_2)}{\cos(\omega_2) - \cos(\omega_1 - \omega_2)}.
\end{aligned}
\tag{5.1}
$$

We also recall that the following values [2] are chosen for the rest of this chapter

$$\omega_1 = 2\pi q_x \quad \text{with} \quad q_x = 0.61803, \tag{5.2}$$

$$\omega_2 = 2\pi q_y \quad \text{with} \quad q_x = 0.4152. \tag{5.3}$$

As presented in the two previous sections, the models exhibit escaping, regular and chaotic orbits in various proportions.

We now would like to stress out the need for good chaos indicators such as the one we have already used before, the SALI. To achieve this goal, we produce in Fig 5.1 graphs [3] of the (IM) and the (CMp0) in the $x_1 - x_3$ phase space : initial conditions are $(x_1(0), 0, x_3(0), 0)$ with $x_1(0)$ and $x_3(0)$ varying in $[-1, 1]$. For each initial condition we have plotted a color code corresponding to the number of iterations needed for the particle to escape.

As explained before, in particle physics, these results are of importance because they give the dynamical aperture of a model and the time-scale a

---

1. Let us remark that F is different from the one presented in the previous chapter that was incorrect due to a typesetting error.

2. In [Vrahatis et al., 1997], they construct a method to find values such that the (IM) has a great dynamical aperture. The chosen q_x and q_y are close to irrational numbers : $0.61803 \sim (\sqrt{5} - 1)/2$ and $0.4152 \sim \sqrt{2} - 1$.

3. As explained below such graphs are time consuming. That is why the corresponding plot for the (CMo4) was not produced for lack of time and because the results were similar to the ones obtained using the other maps.
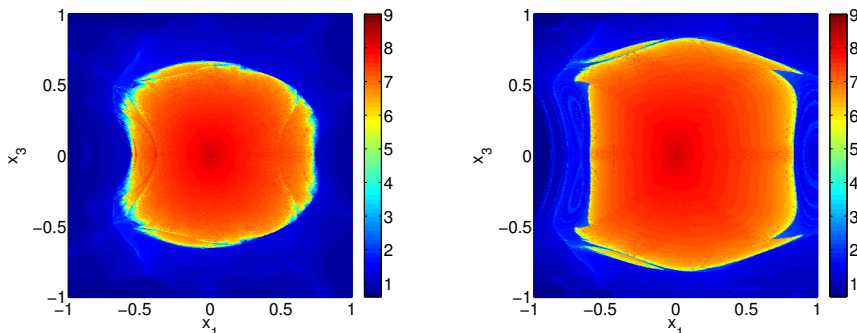
FIGURE 5.1: Escaping time (in $\log_{10}$) for initial conditions taken in the $x_1 - x_3$, on the left for the (IM) and on the right for the (CMp0).

particle turns in the accelerator (time wished as long as possible). Nowadays, real particle accelerators perform runs [Statistics, 2013] lasting several hours, that is between 10^9 and 10^{10} iterations. We are thus glad to see that the studied model complies with these numbers. Despite this observation, we would like to draw the attention on drawbacks of such method.

First, we would like to insist on the CPU time needed to produce such graphs. The mesh size is set to $1/200$ in the x_1 and x_3 axes leading to 16000 initial conditions. For the controlled maps a considerable proportion of initial conditions remains until 10^8 iterations. On a Intel(R) Core(TM) i5-2500 CPU @ 3.30GHz, for (CMo4), it takes about 10 minutes for an initial condition close to the origin. So considering 75% of the set of initial conditions that stay up to 10^8 iterations, we should plan about a year and a half of CPU time. We used a super-calculator [4] that allowed us to obtain results in shorter amounts of time.

Secondly, using chaos indicators, more than producing similar results and thus similar conclusions on the dynamics, we can exhibit other behaviors such as chaotic zones, special directions in the phase space or even analyze the dynamics in other representation spaces. Moreover chaos indicators are able to show the presence of chaos before its onset.

Another representation space is the one of the frequencies, or tunes (q_x and q_y, see above Eqs 5.2 and 5.3) that is more natural for particle physicists : the frequency space is a direct description of their parameters, see Rem. 5.2.1.

We describe and analyze this frequency space using the Frequency Map Analysis (see Chap. 3, Sec. 3.3) in Sec. 5.2.

Finally, in Sec. 5.3, we use an analytical approach to compare and vali-

date results obtained numerically with the FMA : the Normal Form approach presented Chap. 1.

5.2 Frequency Map Analysis of Controlled Particle Accelerators

In this section we apply the Frequency Map Analysis (Sec. 3.3, p. 87) to the different maps (IM), (CMo4) and (CMp0), see Sec. 5.1.

The maps are defined in $\mathbb{R}^4$, so we could consider 4 signals $(x_i(k))_{1 \leq k \leq N}$ $i = 1 \ldots 4$ to treat. But, following [Nadolski and Laskar, 2003], we consider only two complex signals :

$$z_1(k) = x_1(k) + ix_2(k)$$
$$z_2(k) = x_3(k) + ix_4(k)$$

with $k = 1 \ldots N$, i.e. to say signals composed of a position and its associated momentum. We thus have the frequency map F^N :

$$F^N : \mathbb{R}^4 \to \mathbb{R}^2$$
$$\boldsymbol{x} \mapsto (\nu_x, \nu_y)$$

whose image is in a two dimensional space and thus is easier to represent (see Subsec. 5.2.2).

Let us remark that we compute FMA only for non-escaping orbits, i.e. for orbits such that $||\boldsymbol{x}(k)|| < 10 , k = 1 \ldots N$.

We shall first stay in the *classical* phase space of positions $x_1 - x_3$ and observe that FMA is a useful chaos indicator providing similar results to those of SALI.

Then we shall present the new representation space $\nu_x - \nu_y$ with which we shall stay till the end of the chapter. In this plane, we shall analyze the action of the controls through
  – resonances ;
  – reachable frequencies ;
  – diffusion of frequencies.

5.2.1 Towards detecting chaos

Frequency Map Analysis was proved [Nadolski and Laskar, 2003] to be an efficient method to determine the regular or chaotic nature of orbits in conservative systems. As explained Sec. 3.3, we look at the diffusion of the

frequencies : if the orbit is regular, it remains on a torus with a unique frequency, otherwise the orbit goes from one torus to another and we qualify it chaotic.

We first show in Figs 5.2(a,b), 5.3(a,b) and 5.4(a,b), respectively for the (IM), (CMo4) and (CMp0), the value of the gap between the frequency obtained for each initial conditions and (ω_1, ω_2), i.e. we evaluated

$$\Delta(\nu_x) := \log_{10}|\nu_x - \omega_1| \quad \text{and} \quad \Delta(\nu_y) := \log_{10}|\nu_y - \omega_2|.$$

Remark 5.2.1 (Working point) *We call the point (ω_1, ω_2), referencing to particle accelerator physicists, the* working point*. In real experiments, the values of the tunes q_x and q_y, and thus of ω_1 and ω_2 have to be well chosen before the experiment. In fact they constitute the main parameters that can be changed by an experimentalist (see Chap. 2). Their choice is important and leads to various studies, for example [Vrahatis et al., 1997] and references therein.*
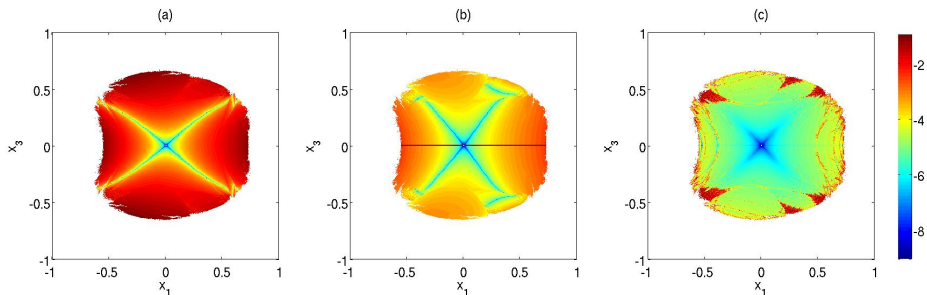

FIGURE 5.2: Color code of $\Delta(\nu_x)$ panel (a) and $\Delta(\nu_y)$ panel (b) of the (IM) in the $x_1 - x_3$ phase space. Panel (c) : diffusion of the frequencies in the $x_1 - x_3$ phase space for the (IM).

As expected, the closer to the origin, the closer to the frequency of the working point. Even more, we observe lower $\Delta(\nu_{x,y})$ for the controlled maps : beyond increasing the dynamical aperture, the controls *flatten*[5] frequencies to the desired ones.

Despite this first good result and the presence of some structures, we do not recover the results obtained with the SALI (see Secs 4.1 and 4.2) : for example, the 4 zones of chaos are not present. This feature is corrected looking at the diffusion of the frequencies.

---

5. By *flatten* we mean that frequencies corresponding to orbits close to the working point vary less in the controlled maps than before the introduction of the control term.
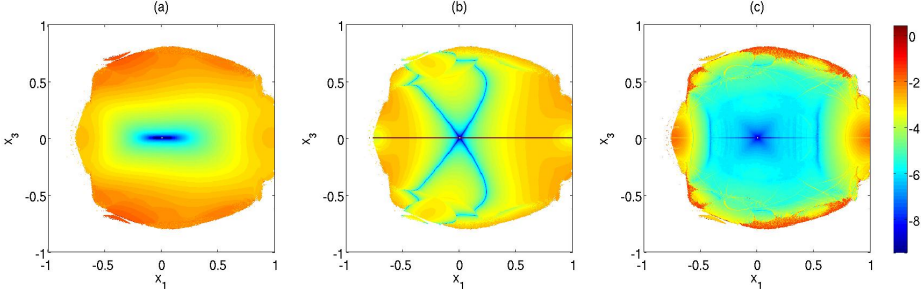
FIGURE 5.3: Color code of $\Delta(\nu_x)$ panel (a) and $\Delta(\nu_y)$ panel (b) of the (CMo4) in the $x_1 - x_3$ phase space. Panel (c) : diffusion of the frequencies in the $x_1 - x_3$ phase space for the (CMo4).
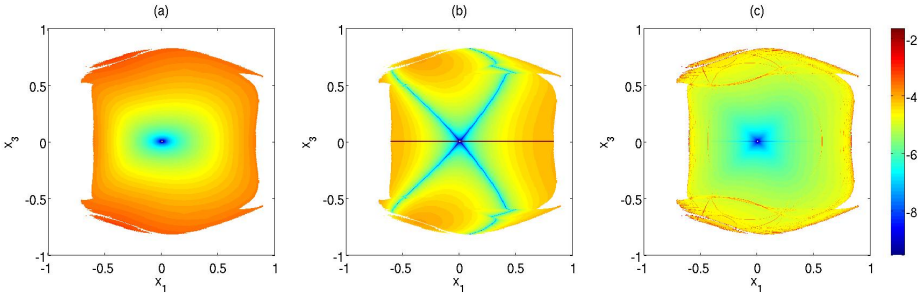

FIGURE 5.4: Color code of $\Delta(\nu_x)$ panel (a) and $\Delta(\nu_y)$ panel (b) of the (CMp0) in the $x_1 - x_3$ phase space. Panel (c) : diffusion of the frequencies in the $x_1 - x_3$ phase space for the (CMp0).

The total number of iterations is $N = 10^4$ for the full signal (constructed from $z_1 = x_1 + ix_2$), called T. We construct a series of sub-signals of T, T_k, such that their length is $N/2$ and the recovery part between two adjacent sub-signals is $N/2 - 10^2$, see Fig. 5.5. The reason of this choice is to emphasize some continuity property of the FMA.

We thus have 50 sub-signals T_k and their corresponding 50 frequencies $\nu_x^{(k)}$. Similarly, we can construct the frequencies $\nu_y^{(k)}$, $k = 1 \ldots 50$ for the second signal (constructed from $z_2 = x_3 + ix_4$).

We show in Figs. 5.2(c), 5.3(c) and 5.4(c) the value of $\log_{10} D$, respectively for the (IM), the (CMo4) and the (CMp0), where the definition (3.9) was chosen. Blue points are initial conditions leading to signals without diffusion of frequencies (regular orbits) while red ones exhibit a high diffusion of the
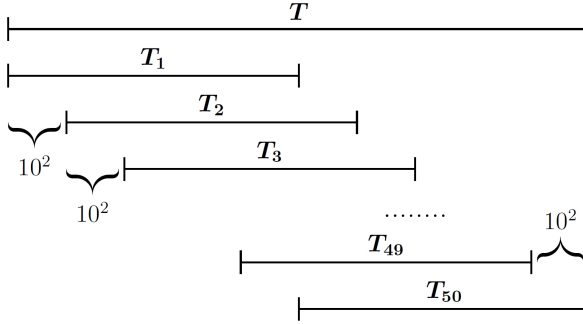
FIGURE 5.5: Cutting of the main signal T and superposition of the sub-signals T_k in order to calculate the diffusion in the frequencies using FMA.

frequencies (chaotic orbits). Color code aside, these plots are similar to the ones obtained with the SALI (see sections 4.1 and 4.2). We could also quantify precisely an orbit as regular or chaotic [6] and get similar [7] increases in the percentages of regular orbit in the full space. We do not go further in that direction already covered with the SALI : the scope of FMA being focused on the frequency space that is introduced in the next section.

5.2.2 Frequency space

The map F^N associates to each initial condition a couple of frequencies (ν_x, ν_y) and a value, D, characterizing the diffusion of that couple along the iterations. We can plot all these values with a color code corresponding to D : this is the *Frequency Space*. We present such plot for the map (IM) that is reported in Figs. 5.6. The corresponding figures for the two considered controls will be presented and analyze later.

In order to analyze the plot, we need to remind that if the map was exactly a rotation, i.e.

$$\boldsymbol{x}' = e^{\{H\}} \boldsymbol{x} \,,$$

that is a linear map, all the frequencies would be the same, in this case (ω_1, ω_2).

So, the initial conditions leading to **frequencies close to the working point** are *good* frequencies ; the map for such points behaves like a rotation. We see that for such points, the diffusion index is small (blue points).

Thus if the map was a rotation, all the points would be sent on the working point. From this observation and the construction of the plot explained before,

---

6. For example by fixing the limit to 10^{-2} : D smaller than it leads to a regular orbit and a chaotic one otherwise.

7. According to the threshold chosen : the proportion would remain close but we cannot expect the exact same results.
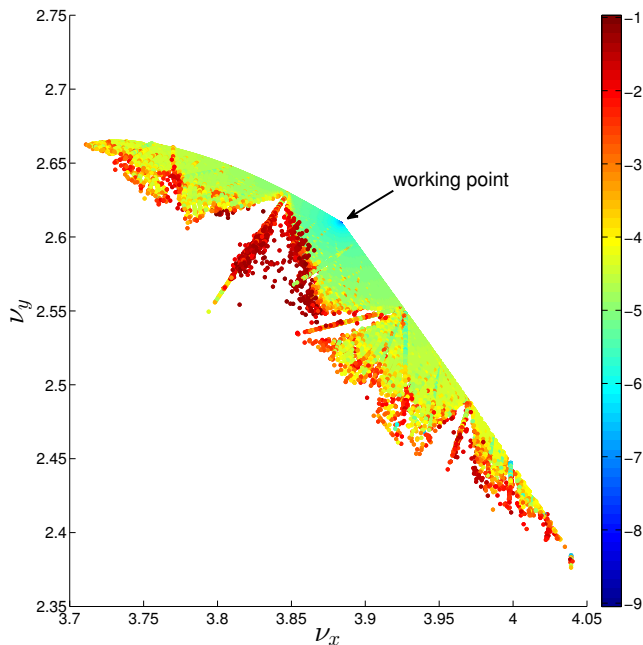
FIGURE 5.6: Frequency space for the (IM) with color code representing the diffusion $\log_{10} D$.

it is important to notice that **the density and the dispersion of points are not constant** : we can imagine a high concentration of the dots in a close neighborhood of the working point while the remaining ones would be spread somewhere else. As we shall see, this dispersion is closely related to the working point.

We also clearly observe special directions, where no points are present or points with a high diffusion index (red points). These are due to **resonances**. They are more or less important, according to their **width**.

Finally, the frequency space has a special **shape** delimited by two curves beyond which no frequencies are reached anymore.

We focus on these 3 peculiarities, namely
– the density of points close to the working point ;
– the shape of the frequency space ;
– the resonances and their width ;

that we now examine and compare with the two controlled maps (see Fig. 5.7 and 5.8).
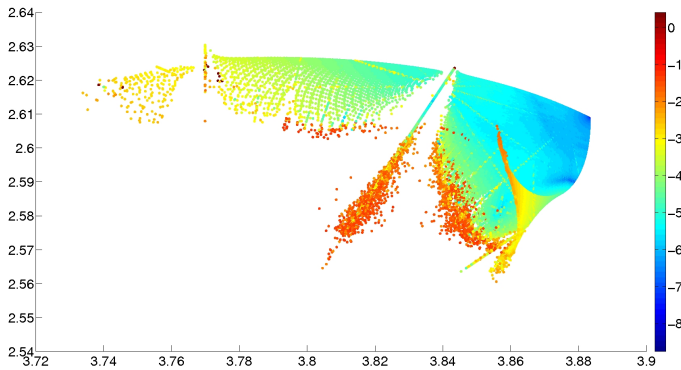

FIGURE 5.7: Frequency space for the (CMo4) with color code representing the diffusion $\log_{10} D$.
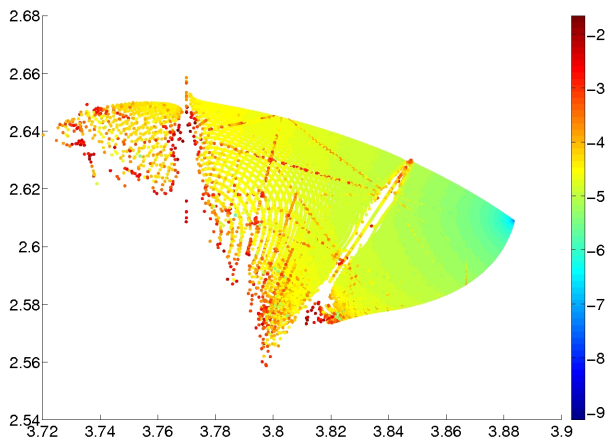

FIGURE 5.8: Frequency space for the (CMp0) with color code representing the diffusion $\log_{10} D$.

5.2.3 Density near the working point

In Secs 4.1 and 4.2, we have presented that (CMo4) and (CMp0), among other properties, increase the number of non-escaping orbits and their *quality* : beyond the number, the proportion of regular orbits is, in both cases, also increased.
We find similar results thanks to FMA and the associated frequency space.

We consider the number of couples (ν_x, ν_y) within a radius r from the working point (ω_1, ω_2). We indicate in table 5.1 the number of couples, its percentage and the density [8] for different values of r.

We observe a high density of points near the working point. This was expected ; the accelerator, and (hopefully) its model, is designed such that most particles turn with the same frequency close to the working point. The two controlled maps preserve that property and reinforce it : the density near the working point is much higher ; many points have their frequency flattened to the desired one. Of course, there are more points to be considered but the higher density is not only due to that increase of points : the percentages of the total number of non-escaping orbits is higher for smaller radii.

With the controlled maps, we thus have increased the number of non-escaping orbits and, globally, they have a better behavior exhibiting frequencies closer to (ω_1, ω_2) and this in great number.

---

8. The density for a given r is the ratio between the number of frequencies within this radius and the area of the circle of such radius.

(IM)				(CMo4)				(CMp0)			
r	Number	%	Density	r	Number	%	Density	r	Number	%	Density
10^{-3}	712	1,21	2.10^8	10^{-3}	1418	1,54	5.10^8	10^{-3}	1394	1,61	4.10^8
10^{-2}	7000	11,85	2.10^7	10^{-2}	14754	16,08	5.10^7	10^{-2}	13886	16,03	4.10^7
2.10^{-2}	13574	22,98	1.10^7	2.10^{-2}	30462	33,19	2.10^7	2.10^{-2}	26918	31,08	2.10^7
3.10^{-2}	19756	33,44	7.10^6	3.10^{-2}	52244	56,93	2.10^7	3.10^{-2}	38984	45,00	1.10^7
4.10^{-2}	24772	41,93	5.10^6					4.10^{-2}	50032	57,76	1.10^7
5.10^{-2}	30526	51,67	4.10^6	$\vdots$	$\vdots$	$\vdots$	$\vdots$	$\vdots$	$\vdots$	$\vdots$	$\vdots$
$\vdots$	$\vdots$	$\vdots$	$\vdots$								
0,28	59068	100	2.10^5	0,15	91768	100	1.10^6	0,166	86618	100	1.10^6

TABLE 5.1: Summary of the concentration of points near the working one (ω_1, ω_2). For different radii, r, from (ω_1, ω_2), the number of points within the considered radius, their percentage (with respect to the total number, see last line) and their density is given. These 3 numbers are much higher for the controlled maps than for the initial one.

5.2.4   Reachable frequencies - Shape of the frequency space

In Fig. 5.9, we plotted the frequency spaces of the three maps at the same scale and with the same axis.
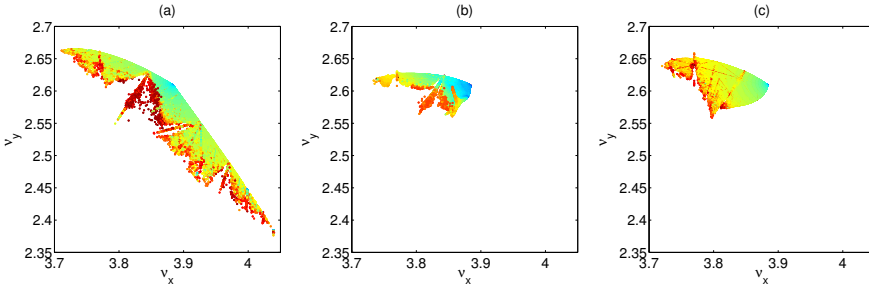

FIGURE 5.9: Frequency spaces of the (IM), the (CMo4) and the (CMp0) from left to right. The plots are at the same scale, the same place and for the same number of initial conditions. The FMA for the controlled maps has a smaller range of values, exhibiting thus a fewer frequencies.

The first observation is the considerable reduction of the frequency space in the controlled cases. This reinforces the conclusion of the previous subsection : even if more points are remaining, the diffusion, the variation, of the reached frequencies has decreased.

Secondly, we observe that the two controlled maps also exhibit a special shape delimited by two curves beyond which no frequencies are reached anymore while in the (IM) such curves are almost flat and thus determine a half plane.
These two curves intersect each other at the working point. Let us call Ψ, the angle formed by the curves at this point. At first approximation, Ψ defines a cone of reachable frequencies. While Ψ is close to $175°$ for the (IM), the controls reduced it to $116°$ and $110°$ for the (CMo4) and the (CMp0) respectively. This is another improvement of the quality of the controls : they reduce the directions where the frequencies can diffuse.

5.2.5   Resonances

The straight lines one can observe in the different frequency spaces are resonances. A resonance appears for an integer linear combination of the tunes q_x, q_y and the s direction $(= 1)$, i.e.

$$mq_x + nq_y + p = 0 \,, \tag{5.4}$$

or, equivalently, in terms of the frequencies, if

$$m\nu_x + n\nu_y + 2\pi p = 0\,,$$

where m, n and p are integers. We define the *resonance order* as the integer $|m| + |n| + |p|$. In the following we denote a resonance verifying Eq. (5.4) by $m : n : p$.

Because the values of q_x and q_y are well chosen (see footnote 2, p. 121), *exact* resonances would occur only for very high order, for example $10^5 : 10^4 : -57651$ verifies Eq. (5.4) but is of order 167651. We thus consider the triplet $m : n : p$ to be a *resonance* if it satisfies

$$|mq_x + nq_y + p| < \epsilon\,, \tag{5.5}$$

for a given small value ϵ. With this definition we avoid the use of large numbers and we are able to draw the resonant lines.

We present in Fig. 5.10, the resonance diagram close to the working point up to order 5, 10 and 15.
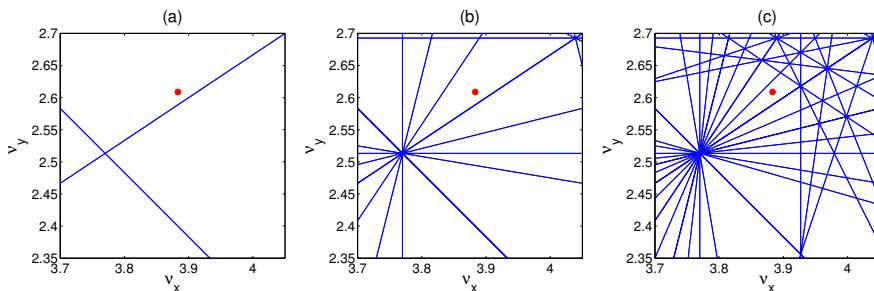

FIGURE 5.10: Resonance diagram up to order 5 (a), 10 (b) and 15 (c). The working point is each time indicated by a red dot. ϵ was set to 0.15.

In the Table 5.2, we give the first resonances, their order and the value of $|mq_x+nq_y+p|$. Let us remark that if $m : n : p$ is such that $|mq_x+nq_y+p| = \epsilon_{mnp}$ so is $-m : -n : -p$. Then we only presented one of the two combinations.

We then superpose these lines found analytically on the frequency space obtained with FMA and observe a perfect match : see Figs. 5.11, 5.12 and 5.13. Once again we observe the very good action of the controls. They both reduce

Order	m	n	p	$|mq_x + nq_y + p|$
3	-1	-1	1	0,0332
5	-2	3	0	0,0095
6	-3	2	1	0,0237
	-1	4	-1	0,0428
7	-4	1	2	0,0569
	0	-5	2	0,0760
8	-5	0	3	0,0901

TABLE 5.2: The first integer combinations up to order 8 of q_x, q_y and 1, leading to a small value of $|mq_x + nq_y + p|$.
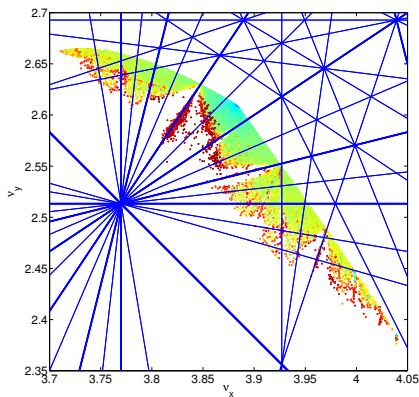

FIGURE 5.11: Resonances up to order 15 in the frequency space of (IM). Thicker lines correspond to resonances up to order 8. All the resonances check the conditions $|mq_x + nq_y + p| < 0.15$

the number of resonances giving diffusion directions, only one important resonance remains, the $-3 : 2 : 1$. Moreover, the (CMp0) even reduce drastically the width of that resonance visible only at small scale.

5.2.6 Conclusion

In the frequency space, we can observe three kinds of zones :

1. Regular areas, where points are regularly spaced with small diffusion index D. These points correspond to regular motion. This is observed especially near the working point.

2. Irregular areas (see for example the vicinity of $(3.84, 2.58)$ in Fig. 5.12) with lost of any structure : chaotic behaviors and/or border of the DA.

3. Resonances, that are straight lines of rational slope. They speed up the
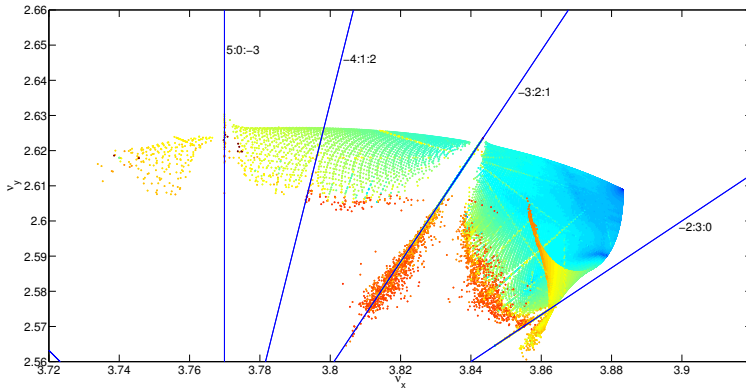
FIGURE 5.12: Resonances up to order 8 in the frequency space of (CMo4). All the resonances check the conditions $|mq_x + nq_y + p| < 0.15$

diffusion process : they empty their neighborhood and the remaining points have a large diffusion index.

Thanks to FMA, we can go further in the description and qualification of the controls (CMo4) and (CMp0) :

1. More then increasing the number of non-escaping orbits, they flatten the frequencies gathering them close to the working point.

2. They drastically decrease the size of the frequency space by reducing the cone of admissible frequencies.

3. Following the two previous points, the strength of the resonances is thus reduced and in the case of the (CMp0), remaining resonances have their width impressively shortened.

In the next section, we use the normal form approach in order to retrieve these results and give them an analytical meaning.
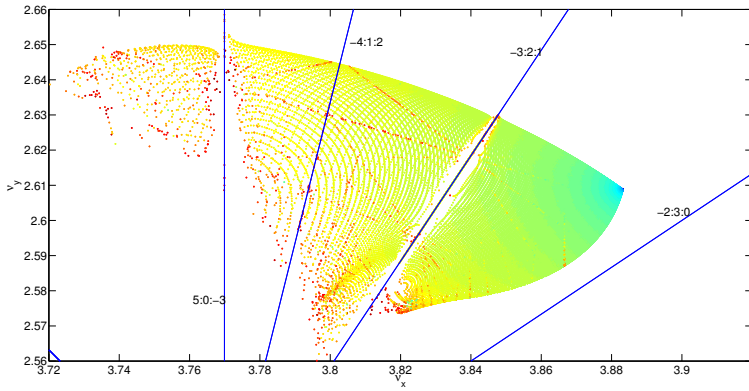
FIGURE 5.13: Resonances up to order 8 in the frequency space of (CMp0). All the resonances check the conditions $|mq_x + nq_y + p| < 0.15$

5.3   Normal Form approach of controlled particle accelerators

Following the method described in Chap. 1, Sec. 1.5 we evaluate the Normal Form (NF) of the three maps at different orders. Using this analytical method, we are able to recover most [9] of the results obtained with the numerical method FMA : the non-resonant frequency space, the high density of frequencies reached near the working point and the general *flattening* of the frequencies due to the controls. Then, we give an analytical prediction (at first order) of the two curves delineating the frequency space.

5.3.1   Normal Forms and conditions

The 3 maps (IM), (CMo4) and (CMp0) can be written in the generic form

$$\boldsymbol{x}' = f(\boldsymbol{x})$$

where $\boldsymbol{x} \in \mathbb{R}^4$. We perform the change of variables

$$\begin{cases} z_1 = x_1 + ix_2 \\ z_2 = x_3 + ix_4 \end{cases}$$

giving us a new map in complex variables

$$\boldsymbol{z}' = F(\boldsymbol{z}, \bar{\boldsymbol{z}})$$

with $\boldsymbol{z} = (z_1 , z_2) \in \mathbb{C}^2$. The normal form algorithm gives us order by order the change of variables (close to the identity)

$$\boldsymbol{z} = \Phi(\boldsymbol{\zeta}, \bar{\boldsymbol{\zeta}})$$

such that

$$\boldsymbol{\zeta}' = e^{i\Omega(\boldsymbol{\zeta}, \bar{\boldsymbol{\zeta}})}\boldsymbol{\zeta}$$

where $\Omega = (\Omega_1, \Omega_2)$ is real and depends only on the square of the modulus of ζ_1 and ζ_2 :

$$\Omega(\boldsymbol{\zeta}, \bar{\boldsymbol{\zeta}}) \equiv \Omega(|\zeta_1|^2, |\zeta_2|^2) \in \mathbb{R}^2.$$

We are especially interested in this vector (Ω_1, Ω_2) which gives the main frequency of the signal composed by the iterations of $\boldsymbol{\zeta}$ and the one of $\boldsymbol{z}$. We can thus reconstruct the frequency space by evaluating the function Ω at the initial conditions leading to non-escaping orbits. Let us already observe that at first order we recover the working point :

$$[(\Omega_1, \Omega_2)]_0 = (\omega_1, \omega_2).$$

---

9. We used the normal form algorithm in the non-resonant case and therefore we will not recover the resonant lines.

The higher the order, the smaller the radius of convergence will be

(see [Birkhoff, 1927]). Moreover, results are expressed in polynomial series. For these reasons, we adopt rules in order to avoid misleading results. We consider points z only if

1. the variables obtained via the change of variables, assume values smaller than 1 :
$$|\zeta_1| < 1 \quad \text{and} \quad |\zeta_2| < 1 \, ; \tag{5.6}$$

2. increasing the order makes only small variations :
$$||[\Omega]_{\leq j} - [\Omega]_{\leq l}|| \sim 0 \, , \tag{5.7}$$

where we introduced the notation

$$[\Omega]_{\leq j} := \sum_{k=1}^{j} [\Omega]_k.$$

Practically, we have chosen $j = 20$ and $l = 5$ and the difference was set to 10^{-3}.

We tested two algorithms, the one developed in [Bazzani et al., 1995] and the one of [Giorgilli, 2013]. They both give the exact same results at machine accuracy. The second one, more recent, and allowing higher orders was used to produce the graphs of this section.
Let us finally precise that both algorithms were used in the non-resonant case : as explained in the previous section, q_x and q_y are chosen irrational.

5.3.2 Reconstruction of the frequency space with Normal Form

We look at the initial conditions remaining after applying conditions (5.6) and (5.7). We then plot the results in the frequency space and comment the results by comparing them with those obtained with FMA.

Remaining initial conditions

Considering the conditions mentioned above, we first show which initial conditions remain in Fig. 5.14.
Referring to graphs like those obtained with the SALI (see Sec. 4.1) or the FMA (see Sec. 5.2), chaotic and leading to resonant motion orbits are removed. We also observe that regular orbits close to the border are absent. This is probably due to the need for crossing a resonance that the NF cannot accomplish : looking at Fig. 5.15 where we plotted in different colors initial conditions leading to orbits with frequencies that are on the main resonances line (precisely the $-3 : 2 : 1$, $-2 : 3 : 0$, $-4 : 1 : 2$ and $5 : 0 : -3$ resonances). We observe
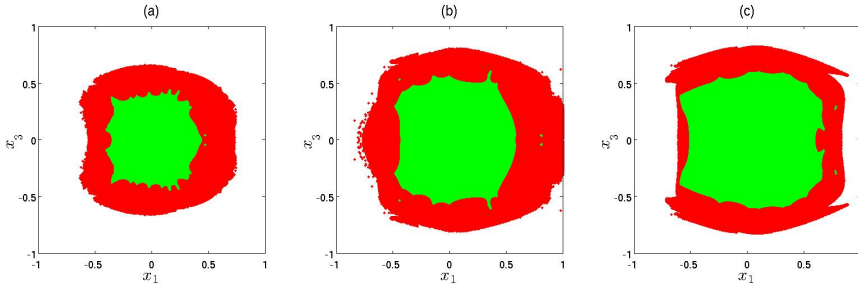
FIGURE 5.14: Remaining initial conditions for the (IM), the (CMo4) and the (CMp0) respectively (a), (b) and (c). In red all initial conditions, in green initial conditions veryfying (5.6) and (5.7).

that they separate the initial phase space into different regions where stand initial conditions of regular orbits. With this plot we show that we achieved what [Weishi and Cary, 2001] already imagined in order to enlarge the dynamic aperture (see Fig. 5.16) : to reduce the size of the resonances around the working point. Moreover we pushed them away.

The frequency space

We now can plot the frequency space without computing thousands of iterations and recover previous non-resonant results : see Figs. 5.17, 5.18 and 5.19. We superpose the results to those obtained by FMA. This helps the comparison. As expected the match around the working point is perfect. We also measure the percentage and density of frequencies at a given distance r from the working point and give them in Table 5.3.

Keeping in mind that most of the considered points are likely to be *good* points [10], we cannot directly compare the values of this table with the one obtained with FMA, table 5.1), but we can compare the percentages and densities. We found similar behaviors (increase of points and densities near (ω_1, ω_2) for the controlled maps), that is an improvement with the (CMo4) and the (CMp0), even with all the *bad guys* removed.

---

10. Replacing the maps in the context of accelerator physicists, the interesting points are those ones : not escaping, not chaotic and non-resonant.
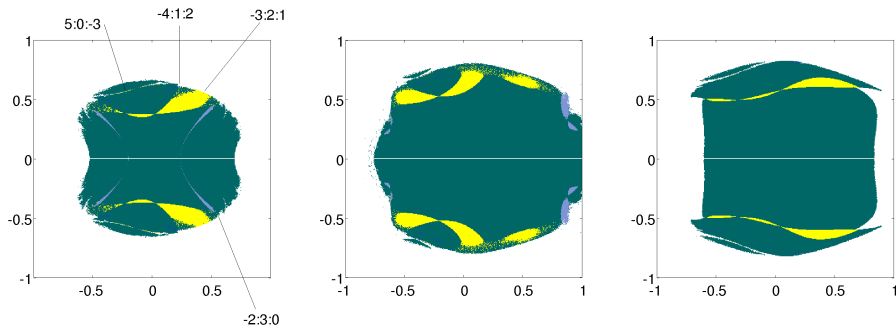
FIGURE 5.15: Initial conditions leading to non-escaping orbits in the $x_1 - x_3$ phase space for the 3 models, from left to right the (IM), the (CMo4) and the (CMp0). Initial conditions leading to frequencies on the resonances $-3 : 2 : 1$, $-2 : 3 : 0$, $-4 : 1 : 2$ and $5 : 0 : -3$ are in yellow, purple, blue and pale yellow respectively.
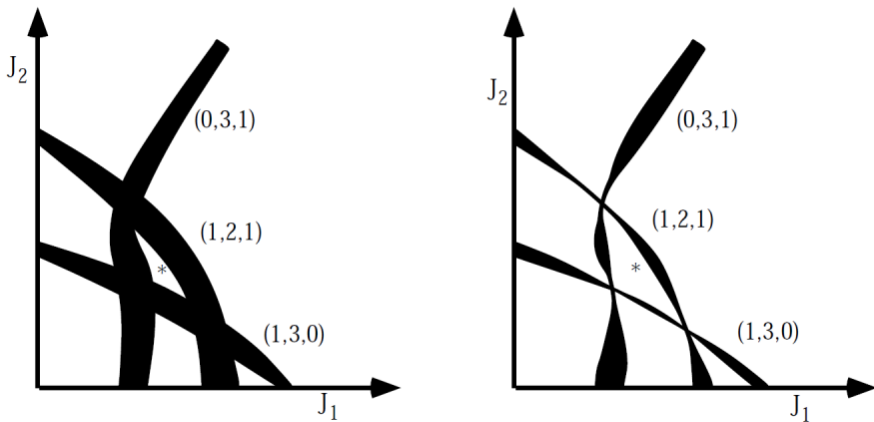

FIGURE 5.16: Drawing of the idea of [Weishi and Cary, 2001] : to find a good set of parameters such that the resonances surrounding the working point have their width reduced. Our control method achieve this goal, see Fig. 5.15. This figure is from [Weishi and Cary, 2001].
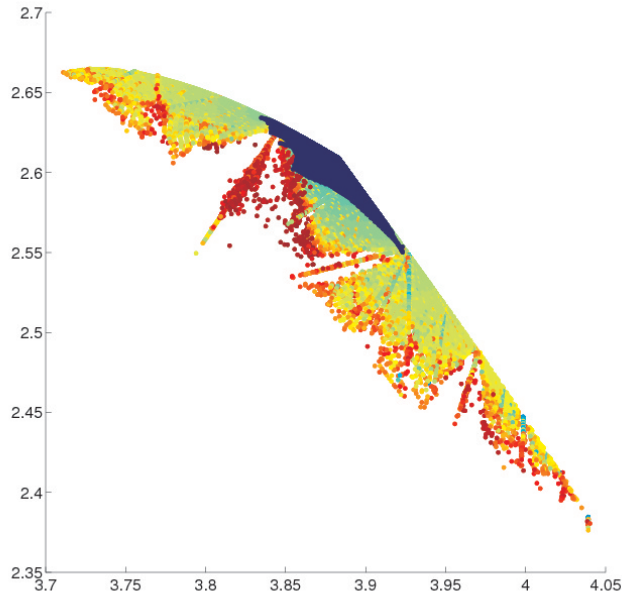
FIGURE 5.17: Frequency space of the (IM) : superposition of the results obtained by a normal form approach on those obtained by FMA.
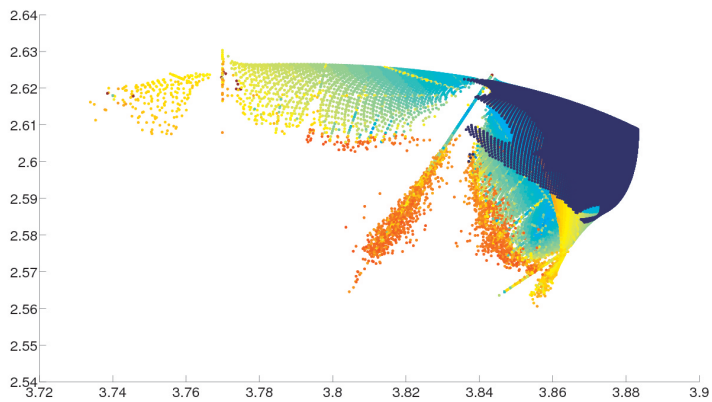

FIGURE 5.18: Frequency space of the (CMo4) : superposition of the results obtained by a normal form approach on those obtained by FMA.
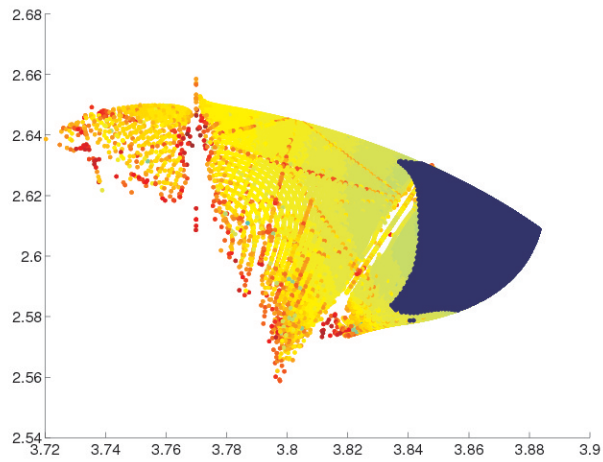
FIGURE 5.19: Frequency space of the (CMp0) : superposition of the results obtained by a normal form approach on those obtained by FMA.

(IM)				(CMp0)				(CMo4)			
r	Number	%	Density	r	Number	%	Density	r	Number	%	Density
10^{-3}	732	3,5	2.10^8	10^{-3}	1438	2,9	5.10^8	10^{-3}	1456	3,8	5.10^8
10^{-2}	7068	33,6	2.10^7	10^{-2}	14014	28,04	4.10^7	10^{-2}	14834	38,09	5.10^7
2.10^{-2}	13036	62,01	1.10^7	2.10^{-2}	27095	54,9	2.10^7	2.10^{-2}	32299	79,6	2.10^7
$\vdots$	$\vdots$	$\vdots$	$\vdots$	$\vdots$	$\vdots$	$\vdots$	$\vdots$	$\vdots$	$\vdots$	$\vdots$	$\vdots$
8.10^{-2}	20993	100	1.10^6	6.10^{-2}	49329	100	5.10^6	6.10^{-2}	38085	100	3.10^6

TABLE 5.3: Table of the points near the working point (ω_1, ω_2) obtained by normal form. For different distances, r, from it, the number of points, their percentage and their density within such distance is given.

5.3.3 The Shape of the frequency space

In this subsection, we derive the shape of the frequency space, that is to say we find the two curves delineating a portion of the plane where the diffusion directions are allowed.

Generally speaking (that is, for the three considered maps), at first order [11], we can write

$$[\Omega_1]_{\leq 2} = \omega_1 + a_1|\zeta_1|^2 + b_1|\zeta_2|^2 \qquad (5.8)$$

$$[\Omega_2]_{\leq 2} = \omega_2 + a_2|\zeta_1|^2 + b_2|\zeta_2|^2 \qquad (5.9)$$

where a_1, a_2, b_1 and b_2 are provided by the normal form algorithm. We recall that we consider $|\zeta_1|$ and $|\zeta_2|$ to lie in the interval $[0\,,1]$.

Initial Map

For the (IM), we find the following values

$$a_1 = 0.19955798013540454 > 0$$
$$b_1 = -0.27632214397086574 < 0$$
$$a_2 = -0.27632214397086574 < 0$$
$$b_2 = 0.1663288024549204 > 0$$

We can consider two extreme cases :

1. with $|\zeta_1| = 0$ and $|\zeta_2| = 1$, $[\Omega_2]_{\leq 2}$ is maximum and thus should have all its values below the straight line [12]

$$D_1 \equiv y = \frac{b_2}{b_1}(x - \omega_1) + \omega_2 \qquad (5.10)$$

for x varying in $[\omega_1 + b_1, \omega_1 + a_1]$;

2. with $|\zeta_1| = 1$ and $|\zeta_2| = 0$, we have a similar behavior : $[\Omega_1]_{\leq 2}$ should be below the straight line

$$D_2 \equiv y = \frac{a_2}{a_1}(x - \omega_1) + \omega_2 \qquad (5.11)$$

for y varying in $[\omega_2 + a_2, \omega_2 + b_1]$;

The intersection of these two portions of the plane delineates the reachable values of $([\Omega_1]_{\leq 2}, [\Omega_2]_{\leq 2})$. The two lines are superposed the frequency space obtained with FMA in Fig. 5.20.
The match is perfect at the working point (where non-linear terms have negligeable effect) and a very good approximation of the border, especially on the right of the working point.

---

11. In the development in the variables $\rho_i = \zeta_i\bar{\zeta}_i$, $i = 1, 2$.
12. This can be obtained by setting $|\zeta_1| = 0$ in Eqs. (5.8) and (5.9) and then substituting $|\zeta_2|^2$.
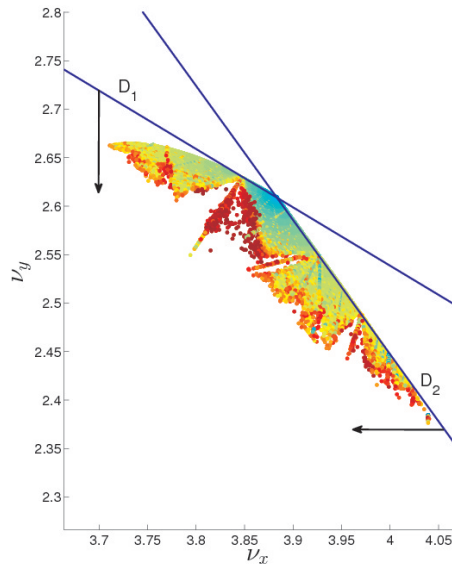
FIGURE 5.20: Lines D_1, Eq. (5.10) and D_2, Eq. (5.11) in superposition on the frequency space.

Controlled maps

A similar reasoning can be applied to the (CMo4) and the (CMp0). The lines D_1 and D_2 have the same equation but the values of a_i and b_i $(i = 1, 2)$ change for each map. We have the results reported in Figs. 5.21 and 5.22. Once again, the matching is excellent.

Higher order

Let us remark that such analysis could be extended to higher order. We would expect a good fit at a greater distance from the working point.

FIGURE 5.21: Lines (with adapted values of a_1, a_2, b_1 and b_2) D_1, Eq. (5.10) and D_2, Eq. (5.11) in superposition on the frequency space of the (CMo4).
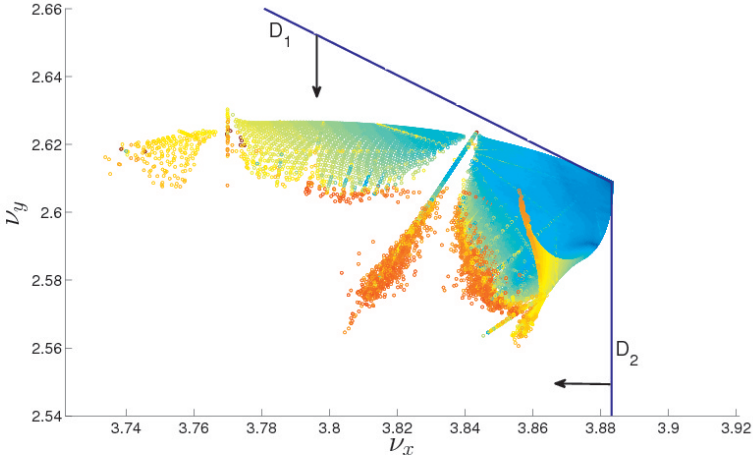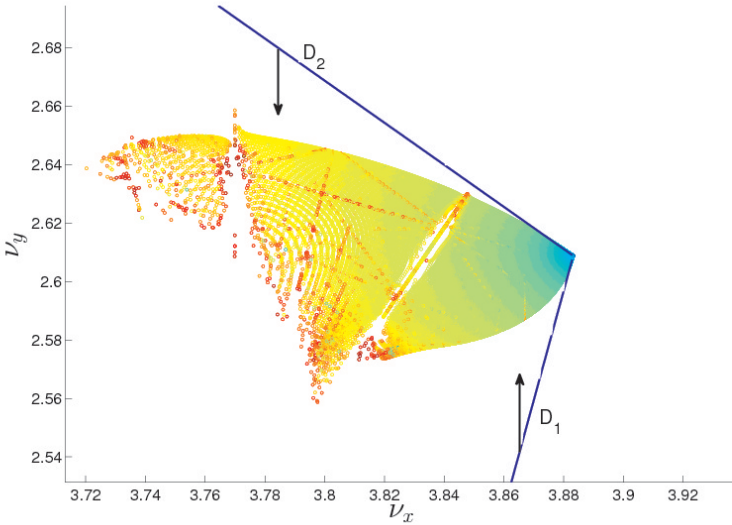

FIGURE 5.22: Lines (with adapted values of a_1, a_2, b_1 and b_2) D_1, Eq. (5.10) and D_2, Eq. (5.11) in superposition on the frequency space of the (CMp0).

Control of dissipative perturbation of integrable systems - An Application to the van der Pol oscillator

Contents

We propose a method to control dissipative systems *close* to integrable systems. To achieve this, a control is added to the original system such that the controlled system exhibits a constant of motion. We apply this procedure to the van der Pol oscillator.

6.1　Introduction

Many physical systems can be represented by a conservative system perturbed by non-conservative forces : we think for instance of friction, tidal forces, atmospheric drag, radiation pressure or an electrical resistance.

Consider an autonomous system of differential equations of first order :

$$\dot{\boldsymbol{x}} = H(\boldsymbol{x}) + V(\boldsymbol{x})$$

where H and V are smooth vector fields. We consider V to be a perturbation (say of size ϵ) of the system H. We assume the existence of a constant of motion h for H i.e. the vector field H preserves h.

The goal is to propose a control method for such perturbed systems. It consists in adding a correction F of size ϵ^2 to the initial system in such a way that the resulting, *controlled*, system possesses a constant of motion $\epsilon-$close to h, the one of the unperturbed system.

In Sec. 6.2, we first expose the framework of vector fields, vector spaces and Lie-Algebras we shall work with, before constructing the control. In Sec. 6.3 we apply the technique to a classical example of damped oscillator : the van der Pol oscillator.

6.2　Theory

Let M be a manifold and TM its tangent bundle. We consider vector fields V on the manifold M, i.e. sections of $TM : V \in \mathcal{C}^\infty(M, TM)$ such that for any $\boldsymbol{x} \in M$, $V(\boldsymbol{x})$ lies in $T_{\boldsymbol{x}}M$, the tangent space at $\boldsymbol{x}$. We denote the space of vector fields on M by $\mathbb{V}$.

For all scalar valued function $f \in \mathbb{Y} = \mathcal{C}^\infty(M, \mathbb{R})$, we shall consider the derivation along the vector field V and we denote it by $L_V f \in \mathbb{Y} : L_V$ is a differential operator of order 1 on $\mathbb{Y}$. We denote the space of those operators by $L_{\mathbb{V}}$.

We recall that the commutator $[L_H, L_V]$ of two elements L_H and L_V of $L_{\mathbb{V}}$ is again of order 1, i.e. it preserves the Leibniz property. Thus there exists some $Z \in \mathbb{V}$ such that $L_Z = [L_H, L_V]$. Z is called the Lie-bracket of the vector fields H and $V : Z = [H, V]$.

In the specific case where $M = \mathbb{R}^n$, we have the following expression for the derivation along a vector field.
Let $f \in \mathbb{Y}$ and $H, V \in \mathbb{V}$, then

$$L_H f := (H \cdot \nabla) f = \sum_{j=1}^n H_j(\boldsymbol{x}) \frac{\partial f}{\partial x_j} \,,$$

and

$$[H, V] = (H \cdot \nabla) V - (V \cdot \nabla) H \,,$$

or, componentwise,

$$([H, V])_i = \sum_{j=1}^n \left(H_j \frac{\partial V_i}{\partial x_j} - V_j \frac{\partial H_i}{\partial x_j} \right) = L_H V_i - L_V H_i \,. \tag{6.1}$$

This is the derivation of the vector field V along the vector field H. For that reason, we also use the notation $[H, V] =: L_H V$. This notation is identical if the argument is either a scalar value function or a vector field. For practical reasons in further calculations, we also introduce the following equivalent notations of such operator L_V :

$$L_V \equiv \{V\} \equiv \mathcal{V} \,.$$

The vector space $\mathbb{V}$ with this bracket is a Lie-Algebra : $\forall\, X\,, Y,\, Z \in \mathbb{V}$ we have (see e.g. [Fasano and Marmi, 2006]) :
  – $[.,.]$ is bilinear ;
  – $[X, Y] = -[Y, X]$;
  – the Jacobi identity

$$[X, [Y, Z]] + [Y, [Z, X]] + [Z, [X, Y]] = 0.$$

We finally need to consider *operators* acting on elements of $L_\mathbb{V}$. Such an operator is defined from an element of $L_\mathbb{V}$ through the commutator :

$$\begin{array}{cccc} \{\mathcal{X}\} : & L_\mathbb{V} & \to & L_\mathbb{V} \\ & \mathcal{Y} & \mapsto & \{\mathcal{X}\} \mathcal{Y} := \mathcal{X}\mathcal{Y} - \mathcal{Y}\mathcal{X} \end{array} \tag{6.2}$$

We shall denote by $\mathbb{U}$ the space of these elements :

$$\mathbb{U} = \{\{\mathcal{X}\} : L_\mathbb{V} \to L_\mathbb{V}\}$$

We have defined the framework that we need in order to construct a control term.

The aim is to construct a new vector field

$$\hat{H} := H + V + F$$

that preserves a certain quantity $\hat{h}$. Let us denote by $\mathbb{V}_h$ the set of vector fields preserving the scalar function h

$$\mathbb{V}_h = \{X \in \mathbb{V} \,|\, L_X h = 0\}$$

and the corresponding sets of *good* operators

$$\mathbb{B}_h = \{\mathcal{X} \in L_\mathbb{V} \,|\, X \in \mathbb{V}_h\}\,.$$

With all those tools, we can present the following [1]

Theorem 6.2.1 *Let* $H \in \mathbb{V}_h$. *If* $\exists\, S \in \mathbb{V}$ *s.t.*

$$B := V - \mathcal{H}S \in \mathbb{V}_h \quad i.e \quad \mathcal{B} \in \mathbb{B}_h \quad and \quad B = \mathcal{O}(V) \tag{6.3}$$

then

$$there\ exists\ \hat{\mathcal{H}} \in \mathbb{B}_{\hat{h}} \quad where \quad \hat{h} = e^{-S} h \tag{6.4}$$

with $\hat{H} = H + V + F$, *where*

$$F = \left(e^{-S} - 1\right) V + \left(\frac{1 - e^{-S}}{S} - e^{-S}\right) \mathcal{H}S. \tag{6.5}$$

Moreover $F = \mathcal{O}(V)^2$.

Proof. We have to check that (6.4) is fulfilled. Let first point out that this is equivalent to

$$e^{\{S\}}\hat{\mathcal{H}} \quad preserves \quad h. \tag{6.6}$$

Indeed, by definition one has

$$e^{\{S\}}\hat{\mathcal{H}}h = 0 \Leftrightarrow e^S \hat{\mathcal{H}} e^{-S} h = 0 \Leftrightarrow \hat{\mathcal{H}} e^{-S} h = 0$$

that is (6.4). We also notice that from Eq. (6.5), the operator $\mathcal{F}$ associated to F is given by

$$\mathcal{F} = \left(e^{-\{S\}} - 1\right) \mathcal{V} + \left(\frac{1 - e^{-\{S\}}}{\{S\}} - e^{-\{S\}}\right) \{\mathcal{H}\}\mathcal{S}$$

---

1. We keep the notation $\mathcal{O}$ that should be understood as the max on each component.

Let us now prove (6.6).

$$
\begin{aligned}
e^{\{S\}}(\mathcal{H} + \mathcal{V} + \mathcal{F}) &= e^{\{S\}}\mathcal{H} + e^{\{S\}}\mathcal{F} + \mathcal{V} + (e^{\{S\}} - 1)\mathcal{V} \\
&= \frac{\{S\}\mathcal{H} - e^{\{S\}}\{\mathcal{H}\}S + \{\mathcal{H}\}S}{\{S\}} + e^{\{S\}}\mathcal{F} + \mathcal{V} + (e^{\{S\}} - 1)\mathcal{V} \\
&= \mathcal{H} - \frac{e^{\{S\}} - 1}{\{S\}}\{\mathcal{H}\}S + \mathcal{V} + e^{\{S\}}\mathcal{F} + (e^{\{S\}} - 1)\mathcal{V} \\
&= \mathcal{H} - \frac{e^{\{S\}} - 1}{\{S\}}\{\mathcal{H}\}S + \mathcal{B} + \{\mathcal{H}\}S + e^{\{S\}}\mathcal{F} + (e^{\{S\}} - 1)\mathcal{V} \\
&= \mathcal{H} + \mathcal{B} + e^{\{S\}}\mathcal{F} + \underbrace{\left(1 - \frac{e^{\{S\}} - 1}{\{S\}}\right)\{\mathcal{H}\}S + (e^{\{S\}} - 1)\mathcal{V}}_{= -e^{\{S\}}\mathcal{F}} \\
&= \mathcal{H} + \mathcal{B} \in \mathbb{B}_h.
\end{aligned}
$$

where we used $\mathcal{H} \in \mathbb{B}_h$.
This achieves the proof.

$\square$

Concretely, we need to find $S \in \mathbb{V}$ verifying (6.3) which is nothing but a partial differential equation with n unknowns $S_1, \ldots, S_n$.

Moreover in order to provide a control term F, we should evaluate e^{-S}, which is generally not possible in a closed analytical form. For that reason we give a version of F correct at $\mathcal{O}(V)^2$.
We shall use the following decomposition :

$$
e^{-S} = \sum_{k \geq 0} \frac{(-S)^k}{k!} = 1 - S + \frac{S^2}{2} + \ldots \tag{6.7}
$$

and use it to calculate F :

$$
\begin{aligned}
F &= \left(e^{-S} - 1\right)V + \left(\frac{1 - e^{-S}}{S} - e^{-S}\right)\mathcal{H}S \\
&= (1 - S - 1)V + \left(\frac{1 - \left(1 - S + \frac{S^2}{2}\right)}{S} - (1 - S)\right)\mathcal{H}S + \mathcal{O}(V)^3 \\
&= -SV + \frac{1}{2}S\mathcal{H}S + \mathcal{O}(V)^3.
\end{aligned}
$$

6.3 Application to the van der Pol oscillator

The model we shall consider was originally developed by van der Pol in the 1920s [van der Pol, 1927] to describe the dynamics of a triode electronic

oscillator.

In the van der Pol model, the electrical charge, denoted by $q(t)$, passing through the triode tube is assumed to be described by the equation

$$\ddot{q} + \epsilon(q^2 - 1)\dot{q} + q = 0. \tag{6.8}$$

This model has been widely studied in the history of nonlinear dynamics and it is used in most of the books in this field as a paradigm model for the existence of limit cycle in non-linear oscillator.

Eq. (6.8) can be written as two ordinary differential equations introducing the variable $p = \dot{q}$ and $\boldsymbol{x} = (q \; p)^t$:

$$\dot{\boldsymbol{x}} = H(\boldsymbol{x}) + V(\boldsymbol{x})$$

where

$$H(\boldsymbol{x}) = \begin{pmatrix} p \\ -q \end{pmatrix} \quad \text{and} \quad V(\boldsymbol{x}) = \epsilon \begin{pmatrix} 0 \\ (1 - q^2)p \end{pmatrix}.$$

The quantity

$$h(\boldsymbol{x}) = \frac{q^2}{2} + \frac{p^2}{2}$$

is preserved by H, indeed :

$$L_H h = H_1(\boldsymbol{x})\partial_q h + H_2(\boldsymbol{x})\partial_p h = p\,q + (-q)p = 0.$$

With these notations, we can try to construct a control F. For this purpose, we first need to find a *good S* i.e. we need (6.3) to be satisfied. In other words we have to solve the following equation

$$\{V - \mathcal{H}S\}h = 0$$
$$\Leftrightarrow \quad L_V h - L_{\mathcal{H}S}h = 0$$
$$\Leftrightarrow \quad L_V h - L_{[H,S]}h = 0$$

where

$$L_V h = V_1(\boldsymbol{x})\partial_q h + V_2(\boldsymbol{x})\partial_p h = \epsilon(1 - q^2)p^2$$

and

$$[H, S] = \begin{pmatrix} H_1\partial_q S_1 + H_2\partial_p S_1 - S_1\partial_q H_1 - S_2\partial_p H_1 \\ H_1\partial_q S_2 + H_2\partial_p S_2 - S_1\partial_q H_2 - S_2\partial_p H_2 \end{pmatrix}$$
$$= \begin{pmatrix} p\partial_q S_1 - q\partial_p S_1 - S_2 \\ p\partial_q S_2 - q\partial_p S_2 + S_1 \end{pmatrix}$$

thus

$$L_{[H,S]}h = (p\partial_q S_1 - q\partial_p S_1 - S_2)q + (p\partial_q S_2 - q\partial_p S_2 + S_1)p.$$

The partial differential equation to solve is then

$$(1 - q^2)p^2 - (p\partial_q S_1 - q\partial_p S_1 - S_2)q - (p\partial_q S_2 - q\partial_p S_2 + S_1)p = 0. \tag{6.9}$$

6.3.1 Solution S

We are looking for $S_1, S_2 : \mathbb{R}^2 \to \mathbb{R}$ verifying (6.9). Ideally, we would like to find them $\mathcal{C}^k$ with $k \in \mathbb{N}$ as high as possible : in order to construct F, we need the derivatives of S. This equation admits possibly many solutions. Indeed, we have one equation with two functions to be determined.

A practical form would be a polynomial solution but we shall show that it is impossible. Secondly, we could try to solve

$$V - [H, S] = 0$$

whose solution would also solves $L_{V-[H,S]}h = 0$.

Polynomials

We first propose a polynomial solution :

$$S_1 = \sum_{n,m \in \mathbb{N}} \alpha_{nm} q^n p^m \quad \text{and} \quad S_2 = \sum_{n,m \in \mathbb{N}} \beta_{nm} q^n p^m$$

where $\alpha_{nm}, \beta_{nm} \in \mathbb{R}$ are to be determined. We evaluate the corresponding partial derivative :

$$\partial_q S_1 = \sum_{n,m \in \mathbb{N}} n\alpha_{nm} q^{n-1} p^m \quad \text{and} \quad \partial_q S_2 = \sum_{n,m \in \mathbb{N}} n\beta_{nm} q^{n-1} p^m$$

$$\partial_p S_1 = \sum_{n,m \in \mathbb{N}} m\alpha_{nm} q^n p^{m-1} \quad \text{and} \quad \partial_p S_2 = \sum_{n,m \in \mathbb{N}} m\beta_{nm} q^n p^{m-1}$$

Eq. (6.9) reads then

$$p^2 - q^2 p^2 - \sum_{n,m \in \mathbb{N}} (n+1)\alpha_{nm} q^n p^{m+1} + \sum_{n,m \in \mathbb{N}} (m+1)\beta_{nm} q^{n+1} p^m$$

$$+ \sum_{n,m \in \mathbb{N}} m\alpha_{nm} q^{n+2} p^{m-1} - \sum_{n,m \in \mathbb{N}} n\beta_{nm} q^{n-1} p^{m+2} = 0.$$

Unfortunately, this equation has no solution : looking at the condition on the coefficients in q^2, we need

$$\alpha_{01} + \beta_{10} = 0 \tag{6.10}$$

and similarly, the condition on those in p^2 is

$$1 - \alpha_{01} - \beta_{10} = 0. \tag{6.11}$$

Eqs. (6.10) and (6.11) are not compatible. Equation (6.9) does not admit a polynomial solution.

Imposing $S_1 = 0$

Imposing $S_1 = 0$, Eq. (6.9) becomes

$$(1 - q^2)p^2 + qS_2 - p^2 \partial_q S_2 + pq \partial_p S_2 = 0.$$

that is a linear partial differential equation of order one which is solved by

$$S = \begin{pmatrix} 0 \\ \arctan\left(\frac{p}{q}\right)\left(\frac{1}{8}p^3 - \frac{1}{2}p + \frac{1}{4}pq^2 + \frac{1}{8}\frac{q^4}{p} - \frac{1}{2}\frac{q^2}{p}\right) + \frac{1}{8}p^2 q - \frac{1}{8}q^3 + \frac{1}{2}q \end{pmatrix}$$
$$(6.12)$$

where we set the constant to 0. Let us remark that this solution is not well defined when p or q vanish.

6.3.2   The control term

Considering the solution S given in Eq. (6.12), we need $\mathcal{SHS}$ to construct the control term F. Noticing that $V_1 = S_1 = 0$, we quickly get

$$\mathcal{SV} = \begin{pmatrix} 0 \\ S_2 \partial_p V_2 - V_2 \partial_p S_2 \end{pmatrix}$$

$$= \begin{pmatrix} 0 \\ \frac{\epsilon}{4p}\left(q^2 - 1\right)\left(p^3 q + pq^3 + \arctan\left(\frac{p}{q}\right)\left(p^4 - q^4 + 4q^2\right) - 4\,pq\right) \end{pmatrix}$$

and, similarly, we can find $\mathcal{SHS}$ to finally express F :

$$F = \begin{pmatrix} F_1 \\ F_2 \end{pmatrix}$$

where

$$F_1 = \frac{-\epsilon^2}{128p^3}\left(\left(\arctan\left(p/q\right)\left(p^4 + 2p^2 q^2 + q^4 - 4p^2 - 4q^2\right) + p^3 q - pq^3 + 4pq\right)\right.$$

$$\left(\arctan\left(p/q\right)\left(3p^4 - 4p^2 + 2p^2 q^2 - q^4 + 4q^2\right) + 3p^3 q + pq^3 - 4pq\right)\right)$$

and

$$F_2 = \frac{\epsilon^2}{128p^4}\left(\left(\arctan\left(\frac{p}{q}\right)\left(p^4 q + 2p^2 q^3 - 4qp^2 + q^5 - 4q^3\right)\right.\right.$$

$$\left. + p^3(8 - 7q^2) + 4p(q^2 - q^4)\right)$$

$$\left(\arctan\left(p/q\right)\left(3p^4 - 4p^2 + 2p^2 q^2 - q^4 + 4q^2\right) + 3p^3 q + pq^3 - 4pq\right)\right).$$

The preserved quantity $\hat{h}$ can also be calculated using Eq. (6.7) :

$$\hat{h}(\boldsymbol{x}) = h - \epsilon \left(\frac{pq}{8} \left(p^2 - q^2 + 2 \right) + \arctan(p/q) \left(\frac{h^2}{2} - h \right) \right)$$

$$+ \frac{\epsilon^2}{2} \left(\frac{pq}{2} + \arctan(p/q) \left(h - 1 \right) \right) \left(\frac{pq}{8} \left(p^2 - q^2 + 2 \right) + \arctan(\frac{p}{q}) \left(\frac{h^2}{2} - h \right) \right)$$

$$+ \mathcal{O}(\epsilon^3).$$

6.3.3   Numerical results

The aim of this subsection is to present some numerical results to support the analytical part of Sec. 6.3. For the initial value $\boldsymbol{x}(0) = (q(0)\ p(0))^t = (-1.97\ 0.3031)^t$ with $\epsilon = 0.2$, we plot in Fig. 6.1 the evolution of $\hat{h}$. In Fig. 6.2
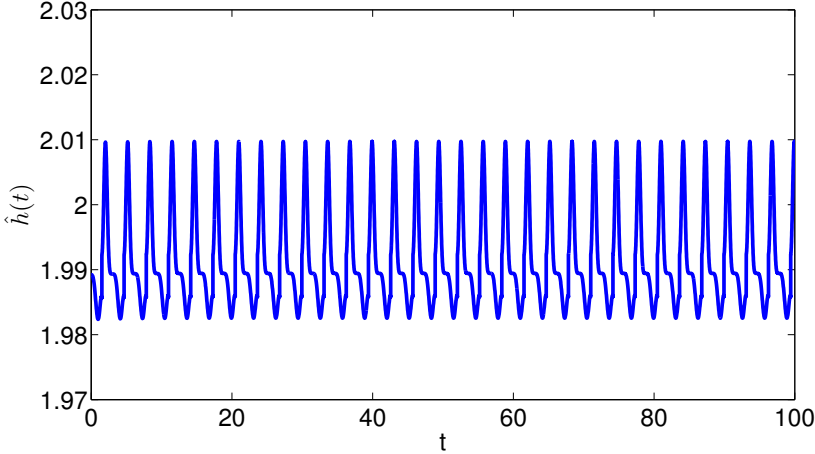
FIGURE 6.1: Evolution of $\hat{h}(t)$.

we give the error

$$err(t) = \frac{|\hat{h}(\boldsymbol{x}(t)) - \hat{h}(\boldsymbol{x}(0))|}{|\hat{h}(\boldsymbol{x}(0))|}$$

of the preserved quantity $\hat{h}$ linked to the system $H + V + F$.

Also, in order to check that the control F is small in front of the initial system $H + V$, we computed for a given initial condition $\boldsymbol{x}(0)$

$$E(\boldsymbol{x}(0)) = \frac{\sup |F|}{\sup |H + V|}$$

where

$$\sup |F| = \sup_{t} \max\{|F_1(\boldsymbol{x}(t))|, |F_2(\boldsymbol{x}(t))|\}$$

FIGURE 6.2: Evolution of $err(t)$.

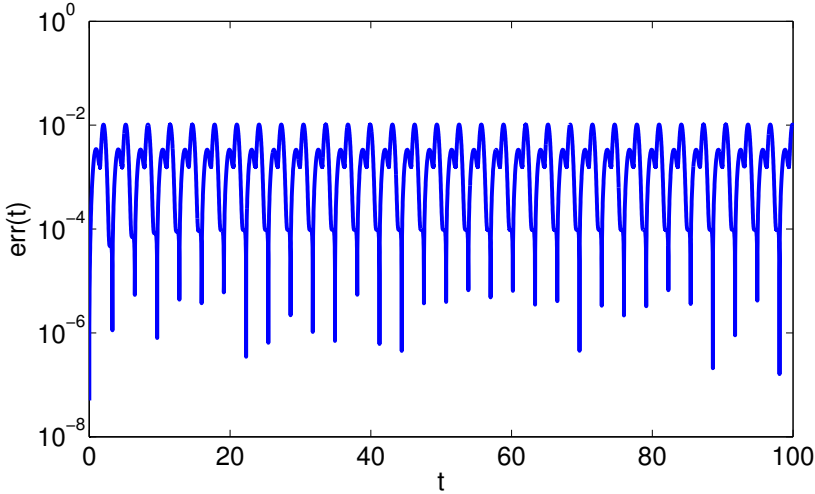and identically for $\sup|H + V|$. We obtain $E(\boldsymbol{x}(0)) = 0.0295$. This means that we constructed a preserved quantity using less than 3% of the energy of the original system for the initial condition $\boldsymbol{x}(0)$.

It is also common to compare the size of the control in front of the energy of the initial system. Considering the kinetic energy being $\frac{|\dot{q}|^2}{2}$, the control is then less than 0.08% of that considered energy.

6.4   Time dependence

The aim of this section is to extend the previous results to an explicit time dependent system ; for example the Duffing oscillator [Holmes, 1979] :

$$\left(\begin{array}{c} \dot{q} \\ \dot{p} \end{array}\right) = \left(\begin{array}{c} p \\ \omega q - \beta q^3 + \epsilon(2\cos\tau - \gamma p) \end{array}\right) = X(q, p, \tau).$$

where the dot symbol denotes the derivative with respect to τ in this section : $(\dot{\ }) = \frac{d}{d\tau}$.

6.4.1   Need to *defrost* the time

Let us observe that the main difference with respect to the previous case is that given a time dependent vector field X, the operator L_X does not anymore induce the flow $e^{\tau L_X(\tau)}$ of any observable ; indeed, the *time*, here represented by the variable τ is frozen. To tackle this problem we propose to complete L_X by adding ∂_τ :

$$\mathcal{H} = L_X + \partial_\tau$$

such that its flow is the correct one if the observable is time-dependent. Indeed for any observable $W(q, \tau)$, we should have

$$W(\tau) = e^{\tau \mathcal{H}} W_0$$

which is the solution of

$$\dot{W} = \mathcal{H} W.$$

On one hand we have that

$$\dot{W} = (\partial_q W)\dot{q} + \partial_\tau W$$

and on the other hand, remembering that $L_X = \dot{q}\partial_q$ we find

$$\begin{aligned} \mathcal{H}W &= (L_X + \partial_\tau)W \\ &= L_X W + \partial_\tau W \\ &= \dot{q}\partial_q W + \partial_\tau W. \end{aligned}$$

Let us also remark that

$$\dot{\tau} = \mathcal{H}\tau = (L_X + \partial_\tau)\tau = 1$$

and thus τ actually plays its role, the time, and can be replaced by the variable t.

6.4.2 Generalization of the PDE

$\mathcal{H}$ being a differential operator of order 1, theorem 6.2.1 still holds. We are thus looking for S such that

$$\mathcal{V} - \{\mathcal{H}\}\mathcal{S} \quad \text{preserves} \quad h$$

More explicitly

$$\mathcal{V} - \{\mathcal{H}\}\mathcal{S} = L_V - [\partial_t + L_H, L_S] = L_V - [\partial_t, L_S] + [L_S, L_H]$$

Let us give some details on the new commutator $[\partial_t, L_S]$:

$$[\partial_t, L_S] = \partial_t L_S - L_S \partial_t = \partial_t L_S$$

because the function on which it will be applied is time-independent. Then, $\forall h \in \mathcal{C}^\infty(M, \mathbb{R})$, we have

$$\begin{aligned} \partial_t(L_S h) &= \partial_t(S \cdot \nabla h) \\ &= (\partial_t S) \cdot \nabla h + S \cdot (\partial_t \nabla h) \\ &= L_{\dot{S}} h \end{aligned}$$

and finally, we have to solve

$$\mathcal{V} - \{\mathcal{H}\}\mathcal{S} = L_V - L_{\dot{S}} + L_{[S,H]}. \tag{6.13}$$

Despite this good theoretical framework, solving Eq. (6.13) remains a hard task (see Subsec. 6.3.1) : our first attempts on the Duffing oscillator did not lead to a solution yet.

Conclusions and Perspectives

Back in the 90s [Scandale and Turchetti, 1990], specialists met together to establish the best possible picture of the problems linked to nonlinearities in present and future particle accelerators. This coincides with LHC project officially approved in December 1994.

In 2008, September 10, a first beam made a full turn of 27km in the LHC. From the CERN press office [press, 2008] :

> "It's a fantastic moment," said LHC project leader Lyn Evans, "we can now look forward to a new era of understanding about the origins and evolution of the universe."

Since then, and amongst other things, this *great milestone of mankind* [Gaudin, 2008] identified the Brout-Englert-Higgs' boson.

In parallel to the great engineering resources established, the talent of scientists was required. The need for constructing models, for simulating such devices and for, already, thinking the design of the future accelerators was and remains huge. The physics of particle accelerators is now a fully-fledged area of science. Tools and techniques were created and adapted to analyze models of particle accelerators and their dynamics.

The present thesis relies in that context. We mainly focused on the dynamical point of view, especially in the framework of conservative systems. On one hand we surveyed the formalism of maps describing such systems as well as the tools to analyze, describe and qualify them. On the other hand we adapted the control methods of Vittot [Vittot, 2004] in order to provide new approaches, new leads, new models of particle accelerators exhibiting robust and excellent properties.

Synthesis

Over the years, physicists, mathematicians or engineers toiled to improve particle accelerators and to increase their energy. We placed ourselves in that mindset.

We first considered the formalism of maps describing effectively ring particle accelerators. Within this formalism we adapted and presented a *theorem of control* and gave explicit steps to apply it.

This theorem gives a methodology to construct a map. This resulting map preserves the main dynamical properties of the initial map : structures, similarities at first order, behaviors. Meanwhile the new map exhibits desired behaviors such as more regularity and bigger percentages of non escaping initial conditions.

We *applied the theorem to ring particle accelerator models*. The resulting map is expressed as an infinite sum of polynomials. We have proposed two techniques to overcome this obstacle in order to provide explicit manipulable maps.
We first operated an obvious choice : truncate the series. This, unfortunately, removes (most of the time) the symplecticity. We balanced this drawback by testing different orders and showed that in the region of interest, namely close to the design orbit, for sufficiently high order, the controlled map can be considered in good approximation as a symplectic one.
Secondly, we made the control independent of the momenta. This method presents two assets : it corresponds to a physical control and it preserves the symplecticity.

Then, we presented tools and methods to analyze the results.

Thanks to the chaos indicator Smaller ALignment Index, we showed that the two controls increase the dynamical aperture of the accelerator up to a factor 2. Many chaotic orbits are removed or pushed to the border of the DA.

With the Frequency Map Analysis, we recovered previous results reinforcing them but, more importantly, we produced the tune-footprints of the maps. With this technique, we were able to find resonances and diffusion directions. The controls weakened many resonant lines and/or decrease the width of the remaining one and drastically reduce the reachable diffusion directions.

We then completed the numerical results obtained by FMA by providing the shape of the frequency space at first order using the Normal Form approach.

Perspectives

The immediate perspective is to go further in the physics of the controls and execute a reverse processing of our development. In Chap. 2 we gave the main steps in the construction of a map modelling a ring particle accelerator. In order to push the quality of our controls to the next level, we would like to trace back the steps to potentially propose an implementable improved accelerator.

A second perspective is to open such techniques of control to dissipative systems.
We provided a first attempt by generalizing the theorem to differential operators of order 1. We applied it to the vector field of the van der Pol oscillator and were able to compute a controlled version with a constant of motion. This attempt is very new and should still be improved, especially in the direction of solving partial differential equations. Indeed, when we resolved the PDE, we should be able to improve the general solution using the fact that the solution is not unique.

Bibliographie

[Arnold, 1963] Arnold, V. (1963). Proof of a theorem by a. n. kolmogorov on the invariance of quasi-periodic motions under small perturbations of the hamiltonian. *Russian Mathematical Survey*, 18 :13–40.

[Bachelard et al., 2006] Bachelard, R., Chandre, C., and Leoncini, X. (2006). Reducing or enhancing chaos using periodic orbits. *Chaos*, 16 :023104–023110.

[Banks et al., 2003] Banks, J., Dragan, V., and Jones, A. (2003). *Chaos - A mathematical introduction.* Cambridge University Press.

[Bazzani, 1988] Bazzani, A. (1988). Normal forms for symplectic maps of $\mathbb{R}^{2n}$. *Celestial Mechanichs*, 42 :107–128.

[Bazzani et al., 1995] Bazzani, A., Giovannozzi, M., and Todesco, E. (1995). A program to compute birkhoff normal forms of symplectic maps in $\mathbb{R}^4$. *Computer Physics Communications*, 86 :199–207.

[Bazzani et al., 1990] Bazzani, A., Marmi, S., and Turchetti, G. (1990). Nekhoroshev estimate for isichronous non resonant symplectic maps. *Celestial Mechanics and Dynamical Astronomy*, 47 :333–359.

[Bazzani et al., 1988] Bazzani, A., Mazzanti, P., Servizi, G., and Turchetti, G. (1988). Normal forms for hamiltonian maps and nonlinear effects in a particle accelerator. *Il nuovo cimento*, 102B :51–80.

[Bazzani et al., 1994] Bazzani, A., Todesco, E., Turchetti, G., and Servizi, G. (1994). *A normal form approach to the theory of nonlinear betatronic motion.* CERN - Service d'information scientifique.

[Benettin et al., 1980] Benettin, G., Galgani, L., Giorgilli, A., and Strelcyn, J.-M. (1980). Lyapunov characteristic exponents for smooth dynamical systems and for hamiltonian systems ; a method for computing all of them. part 1 : Theory. *Meccanica*, 15 :9–20.

[Benson, 1999] Benson, H. (1999). *Mécanique (2nd Edition).* DeBoeck Université.

[Benzekri et al., 2006] Benzekri, T., Chandre, C., Leoncini, X., Lima, R., and Vittot, M. (2006). Chaotic advection and targeted mixing. *Physical Review Letters*, 96 :124503.

[Birkhoff, 1927] Birkhoff, G. (1927). *Dynamical system*. American mathematical society.

[Boreux et al., 2012a] Boreux, J., Carletti, T., Skokos, C., Papaphilippou, Y., and Vittot, M. (2012a). Efficient control of accelerator maps. *International Journal of Bifurcation and Chaos*, 22(9) :1250219.

[Boreux et al., 2012b] Boreux, J., Carletti, T., Skokos, C., and Vittot, M. (2012b). Hamiltonian control used to improve the beam stability in particle accelerator models. *Communications in Nonlinear Science and Numerical Simulation*, 17 :1725–1738.

[Bountis and Kollmann, 1994] Bountis, T. and Kollmann, M. (1994). Diffusion rates in a 4-dimensional mapping model of accelerator dynamics. *Physica D*, 71 :122–131.

[Bountis and Skokos, 2006] Bountis, T. and Skokos, C. (2006). Application of the sali chaos detection method to accelerator mappings. *Nuclear Instruments and Methods in Physics Research A*, 561 :173–179.

[Bountis and Skokos, 2012] Bountis, T. C. and Skokos, C. (2012). *Complex Hamiltonian Dynamics*. Springer-Verlag.

[Bourbaki, 1972] Bourbaki, N. (1972). *Eléments de Mathématiques : Groupes et Algèbres de Lie*.

[Breiter et al., 2005] Breiter, S., Wytrzyszczak, I., and Melendo, B. (2005). Long-term predictability of orbits around the geosynchronous altitude. *Advances in space research*, 35 :1313–1317.

[Callier and Desoer, 1991] Callier, F. and Desoer, C. (1991). *Linear system theory*. Springer-Verlag.

[Casas et al., 2012] Casas, F., Murua, A., and Nadinic, M. (2012). Efficient computation of the zassenhaus formula. *Computer Physics Communications*, 183 :2386–2391.

[Chandre, 2006] Chandre, C. (2006). personal communication.

[Chandre et al., 2005a] Chandre, C., Ciraolo, G., Doveil, F., Lima, R., Macor, A., and Vittot, M. (2005a). Channelling chaos by building barriers. *Physical Review Letters*, 94 :074101.

[Chandre and Jauslin, 2002] Chandre, C. and Jauslin, H. (2002). Renormalization-group analysis for the transition to chaos in hamiltonian systems. *Physics Reports*, 365 :1–64.

[Chandre et al., 2006] Chandre, C., Vittot, M., Ciraolo, G., Ghendrih, P., and Lima, R. (2006). Control of stochasticity in magnetic field lines. *Nuclear Fusion Journal of Plasma Physics and Thermonuclear Fusion*, 45 :1–13.

[Chandre et al., 2005b] Chandre, C., Vittot, M., Elskens, Y., Ciraolo, G., and Pettini, M. (2005b). Controlling chaos in aera preserving maps. *Physica D*, 208 :131–146.

[Chao and Chou, 2008] Chao, A. and Chou, W., editors (2008). *Reviews of Accelerator science and technology*. World Scientific.

[Chirikov, 1979] Chirikov, B. (1979). A universal instability of many-dimensional oscillator systems. *Physics Reports*, 52(5) :265–379.

[Cincotta et al., 2003] Cincotta, P. M., Giordano, C. M., and Simó, C. (2003). Phase space structure of multi-dimensional systems by means of the mean exponential grwth factor of nearby orbits. *Physica D*, 182 :151–178.

[Cincotta and Simó, 2000] Cincotta, P. M. and Simó, C. (2000). Simple tools to study global dynamics in non-axisymmetric galactic potential. *Astronomy and Astrophysics Supplement Series*, 147 :205–228.

[Ciraolo et al., 2004a] Ciraolo, G., Briolle, F., Chandre, C., Floriani, E., Lima, R., Vittot, M., Pettini, M., Figarella, C., and Ghendrih, P. (2004a). Control of hamiltonian chaos as a possible tool to control anomalous transport in fusion plasmas. *Physical Review E*, 69 :056213.

[Ciraolo et al., 2004b] Ciraolo, G., Chandre, C., Lima, R., Vitto, M., and Pettini, M. (2004b). Control of chaos in hamiltonian systems. *Celestial Mechanics and Dynamical Astronomy*, 90 :3–12.

[Close, 2004] Close, F. (2004). *Particle physics - A very short introduction*. Oxford university press.

[Compère et al., 2012] Compère, A., Lemaître, A., and N., D. (2012). Detection by megno of the gravitational resonances between a rotating ellipsoid and a point mass satellite. *Celestial Mechanics and Dynamical Astronomy*, 112 :75–98.

[Courant and Snyder, 1958] Courant, E. and Snyder, H. (1958). Theory of the alternating-gradient synchrotron. *Annals of Physics*, 3 :1–48.

[Darriba et al., 2012] Darriba, L., Maffione, N., Cincotta, P., and Giordano, C. (2012). Comparative study of variational chaos indicators and odes' numerical integrators. *International Journal of Bifurcation and Chaos*, 22 :1230033.

[Delsate et al., 2010] Delsate, N., Robutel, P., Lemaître, A., and Carletti, T. (2010). Frozen orbits at high eccentricity and inclination : application to mercury orbiter. *Celestial Mechanics and Dynamical Astronomy*, 108 :275–300.

[Dynkin, 1947] Dynkin, E. (1947). Calculation of the coefficients in the campbell-hausdorff formula. *Doklady Akademii Nauk SSSR*, 57 :323–326.

[Fasano and Marmi, 2006] Fasano, A. and Marmi, S. (2006). *Analytical mechanics - An introduction*. Oxford university press.

[Fischer et al., 1995] Fischer, W., Giovannozzi, M., and Schmidt, F. (1995). The dynamic aperture experiment at the cern sps.

[Flake, 1998] Flake, G. (1998). *The computational beauty of nature.* the MIT Press.

[Floyd et al., 1942] Floyd, P., Barthelemy, J., and Boreux, J. (1942). On the sublimation of the constant τ by jojo. *Review of good old memories*, 3 :141–592.

[Forest, 1998] Forest, E. (1998). *Beam Dynamics - A new attitude and framework.* Harwood academic.

[Franklin et al., 2010] Franklin, G., J.D., P., and Emani-Naeini, A. (2010). *Feedback control of dynamic systems.* Pearson.

[Gaudin, 2008] Gaudin, S. (2008). Collider test called a 'great milestone of mankind' - www.computerworlduk.com/news/infrastructure/10948/collider-test-called-a-great-milestone-of-mankind/.

[Gayon et al., 2008] Gayon, J., Marzari, F., and Scholl, H. (2008). Stable chaos in the 55cnc exoplanetary system ? *The Monthly Notices of the Royal Astronomical Society*, 389 :L1–L3.

[Giorgilli, 2013] Giorgilli, A. (2013). On the representation of maps by lie transforms. arXiv :1211.56/4v2.

[Giovannozzi et al., 1997] Giovannozzi, M., Scandale, W., and Todesco, E. (1997). Prediction of long-term stability in large hadron colliders. *Particle accelerators*, 56(4) :195–226.

[Goździewski et al., 2001] Goździewski, K., E., B., Maciejewski, A., and L., K.-E. (2001). Global dynamics of planetary systems with the megno criterion. *Astronomy and Astrophysics*, 378 :569–586.

[Greene, 1968] Greene, J. (1968). Two-dimensional measure-preserving mapping. *Journal of mathematical physics*, 9(5) :760–768.

[Greene, 1979] Greene, J. (1979). A method for determining a stochastic transition. *Journal of mathematical physics*, 20(6) :1183–1201.

[Gustavson, 1966] Gustavson, F. (1966). On constructing formal integrals of a hamiltonian system near an equilibrium point. *Astronomical Journal*, 71 :670–686.

[Guzzo and Benettin, 2001] Guzzo, M. and Benettin, G. (2001). A spectral formulation of the nekhoroshev theorem and its relevance for numerical and experimental data analysis. *Discrete and Continuous Dynamical Systems - Series B*, 1 :1–28.

[Hairer et al., 2006] Hairer, E., Lubic, C., and Wanner, G. (2006). *Geometric Numerical Integration. Structure-preserving Algorithms for ordinary differential equations.* Berlin Heidelberg, 2nd edition.

[Hanson and Cary, 1984] Hanson, J. and Cary, J. (1984). Elimination of stochasticity in stellerators. *Physics of fluids*, 27 :767–769.

[Henke et al., 1992] Henke, H., Homeyer, H., and Petit-Jean-Genaz, C., editors (1992). *EPAC 92 - Proceedings of the third european particle accelerator conference.* Editions Frontières.

[Hénon, 1969] Hénon, M. (1969). Numerical study of quadratic area-preserving mappings. *Quarterly of Applied Mathematics*, 27 :291.

[Hénon, 1976] Hénon, M. (1976). A two-dimensional mapping with a strange attractor. *Communications in mathematical physics*, 50 :69–77.

[Hilborn, 1994] Hilborn, R. (1994). *Chaos and nonlinear dynamics*. Oxford university press.

[Hinrichsen and Pritchard, 2005] Hinrichsen, D. and Pritchard, A. (2005). *Mathematical systems theory I modelling, state space analysis, stability and robustness*. Springer-Verlag.

[Hinse et al., 2010] Hinse, T., Christou, A., Alvarellos, J., and Goździewski, K. (2010). Application of the megno technique to the dynamics of jovian irregular satellites. *The Monthly Notices of the Royal Astronomical Society*, 404 :837–857.

[Holmes, 1979] Holmes, P. (1979). A nonlinear oscillator with a strange attractor. *Philosophical Transactions of the Royal Society A*, 292 :419–448.

[Huang et al., 2006] Huang, S., Chandre, C., and Uzer, T. (2006). Reducing multiphoton ionization in a linearly polarized microwave field by local control. *Physical review. A*, 74 :053408.

[Hubaux et al., 2013] Hubaux, C., Libert, A.-S., Delsate, N., and Carletti, T. (2013). Influence of earth's shadowing effects on space debris stability. *Advances in Space Research*, 51 :25–38.

[Kolmogorov, 1954] Kolmogorov, A. (1954). The conservation of quasi periodic motion for small changes in the hamiltonian function. *Doklady Akademii Nauk USSR*, 98 :527.

[Laskar, 1990] Laskar, J. (1990). The chaotic motion of the solar system : a numerical estimate of the size of the chaotic zones. *Icarus*, 88 :266–291.

[Laskar, 1993a] Laskar, J. (1993a). Frequency analysis for multi-dimensional systems. global dynamics and diffusion. *Physica D*, 67 :257–281.

[Laskar, 1993b] Laskar, J. (1993b). Frequency analysis of dynamical system. *Celestial Mechanichs and Dynamical Astronomy*, 56 :191–196.

[Laskar, 1999] Laskar, J. (S'Agaro, 1999). Introduction to frequency map analysis. *In Proceedings of 3DHAM95 NATO Advanced Institute*, 533 :134–150.

[Laskar and Robutel, 2001] Laskar, J. and Robutel, P. (2001). High order symplectic integrators for perturbed hamiltonian systems. *Celestial Mechanichs and Dynamical Astronomy*, 80 :39–62.

[Lee, 2012] Lee, S. (2012). *Accelerator Physics - Third Edition*. World Scientific.

[Locatelli, 2001] Locatelli, A. (2001). *Optimal control : an introduction*. Birkhaüser.

[Lorenz, 1963] Lorenz, E. (1963). Deterministic nonperiodic flow. *Journal of the Atmospheric Sciences*, 20 :130–141.

[MacKay and Conte, 2012] MacKay, W. and Conte, M. (2012). *Accelerator physics - Example problems with solutions*. World Scientific.

[Macor et al., 2007] Macor, A., Doveil, F., Chandre, C., Ciraolo, G., Lima, R., and Vittot, M. (2007). Channeling chaotic transport in a wave-particle experiment. *European Physical Journal D*, 41 :519–530.

[Maffione et al., 2011] Maffione, N., Darriba, L., Cincotta, P., and Giordano, C. (2011). A comparison of different indicators of chaos based on the deviation vectors : application to symplectic mappings. *Celestial Mechanics and Dynamical Astronomy*, 111 :285–307.

[Maschke et al., 2000] Maschke, B., Ortega, R., and van der Schaft A.J. (2000). Energy-based lyapunov functions for forced hamiltonain systems with dissipation. *IEEE transactions on automatic control*, 45(8) :1498–1502.

[Mestre et al., 2011] Mestre, M., Cincotta, P., and Giordano, C. (2011). Analytical relation between two chaos indicators : Fli and megno. *The Monthly Notices of the Royal Astronomical Society*, 414 :L100–L103.

[Meyer, 1974] Meyer, K. (1974). Normal forms for hamiltonian systems. *Celestial Mechanichs*, 9 :517–522.

[Miller and Michel, 1982] Miller, R. and Michel, A. (1982). *Ordinary differential equations*. Academic Press.

[Moser, 1962] Moser, J. (1962). On invariant curves of area-preserving mappings of an annulus. *Nachrichten der Akademie der Wissenschaften in Göttingen. II. Mathematisch-Physikalische Klasse*, 1 :1–20.

[Nadolski and Laskar, 2002] Nadolski, L. and Laskar, J. (2002). Application of a new class of symplectic integrators to accelerator tracking. In *EPAC*, pages 1276–1278.

[Nadolski and Laskar, 2003] Nadolski, L. and Laskar, J. (2003). Review of single particle dynamics for third generation light sources through frequency map analysis. *Physical Review Special Topics - Accelerators and Beams*, 6 :114801.

[Ott et al., 1990] Ott, E., Grebogi, C., and Yorke, J. (1990). Controlling chaos. *Physical review letters*, 64 :1996–1999.

[Petalas et al., 2008] Petalas, Y. G., Antonopoulos, C. G., Bountis, T. C., and Vrahatis, M. N. (2008). Evolutionary methods for the approximation of the stability domain and frequency optimization of conservative maps. *International Journal of Bifurcation and Chaos*, 18 :2249–2264.

[Polymilis et al., 1997] Polymilis, C., Servizi, G., and Skokos, C. (1997). A quantitative bifurcation analysis of hÃ©non-like 2d maps. *Celestial Mechanics and Dynamical Astronomy*, 66 :365–385.

[press, 2008] press, C. (2008). First beam in the lhc - accelerating science.

[Raubenheimer, 1993] Raubenheimer, T. (1993). The preservation of low emittance flat beams. *SLAC-PUB-6117*, pages 1–5.

[Scandale and Turchetti, 1990] Scandale, W. and Turchetti, G. (1990). *Nonlinear problems in future particle accelerators*. World Scientific.

[Servizi and Turchetti, 1986] Servizi, G. and Turchetti, G. (1986). Perturbative expansions for area-preserving maps. *Il nuovo cimento*, 95B :121–154.

[Skokos, 2001] Skokos, C. (2001). Alignement indices : a new, simple method for determining the ordered or chaotic nature of orbits. *Journal of Physics A : Mathematical and General*, 34 :10029–10043.

[Skokos, 2010] Skokos, C. (2010). *The Lyapunov Characteristic Exponents and their computation*, pages 63–135. Springer.

[Skokos et al., 2007] Skokos, C., Bountis, T. C., and Antonopoulos, C. (2007). Geometrical properties of local dynamics in hamiltonian systems : the generalized alignment index (gali) method. *Physica D*, 231 :30–54.

[Statistics, 2013] Statistics, L. P. (2013). lhc-statistics.web.cern.ch/lhc-statistics/.

[Steffen, 1985] Steffen, K. (1985). *Basic Course on Accelerator Optics*. Deutsches Elektronen-Synchrotron.

[Strogatz, 1994] Strogatz, S. (1994). *Nonlinear dynamics and chaos*. Perseus books.

[Thiry, 2002] Thiry, P. (2002). *Physique générale. Electromagnétisme*.

[Todesco et al., 1997] Todesco, E., Gemmi, M., and Giovannozzi, M. (1997). Nero : a code for the nonlinear evaluation of resonances in one-turm mapppings. *Computer Physics Communications*, 106 :169–180.

[Turner, 1994] Turner, S., editor (1994). *Cern acclerator school - Fifth general accelerator physics course*. Cern.

[Valk et al., 2009] Valk, S., Delsate, N., Lemaître, A., and Carletti, T. (2009). Global dynamics of high area-to-mass ratios geo space debris by means of the megno indicator. *Advances in Space Research*, 43 :1509–1526.

[van der Pol, 1927] van der Pol, B. (1927). On relaxation oscillations. *Philosophical Magazine*, 2(7) :978–992.

[Vittot, 2004] Vittot, M. (2004). Perturbation theory and control in classical or quantum mechanics by inversion formula. *Journal of Physics A : Mathematics and General*, 37 :6337–6357.

[Vittot et al., 2005] Vittot, M., Chandre, C., and Lima, R. (2005). Localized control for non-resonant hamiltonian systems. *Nonlinearity*, 18 :423–440.

[Vrahatis et al., 1996] Vrahatis, M., Bountis, T., and Kollmann, M. (1996). Periodic orbits and invariant surfaces in 4-d nonlinear mappings. *International Journal of Bifurcation and Chaos*, 6(8) :1425–1437.

[Vrahatis et al., 1997] Vrahatis, M., Isliker, H., and Bountis, T. (1997). Structure and breakdown of invariant tori in a 4-d mapping model of accelerator dynamics. *International Journal of Bifurcation and Chaos*, 7 :2707–2722.

[Weishi and Cary, 2001] Weishi, W. and Cary, J. (2001). Method for enlarging the dynamic aperture of accelerator lattices. *Physical review special topics - Accelerators and beams*, 4 :084001.

[Wilson, 2001] Wilson, E. (2001). *An introduction to particle accelerators*. Oxford university press.

[Yoshida, 1990] Yoshida, H. (1990). Construction of higher order symplectic integrators. *Physics Lettres A*, 150 :262–268.